



The  
University  
Of  
Sheffield.

# **Study of macromolecule-mineral interactions on nuclear related materials**

by

Lygia Eleftheriou

Submitted in partial fulfillment of the requirements for the degree of

Doctor of Philosophy

Supervised by:

Prof John Harding

Dr Maria Romero-González

The University of Sheffield

Faculty of Engineering

Department of Materials Science and Engineering

September 2016







# Declaration

The work described within this thesis has been completed under the supervision of Prof J. Harding and Dr M. Romero-González at the University of Sheffield between September 2012 and September 2016.

This thesis along with the work described here has been completed by the author with some exceptions indicated clearly at the relevant chapters. These include:

- (1) the construction of ceria models for the computational work that was completed by Dr Colin Freeman and Dr Shaun Hall (described in chapter 5),
- (2) the purification of peptidoglycan completed by Dr Stephane Mesnage (described in chapter 4) and
- (3) the electron microscopy analysis completed by Dr Mohamed Merroun (described in chapter 2).

Lygia Eleftheriou

September 2016



# Acknowledgements

I would like to express my sincere gratitude to my supervisors Dr Maria Romero González and Prof John Harding for all their support during the past four years. This work would not have been possible without their endless encouragement, guidance and advice.

I would also like to thank Dr Colin Freeman, Dr Shaun Hall and Riccardo Innocenti Malini for all the hours they spent trying to make things work and all their help with the computational part of this project.

In addition, I would like to thank Dr Simon Thorpe, Dr Stephane Mesnage and Mr Robert Hanson for their help with the analytical methods of this project.

Special thanks should go to Debbie Hill, Emma Wharfe and Gordon Brown for being my first contact for basically everything, from outreach activities to student support.

Lastly, I would like to thank my family and friends. My parents were the ones to support me the most during this journey. I could never thank them enough. My dear friends, Gifty Tetteh and Joe Hufton who in one way or another shared their support and of course my partner-in-crime, Panagiotis Koulouris who has been next to me during the endless nights of analysing, correcting, writing, re-writing and so on. Thank you!

The research was sponsored financially by the EPSRC Doctoral Training Centre (DTC) in Nuclear Fission Research Science and Technology and the EPSRC consortium 'Hard-soft matter interfaces: from understanding to engineering' (EP/I001514/1).



# Abstract

Microbes have been identified close to contaminated sites such as nuclear-waste repositories indicating their ability to interact with radionuclides. One of the main mechanisms bacteria use involves the reduction of highly mobile radionuclides to less mobile minerals, often in the form of oxides. The precipitated minerals are found located at the cell wall or close to the external components of the bacterial cell suggesting a possible interaction of cell wall components or external components of the tested bacteria with the precipitated particles. Tests on ceria, uranium, thorium and europium oxide confirmed that several biomolecules are responsible for the observed localisation. The first experiments used lipopolysaccharides (LPS), found at the outer site of Gram negative bacterial cells and resulted in successful sorption of LPS on all four minerals. The Purpald assay was used to quantify LPS before and after the interaction and confirmed the attachment of the biopolymers to the oxides with  $\Delta G$  values in the range of physisorption (-3 to -25 kJ/mol) for all systems. ATR-FTIR, zeta potential analysis and electron microscopy also confirmed the attachment of the biomolecules on the minerals. Mycolic acids and peptidoglycans, components of Gram positive bacteria, were also assessed for their ability to interact with ceria and europium oxide. Mycolic acids showed successful sorption profiles with  $\Delta G$  values in the physisorption range (-10 to -17 kJ/mol) for all systems, highly dependent on the experimental conditions. In addition, Molecular Dynamics simulations were used to examine the interaction of mycolic acid with ceria under natural conditions (pH7) in the presence of  $\text{Na}^+$  and the calculated binding energy (-11.598 kJ/mol) agreed well with the experimental results for the corresponding system (-16.485 kJ/mol). Additionally, preliminary tests on peptidoglycan interactions resulted in successful sorption of the biomolecule on both ceria and europium oxide with  $\Delta G$  values in the physisorption range (-8 to -10 kJ/mol). ATR-FTIR and zeta potential analysis confirmed the attachment of mycolic acid and peptidoglycan on the minerals tested. These results suggest that the observed localisation of mineral within the

bacterial cell walls are related to lipopolysaccharide and peptidoglycan-mediated sorption and have potential uses in treatment of nuclear waste and biomining processes.

# Contents

# Page

|   |           |
|---|-----------|
| <b>Chapter 1</b> .....  | <b>15</b> |
| <b>Introduction</b> .....   | <b>15</b> |
| <b>Background</b> .....   | <b>16</b> |
| <b>Objectives</b> .....   | <b>17</b> |
| <b>Literature review</b> .....  | <b>18</b> |
| 1.1 Nuclear Materials: Existence and Usage.....   | 18        |
| 1.2 The issue .....   | 19        |
| 1.3 Bacterial interactions with nuclear-related materials .....   | 19        |
| 1.3.1 Bacterial cell structure .....  | 22        |
| 1.3.1.1 Gram negative and Gram positive bacteria .....  | 22        |
| 1.3.1.2 The Mycolata family .....   | 23        |
| 1.4. Interactions of cell wall bio-components with minerals .....   | 24        |
| 1.4.1 Lipopolysaccharides .....   | 24        |
| 1.4.2 Peptidoglycans.....   | 25        |
| 1.4.3 Mycolic acids .....   | 25        |
| 1.5. Importance and applications of interactions between bacterial components and nuclear-related minerals..... | 26        |
| 1.6 Experimental techniques to evaluate macromolecule-mineral interactions .....                                | 28        |
| 1.6.1 Spectrophotometric Techniques .....   | 28        |
| 1.6.2 Spectroscopic techniques-FTIR .....   | 30        |
| 1.6.3 Computational Methods.....  | 31        |
| 1.6.3.1 Molecular Dynamics .....  | 33        |
| <b>Chapter 2</b> .....  | <b>45</b> |
| <b>Lipopolysaccharide Interactions with Nuclear Related Minerals</b> .....                                      | <b>45</b> |
| <b>2.1 Introduction</b> .....   | <b>46</b> |
| 2.1.1 Functions of LPS.....   | 48        |
| 2.1.1.1 Interactions of LPS with surfaces .....   | 49        |
| 2.1.2 Objectives .....  | 51        |
| <b>2.2 Materials and Methods</b> .....  | <b>52</b> |
| 2.2.1 Chemicals.....  | 52        |
| 2.2.2 Macromolecules .....  | 52        |
| 2.2.2.1 Molecular Weight Determination of LPS .....   | 53        |
| 2.2.3 Minerals .....  | 53        |
| 2.2.3.1 Synthesis of UO <sub>2</sub> .....  | 54        |
| 2.2.3.1.1 Stainless Steel Reactor Design .....  | 54        |
| 2.2.3.1.2 X-ray Diffraction Analysis .....  | 56        |
| 2.2.3.1.3 Experimental conditions.....  | 56        |

|  |            |
|--|------------|
| 2.2.3.2 Ceria, Europium oxide, Thoria .....  | 57         |
| 2.2.4 Adsorption Experiments .....   | 57         |
| 2.2.4.1 Isotherm Models.....   | 58         |
| 2.2.4.2 Quantification of LPS using the Purpald Assay .....                                | 59         |
| 2.2.5 Zeta Potential Analysis .....  | 60         |
| 2.2.6 Attenuated Total Reflection-Fourier Transform Infrared Spectroscopy (ATR-FTIR) ..... | 60         |
| 2.2.7 Electron Microscopy.....   | 61         |
| <b>2.3 Results and Discussion.....</b>   | <b>62</b>  |
| 2.3.1 Determination of LPS Molecular Weight .....  | 62         |
| 2.3.2 Characterization of minerals .....   | 64         |
| 2.3.2.1 Urania Synthesis.....  | 64         |
| 2.3.2.2 Characterization of Ceria and Europium oxide .....                                 | 65         |
| 2.3.3 Adsorption of LPS on Ceria .....   | 66         |
| 2.3.3.1 Zeta Potential of LPS – Ceria interactions .....                                   | 66         |
| 2.3.3.2 Quantification of LPS - Calibration Curve.....                                     | 69         |
| 2.3.3.3 Experimental Isotherms for sorption of LPS onto Ceria .....                        | 71         |
| 2.3.3.3.1 Equilibrium Modelling of LPS sorption onto Ceria .....                           | 74         |
| 2.3.3.4 Kinetics .....   | 78         |
| 2.3.3.5 ATR-FTIR of Ceria-LPS interactions.....  | 81         |
| 2.3.3.6 Electron Microscopy.....   | 84         |
| 2.3.4 Adsorption of LPS onto europium oxide .....  | 86         |
| 2.3.4.1 Quantification of LPS- Calibration curve.....                                      | 86         |
| 2.3.4.2 Experimental Isotherms for sorption of LPS onto europium oxide.....                | 86         |
| 2.3.4.3 Equilibrium Modelling of LPS sorption onto Europium oxide .....                    | 89         |
| 2.3.4.4 Kinetics.....  | 91         |
| 2.3.4.5 ATR-FTIR of europium oxide-LPS interactions.....                                   | 93         |
| 2.3.5 Adsorption of LPS onto thoria.....   | 95         |
| 2.3.5.1 Quantification of LPS- Calibration curve.....                                      | 95         |
| 2.3.5.2 Experimental Isotherms for sorption of LPS onto thoria.....                        | 95         |
| 2.3.5.2.1 Equilibrium Modelling of LPS sorption onto Thoria .....                          | 98         |
| 2.3.5.3 Kinetics .....   | 100        |
| 2.3.6 Adsorption of LPS onto urania .....  | 102        |
| 2.3.6.1 Quantification of LPS- Calibration curve.....                                      | 102        |
| 2.3.6.2 Experimental Isotherms for sorption of LPS onto urania .....                       | 102        |
| 2.3.6.2.1 Equilibrium Modelling of LPS sorption onto Urania.....                           | 105        |
| 2.3.6.3 Kinetics .....   | 108        |
| 2.3.7 Comparison of LPS sorption profiles .....  | 110        |
| <b>2.4 Conclusions.....</b>  | <b>113</b> |
| <b>Chapter 3.....</b>  | <b>115</b> |

|   |            |
|---|------------|
| <b>Mycolic acid interactions with nuclear related materials .....</b>                     | <b>115</b> |
| <b>3.1 Introduction .....</b>   | <b>116</b> |
| 3.1.1 Adsorption of MCA onto surfaces .....   | 118        |
| 3.1.2 Extraction and Purification Techniques for MCA .....                                | 119        |
| 3.1.3 Objectives .....  | 122        |
| <b>3.2 Materials and Methods .....</b>  | <b>123</b> |
| 3.2.1 Chemicals .....   | 123        |
| 3.2.2 Macromolecules .....  | 123        |
| 3.2.3 MCA solubility tests .....  | 124        |
| 3.2.4 Minerals .....  | 124        |
| 3.2.5 Method for MCA-Mineral Interactions .....   | 124        |
| 3.2.5.1 Isotherm Models .....   | 125        |
| 3.2.6 Mass Spectrometry for Quantification of MCAs .....                                  | 126        |
| 3.2.7 Attenuated Total Reflection-Fourier Transform Infrared Spectroscopy (ATR-FTIR)..... | 127        |
| <b>3.3 Results and Discussion .....</b>   | <b>128</b> |
| 3.3.1 MCA solubility tests and solvent choice .....                                       | 128        |
| 3.3.2 Characterization of Ceria and Europium Oxide .....                                  | 129        |
| 3.3.3 MCA quantification – Calibration .....  | 130        |
| 3.3.4 Adsorption of MCA onto Ceria.....   | 133        |
| 3.3.4.1 MCA interactions with ceria – Kinetics .....                                      | 133        |
| 3.3.4.2 Experimental Isotherms for sorption of MCA onto Ceria .....                       | 138        |
| 3.3.5 Adsorption of MCA on europium oxide .....   | 146        |
| 3.3.5.1 MCA interactions with europium oxide- Kinetics .....                              | 146        |
| 3.3.5.2 MCA interactions with europium oxide – Isotherms .....                            | 151        |
| 3.3.5.3 ATR-FTIR of Europium Oxide - MCA interactions .....                               | 157        |
| 3.3.6 Comparison between Ceria-MCA and Europium Oxide-MCA interactions.....               | 158        |
| <b>3.4 Conclusions .....</b>  | <b>162</b> |
| <b>Chapter 4.....</b>   | <b>165</b> |
| <b>Peptidoglycan Interactions with Nuclear Related Materials .....</b>                    | <b>165</b> |
| <b>4.1 Introduction .....</b>   | <b>166</b> |
| 4.1.1 Quantification of PGN .....   | 168        |
| 4.1.2 PGN interactions with surfaces .....  | 170        |
| 4.1.3 Objectives .....  | 172        |
| <b>4.2 Materials and Methods .....</b>  | <b>173</b> |
| 4.2.1 Chemicals.....  | 173        |
| 4.2.2 Macromolecules .....  | 174        |
| 4.2.2.1 Purification of PGN .....   | 174        |
| 4.2.2.1.1 Analysis of peptidoglycan purity using HPLC .....                               | 175        |
| 4.2.3 Minerals .....  | 176        |
| 4.2.4 Method for PGN and Surface Interactions .....                                       | 176        |
| 4.2.4.1 Isotherm Models .....   | 177        |

|  |            |
|--|------------|
| 4.2.5 Quantification of PGN – Colorimetric Method .....                                    | 177        |
| 4.2.6 Attenuated Total Reflection-Fourier Transform Infrared Spectroscopy (ATR-FTIR) ..... | 178        |
| 4.2.7 Zeta Potential Analysis .....  | 179        |
| <b>4.3 Results and Discussion.....</b>   | <b>180</b> |
| 4.3.1 Adsorption of PGN onto Ceria .....   | 180        |
| 4.3.1.1 Zeta Potential of PGN – Ceria interactions .....                                   | 180        |
| 4.3.1.2 Muramic Acid Assay-Calibration Curve .....   | 183        |
| 4.3.1.3 Adsorption of PGN onto Ceria-Kinetics .....  | 184        |
| 4.3.1.4 Adsorption of PGN onto Ceria-Isotherm .....  | 187        |
| 4.3.1.5 ATR-FTIR of Ceria - PGN interactions .....   | 190        |
| 4.3.2 Adsorption of PGN onto europium oxide .....  | 193        |
| 4.3.2.1 ATR-FTIR of europium oxide - PGN interactions.....                                 | 193        |
| <b>4.4 Conclusions.....</b>  | <b>197</b> |
| <b>Chapter 5.....</b>  | <b>199</b> |
| <b>Computational Simulation of Mycolic Acid Adsorption onto Ceria.....</b>                 | <b>199</b> |
| <b>5.1 Introduction.....</b>   | <b>200</b> |
| 5.1.1 Simulations of Mineral-Organics systems .....  | 200        |
| 5.1.1.1 Simulation of Biomineralisation Processes .....                                    | 201        |
| 5.1.2 Simulation of Inorganic surfaces .....   | 203        |
| 5.1.3 Objectives .....   | 204        |
| <b>5.2 Materials and Methods.....</b>  | <b>205</b> |
| 5.2.1 Ceria modeling .....   | 206        |
| 5.2.2 Mycolic acid modeling .....  | 207        |
| 5.2.3 Simulation Parameters .....  | 209        |
| <b>5.3 Results and Discussion.....</b>   | <b>210</b> |
| 5.3.1 Structure of Ceria.....  | 210        |
| 5.3.2 Simulation binding energies .....  | 211        |
| 5.3.3 Effect of ions in binding .....  | 214        |
| 5.3.4 Comparison to experimental results .....   | 215        |
| <b>5.4 Conclusions.....</b>  | <b>222</b> |
| <b>General Discussion .....</b>  | <b>223</b> |
| <b>General Conclusions .....</b>   | <b>231</b> |
| <b>Future Work.....</b>  | <b>232</b> |
| <b>References .....</b>  | <b>239</b> |
| <b>Appendices.....</b>   | <b>261</b> |

| <b>List of Figures</b>   | <b>Page</b> |
|--|-------------|
| Figure 1.1 Urania precipitates on Shewanella oneidensis                        | 20          |
| Figure 1.2 U [IV] precipitates formed by G. sulfurreducans                     | 20          |
| Figure 1.3 Eu precipitates on E. coli  | 20          |
| Figure 1.4 Technetium oxides at the periphery of G. Sulfurreducens             | 21          |
| Figure 1.5 Gram Negative and Gram Positive bacterial cell wall                 | 22          |
| Figure 1.6The ‘Minnikin model’ for the Mycobacterium cell envelope             | 23          |
| Figure 1.7The different levels of microscale/mesoscale computational modelling | 32          |
| Figure 1.8The Morse potential  | 34          |
| Figure 1.9 The Lennard -Jones potential  | 35          |
| Figure 1.10The Coulomb potential compared to van der Waals                     | 35          |
| Figure 1.11 Hydrogen Bonding and different water molecule models               | 35          |
| Figure 1.12 Example of a coarse grained molecule                               | 37          |
| Figure 1.13 Periodic boundary conditions used to replicate the system          | 40          |
| Figure 1.14The canonical and isothermal ensembles                              | 42          |
| Figure 1.15 Flow Chart of a molecular dynamic simulation                       | 43          |
| Figure 2.1 General structure for bacterial LPS                                 | 47          |
| Figure 2.2 Reaction mechanism of the Purpald Assay                             | 49          |
| Figure 2.3The stainless steel reactor used for UO <sub>2</sub> synthesis       | 55          |
| Figure 2.4 Example of a UO <sub>2</sub> PDF card by ICDD                       | 56          |
| Figure 2.5 Molecular Weight of LPS by GPC analysis                             | 63          |
| Figure 2.6 XRD results for synthesised UO <sub>2</sub>                         | 65          |
| Figure 2.7 Eu <sub>2</sub> O <sub>3</sub> characterization                     | 66          |
| Figure 2.8The structure of the electric double layer                           | 67          |
| Figure 2.9 Zeta potential of LPS and Ceria before and after the interaction    | 68          |
| Figure 2.10 Calibration curves for the Purpald Assay                           | 70          |
| Figure 2.11 Isotherm of LPS-Ceria interactions at pH3                          | 72          |
| Figure 2.12 Isotherm of LPS-Ceria interaction (pH7)                            | 72          |
| Figure 2.13 Isotherm of LPS-Ceria interactions(pH10)                           | 72          |
| Figure 2.14 Kinetics of LPS-Ceria interactions(pH3)                            | 78          |
| Figure 2.15 Kinetics of LPS-Ceria interactions (pH 7)                          | 78          |
| Figure 2.16 Kinetics of LPS-Ceria interactions (pH10)                          | 78          |

|   |     |
|---|-----|
| Figure 2.17 Pseudo-second order fitting of LPS-Ceria interactions (pH10)                    | 80  |
| Figure 2.18 ATR-FTIR of LPS interacted with Ceria   | 82  |
| Figure 2.19 ATR-FTIR of LPS controls under different conditions                             | 83  |
| Figure 2.20 Transmission Electron Microscopy analysis of Ceria-LPS                          | 85  |
| Figure 2.21 Isotherm of LPS-europium oxide interactions at pH3                              | 87  |
| Figure 2.22 Isotherm of LPS-europium oxide interactions at pH7                              | 87  |
| Figure 2.23 Isotherm of LPS-europium oxide interaction at pH10                              | 87  |
| Figure 2.24 Kinetics of LPS-europium oxide interaction pH3                                  | 91  |
| Figure 2.25 Kinetics of LPS-europium oxide interactions pH7                                 | 91  |
| Figure 2.26 Kinetics of LPS-europium oxide interactions pH10                                | 91  |
| Figure 2.27 Pseudo-second order fitting of LPS-europium oxide interactions                  | 92  |
| Figure 2.28 ATR-FTIR of LPS interacted with europium oxide                                  | 94  |
| Figure 2.29 Isotherm of LPS- thoria interactions at pH3                                     | 96  |
| Figure 2.30 Isotherm of LPS- thoria interactions at pH7                                     | 96  |
| Figure 2.31 Isotherm of LPS- thoria interaction pH10  | 96  |
| Figure 2.32 Kinetics of LPS- thoria interactions  | 100 |
| Figure 2.33 Pseudo-second order fitting of LPS- thoria interactions                         | 101 |
| Figure 2.34 Isotherm of LPS- urania interactions at pH3                                     | 103 |
| Figure 2.35 Isotherm of LPS- urania interactions at pH7                                     | 103 |
| Figure 2.36 Isotherm of LPS- urania interactions at pH10                                    | 103 |
| Figure 2.37 Example fitting on the Freundlich model for the adsorption of LPS onto Urania   | 105 |
| Figure 2.38 Kinetics of LPS- urania interactions  | 108 |
| Figure 2.39 Pseudo-second order fitting of LPS- urania interactions                         | 109 |
| Figure 2.40 Surface charge and point of zero charge of all minerals tested                  | 110 |
| Figure 2.41 LPS sorption onto minerals under acidic conditions                              | 112 |
| Figure 2.42 LPS sorption onto minerals under basic conditions                               | 112 |
| Figure 3.1 The three major forms of MCA   | 118 |
| Figure 3.2 Basic characteristics of MCAs from Mycobacterium tuberculosis                    | 120 |
| Figure 3.3 Theoretical peaks of MCA produced ions when analysed with mass spectrometry      | 121 |
| Figure 3.4 Mass Spectrometry Calibration curve for quantification of MCA                    | 130 |
| Figures 3.5 Examples of Mass Spectrometry results for MCA identification and quantification | 132 |

|   |     |
|---|-----|
| Figure 3.6 Kinetics of adsorption of MCA with Ceria pH3                                 | 133 |
| Figure 3.7 Kinetics of adsorption of MCA with Ceria pH7                                 | 133 |
| Figure 3.8 Kinetics of adsorption of MCA with Ceria-pH10                                | 133 |
| Figure 3.9 Example fitting (Langmuir) for adsorption of MCA onto ceria                  | 138 |
| Figure 3.10 Freundlich Isotherm Model for adsorption of MCA onto ceria                  | 139 |
| Figure 3.11 Sips Isotherm Model for adsorption of MCA onto ceria (n=0.4)                | 141 |
| Figure 3.12 Sips Isotherm Model for adsorption of MCA onto ceria (n=0.5)                | 141 |
| Figure 3.13 Kinetics of adsorption of MCA with europium oxide- pH3                      | 147 |
| Figure 3.14 Kinetics of adsorption of MCA with Europium oxide-pH7                       | 147 |
| Figure 3.15 Kinetics of adsorption of MCA with Europium oxide-pH10                      | 147 |
| Figure 3.16 ATR-FTIR results for MCA adsorption onto europium oxide                     | 157 |
| Figure 3.17The surface charge of ceria and europium oxide                               | 158 |
| Figure 3.18The effect of chloroform in the solubility of MCA                            | 160 |
| Figure 3.19 Sorption of An and Ln onto bacterial cells                                  | 161 |
| Figure 4.1 PGN in Gram negative and Gram positive bacterial cell walls                  | 168 |
| Figure 4.2 Structure of the repeating unit of PGN                                       | 168 |
| Figure 4.3The muramic acid structure  | 169 |
| Figure 4.4 HPLC results for purity of PGN-treated                                       | 175 |
| Figure 4.5 Measured zeta potential as a function of pH for ceria-PGN                    | 181 |
| Figure 4.6 Calibration curve for muramic acid quantification with varying electrolytes  | 183 |
| Figure 4.7 Kinetics of adsorption of PGN with Ceria -pH7                                | 185 |
| Figure 4.8 Pseudo second order kinetics for PGN-Ceria at pH 7                           | 187 |
| Figure 4.9 Fitting on the Langmuir isotherm of Ceria-PGN with CaCl <sub>2</sub>         | 188 |
| Figure 4.10 ATR-FTIR spectra of PGN controls  | 191 |
| Figure 4.11 FT-IR of PGN measuring absorbance   | 192 |
| Figure 4.12 ATR-FTIR spectra of Ceria- PGN  | 193 |
| Figure 4.13 ATR-FTIR spectra of Europium oxide- PGN                                     | 195 |
| Figure 5.1 The Ceria model shown from different angles                                  | 207 |
| Figure 5.2The model of (pseudo-)mycolic acid  | 208 |
| Figure 5.3 Ce–Ce Radial Distribution Functions  | 210 |
| Figure 5.4The binding of mycolic acid onto ceria when starting at <3Å away from surface | 212 |
| Figure 5.5 Repulsion of mycolic acid from surface when starting >5 Å from surface       | 212 |

|  |     |
|--|-----|
| Figure 5.6 Starting and final simulation configurations Ceria-pseudo-MCA- water          | 213 |
| Figure 5.7 Starting and final simulation configurations Ceria-pseudo-MCA- water          | 213 |
| Figure 5.8 Starting and final simulation configurations Ceria-pseudo-MCA- water          | 213 |
| Figure 5.9 Starting and final simulation configurations Ceria-pseudo-MCA- water          | 213 |
| Figure 5.10 The role of Na ion   | 214 |
| Figure 5.11 The bringing effect of Ca <sup>2+</sup> ions in the binding of DNA to Silica | 214 |
| Figure 5.12 The three different forms of mycolic acid                                    | 219 |
| Figure 5.13 The different modes of polymer adsorption onto surfaces                      | 220 |

## List of Tables

## Page

|  |     |
|--|-----|
| Table 1.1. Water molecule model and parameters                                     | 36  |
| Table 2.1. Equilibrium Models  | 59  |
| Table 2.2 pH at point of zero charge   | 71  |
| Table 2.3. Modified Freundlich Model-Results of LPS adsorption on Ceria            | 76  |
| Table 2.4. $\Delta G$ calculations for LPS adsorption to ceria                     | 77  |
| Table 2.5. Results of kinetic analysis of LPS adsorption to Ceria                  | 80  |
| Table 2.6. IR Assignments for LPS  | 81  |
| Table 2.7. Modified Freundlich Model-Results of LPS adsorption on europium oxide   | 90  |
| Table 2.8. $\Delta G$ calculations for LPS adsorption to europium oxide            | 90  |
| Table 2.9. Results of kinetic analysis of LPS adsorption to europium oxide         | 93  |
| Table 2.10. Freundlich Model-Results of LPS adsorption on thoria                   | 98  |
| Table 2.11. $\Delta G$ calculations for LPS adsorption to thoria                   | 99  |
| Table 2.12. Results of kinetic analysis of LPS adsorption to thoria                | 101 |
| Table 2.13. Modified Freundlich Model-Results of LPS adsorption on thoria          | 106 |
| Table 2.14. $\Delta G$ calculations for LPS adsorption to Urania                   | 107 |
| Table 2.15. Results of kinetic analysis of LPS adsorption to Urania                | 109 |
| Table 3.1. Variation in size of MCA  | 118 |
| Table 3.2. MS – Characterization of the MCAs                                       | 120 |
| Table 3.3. Equilibrium Models  | 126 |
| Table 3.4. MCA solubility tests  | 129 |
| Table 3.5. Equations obtained for the Calibration Curves of MCAs                   | 130 |
| Table 3.6. Mass spectrometry results for MCA quantification compared to literature | 131 |
| Table 3.7. Results of kinetic analysis of MCA adsorption to ceria                  | 137 |
| Table 3.8. Langmuir Isotherm for MCA adsorption on ceria                           | 138 |
| Table 3.9. Freundlich Isotherm for MCA adsorption on ceria                         | 139 |
| Table 3.10. Sips Isotherm for MCA adsorption on ceria (for n=0.4)                  | 140 |
| Table 3.11. Sips Isotherm for MCA adsorption on ceria (for n=0.5)                  | 141 |
| Table 3.12. Sips isotherm fitting for n=0.4  | 142 |

|  |     |
|--|-----|
| Table 3.13. Sips Model-Results of MCA adsorption on europium oxide and ceria (n=0.5)           | 143 |
| Table 3.14. $\Delta G$ calculations for MCA adsorption onto ceria -Freundlich for Sips (n=0.4) | 145 |
| Table 3.15. Results of kinetic analysis of MCA adsorption to europium oxide                    | 151 |
| Table 3.16. Langmuir Isotherm for MCA adsorption on europium oxide                             | 152 |
| Table 3.17. Freundlich Isotherm for MCA adsorption on europium oxide                           | 153 |
| Table 3.18. Sips Isotherm for MCA adsorption on europium oxide (for n=1)                       | 154 |
| Table 3.19. Sips Isotherm for MCA adsorption on europium oxide (for n=0.2)                     | 154 |
| Table 3.20. Sips isotherm fitting for n=0.2  | 155 |
| Table 3.21. $\Delta G$ calculations for MCA adsorption to europium oxide-Freundlich Isotherm   | 156 |
| Table 4.1. Equilibrium Models  | 177 |
| Table 4.2.pKa associated with PGN moieties   | 186 |
| Table 4.3. Results of kinetic analysis of PGN adsorption to ceria                              | 187 |
| Table 4.4. Langmuir Isotherm for PGN adsorption on ceria                                       | 188 |
| Table 4.5. Langmuir Model-Results of PGN adsorption on ceria                                   | 189 |
| Table 4.6. $\Delta G$ for PGN adsorption onto ceria according to Langmuir                      | 190 |
| Table 5.1. Sayle potentials for modelling of ceria slabs                                       | 206 |
| Table 5.2 Energy of adsorption ( $U_{\text{binding}}$ ) of pseudo-mycolic acid onto ceria      | 211 |
| Table 5.4. $\Delta G$ calculations for MCA adsorption onto ceria - Freundlich for Sips (n=0.4) | 216 |

## List of Abbreviations:

**LPS:** Lipopolysaccharides;

**KDO:** 3-deoxy- $\alpha$ -D-mannooctulosonic acid;

**Hep:** Heptulose (ketoheptose);

**NGa:** Galactosamine;

**NGc:** Glucosamine;

**GPC:** Gel Permeation Chromatography;

**MW:** Molecular Weight;

**CMC:** Critical Micelles Concentration;

**XRD:** X-Ray Diffraction;

**PGN:** Peptidoglycan;

**MCA:** Mycolic acid;

**MS:** Mass Spectrometry;

**MD:** Molecular Dynamics;

**ICDD:** International Centre of Diffraction Data;

**ATR-FTIR:** Attenuated Total Reflection-Fourier Transform Infrared Spectroscopy;

**PBS:** Phosphate Buffered Saline;

**HPLC:** High Performance Liquid Chromatography;

**TLC:** Thin Layer Chromatography;

**IR:** Infrared Spectroscopy;

**NMR:** Nuclear Magnetic Resonance;

**LC:** Liquid Chromatography;

**ESI** Electro-Spray Ionization;

**AFM:** Atomic Force Microscopy;

**SEM:** Scanning Electron Microscopy;

**THF:** Tetrahydrofuran;

**IEP:** Isoelectric Point.



## **Thesis Outline**

The first chapter of this thesis starts with the basic background of the project and introduces the hypothesis and objectives of this work. A literature review on what is known on bacterial interactions with nuclear-related materials is then introduced along with a summary of the basic theory of the techniques used during this project. Four chapters that include the practical work then follow. Each one of those four chapters contains an introduction to the tested biomolecule, the methodology used, the results obtained and a discussion on the meaning of the results. Chapter 2 includes the laboratory experiments carried out to examine the interaction of bacterial lipopolysaccharides with four nuclear-related minerals. Chapter 3 includes the laboratory experiments carried out to examine the interaction of bacterial mycolic acids with two nuclear-related minerals. Chapter 4 includes the preliminary results of the work carried out to examine the interaction of bacterial peptidoglycan with two nuclear-related minerals. Chapter 5 includes computational simulations carried out to examine the interaction of bacterial mycolic acid with ceria. A general discussion of the results along with their significance in the context of natural systems and possible applications is found after chapter 5. The thesis is completed with general conclusions and notes on future work.



# Chapter 1

## Introduction

# Background

Micro-organisms found in aquatic and terrestrial sites are able to interact with their surroundings in order to obtain the nutrients needed for their survival but also to protect themselves from toxic matter (Anderson and Lovley, 2002). Certain bacterial species have been discovered close to uranium mines indicating their ability to survive under high levels of radioactivity (Trujillo *et al.*, 2004; Neu *et al.* 2010). Since then, extensive research on the functionalities and metabolisms of these species has been carried out. This ability of microbes is of great interest to the nuclear industry because it could offer essential knowledge for a suitable treatment method for the waste produced during nuclear processes. At the same time, this ability of microbes could be used to mediate the extraction of metals from ores (such as uranium, copper and iron) without the need for human involvement (Ananthi *et al.*, 2012; Tomioka *et al.*, 1992; Markai *et al.*, 2003; Takenaka *et al.*, 2007).

Microbes have been found to affect radionuclides by two major mechanisms: redox transformation or complexation. Redox transformation, which includes the reduction of highly mobile and toxic ions and results in precipitation of biogenic minerals (Renshaw *et al.*, 2007) is particularly interesting. One such example is the reduction of highly mobile uranyl ions (U[VI]) which results in the formation of uranium biominerals (U[IV]) and specifically, urania (UO<sub>2</sub>). A preferred localisation of the biogenic mineral within the cell wall (intracellularly) or at specific positions closely-related to the cell structure (extracellularly) was observed (Lloyd and Renshaw, 2005). This specific localisation of the biominerals results in the hypothesis that:

**'one or more bacterial cell wall components (or components present at the outer boundaries of the bacterial cells) interact with the uranium biomineral (and the other biominerals formed) which results in localisation of the mineral particles inside or close to the cell wall'.**

# Objectives

In order to examine whether the above hypothesis was true, three main objectives were proposed:

1. To examine whether the individual macromolecules present at the bacterial cell wall or associated positions are able to interact with  $\text{UO}_2$  and other chemogenic or biogenic minerals.
2. To calculate the energy associated with the interaction between the biominerals and the bacterial components.
3. To examine whether other radioactive species important to the nuclear industry can interact in a similar manner with the identified biological components. These include  $\text{Eu}^{152}$ ,  $\text{Eu}^{154}$  and  $\text{Eu}^{155}$  (present as the oxide and often found as uranium fission products),  $\text{Th}^{232}$  (present as the oxide and used as the alternative to uranium in nuclear power processes) and  $\text{Ce}^{140}$ , (present as the oxide and usually used as the analogue of radioactive minerals and specifically plutonium and uranium oxides).

# Literature review

## 1.1 Nuclear Materials: Existence and Usage

Natural uranium consists of three isotopes,  $U^{238}$ ,  $U^{234}$  and  $U^{235}$  of which  $U^{238}$  has the highest percentage in natural samples (~99.2%) with  $U^{235}$  being the second most abundant isotope (~0.7%). Uranium is found in the earth's crust mostly in the form of oxides such as  $UO_2$ , known as urania (Weil, 2012; Housecroft and Constable, 2006). Other uranium complexes are also found in nature due to erosion and weathering that result in dissolution of ores and mobilisation of uranyl ions in soil and groundwater repositories (Merroun and Selenska-Pobell, 2008).

Another important nuclear-related element is thorium. Natural thorium is almost exclusively found as the  $Th^{232}$  isotope. A number of other Th isotopes are also known but due to their short half-lives and instability, they are not often identified in natural samples. Thorium is found in the earth's crust mostly in the form of oxides such as  $ThO_2$  known as thoria (Housecroft and Constable, 2006). Thoria is considered as a suitable alternative to urania in nuclear-power processes while an increase in its availability in the environment is observed due to its usage as an alloy for high temperature procedures (Peterson *et al.*, 1965).

Nuclear-related accidents and problems associated with long-term treatment of waste produced during nuclear-power processes have resulted in the release of high amounts of radionuclides in the environment (Kosog *et al.* 2012). Examples of such radionuclides are isotopes of plutonium, Pu, neptunium, Np, americium, Am and europium, Eu produced during the uranium fission cycle (Roeser *et al.*, 2012).

## 1.2 The issue

Radionuclides are unstable and continuously emit particles which are harmful to almost all living organisms. Thus, their increased availability in the environment has resulted in a major need for a removal method. Surprisingly, tests close to mining sites and nuclear-related waste repositories have shown that certain families of bacteria are able to trap radioactive nuclides and remove them from contaminated regions. *Actinomycelates*, *β-Proteobacteria*, *Bacillus* and *Staphylococcus* are only a few examples of bacterial species that have been found to sequester nuclear-related species (Lloyd and Renshaw, 2005; Chicote *et al.*, 2004).

## 1.3 Bacterial interactions with nuclear-related materials

Several articles related to the interactions of bacteria and radioactive species have already been published (Ananthi *et al.*, 2012; Tomioka *et al.*, 1992; Markai *et al.*, 2003; Takenaka *et al.*, 2007). Microbes have been found to affect radionuclides by two major methods: redox transformation or complexation. Each method has been associated with several mechanisms including bacterial accumulation, biosorption, biomineralisation and ligand complexation. Redox transformation which includes the reduction of highly mobile and toxic ions and results in precipitation of biogenic minerals (Renshaw *et al.*, 2007) is particularly interesting. One such example is the reduction of U[VI] ions to U[IV] oxide induced by bacteria under anaerobic conditions which leads to the precipitation and localisation of biogenic urania within the cell wall (intracellularly) or extracellularly, closely-related to the cell structure (figures 1.1 and 1.2) (Lloyd and Renshaw, 2005).

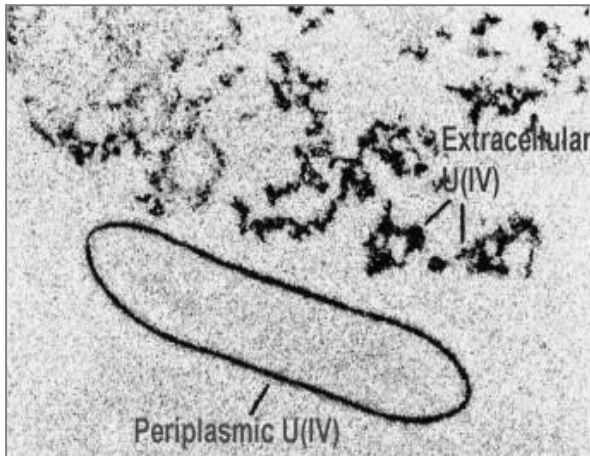


**Figure 1.1.** Urania precipitates on *Shewanella oneidensis* (Burgos *et al.*, 2008)

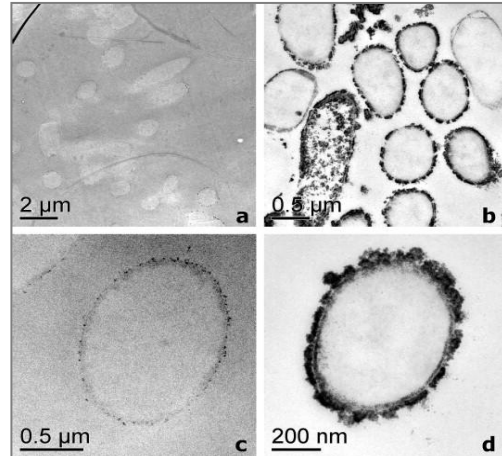


**Figure 1.2.** U [IV] precipitates formed by *G. sulfurreducans* (Lloyd *et al.*, 2002)

In addition to urania precipitation, preliminary tests on europium reduction were reported (Macaskie *et al.* 1994) following studies that demonstrated the precipitation of insoluble europium compounds when growing bacteria were treated with europium ions (figure 1.3- Bayer *et al.*, 1991).

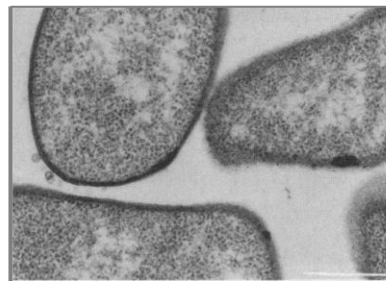


**Figure 1.3.** Europium precipitates on *E.coli* (Bayer *et al.*, 1991)

Reduction and precipitation of complexes related to uranium, thorium and technetium were also reported when Gram negative bacteria were interacted with the respective ions. The resulting biogenic oxides were located at the cell wall of the bacteria (figure 1.4).

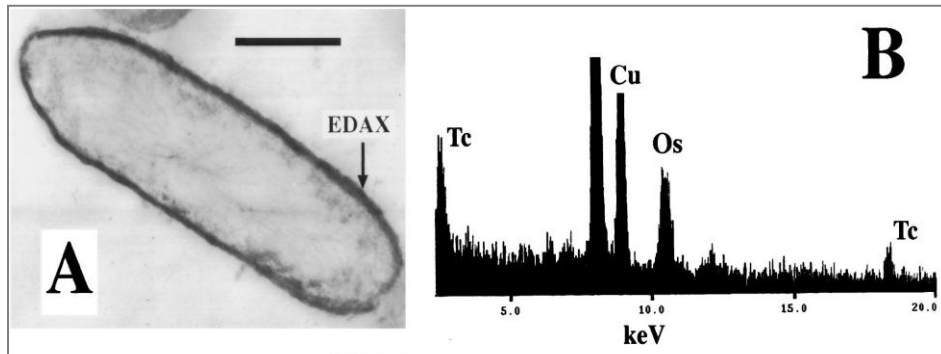


**Figure 1.4. Technetium oxides at the periphery of *G. sulfurreducens* (A). The composition of the precipitate was assessed through EDAX (B) (Lloyd *et al.*, 2000)**

In the given examples and in a significant number of additional cases associated with biomineralisation processes (i.e. the processes involving reduction and biogenic synthesis of minerals) under anaerobic conditions, bacteria were found to retain the biominerals formed inside their own cells and specifically within the bacterial cell wall or closely associated with their external bio-components. This observation resulted in a hypothesis that one or more bacterial macromolecules located at those specific positions were interacting with the produced minerals and were therefore holding them in place. Knowledge on the nature and basic characteristics of the bacterial macromolecules present at the cell wall and the outer boundaries of the bacterial cell was therefore needed in order to test whether the starting hypothesis was correct.

## 1.3.1 Bacterial cell structure

### 1.3.1.1 Gram negative and Gram positive bacteria

Bacteria are divided into two major groups: The Gram negative and the Gram positive. The main difference between these two types is the presence of an additional outer membrane which controls how the Gram negative bacteria interact with their surroundings (figure 1.5) (Murray *et al.*, 2010). The outer membrane of the gram negative bacteria consists of lipopolysaccharides (LPS), phospholipids, a specific protein known as porin, peptidoglycan (PGN) and arabinogalactan. Examples of gram negative bacteria known for their ability to interact with radioactive species are some *Actinobacteria* (Akob *et al.*, 2007).

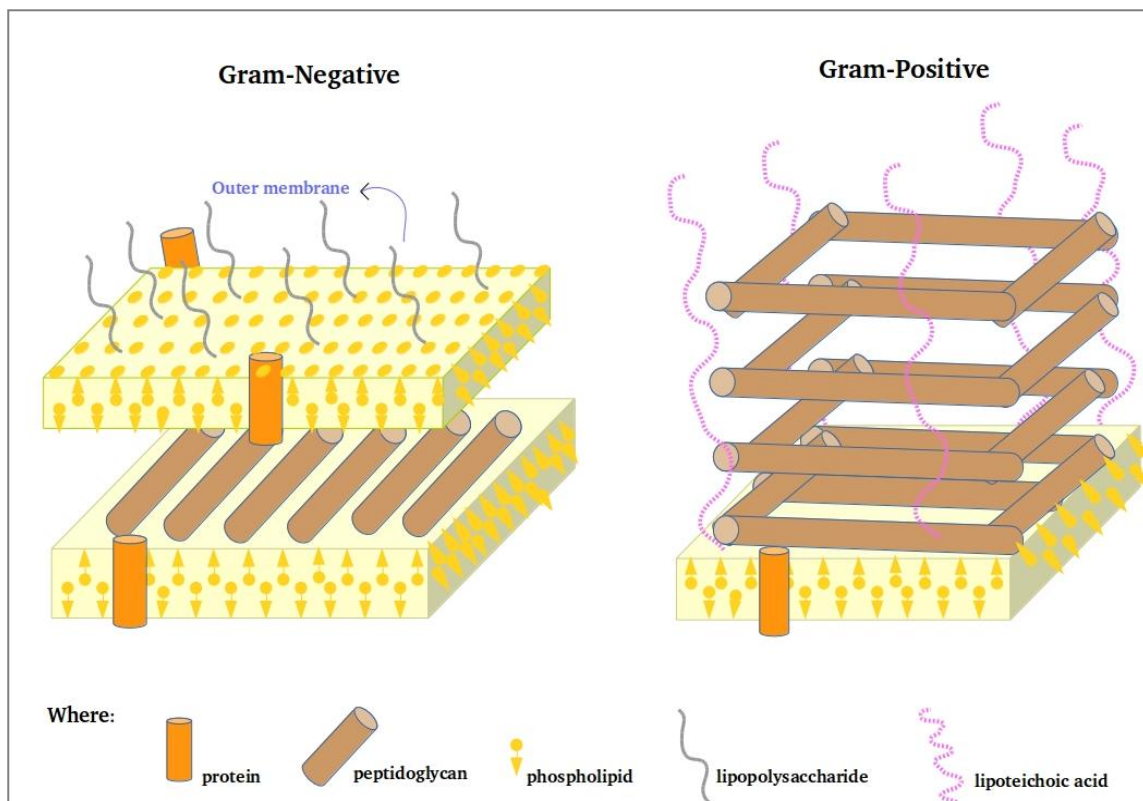


**Figure 1.5. Gram Negative and Gram Positive bacterial cell wall**

Gram positive bacteria do not have an outer protective membrane but have a thick layer of peptidoglycans instead. Lipoproteins and lipoteichoic acids are also found at the outer layer of the

Gram positive bacterial cells. Examples would be some members of the *Proteobacteria* group which were identified for their ability to trap radioactive particles (Akob *et al.*, 2007; Sutcliffe, 1998; Butler and Kilburn, 1988; Davidson *et al.*, 1982; Sihavy *et al.*, 2010; Rieβ *et al.*, 2003).

### 1.3.1.2 The Mycolata family

An exception to these two major groups is the *Mycolata* family. Unlike most of the Gram positive bacteria (that lack a protective membrane), the members of the *Mycolata* family are considered as Gram positive but have an extra cell wall similar to the outer membrane of the Gram negative bacteria. This outer membrane consists of a series of phospholipids and mycolic acids (MCA); arabinogalactan, peptidoglycan and phospholipids come next (figure 1.6).

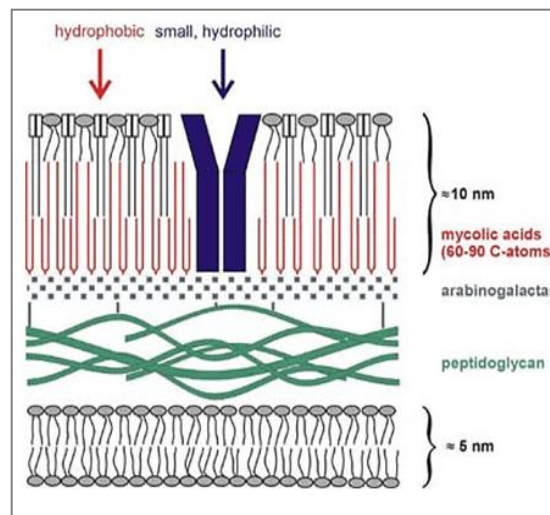


**Figure 1.6. Members of the *Mycolata* family: the ‘Minnikin model’ for *Mycobacterium*. Adapted from Sutcliffe (Brennan and Nikaido, 1995; Hong and Hopfinger, 2004)**

Simulation methods have been used to model and evaluate the basic structure of the *Mycolata*-related cell wall (Hong and Hopfinger, 2004). An example of the simulated cell wall of *Mycobacterium tuberculosis* is shown in figure 1.6.

## **1.4. Interactions of cell wall bio-components with minerals**

### **1.4.1 Lipopolysaccharides**

The sorption capacities of individual bio-components in relation to a number of minerals have already been assessed by different research groups, in an attempt to evaluate the mechanisms bacteria use to interact with their surroundings. Since lipopolysaccharides are the last bio-components of the outer layer of Gram negative bacterial cells, it is assumed that they are the first bacterial components to interact with extracellular species such as approaching particles. Lipopolysaccharides are not only found as components of live bacteria but they are also freely available in natural systems because of cell lysis. Thus, adhesion processes have been examined when free and bound-LPS was left to interact with different minerals (Lu *et al.*, 2011). Adhesion on TiO<sub>2</sub>, SiO<sub>2</sub>, and Al<sub>2</sub>O<sub>3</sub> surfaces was assessed with the biomolecules showing high sorption capacities (Jucker *et al.*, 1997). In addition, ATR-FTIR studies on LPS adsorption on GeO<sub>2</sub>, α-Fe<sub>2</sub>O<sub>3</sub> and Al<sub>2</sub>O<sub>3</sub> have shown that the process is pH and electrolyte dependent. LPS was found to adsorb successfully on the tested minerals while intermolecular interactions were observed when calcium ions were present in solution. The authors proposed that sorption was mediated by functional groups present in the O-antigen region of the molecule (more details in chapter 2) and small differences were reported between the adsorption profile of LPS on hydrophilic or hydrophobic surfaces (Parikh and Chorover, 2008).

## 1.4.2 Peptidoglycans

Studies involving bacterial polysaccharides were performed in an attempt to examine whether sorption is possible between the bacterial compounds and several natural minerals. Bacterial polysaccharides were used to mimic bacterial peptidoglycan which is found in the outer layer of Gram positive species and in a smaller percentage in the inner layer of the Gram negative bacterial cell. Haematite, calcite and aluminium oxide were all affected by the presence of polysaccharides in solution in terms of surface charge and flotation and it was proved that adsorption of polysaccharides on the minerals is pH dependent (Natarajan and Namita, 2001). Peptidoglycan moieties were proposed to show similar sorption profiles to the ones observed for the bacterial polysaccharides due to the structural similarities exhibited by the two bio-components.

Strong adsorption of peptidoglycan onto kaolinite was also reported (Spencer and Kelleher, 2012). Results indicated that complexes resulting from such interactions remained dominant after acid hydrolysis suggesting a very strong sorption product. Furthermore, several studies have examined the adsorption of heavy metal oxides and other toxic ions including  $\text{UO}_2^{2+}$ ,  $\text{Pd}^{2+}$ ,  $\text{Cd}^{2+}$  onto peptidoglycan layers (Barkleit *et al.*, 2009; Johnson *et al.*, 2006). Specific complexation sites were identified including carboxylic sites of glutamic acid and diaminopimelic acid, as well as hydroxyl and amino groups (Barkleit *et al.*, 2009). The identification of mechanisms involving strong complexation initiated by adhesion suggested that bacterial peptidoglycan is a possible candidate for bioremediation processes.

## 1.4.3 Mycolic acids

Mycolic acids (MCA) are components of the *Mycolata* family and are found attached to peptidoglycan via arabinogalactan. Their location suggests that interaction of the bio-components with approaching minerals may be possible. The binding of mycolic acids on hydrophilic and

hydrophobic surfaces was previously reported and two different mechanisms were proposed depending on the extent of hydrophobicity exhibited by the tested surfaces. The dependence of the extent of interaction on the number of available water molecules in solution was also exploited (Zhang *et al.*, 2010). Another study examining macromolecule adhesion onto surfaces involved polyacrylic acid, a polymer that contains carboxylic acid functional groups similar to that of MCA. This study showed a dependence of the adhesion capacity on the pH conditions and the conformation of the molecule (Sparks *et al.*, 2015).

## **1.5. Importance and applications of interactions between bacterial components and nuclear-related minerals**

A review of the current literature suggests that no results on the sorption profiles of bacterial components with nuclear-related minerals have been published. This knowledge is needed in order to obtain an in-depth understanding of the bacterial processes involving nuclear-related species. At the same time, and maybe most importantly, this knowledge is needed in order to establish a generic mechanism that can mediate the binding and thus, collection of reduced radioactive species from contaminated sites. Such methods would be of great interest to the nuclear waste treatment industry as well as the mining of nuclear-related ores.

The current practices involved in nuclear waste treatment include deep geological repositories where spent nuclear fuel (mostly urania and thoria in the form of oxides along with fission products) or products of the nuclear cycle (mostly radioactive elements that cannot be of use) are deposited. The efficiency of these methods is now questioned due to the release of investigations reporting potential contamination of areas in close proximity to the nuclear repositories (Liu *et al.*, 2013; Gomez *et al.*, 2006). These reports showed that migration of radionuclides after dissolution of oxides such as urania or thoria is highly possible. Hence, alternative methods for nuclear-waste treatment are required in order to make sure that the treated materials do not affect the ecosystem and are not hazardous to living organisms.

The use of microbes in order to reduce and immobilise nuclear-waste has already been suggested as a possible alternative to the current practices by several research groups (Johnson, 2014). Microbes can mediate the precipitation of soluble radioactive particles into insoluble minerals that can then be collected, treated and reused in nuclear power plants. Unfortunately, a disadvantage of this approach is the very slow reaction rate and the enormous amounts of biomass needed to treat the continuously increased waste. Another disadvantage is the lack of a technique to recover the immobilised radioactive materials after the bacterially induced reduction, without human involvement (Johnson, 2014). If reduction was induced by other means (e.g. chemical substances), recovery of the reduced minerals could be obtained via polymeric substances similar to the ones present in the bacterial cell wall that have been associated with binding of minerals. Knowledge on the adsorption capacity of such biomolecules is therefore essential. An immediate application of a successful polymer would be the recovery of oxide minerals from nuclear wastes and other contaminated sites.

Another example of an ongoing industrial application is the use of bacteria to extract useful metals from ores, known as '*biomining*'. For example, copper from low-grade ores is now extracted by bacteria using two main processes: bioleaching and biooxidation (Schippers *et al.*, 2014). The first process refers to the bacterially mediated conversion of an insoluble metal into a soluble form for extraction from ores while the second process refers to the bacterially induced change of oxidation states for further processing steps. Copper, gold, uranium, zinc, nickel and cobalt are just a few of the metals where biomining has been used. Unfortunately, the main disadvantage of this approach is the time bacteria need for the completion of the reactions as well as the very small size of the microbes which indicates that a large number of them is needed in order to extract large quantities of the wanted elements from the ores. Thus, if a suitable biopolymer that can bind and capture the wanted metals or oxides was identified, it could potentially find uses at the recovery stage of biomining processes (Johnson, 2014; Rawlings *et al.*, 1997; Siddiqui *et al.*, 2009).

## 1.6 Experimental techniques to evaluate macromolecule-mineral interactions

Several experimental and computational methods can be used to observe and explain the interaction of macromolecules with minerals. To quantify the macromolecules in solution, useful methods include chromatographic or spectrophotometric techniques as well as spectroscopic methods. In this study, suitable spectrophotometric techniques were identified for biopolymer quantification while spectroscopic techniques were used to identify and characterise the functional groups present in the reacted samples. Mass spectrometry was also used for quantification of some biomolecules while computational modelling was used to examine the interaction of biomolecules with minerals at the atomic level.

### 1.6.1 Spectrophotometric Techniques

Spectrophotometric techniques are based on quantification of light absorption when photons interact with matter (e.g. a sample). Light is electromagnetic radiation thus, it is described by the means of energy (E), wavelength ( $\lambda$ ) and frequency ( $\nu$ ). Photons carry electromagnetic radiation and when they interact with matter, they transfer their energy according to equation (1).

$$E = \frac{hc}{\lambda} = h\nu \quad \text{equation (1)}$$

where E is energy, h is Planck's constant, c is the velocity of light,  $\lambda$  is wavelength and  $\nu$  is the frequency.

Energy derived from electromagnetic radiation results in the theoretical construction of an '*absorption spectrum*'. This spectrum basically describes the transition between energy states that an electron exhibits when such a transfer of energy occurs. The more atoms in a molecule, the more complex the absorption spectrum will be due to the increased number of possible transitions. The number of transitions depends on the molecular geometry. Different types of bonds for example (i.e. single, double or triple) offer different kinds of transition states hence, different

absorption spectra can be produced. Biological samples are usually observed at the UV/Vis region of the electromagnetic spectrum due to the presence of 'chromophores' within the molecular structures. These are specific groups that exhibit specific transitions relevant to the UV/Vis region, such as melanin and carotene (Trumbo *et al.* 2013).

When it comes to the physical experiment related to these transition states, a light source (usually a bulb relevant to the region of the electromagnetic spectrum needed, e.g. deuterium bulb for UV) provides the photons which are directed on the sample. A monochromator is placed between the sample and the bulb, to allow for wavelength selection. In colorimetry, coloured filters that absorb all the wavelengths except the ones to be tested are used as monochromators. An example would be a red filter which is transmitting red light and absorbs all other wavelengths. The range of permitted wavelengths is known as the 'bandwidth' of the filter. In spectrophotometry, the wavelengths are selected by a prism, which splits the incoming light by refraction, acting as the monochromator. When the light (i.e. photons) of the selected wavelength hits the sample, energy changes occur. The photons transfer their energy to the sample's electrons causing changes in the transitions states of the electrons and hence, an absorption spectrum is produced. The absorbed light at the given wavelength is calculated by measuring the transmitted beams of light after those are collected by a beam collector and detected (measured) by a detector sited at the end of the process line (Trumbo *et al.* 2013).

The probability of a photon being absorbed by the tested compound is known as the 'absorption coefficient' (or 'extinction coefficient'),  $\epsilon$ . The light of intensity  $I_0$  travels through the tested compound which is usually put in a sample holder (possibly a cuvette) of path length,  $d$ . As the light travels, its intensity decreases exponentially. Thus, a relationship can be extracted between the initial intensity, the path length and the decreasing intensity by naming a constant  $\alpha$  where  $I = I_0 e^{-\alpha d}$ . Also, the ratio  $I/I_0$  is known as the transmission,  $T$ . Biological and chemical samples are usually characterised by a molar concentration,  $c$  which is related to the exponential equation by the Beer-Lambert Law where:

$$\text{Log}\frac{1}{T}=\text{Log}\frac{I_0}{I}=\varepsilon\cdot c\cdot d=A \quad \text{equation (2)}$$

where  $d = \text{cm}$ ,  $c = \text{mol L}^{-1}$ ,  $\varepsilon = \text{L mol}^{-1}\text{cm}^{-1}$  and  $A$  is the sample absorbance as that has been measured by the detector on the spectrophotometer.

Several complexation methods have been employed in order to allow for quantification of biological samples that do not contain chromophores. A series of reagents including anthrone (Somani *et al.*, 1987), phenol (Liu *et al.* 1973) and p-phenylenediamine (Bailey and Rankin, 1971) produce complexes with biological samples based on hydrocarbons that absorb in the visible region of the electromagnetic spectrum. Metal-catalysed interactions have also been used to enable researchers to evaluate bacterial samples through spectrophotometric and colorimetric techniques (Trumbo *et al.* 2013).

## 1.6.2 Spectroscopic techniques-FTIR

Similarly to spectrophotometric techniques, Fourier Transform Infrared (FTIR) relies on the absorption of radiation by a molecule in order to produce a spectrum of peaks that describes its basic vibrational characteristics. As the name suggests, the technique is based on absorption of Infrared radiation. The main difference of FTIR and spectrophotometric techniques is that FTIR uses a beam that contains many light frequencies instead of a single frequency (which is selected via the monochromator in spectrophotometric methods). Hence, the absorption of light at each frequency is measured and then transformed into absorption at each wavelength. The wavelength is recorded as absorption per wavenumber and a spectrum is created either for absorption per wavenumber or transmission percentages per wavenumber. Similarly to spectrophotometric techniques, the absorption of light directly affects the energy states of the electrons and thus, it can be related to the vibration of bonds within a molecule. Hence, FTIR can be used to identify all the functional groups present in the sample via their vibrational modes (Yuji and Sparks, 2001).

In terms of instrumentation, FTIR is equipped with a light source and an '*interferometer*'. The latter consists of a beam-splitter which divides the incoming light into two separate beams. The first beam is directed to a fixed mirror (and thus, reflects back to the beam-splitter) and the second beam is directed to a moving mirror (and thus, has a different path length compared to that directed on the fixed mirror). The two eventually recombine at their origin and an interferogram is created by the difference in path lengths between the two separate beams. The recombined beam is then directed to the sample which absorbs specific wavelengths depending on its functional groups. The wavelengths absorbed by the sample's functional groups are then subtracted from the interferogram and a detector at the end of the process line collects information on the changes in energy for all wavelengths in relation to time. Fourier transform is then used to convert the recorded energy changes (thus, intensity) versus time to intensity versus frequency. The resulting spectrum is then used to identify peaks directly related to the functional groups present in the sample (Smith, 1995).

The attenuated total reflection (ATR) tool is a sampling equipment item that can be used in combination with FTIR instrumentation in order to examine solids and liquids without any sample preparation. ATR relies on a crystal, used as the sample holder, that reflects the incoming light from the source, creating an evanescent wave. The wave is extended into the sample and the light is collected by the detector as it exits the crystal (Yuji and Sparks, 2001).

### **1.6.3 Computational Methods**

Modelling studies of water-solvated biomolecules near an inorganic interface can be used to elucidate the basic characteristics of the system providing necessary information that is not easily accessible with traditional experimental techniques. Two such examples are the exploration of highly radioactive materials that are very difficult to handle experimentally (Boyarchenkov *et al.* 2012) and the exploration of costly biomolecules that are not easily extracted from their origin (Cornell *et al.* 1995). Computational modelling can therefore be used as a tool to explore chemical

and biological interactions, providing information on the associated energies, the configurations each component in a reaction takes as well as the physical properties of the reactants or the products such as distances between atoms, vibration and rotation of bonds, geometry and others (Allen, 2004).

Studies involving computational modelling can be carried out on different time and size scales, from individual atoms to large molecules, nanoseconds to hours (Allen, 2004). Studies at the atomic scale include quantum mechanics and range from Angstroms to nanometre length scales, followed by mesoscale studies that range from nanometre to micron length scales. Bigger length scales are referred to as the '*macroscale level*', with length scales ranging from millimetres to metres and kilometres and usually use the continuum mechanics of classical physics. The adsorption of biomolecules onto different surfaces is often explored in the atomistic to mesoscale range with quantum mechanics and molecular mechanics studies involving several possible techniques including atomistic simulations and coarse grained models as shown in figure 1.7 (Allen, 2004). Examples of such biomolecule-to-surface adsorption processes are discussed in Chapter 5. The following sub-sections include the basic theory and methodology used for molecular dynamics simulations adapted from Leach and Frenkel and Smit (Leach, 2001; Frenkel and Smit, 2002).

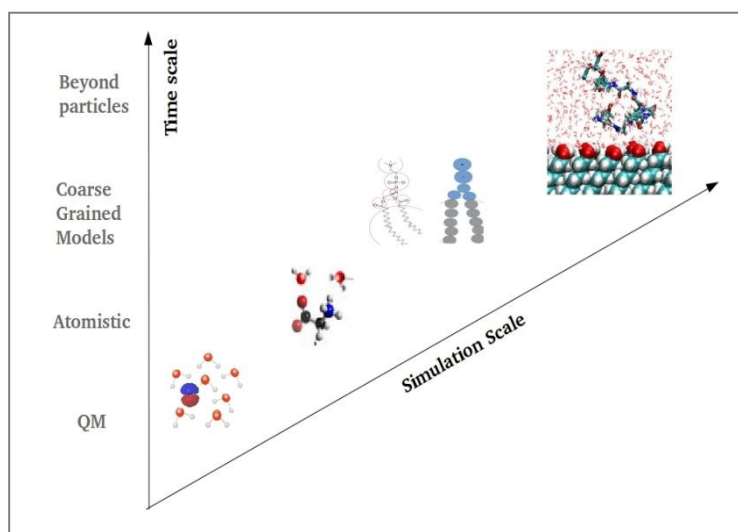


**Figure 1.7** The different levels of microscale/mesoscale computational modelling from nm to mm length scales. The horizontal axis corresponds to time.

### 1.6.3.1 Molecular Dynamics

A widely known tool of computational modelling used for exploration of interactions at the atomic level is Molecular Dynamics (MD). MD is a computer simulation of a system that examines the arrangement of atoms and molecules in space, when those are allowed to interact for a given period of time. The trajectories of atoms and molecules are determined using Newton's equation of motion which relates the force (F) exerted on an atom/particle, its mass (m) and its acceleration (a) as shown in equation (3).

$$F = ma \quad \text{equation (3)}$$

Knowing the force exerted on each atom at a given time (and therefore all the accelerations) yields the trajectory of each particle or atom examined within the system. Given the positions and velocities of the atoms at any given time, they can be calculated at a later time. The forces are given by equation (4) which relates them to the potential energy  $U(r_1, \dots, r_n)$  of the system.

$$F_i = - \frac{\partial U(r_1, r_2, \dots, r_i, \dots, r_n)}{\partial r_i} = ma = m \frac{dv}{dt} \quad \text{equation (4)}$$

Note that the potential energy is a function of all the coordinates so it will change (and therefore the forces will change) as the system evolves. The trajectory must be calculated numerically, the forces are used to calculate the accelerations, the accelerations are in turn used to calculate new atomic positions and velocities and the new positions to calculate new forces and so on. We therefore first need to consider how to calculate the potential energy and then how to perform the calculation of the trajectory.

#### 1.6.3.1.1 Force Field and Potentials

In MD, the potential energy of a system is usually calculated with the help of '*force fields*'. These are sets of parameters and inter-atomic potential functions (equations) that include bonding

(intramolecular) and non-bonding (intermolecular) terms describing the interactions within a system. The bonded terms refer to covalent bonds and are related to the geometry of the bonds between the atoms of a molecule (bond stretching, bending, proper dihedrals, improper dihedrals) while the non-bonded terms refer to the long range electrostatic (Coulomb) and van der Waals forces, hydrogen bonding and  $\pi$ - $\pi$  interactions which are independent of the bond geometry, as shown in equations (5), (6) and (7).

$$U_{\text{total}} = U_{\text{bonded}} + U_{\text{non-bonded}} \quad \text{equation (5)}$$

where  $U_{\text{bonded}} = U_{\text{bond}} + U_{\text{angle}} + U_{\text{dihedral}} \quad \text{equation (6)}$

$$U_{\text{non-bonded}} = U_{\text{electrostatic}} + U_{\text{vdW}} + U_{\text{other}} \quad \text{equation (7)}$$

Some characteristic interatomic potentials often used for the description of these terms are (a) the harmonic potential that describes bond stretching or the Morse potential that describes bonded interactions where the bond can break, (equation (8), figure 1.8) (b) the Lennard-Jones potential for the non-bonded van der Waals term shown in equation (9) and figure 1.9, (c) Coulomb's law for the electrostatic interactions as shown in figure 1.10 and (d) various models of water molecules describing different characteristics of the molecule according to the system it is being introduced in, as shown in table 1.1 and figure 1.11.

$$U_M(r) = D_e [e^{-2a(r-r_e)} - 2e^{-a(r-r_e)}] \quad \text{equation (8)}$$

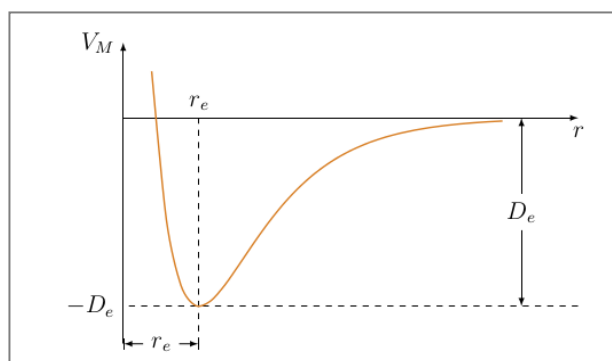


**Figure 1.8.**The Morse potential.  $D_e$  is the depth,  $r_e$  is the equilibrium bond distance and  $a$  is a parameter that controls the width of the well (Bartha *et al.* 2003).

$$U_{LJ} = 4\epsilon \left[ \left( \frac{\sigma}{r} \right)^{12} - \left( \frac{\sigma}{r} \right)^6 \right] = \epsilon \left[ \left( \frac{r_m}{r} \right)^{12} - 2 \left( \frac{r_m}{r} \right)^6 \right] \quad \text{equation (9)}$$

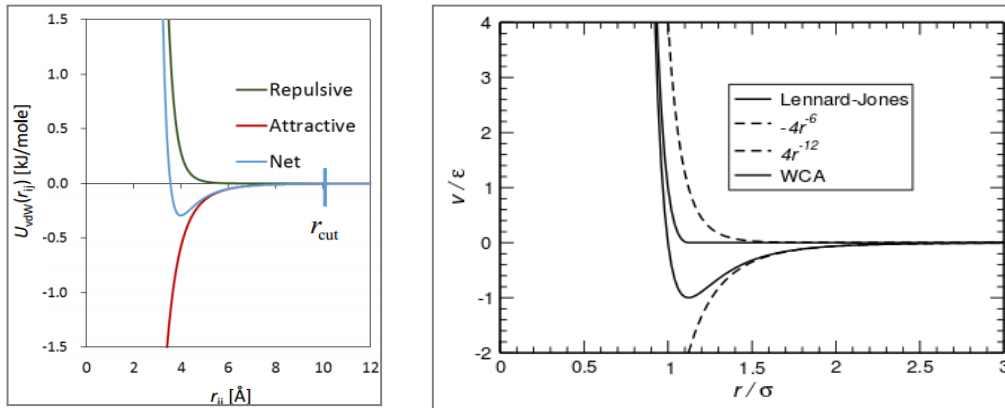


**Figure 1.9.**The Lennard -Jones potential.  $\epsilon$  is the depth,  $r$  is the distance between the particles,  $\sigma$  is the distance at which the potential is zero, WCA is the Weeks Chandler Andersen (a forcefield that is cut off at the minimum and shifted up so that the minimum is on the distance ( $x$ ) axis),  $r_m$  is the distance at minimum potential and  $r_{cut}$  is the potential cut-off distance (Schravendijk, 2007; Allen, 2004).

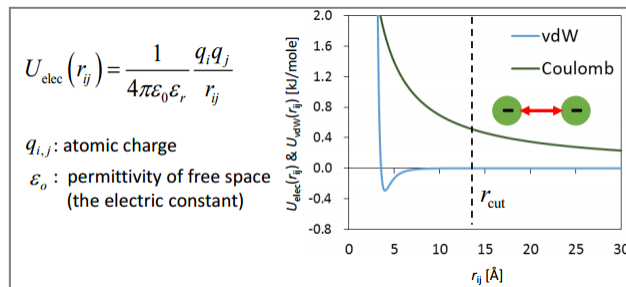


**Figure 1.10.** The Coulomb potential compared to van der Waals (Fujiwara and Fukukawa, 2012).

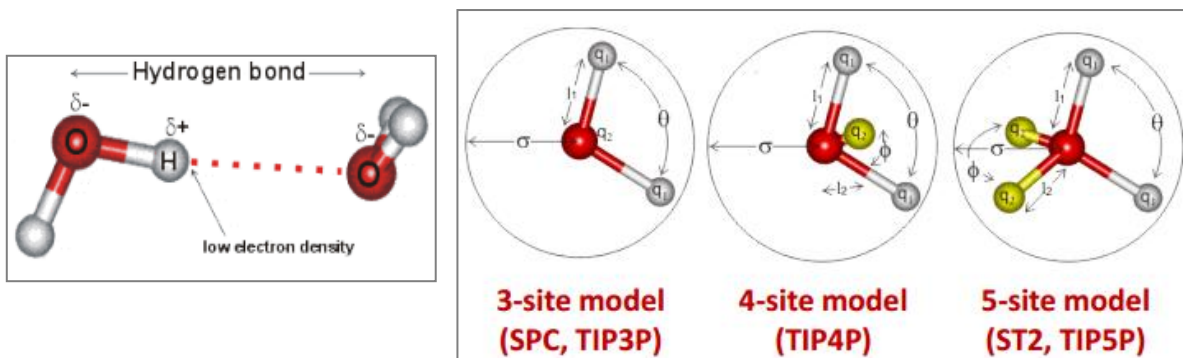


**Figure 1.11.** Hydrogen Bonding (left) and different water molecule models (right-Chaplin, 2016). In MD Hydrogen bonds are usually measured in terms of the distance between two oxygen atoms (from separate water molecules as shown in left image) rather than the distance between a hydrogen and an oxygen atom (from separate water molecules).

The reason for the existence of several models of water is mainly the lack of a 'perfect' model that can be used in all systems (Chaplin, 2016). A recent review on water simulations listed 46 different models of the molecule (Chaplin, 2016). What this really suggests is that the existing models cannot yet reproduce the properties of real water but do however give an insight into its behavior. Some of the most widely used models are shown in table 1.1 where  $I_1$ ,  $I_2$ ,  $q_1$ ,  $q_2$ ,  $\theta$  and  $\varphi$  are shown in figure 1.11 on the individual water molecules and  $\sigma$  &  $\varepsilon$  are Lennard-Jones parameters as shown in figure 1.9 (separation and depth of the potential energy minimum as shown on graph - equivalent to the diameter in the case of water, shown in figure 1.11). It should be noted that the different models, not only differ in simulation parameters, but also have different abilities to predict different physical properties of water (not shown here).

| <b>Model</b> | $\sigma$ | $\varepsilon$ | $I_1$  | $I_2$ | $Q_1$ | $Q_2$   | $\theta$ | $\varphi$ | <b>Max density<br/>Temp. °C</b> |
|--------------|----------|---------------|--------|-------|-------|---------|----------|-----------|---------------------------------|
| <b>TIP3P</b> | 3.151    | 0.636         | 0.9572 | -     | 0.417 | -0.8340 | 104.52   | -         | -91                             |
| <b>TIP4P</b> | 3.153    | 0.648         | 0.9572 | 0.15  | 0.520 | -1.0400 | 104.52   | 52.26     | -25                             |
| <b>TIP5P</b> | 3.120    | 0.669         | 0.9572 | 0.70  | 0.241 | -0.2410 | 104.52   | 109.47    | +4                              |

### **1.6.3.1.2 Types of Force Fields**

Depending on the system to be examined, different force fields can be used. There are three types of force fields: all atom, united atom and coarse grained force fields. As the names suggest, the 'all atom' force field includes parameters for every single atom in the system, 'united atoms' includes parameters for all atoms except non-polar hydrogens and coarse grained includes a representation of molecules after grouping several atoms and creating a less-detailed system as shown in figure 1.12.

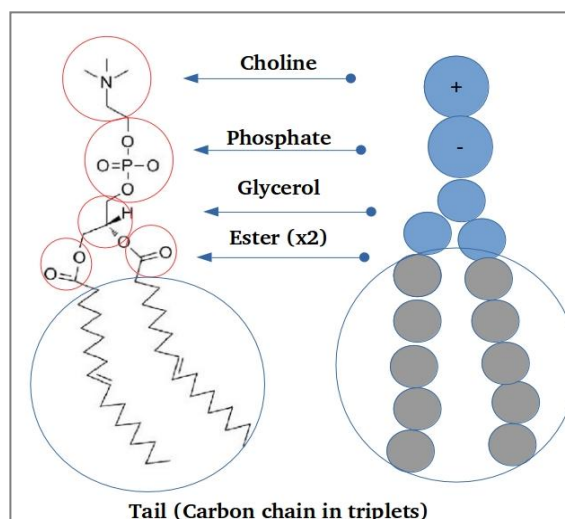


**Figure 1.12.** Example of a coarse grained molecule

The type of force field is not only related to the grouping of atoms involved but also the type of interactions to be simulated. A special family of codes for MD includes AMBER and CHARMM which are used for simulation studies of large molecules such as bio-components (e.g. proteins and lipids) that are often hard to observe with the detail that simulation can provide. Cornell *et al.* described the AMBER forcefield in 1995 defining the energy of the system using the sum of all the bonding terms involved as shown in equation (10) (Cornell *et al.*, 1995).

$$U_{total} = \sum K_r (r - r_{eq})^2 + \sum K_\theta (\theta - \theta_{eq})^2 + \sum \left(\frac{V_n}{2}\right) [1 + \cos(n\phi - \gamma)]$$

$$+ \sum \left(\frac{A_{(ij)}}{R_{(ij)}^{12}} - \frac{B_{(ij)}}{R_{(ij)}^6} + \frac{(q_i)(q_j)}{\epsilon R_{(ij)}}\right)$$

equation (10)

The first term of the equation represents the energy needed to stretch (or compress) the bond from its equilibrium length for all covalently bonded atoms in the system while the second term represents the energy resulting from the angles between the bonds. The third term of the equation represents the energy due to torsions (twisting of bonds) which varies depending on the type of the bond (single, double or triple) and the final term represents the non-bonded energy between atom pairs which was described in previous sub-sections (1.6.3.1.1.).

### 1.6.3.1.3 Calculating the trajectory in Molecular Dynamics

In most MD simulations the potential energy of the system is calculated at each time step according to the force field and integration takes place to calculate the trajectory (and hence the force, position, velocity and acceleration for each atom) as shown previously. For the integration step, several algorithms can be used, with the Verlet algorithm (integrator) being commonly chosen. The Verlet algorithm is a finite difference method obtained from two Taylor expansions about a time  $t$ .

$$r(t + \Delta t) = r(t) + v(t)\Delta t + (1/2)a(t)\Delta t^2 + (1/6)b(t)\Delta t^3 + O(\Delta t^4) \quad \text{equation (11)}$$

$$r(t - \Delta t) = r(t) - v(t)\Delta t + (1/2)a(t)\Delta t^2 - (1/6)b(t)\Delta t^3 + O(\Delta t^4) \quad \text{equation (12)}$$

Equation (11) describes the position  $r(t + \Delta t)$  at time  $t + \Delta t$  with respect to the position  $r(t)$  at time  $t$ . Equation (12) describes the position  $r(t - \Delta t)$  at time  $t - \Delta t$  with respect to the position  $r(t)$  at time  $t$ .  $O(\Delta t^4)$  is the error associated with the truncation of the Taylor expansion. Adding the two equations together results in equation (13) which is the basic form of the Verlet algorithm. This can directly lead to the force as a function of position while the acceleration at time  $t$  can be calculated by dividing the force by the mass and hence results in equation (14).

$$r(t + \Delta t) = 2r(t) - r(t - \Delta t) + a(t)\Delta t^2 + O(\Delta t^4) \quad \text{equation (13)}$$

$$a(t) = -(1/m)\nabla U(r(t)) \quad \text{equation (14)}$$

The velocities of the particles, if necessary, can be determined from the difference in positions at times  $t + \Delta t$  and  $t - \Delta t$  divided by twice the time step ( $v(t) = (r(t + \Delta t) - r(t - \Delta t))/2\Delta t$ ) but a main problem with the Verlet algorithm is that velocities are not generated directly from the integrations and even if they are not always necessary, they might be required on several occasions, especially if knowledge of the kinetic energy of a system is needed. To avoid this, several versions of the Verlet algorithm have been developed including the *leap-frog* algorithm and the *Velocity Verlet* algorithm which is a better implementation of the basic Verlet

scheme that includes velocities with the main algorithm (equations (15) -(18)) and so gives velocities.

$$r(t + \Delta t) = r(t) + v(t)\Delta t + (1/2)a(t)\Delta t^2 \quad \text{equation (15)}$$

$$v(t + \Delta t/2) = v(t) + (1/2)a(t)\Delta t \quad \text{equation (16)}$$

$$a(t + \Delta t) = -(1/m)\nabla U(r(t + \Delta t)) \quad \text{equation (17)}$$

$$v(t + \Delta t) = v(t + \Delta t/2) + (1/2)a(t + \Delta t)\Delta t \quad \text{equation (18)}$$

The leap-frog algorithm involves calculations of velocities at time  $t + \frac{1}{2} \Delta t$  and therefore positions at  $t + \Delta t$  and the velocities at time  $t$  are the average of velocities at  $t + \frac{1}{2} \Delta t$  and  $t - \frac{1}{2} \Delta t$  (not shown here).

#### 1.6.3.1.4 Periodic Boundaries

When running MD simulations, each collection of atoms is being held within the boundaries of an imaginary box. A number of atoms are in contact with the boundaries of the system (or the box), which suggests that these atoms will exhibit different forces than the bulk material and hence, only a few of the tested atoms will actually behave as the bulk material (Leach, 2001). In order to observe the whole system as the bulk material, periodic boundary conditions are introduced where copies of the system are placed around the original system (Allen, 2004) as shown in figure 1.13. This suggests that interactions are not only calculated for atoms in the centre of the box (known as the *unit cell*) but also for atoms in the surrounding boxes. Such systems would be far too great to calculate and hence a cut-off range is usually introduced. This results in fewer calculations that only include the atoms within the set cut-off range but at the same time, interaction calculations are done for the bulk material.

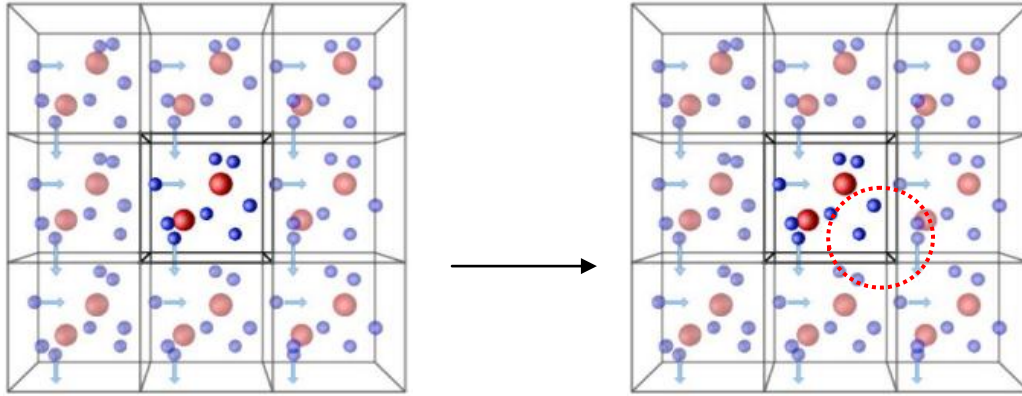


**Figure 1.13.** Periodic boundary conditions used to replicate the system – as a particle moves out of the central/simulation box, a ‘mirror’ particle moves in to replace it. The red circle represents the cut-off range (Leach, 2001).

### 1.6.3.1.5 Ensembles and Ensemble Averages

Depending on the system of interest and the actual simulation, macroscopic terms such as pressure and temperature can be retrieved from the available information at the microscopic level (positions, velocities etc.) If the coordinates of the particles  $q^N$  and their momenta  $p^N$  of the particles within a microstate are known, the Hamiltonian,  $H$ , of the system can be defined. This corresponds to the overall sum of the kinetic and potential contributions resulting from the interactions between the particles. The averages of the microstate quantities are known as the ensemble average,  $f(q^N, p^N; t)$  and it is a probability distribution of the state of the system (or else, the possible microstates of the system) at time  $t$  as shown in equation (19).

$$\iint f(q^N, p^N; t) dq^N dp^N = 1 \quad \text{equation (19)}$$

The ensemble consists of virtual copies of the system of interest, each of which represents a possible state of the real system and it relates the total energy of each micro-state with the different macroscopic terms as shown in figure 1.14. The three most known ensembles are the micro-canonical, the canonical and the isothermal-isobaric ensembles. The micro-canonical

ensemble assumes a constant number of molecules ( $N$ ), constant volume ( $V$ ) and constant energy ( $E$ ). The usage of this ensemble is quite rare due to the constant energy that is required. The density function of the ensemble  $f(q^N, p^N)$  is defined by equation (20) where  $H(q^N, p^N)$  is the Hamiltonian of the system,  $W(N, V, E)$  is the sum of all accessible states and hence, equation (21) can be extracted (Leach, 2001).

$$f(q^N, p^N) = \frac{1}{W(N, V, E)} \delta[(H(q^N, p^N) - E)] \quad \text{equation (20)}$$

$$W(N, V, E) = \iint \delta[H(q^N, p^N) - E] dq^N dp^N \quad \text{equation (21)}$$

A canonical ensemble represents the mechanical system where temperature ( $T$ ), number of particles ( $N$ ) in the system and the system's volume ( $V$ ) are fixed (constant) and is also known as the 'NVT' ensemble. This is one of the most commonly used ensembles due to the close correlation with experimental systems and at the same time, low computational costs. The probability density of the canonical ensemble is shown in equation (22) where  $\beta$  is the inverse product of the Boltzmann factor  $k_B$ . Equation (23) can therefore be extracted.

$$f(q^N, p^N) = \frac{1}{W(N, V, T)} \exp(-\beta H(q^N, p^N)) \quad \text{equation (22)}$$

$$W(N, V, T) = \iint \exp(-\beta H(q^N, p^N)) dp^N dq^N \quad \text{equation (23)}$$

An isothermal-isobaric ensemble refers to the systems where temperature, pressure ( $P$ ) and number of particles are constant. The probability density of this ensemble is shown in equations (24) and (25).

$$f(q^N, p^N) = \frac{1}{W(N, P, T)} \exp(-\beta[H(q^N, p^N) + PV]) \quad \text{equation (24)}$$

$$W(N, P, T) = \int_0^\infty \exp(-\beta PV) W(N, V, T) dV \quad \text{equation (25)}$$

The last two ensembles assume the system exchanges energy with the surroundings (usually a heatbath) so the total energy of each microstate differs (figure 1.14).

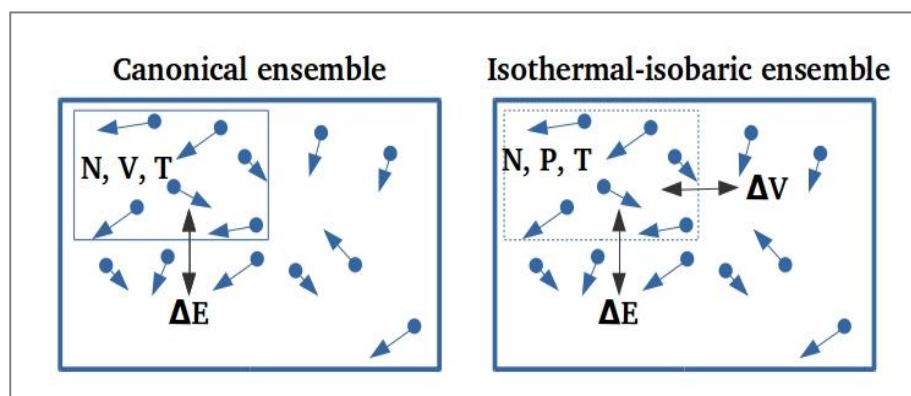


**Figure 1.14. The canonical and isothermal ensembles**

In order to comply with the ensemble conditions and make sure temperature (or pressure depending on the ensemble) is always constant, a thermostat and a barostat have to be introduced to the simulation parameters. There is a range of available thermostats and barostats that can be used, including the Nose-Hoover thermostat, the Langevin thermostat, the MTK barostat or the Berendsen thermostat. The Berendsen thermostat is known for its inaccuracy to generate correct canonical ensembles for small systems but it is quite efficient for systems that include large amounts of molecules/particles (Frenkel and Smit, 2002). According to the thermostat, the temperature of the system is corrected so that the temperature difference exponentially decays with time constant  $\tau$  (shown in equation (26) where  $T_0$  is the temperature the system should be maintained constant at).

$$\frac{dT}{dt} = \frac{T_0 - T}{\tau} \quad \text{equation (26)}$$

### 1.6.3.1.6 Practical Aspects of a Molecular Dynamics Simulation

In order to run a molecular dynamics simulation one should (a) Input the initial conditions (positions of all atoms and system variables including temperature, time steps cut-off etc.), (b) Compute Forces (calculate molecular interactions and external forces), (c) Update configuration

(solve Newton's equation of motion and simulate the movement of atoms, (d) Compute the scaling factors, (e) Update the positions and (f) Check results (updated positions, energies etc.) as shown in figure 1.15.

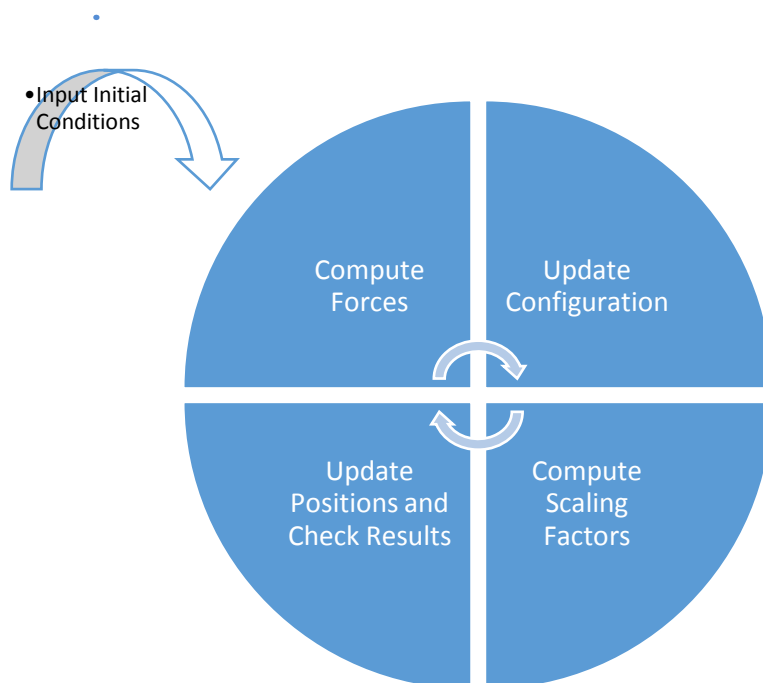


**Figure 1.15. Flow Chart of a molecular dynamics simulation**

In this study, the above steps are done using DL\_POLY, a general purpose molecular dynamics simulation software which was developed by I. T Todorov and W. Smith at Daresbury Laboratory, UK (Smith *et al.*, 2010). In order to perform a MD simulation, 3 main input files are needed: the CONFIG file which consists of all the starting positions of the atoms, the FIELD file which contains all the force field parameters (the molecular interactions and potentials) and the CONTROL file that contains all the system parameters such as pressure, temperature, thermostat, ensemble, time steps and others.

The above experimental and computational techniques have been used to explore the type (e.g. physisorption, chemisorptions etc.) and strength of interaction (i.e.  $\Delta G$  values, binding energy etc.) between nuclear-related materials and specific bacterial cell-wall components. The

chosen biomolecules were lipopolysaccharides (LPS), mycolic acids (MCA) and peptidoglycans (PGN) all found within the bacterial cell wall of Gram negative or Gram positive bacteria. Zeta potential analysis, adsorption experiments, spectrophotometric techniques and ATR-FTIR were the experimental techniques used to explore the interaction of the individual minerals (ceria, urania, thoria and europium oxide) with the three molecules (one at a time) while Molecular Dynamics simulations were performed to examine the interaction of ceria with MCA at the atomic level. The combination of these experimental and computational methods provided the confidence that the results presented here can be used as evidences to explain the observed localisation of minerals within the bacterial cell walls and could therefore be used to enable a more efficient bioremediation of nuclear waste.

# **Chapter 2**

## **Lipopolysaccharide Interactions with Nuclear Related Minerals**

## 2.1 Introduction

The findings of sorption of lipopolysaccharide (LPS) to nuclear related materials are presented in Chapter 2. LPS was previously found to play a role in bacterial interactions with surfaces. More specifically, minerals synthesised during biomineralisation were found to stay located close to LPS strains (Lloyd *et al.*, 2002; Burgos *et al.*, 2008).

LPS is a component of the outer membrane of Gram negative bacteria. Since it is not found in Gram positive bacteria, LPS is an ideal candidate for the identification of any differences in the adsorption mechanisms used by Gram negative and Gram positive bacteria.

LPS is located in the outer layer of the membrane of Gram negative bacteria and is exposed on the cell surface, in long fibrous-like strains. More than 90% of the cell surface is covered with LPS molecules, which suggests that LPS is possibly the first bacterial component that comes into contact with external molecules and therefore, the first component that interacts with the surfaces of interest, the nuclear minerals (Rosenfeld and Shai, 2006).

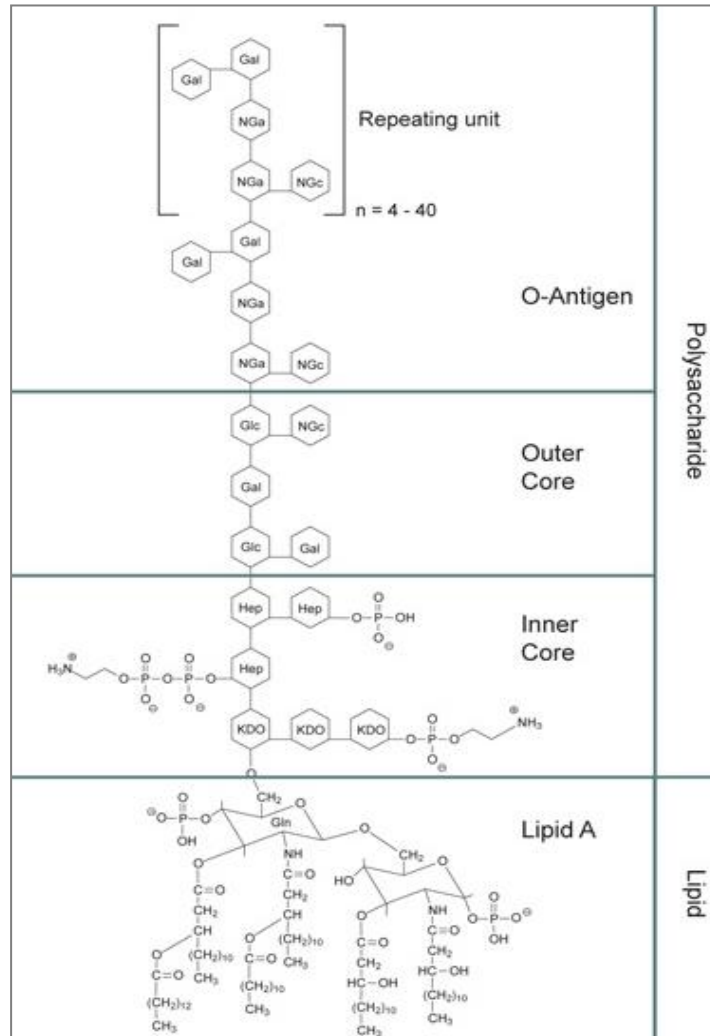


**Figure 2.1. General structure for bacterial LPS. (Clifton *et al.* 2013)**

The basic structure of LPS consists of 3 major groups: a lipid section, a hydrophilic polysaccharide chain and a hydrophilic O-antigenic oligosaccharide chain. LPS from different families and usually from different strains within the same family have small differences which explain the variation of the molecular mass that ranges from 100 to 500kDa (Clifton *et al.*, 2013; Jucker *et al.* 1998; Marchetti *et al.*, 2013).

The lipid A core consists of a  $\beta$ -glucosamine-(1,2,3,4,5,6)-glucosamine-1-phosphate base with fatty acid esters attached to both carbohydrate ends, connecting it to the rest of the cell wall. The inner polysaccharide core contains between 1 to 4 molecules of 3-deoxy- $\alpha$ -D-mannooctulosonic acid (KDO), depending on the bacterial species. KDO is specifically associated with

LPS and its quantification. A few assays have already been reported identifying the terminal vicinal glycol group present in the KDO component of LPS as the key component for spectrophotometric techniques (Karkhanis *et al.*, 1978; Osborn *et al.*, 1972). The inner core also consists of a heptulose monosaccharide, typically L-glycero- $\alpha$ -D-manno-heptopyranose. The inner core glycan residues are usually found to be phosphorylated which is one of the reasons why LPS has an overall negative charge. This helps stabilize the overall structure and plays a key role in the interaction of bacterial cells with external molecules and especially ions.

The outer core of LPS contains a combination of hexoses, including galactose, glucose and N-acetylglucosamine, the frequency in appearance of which depends mainly on the bacterial species and the strains examined (Clifton *et al.*, 2013; Jucker *et al.* 1998; Marchetti *et al.*, 2013).

The O-antigen region of the LPS macromolecule usually consists of repeated units of two to six sugars. The O-antigen is the main region tested for differentiation between different families of bacteria as there are some distinctive O-antigen structures associated with individual groups including *Escherichia coli*, *Salmonella enterica*, *Vibrio cholerae* and many more (Strauss *et al.*, 2009). It is usually the most reactive site of the molecule, especially in adhesion as it is the only exposed region and controls the interaction with approaching molecules, including surfaces (Strauss *et al.*, 2009).

An overall negative charge exhibited by the molecule at varying pH conditions (pH>3) is associated with moieties present in all the different regions of the molecule such as phosphate groups (Rosenfeld and Shai, 2006).

## **2.1.1 Functions of LPS**

It is believed that the main role of LPS is to protect bacteria from external threats. For example, lipophilic antibiotics are not efficient when used against LPS-containing bacteria because the biomolecule can detect and destroy them (Aurell and Wistrom, 1998).

Research has been carried out to explore the LPS structure fully, its association with bacterial metabolism, its relation to possible toxicity of different bacterial species and its biosynthesis. Because of its connection to different diseases, LPS has been studied to identify possible inhibitors to LPS biosynthesis (Rietschel *et al.*, 1994). Therefore, a number of assays have been developed for LPS quantification, one of which relies on UV absorbance by purple 'adducts', products of LPS oxidation. This is known as the Purpald assay and was first described by Lee and Tsai in 1999 (Lee and Tai, 1999). The assay is based on the oxidation of the terminal vicinal glycol groups found in the KDO regions of LPS molecules by periodate which results in the production of formaldehyde (figure 2.2). Formaldehyde is then reacted with the Purpald reagent and the purple Purpald adduct created is finally quantified by measuring its absorption at 550nm. The Purpald assay has been used for the detection of different types of LPS as each bacterial strain of LPS consists of different numbers of terminal vicinal glycols (Lee and Tsai, 1999).

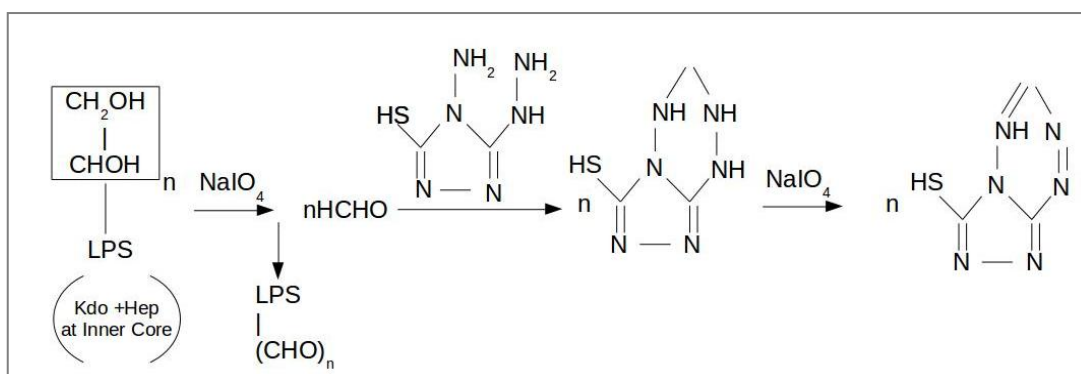


**Figure 2.2. Reaction mechanism of the Purpald Assay (Adapted from Lee and Tsai, 1999)**

### 2.1.1.1 Interactions of LPS with surfaces

In a system where LPS is approaching a surface, a series of different interactions are possible depending on the different conformations of the molecule, which are directly related to the pH conditions, as well as the ions in solution. Adhesion processes have been observed when free and bound-LPS was left to interact with different surfaces (Lu *et al.*, 2011). In the case of bound-

LPS, these processes are driven by functional groups present at the O-antigen region of the molecule. So far, no results regarding the chemical composition of the O-antigen region responsible for adhesion processes have been obtained. However, interactions of sugars are generally mediated by hydrogen bonds (Strauss *et al.*, 2009). Therefore, hydrogen bonds could be possible candidates for a controlled system where only bound-LPS is included in the interaction and only the O-antigen region is exposed for interaction.

In addition, tests on isolated O-antigens for adhesion on SiO<sub>2</sub> and Al<sub>2</sub>O<sub>3</sub> resulted in high dependence of the process on hydrogen bonding (Jucker *et al.*, 1997). Another study on adhesion forces of O-antigens from different strains approaching SiO<sub>2</sub> resulted in significant variations of the measured adhesion forces. This was attributed to the different chemical compositions of the O-antigens even though no information was available on the exact chemical bonding of the mentioned systems (Strauss *et al.*, 2008). An additional study on LPS adhesion onto different surfaces showed that electrostatic interaction and steric effects were the major contributors to the interaction while the presence of long O-antigen chains was associated with reduced bacterial adhesion. This again is a case of bound-LPS where an energetic barrier to the process was suggested and a hypothesis proposed by the authors is that the affinity of hydrophilic neutral O-antigen chains to water is responsible for the observed reduction in bacterial adhesion to minerals. These studies suggest that several different scenarios can arise depending on (a) the length of the LPS chain (and specifically the length of the O-antigen region when bound-LPS is of concern), (b) the chemical composition of the LPS and (c) the experimental conditions such as water quantity and pH (Lu *et al.*, 2011).

## 2.1.2 Objectives

The aim of this work was to examine the interaction of LPS with nuclear related materials at varying pH conditions and in the presence of different counter ions in order to examine whether a universal rule can be drawn for the adhesion of LPS onto minerals. The mineral chosen for this part of the project were: (a) ceria, (b) europium oxide, (c) thoria, and (d) urania. The sorption of LPS onto the minerals was examined using experimental techniques solely.

## **2.2 Materials and Methods**

### **2.2.1 Chemicals**

All chemicals were purchased from Sigma-Aldrich (UK) and were of analytical grade unless stated otherwise. Double distilled water was used for all the experiments. The experiments were conducted at least in triplicate and the values reported here are average values of at least 3 results. Variation in these results is given as standard deviation and standard error values.

### **2.2.2 Macromolecules**

Lipopolysaccharides (from *Escherichia coli*0111: B4), purified by gel-filtration chromatography were purchased from Sigma-Aldrich and used as received. Stock solutions of LPS

dissolved in water, NaCl or CaCl<sub>2</sub> were prepared before any analysis. These were prepared above the *critical micelle concentration* (CMC) of the *E. Coli* LPS strain 0111: B4 which is 0.022 mgml<sup>-1</sup> of water (Aurell and Wistrom, 1998) and the pH was adjusted to 3, 7 or 10 with 0.01M HCl or 0.01M NaOH. All stock solutions were vortexed, sonicated for 10 min, and stored overnight at 4 °C before re-equilibration the following day at room temperature.

### **2.2.2.1 Molecular Weight Determination of LPS**

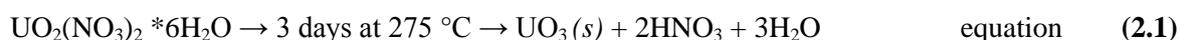
The molecular weight of each LPS batch purchased was analysed by Gel Permeation Chromatography (GPC). A Hewlett-Packard 1090A GPC was used with pure water as the eluent and a series of polyethylene oxide (PEO) and polyethylene glycol (PEG) standards with molecular weights ranging from 106 to 1552000 to calibrate the GPC columns. 1-2 mg of LPS were diluted in pure water and filtered through a 0.45 µm polytetrafluoroethylene (PTFE) syringe filter before injection. The results were analysed with the Agilent GPC/SEC Software.

### **2.2.3 Minerals**

Four different minerals were used in this study: thoria ThO<sub>2</sub>, urania UO<sub>2</sub>, europium oxide Eu<sub>2</sub>O<sub>3</sub> and ceria CeO<sub>2</sub>. Eu<sub>2</sub>O<sub>3</sub>, ThO<sub>2</sub> and CeO<sub>2</sub> were purchased from Sigma-Aldrich (UK) and UO<sub>2</sub> was prepared by hydrogen induced reduction of studtite (details in sub-section 2.2.3.1). X-ray Diffraction (XRD) analysis was carried out for characterisation of the materials which were compared to known PDF cards from the literature.

### 2.2.3.1 Synthesis of UO<sub>2</sub>

Synthetic UO<sub>2</sub> was prepared by reduction of studtite at 400° Celsius for 4 hours in an in-house made stainless steel reactor in the presence of hydrogen gas. The reactor design and build is covered in the next section. Studtite was precipitated after several steps of treatment of uranyl nitrate. The uranyl nitrate was heated for 3 days at 275 °C and the resulting UO<sub>3</sub> was then dissolved in 0.5 M HCl (trace meta grade, Fisher Scientific). Aliquots of 88mM H<sub>2</sub>O<sub>2</sub> were then added to 2.5mM UO<sub>2</sub>Cl<sub>2</sub> and after a three-day reaction a yellow precipitate settled out (UO<sub>2</sub>O<sub>2</sub>\*4H<sub>2</sub>O(s)). The solid was dialysed against double distilled, oxygen-free water, dried and finally reduced in a stainless steel reactor at 400° Celsius in the presence of pure hydrogen gas (zero grade, BOC UK). The product was tested with X-ray Diffraction and the resulting pattern was compared to reference PDF cards. The chemical equations are given in equations (2.1)-(2.4).



#### 2.2.3.1.1 Stainless Steel Reactor Design

An in-house built reactor was required to complete the urania synthesis. The main body of the reactor consists of a block of stainless steel with a void chamber on the inside where the solid is placed. The centre of this unit is connected with cartridge heaters that provide heat and an electronic device that controls the temperature. The two end-sides of the stainless steel hold an inlet and an outlet pipe for hydrogen gas circulation (figure 2.3).

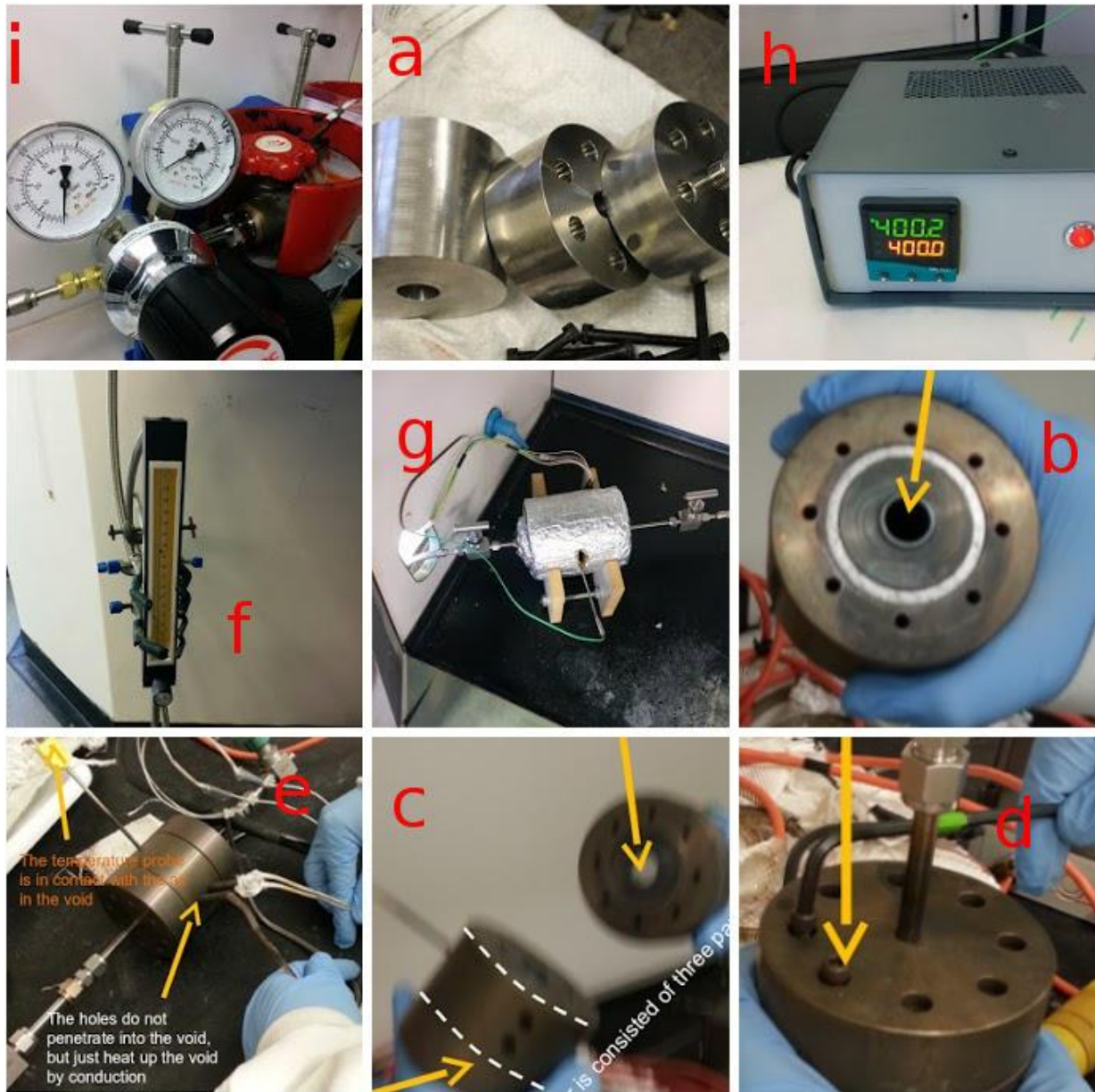


Figure 2.3. The stainless steel reactor used for  $\text{UO}_2$  synthesis. It consists of a block cylinder 10 cm x 8 cm (length: diameter).[a] Inside there is a void chamber of cylindrical shape (6 cm x 2 cm; length: diameter) while the two sides hold an inlet and an outlet pipe for the  $\text{H}_2$  gas.[g] Ceramic filters are placed at both ends of the void chamber to ensure no loss of powder during the reaction.[c] The main body of the reactor consists of 3 pieces, screwed together after filling in the void with the reactants.[d] There is a hole for a temperature probe that does not penetrate the void chamber and 2 more for the cartridge heaters facing each other. [e] The whole block is wrapped with insulating material and an electronic device controlling the temperature is connected. [g+h] The inlet of the  $\text{H}_2$  gas is connected to a gas cylinder with an appropriate gas regulator and a flow meter. [i] (Dr K. Ulrich 2012 pers. comm.)

### 2.2.3.1.2 X-ray Diffraction Analysis

The product of the  $\text{UO}_2(\text{NO}_3)_2$  reduction was tested and compared against the  $\text{UO}_2$  template (PDF card) from the International Centre of Diffraction Data (ICDD). The analysis was run on the fully automated X'Pert<sup>3</sup> Powder by PANalytical on reflection mode for 15 minutes. Details on the instrumental parameters can be found in appendix 1.

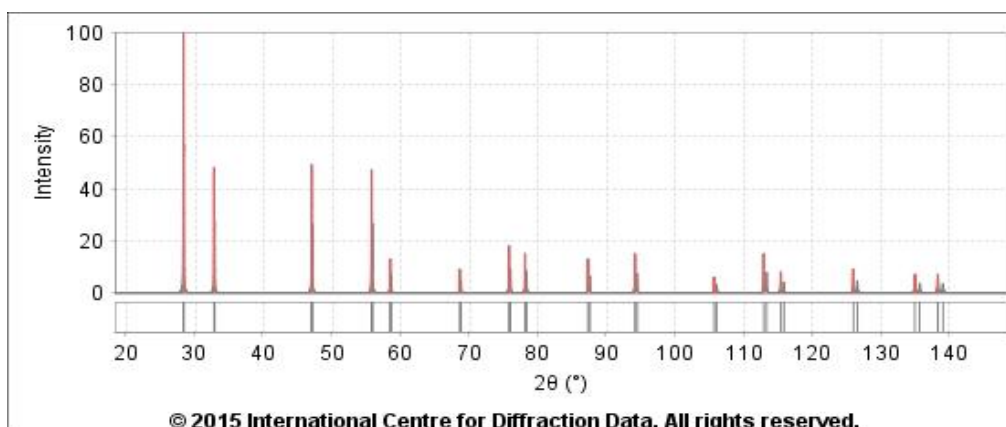


Figure 2.4. Example of a  $\text{UO}_2$  PDF card by ICDD

### 2.2.3.1.3 Experimental conditions

The measured diffusion of oxygen in  $\text{UO}_2$  (Chen *et al.*, 2010; Fayek *et al.*, 2012; Skomurski *et al.*, 2007), the proposed dissolution of uranium ores under oxic conditions (Gomez *et al.*, 2006) along with the high solubility rates of urania directly related to the acidity of the environment (Merroun and Selenska-Pobell, 2008; Boyanov *et al.*, 2011) suggested that anaerobic conditions for all experiments involving  $\text{UO}_2$  were needed. In order to achieve the minimum oxygen interference with  $\text{UO}_2$  a COY anaerobic chamber was used and the oxygen/hydrogen content was monitored with an oxygen analyser. All chemicals and solvents used for the interactions between  $\text{UO}_2$  and macromolecules were first treated with nitrogen gas and were held under vacuum to remove all dissolved gases including oxygen. The oxygen content of the anaerobic chamber was 0 ppm at all times while the hydrogen content ranged from 2 to 4 %.

### 2.2.3.2 Ceria, Europium oxide, Thoria

The rest of the mineral surfaces, thoria, europium oxide and ceria were used as purchased from Sigma-Aldrich. All three minerals were analysed using the X'Pert<sup>3</sup> Powder by PANalytical on reflection mode for 15 minutes to compare with existing templates (PDF cards) available from the International Centre of Diffraction Data.

### 2.2.4 Adsorption Experiments

An experiment was designed to examine the adsorption of LPS on different minerals (thoria, urania, europium oxide and ceria) at different pH conditions and different electrolytes (ionic strength) including CaCl<sub>2</sub>, NaCl and H<sub>2</sub>O. Sample portions of  $3 \pm 0.5$ mg of minerals were weighted and transferred into 2.5ml Eppendorf tubes. To the samples, 250  $\mu$ L of 0.01M NaCl solution, 0.01M CaCl<sub>2</sub> solution or pure H<sub>2</sub>O were added and the pH was adjusted to 3, 7 or 10 with 0.01M NaOH or 0.01M HCl. The contents of the tubes were mixed and left stirring for 24 hours at 22 °C to equilibrate. The pH was tested again and adjusted accordingly and 50 $\mu$ L of the stock macromolecule solution was then added to the equilibrated tubes. The tubes were mixed and then centrifuged at 5000g for 10 minutes. Samples were taken at specific times (10 min, 30 min, 1h, 2h, 24h) for identification of the kinetics of the interaction (constant concentration, temperature, pressure and pH, changing times).

A second experiment examined the adsorption capacity at varying LPS concentrations for the construction of experimental isotherms (set time 200 min, pressure, temperature and pH, changing concentration of macromolecule). The stock solutions of LPS used for the isotherms were 1 mg ml<sup>-1</sup>, 2 mg ml<sup>-1</sup>, 3 mg ml<sup>-1</sup>, 4 mg ml<sup>-1</sup> and 0.5 mg ml<sup>-1</sup> (always higher than the '*critical micelle concentration*' (CMC) which is 0.022 mg ml<sup>-1</sup> LPS in water (Aurell and Wistrom, 1998)). The amount of macromolecule adsorbed was calculated by equation (2.5).

$$Q = \frac{(C_o - C_e)V}{m} \quad \text{equation (2.5)}$$

where Q = amount of LPS adsorbed on mineral ( $\text{mg g}^{-1}$ ),  $C_o$ = initial concentration of LPS in solution ( $\text{mg L}^{-1}$ ),  $C_e$ = final concentration of LPS in solution ( $\text{mg L}^{-1}$ ), m=mass of mineral used (g) and V= volume (L).

### 2.2.4.1 Isotherm Models

In order to describe the isotherms, the *Langmuir* and the *Freundlich* models were used. The Langmuir model is based on the assumptions that: (a) a fixed number of adsorption sites (or 'vacant' sites) is available on the surface of the mineral, (b) all the vacant sites are of equal size (c) each site can hold maximum of one molecule of the adsorbent and (d) adsorption is a monolayer. These assumptions are ideal for the description of gas adsorption onto solid surfaces. In systems of liquid to solid adsorption, the use of such a model becomes challenging due to hydration forces and mass transport, effects that result in a more complicated situation. The Freundlich isotherm is empirical and while the Langmuir model works on the basis that only a monolayer of the approaching molecule will end up on the surface, the Freundlich isotherm does not have this 'restriction' and is preferred when 'stacking' of adsorbed molecules onto the surface is observed or when sorption occurs to sites of different characteristics. Table 2.1 shows the equations as derived from the models.

| <b>ID</b>           | <b>Equation (linear form)</b>  | <b>Y</b>                          | <b>X</b>   | <b>Intercept</b>     | <b>Slope</b>           |
|---------------------|--|-----------------------------------|------------|----------------------|------------------------|
| Langmuir            | $\frac{C_e}{Q_e} = \frac{1}{Q_m} \cdot C_e + \frac{1}{(K_l)Q_m}$                             | $\frac{C_e}{Q_e}$                 | $C_e$      | $\frac{1}{(Q_m)K_l}$ | $\frac{1}{Q_m}$        |
| Freundlich          | $\ln(Q_e) = \ln(K_f) + \frac{1}{n_f} \cdot \ln(C_e)$   | $\ln(Q_e)$                        | $\ln(C_e)$ | $\ln(K_f)$           | $\frac{1}{n_f}$        |
| Modified Freundlich | $\ln\left(\frac{Q_e}{C_e}\right) = \ln(K_{MF}) + \left(\frac{1}{n_{MF}} - 1\right) \ln(C_e)$ | $\ln\left(\frac{Q_e}{C_e}\right)$ | $\ln(C_e)$ | $\ln K_{MF}$         | $\frac{1}{n_{MF}} - 1$ |

Where  $C_e$ =LPS concentration at equilibrium ( $\text{mg L}^{-1}$ ),  $Q_e$ =equilibrium adsorption capacity ( $\text{mg g}^{-1}$ ),  $K_l$ = Langmuir adsorption constant ( $\text{L/mg}$ ),  $Q_m$ =maximum adsorption capacity ( $\text{mg g}^{-1}$ ),  $K_f$ = Freundlich constant ( $\text{L/g}$ ),  $n_f$  = heterogeneity factor of adsorption sites,  $K_{MF}$ =modified Freundlich constant ( $\text{L/g}$ ),  $n_{MF}$ =modified heterogeneity factor of adsorption sites. Adapted from Bhatt *et al.*, 2012.

### 2.2.4.2 Quantification of LPS using the Purpald Assay

The Purpald assay was used as described by Lee and Tsai (1999). Briefly, 50  $\mu\text{L}$  of 32 mM  $\text{NaIO}_4$  were interacted with 50  $\mu\text{L}$  of a sample containing LPS for 25 minutes. Addition of 50  $\mu\text{L}$  of 136 mM purpald reagent (in 2N NaOH) followed and the solution was incubated at 30  $^\circ\text{C}$  for 20 minutes. After the incubation, 50  $\mu\text{L}$  of 64 mM  $\text{NaIO}_4$  was added and the solution was left to interact for another 20 minutes. The absorbance was then measured and the expected peak at 550 nm was observed (Lee and Tsai, 1999). This method required the development of a calibration curve with standard solutions of known LPS concentrations. That was constructed according to the Beer-Lambert Law where absorbance ( $A$ ) is directly related to the analyte concentration and is equal to the absorptivity coefficient ( $\epsilon$ ) multiplied by the analyte concentration ( $C$ ) and the path length ( $l$ ) (equation (2.6)).

$$A = \epsilon \cdot C \cdot l \quad \text{equation (2.6)}$$

The Purpald assay was performed in transparent 96-well plates (Fisher Scientific) and a

Biotek Plate Reader. The data were analysed for absorbance using the Gen5 and Microsoft Excel software. All reagents were made fresh daily and kept wrapped in foil because of their sensitivity to sunlight.

## **2.2.5 Zeta Potential Analysis**

Information on the surface charge of LPS and minerals was obtained by measuring the zeta potential using a Zeta Potential Analyzer (ZetaPALS by Brookhaven Instruments Corporation). The zeta potential was also measured to confirm the adsorption of macromolecules onto the minerals. Suspensions of  $0.25 \text{ mg L}^{-1}$  minerals in 0.01M  $\text{CaCl}_2$ , 0.01M NaCl solution or  $\text{H}_2\text{O}$  and at different pH conditions (3, 7 or 10 adjusted with 0.01M NaOH and 0.01M HCl) were prepared and left to equilibrate for 24 hours before zeta potential measurements. Approximately 1 ml of the cell suspension was transferred to a glass cuvette and the zeta potential was obtained from the average of 10 measurements, presented at a 95% confidence level. The same procedure was followed after the addition of  $25 \mu\text{L}$  of  $1 \text{ mg ml}^{-1}$  LPS stock solutions at the corresponding pH conditions and after 24 hours of equilibration.

## **2.2.6 Attenuated Total Reflection-Fourier Transform Infrared Spectroscopy (ATR-FTIR)**

The various functional groups of LPS were characterised using ATR-FTIR before and after the interaction of the macromolecules with the mineral surfaces. Sample portions of  $3 \pm 0.5 \text{ mg}$  of minerals were transferred into 2.5 ml Eppendorf tubes. To the tubes,  $250 \mu\text{L}$  of 0.01M NaCl solution, 0.01M  $\text{CaCl}_2$  solution or  $\text{H}_2\text{O}$  were then added and the pH was adjusted to 3, 7 or 10 with 0.01M NaOH or 0.01M HCl. The contents of the tubes were mixed and left on the shaker for 24 hours at room temperature to equilibrate. The pH was then tested and adjusted and  $50 \mu\text{L}$  of  $4 \text{ mg}$

ml<sup>-1</sup> macromolecule solution was added to the equilibrated suspensions. The tubes were left to interact for a given time (chosen according to the sorption profiles obtained for each mineral) and were centrifuged at 5000rpm for 10 minutes. The supernatant was discarded and the sample left was freeze dried for 24 hours. ATR-FTIR spectra were collected from 400-4000 cm<sup>-1</sup>, with a resolution of 4 cm<sup>-1</sup>. Background spectra of the different electrolytes, LPS stock and the mineral surfaces with no macromolecules (controls) were also collected.

## 2.2.7 Electron Microscopy

Representative samples of the interactions of LPS with ceria and europium oxide were analysed. The measurements were performed at the Centro de Instrumentacion Cientifica, Universidad de Granada, Spain. Two representative samples were selected from the ceria-LPS and europium oxide-LPS systems. The samples at pH 7 were considered the best samples to analyse since most interactions in the natural environment will occur around neutral pH.

Samples were prepared for Transmission Electron Microscopy (TEM) as described previously (Merroun *et al.*, 2005). The samples were analysed using a Phillips CM 20 high-resolution TEM. A High-Angle Annular Dark Field-Scanning Transmission Electron Microscope (HAADF-STEM), equipped with an Energy-dispersive X-ray (EDX) analyser (200 kV acceleration voltage) was also used for the examination of elemental maps of cerium and carbon within LPS-treated ceria particles. Similarly, elemental maps of europium and carbon were prepared for the europium oxide-LPS samples.

## **2.3 Results and Discussion**

### **2.3.1 Determination of LPS Molecular Weight**

Each batch of LPS was analysed with GPC to determine the molecular weight of the macromolecule. An example distribution plot with the associated molecular weight averages obtained from the GPC analysis is given in figure 2.5.

The results were different from the ones reported by the provider (Sigma-Aldrich). According to the manufacturer, the commercial bacterial LPSs are of molecular mass 10-20 kDa which is much lower than what GPC characterisation results showed. The results indicated a molecular weight of approximately 400 kDa which is an order of magnitude higher than expected. For verification, the analysis was repeated using different solvents to test if there was an effect on the weight determination. When phosphate buffered saline (PBS) was used, the resulting molecular weight was even higher. That was attributed to the fact that LPS tends to form aggregates of

varying sizes when cations are present which would have an immediate effect on the determination of the molecular weight using GPC. GPC determinations rely on separation of molecular fractions by size as the polymer molecules travel through the column, hence, the larger the fraction, the higher the mass associated with it. Therefore, LPS aggregates formed due to intermolecular binding of cations will produce higher molecular weights.

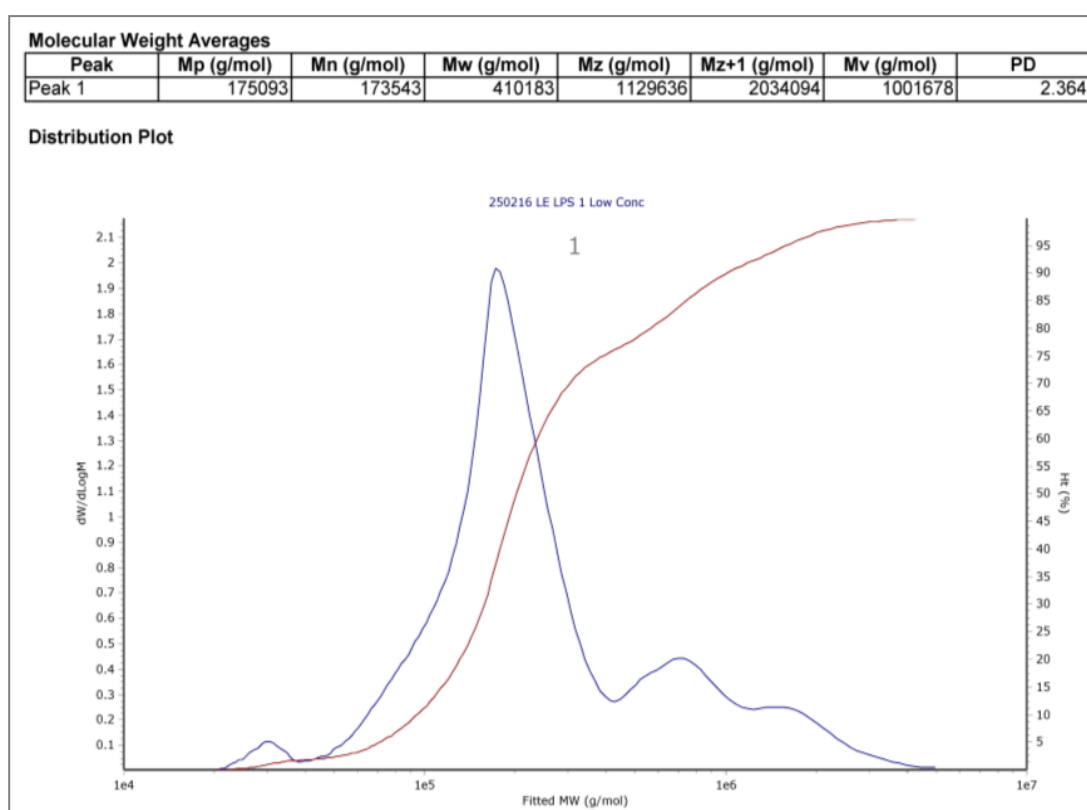


**Figure 2.5. Molecular Weight of LPS by GPC analysis**

A reported range of 1-4 million Da from different literature sources (Rietschel *et al.*, 1994; Jann, Reske and Jann, 1975) suggests that the resulting molecular weight of LPS is dependent on several parameters. These include the presence or absence of cations in solution, the solvent used, the method used and the presence or absence of surface agents. It has been previously suggested that to determine the molecular weight of LPS in its purest form, strong active surface agents and complete absence of divalent cations are needed. Deviating from these conditions would result in a

micelle arrangement with molecular weight of approximately 1000kDa (Aurell and Wistrom, 1998).

In order to avoid the formation of any clusters/micelles, a concentration of less than 14  $\mu\text{g/mL}$  of LPS in double distilled water was chosen (Santos *et al.*, 2003). This concentration was chosen for safety even though the critical micelle concentration of the specific strain that was used in this project is 22  $\mu\text{g/mL}$  (Aurell and Wistrom, 1998). This suggests that no micelles were formed and that GPC analysis provided the most accurate number for the molecular weight of LPS. Since the results were repeatable and micelles were avoided, the resulting molecular weight of LPS was found to be 410183 g/mol.

## **2.3.2 Characterization of minerals**

### **2.3.2.1 Urania Synthesis**

The results of the XRD analysis of synthetic  $\text{UO}_2$  prepared by reduction of studtite confirmed that the product was pure urania. Clear sharp peaks for urania were obtained at  $2\Theta = 28^\circ, 33^\circ, 47^\circ, 56^\circ, 58^\circ, 69^\circ, 76^\circ, 78^\circ$  representing the (111), (200), (220), (311), (222), (400), (331) and (422) phases respectively. The resulting peaks agreed with previously published data on synthetic urania as well as chemogenic urania (Sanjay *et al.*, 2016).

As discussed by Kumar *et al.*, (2010) most cases of synthetic urania reveal  $\text{UO}_3$  or other  $\text{UO}_x$  phases, which are usually present due to incomplete reduction of the starting materials into pure urania. However, the reaction conducted here reached completion, since all urania peaks obtained by XRD are sharp, indicating the presence of the fluorite structure and no extra peaks were observed (figure 2.6).

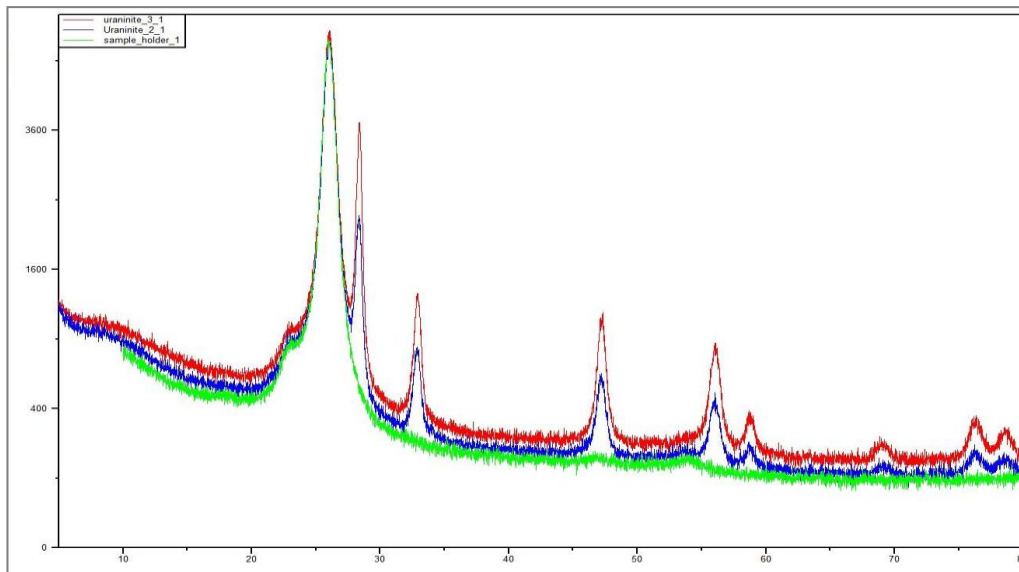


**Figure 2.6.** XRD results for synthesised  $\text{UO}_2$  (blue) compared with given PDF card (red- PDF Card: 00-005-0550). The green peak is the result of the sample holder used. X axis =  $2\theta$ , Y axis = Intensity (counts).

### 2.3.2.2 Characterization of Ceria and Europium oxide

Europium oxide and ceria were characterised using the X'Pert<sup>3</sup> Powder by PANalytical on reflection mode for 15 minutes to compare with existing templates available from the International Centre of Diffraction Data (ICDD). An example of the results is shown in figure 2.7. Both the europium oxide and ceria samples resulted in the expected peaks indicating that the minerals used were of the purest forms with no other phases interfering in the interactions. As shown in figure 2.7, the resulting peaks from the XRD analysis were compared with previously published data and were found to be identical. No extra peaks were observed indicating no contamination. The size of the particles was assessed using AFM and was found to be 50-100 nm for europium oxide and <50 nm for ceria.

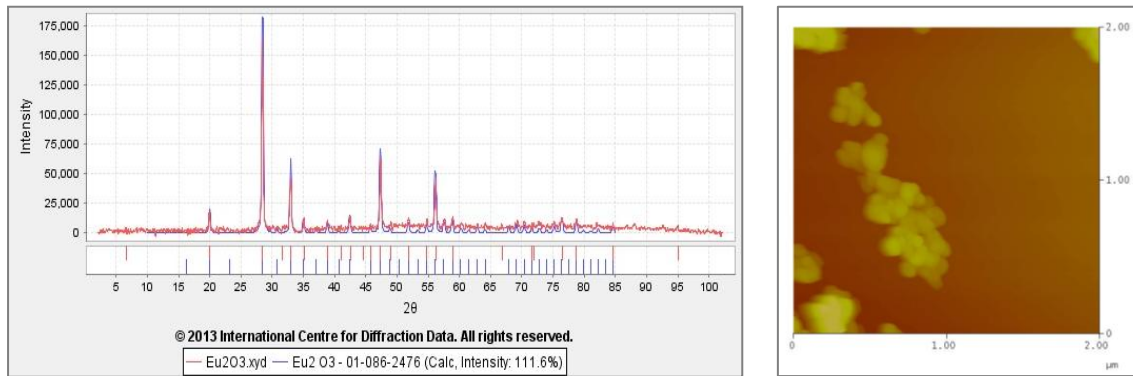


**Figure 2.7. Eu<sub>2</sub>O<sub>3</sub> characterization with XRD (left) and AFM (right) [PDF: 01-086-2476]**

## 2.3.3 Adsorption of LPS on Ceria

### 2.3.3.1 Zeta Potential of LPS – Ceria interactions

Surface charge is a key component describing the behavior of microorganisms. Therefore, the behavior of their bio-components such as LPS can be used to access important information regarding cell interactions (Tofail, 2012). The observed charge is a result of an increase in net charge at the particle surface. This affects the distribution of ions in the close surrounding region which results in the formation of a double layer as shown in figure 2.8. The double layer was firstly introduced by Helmholtz in 1850 who described the existence of two layers, the inner layer known as the '*Stern layer*' which consists of the surface and the closely related ions and one outer layer that consists of ions less affected by the surface. The surface charge of particles is usually examined with zeta potential measurements and electrophoretic mobility (Tofail, 2012).

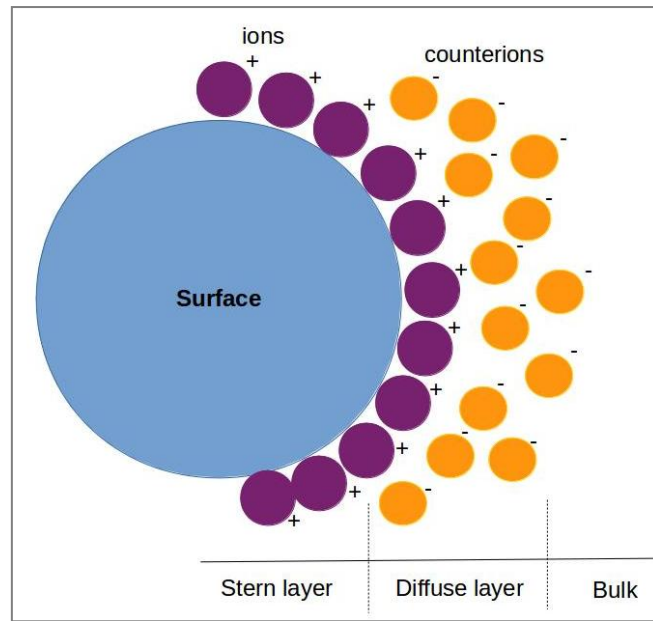


**Figure 2.8. The structure of the electric double layer**

Figure 2.9 shows the results of zeta potential of ceria before and after the interaction with LPS at different electrolytes and pH conditions. Control LPS showed a negative potential at neutral pH conditions. This result agreed with previously published work on zeta potential of LPS that proposed a low point charge of bacterial cells in close-to-neutral environments like natural water (Jiang *et al.*, 2013). The same was shown for *P. fluorescens* biofilms, the zeta potential of which is primarily controlled by LPS (Takenaka *et al.*, 2007).

Slightly positive zeta-potential is expected for acidic solutions due to the added protons found in the samples which are directly related to zeta potential measurements (Yukselen-Aksoy and Kaya, 2011). Hence, control LPS at pH3 is slightly positive (~10mV - figure 2.9). Similarly, ceria controls at acidic conditions resulted in positive zeta potential for all three different electrolytes while neutral and basic conditions resulted in negative zeta potential measurements for all blank samples (ceria controls).

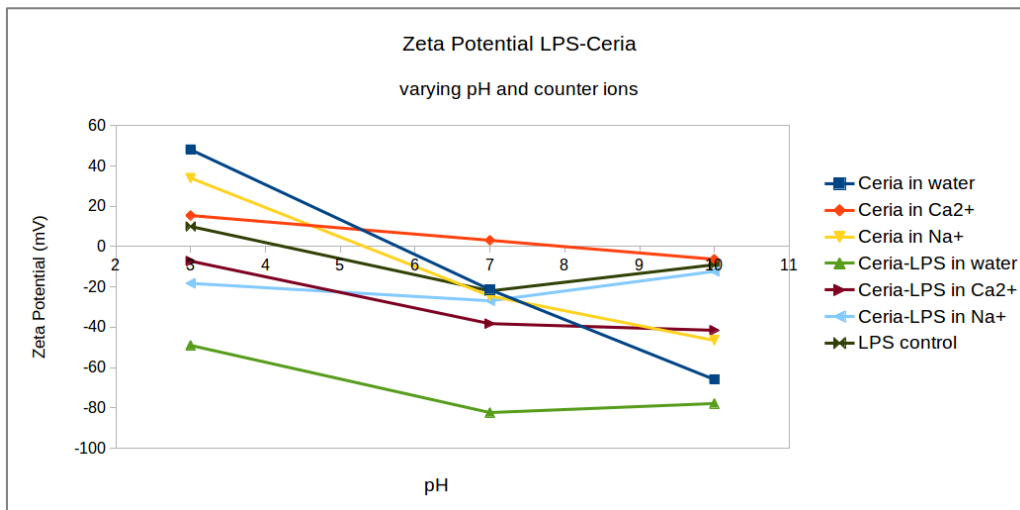


**Figure 2.9.** Zeta potential of LPS and Ceria before and after the interaction at different electrolytes and pH conditions. Y axes is zeta potential (mV) and x axes is pH. Data at a 95% confidence level.

When the macromolecule is interacted with the mineral (indicated as 'Ceria-LPS' in figure 2.9), a change in zeta potential is observed. The zeta potential of LPS-Ceria at acidic conditions in the presence of water, CaCl<sub>2</sub> and NaCl was ~-50, ~-10 and ~-20 mV respectively. The zeta potential of the control ceria sample at pH3 was always higher than 0 mV. This change from positive to negative zeta potential when the macromolecule is added in the system indicates that a large change at the surface charge of the mineral was observed, likely to be due to an adsorption process. Similarly, the zeta potential of LPS-Ceria at neutral conditions in the presence of water, CaCl<sub>2</sub> and NaCl was ~-80, ~-40 and ~-20 mV respectively. The zeta potential of the control ceria sample at pH7 was always higher than the measured value for the Ceria-LPS systems. Lastly, the zeta potential of LPS-Ceria at basic conditions in the presence of water, CaCl<sub>2</sub> and NaCl was ~-75, ~-40 and ~-15 mV respectively. The respective zeta potential measured for the ceria control samples was always higher than the respective Ceria-LPS samples (with the exception of NaCl containing samples where the value of zeta potential was reversed), again indicating the change in surface charge and hence the adsorption process that took place on the surface of ceria. In general, it was observed that in all acidic Ceria-LPS samples, the zeta potential was reversed compared to

the starting zeta potential (without the added macromolecule) while the neutral and basic systems showed a decrease in the measured zeta-potential values when the macromolecule was added to the system. These results agreed with the observed reduction in zeta potential with increasing hydrophobicity of hydrocarbon adsorption onto *Staphylococcus aureus* (Wilson *et al.*, 2001) and suggested that an adsorption process has taken place.

### 2.3.3.2 Quantification of LPS - Calibration Curve

Experimental LPS uptake kinetics onto ceria were calculated using the Purpald assay (subsection 2.2.4.2) for quantification of LPS before and after the interaction with the minerals. A calibration curve was constructed showing the relationship of absorbance,  $A$ , with LPS concentration,  $C$ , as derived from the Beer-Lambert Law (equation (2.6)). Since  $\epsilon$  and  $l$  are constant in the given example (all experiments were carried out in 96-well plates and  $\epsilon$  is constant for a given substance), the absorbance is directly related to the concentration of LPS and hence, a linear graph was obtained (figure 2.10).

In most cases of studies involving quantification a single calibration curve is used for all different conditions to evaluate the effect each condition has on a given system. In the case of LPS quantification a single calibration was not possible due to interference from the presence of cations which was evident from the high error bars obtained. To avoid interference, calibration curves that matched the matrix of experimental conditions were constructed (different calibration curves reflecting the inclusion of different electrolytes and pH conditions). The reason behind the observed differences between the calibration curves was that the different conformations LPS adapted at different pH conditions had an effect on the efficiency of the Purpald assay. It has been previously shown that the presence of positive ions such as protons,  $\text{Ca}^{2+}$  and  $\text{Na}^{+}$  has a direct effect on the conformation of LPS (Parikh and Chorover, 2007). That is due to bridging by cations that increases intermolecular binding and thus, affects the availability of LPS moieties. A matrix match approach was taken to calibration where the linear relationship was verified for each pH value

studied. LPS standards with identical conditions to the experiment were used to ensure that the LPS-cation interactions were included when accounting for the concentration of LPS in solution. An example of the  $\text{Ca}^{2+}$ - related calibration curves can be found in figure 2.10. All the different calibration curves can be found in appendix 2.

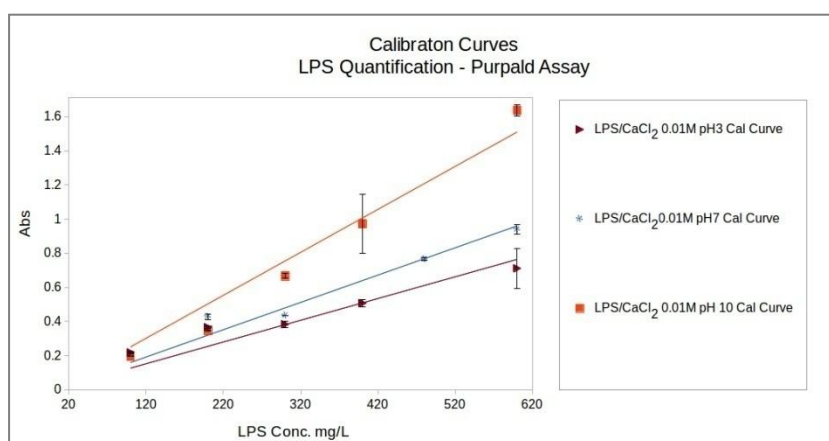


**Figure 2.10. Calibration curves for the Purpald Assay**

The differences observed when comparing the calibration curves confirm the hypothesis that suggested different conformations of LPS under different conditions that affect the availability of the LPS moieties. As can be seen from figure 2.10 and appendix 2, all calibration curves constructed for pH10 showed higher light absorption compared to the pH3 and pH7 curves. It is also observed that the inclusion of  $\text{Ca}^{2+}$  under acidic condition (pH3) showed the lowest absorption with the highest LPS concentration resulting in less than one third of the absorption observed when  $\text{Ca}^{2+}$  were present under basic conditions (pH10). Furthermore, the water and NaCl solutions showed similar behavior under acidic and neutral conditions which further supports the literature that suggested only small differences between the conformation of LPS when  $\text{Na}^+$  or protons are present (Parikh and Chorover, 2007). In general, the calibration curves fit well with previously published work suggesting conformational changes of the LPS molecules according to pH conditions and inclusion or not of ions in solution.

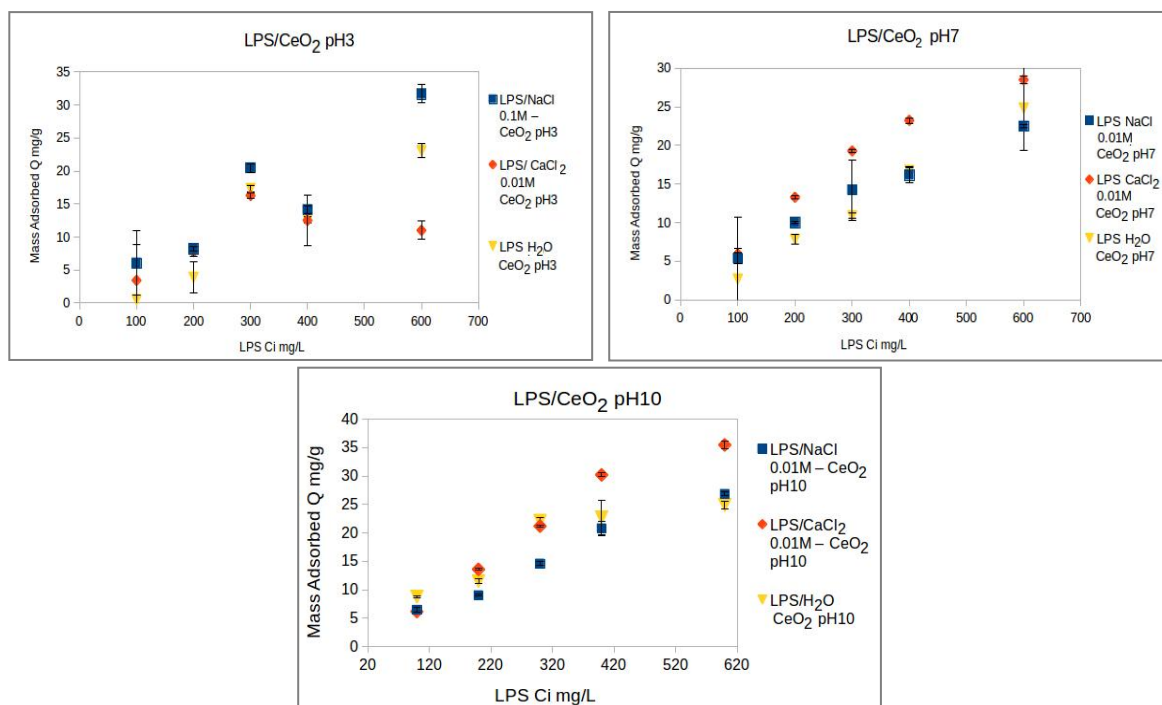
### 2.3.3.3 Experimental Isotherms for sorption of LPS onto Ceria

The Purpald Assay was used to quantify LPS before and after its interaction with ceria. Ceria (cerium oxide,  $\text{CeO}_2$ ) is a cubic fluorite-type oxide similar to  $\text{UO}_2$ . The structural similarities with thorium and uranium, as well as americium oxides usually found in nuclear waste, render ceria as a suitable analogue of the mentioned minerals when surface interactions are considered (Watkinson *et al.*, 2015). According to Kosmulsko (2002) and Nolan and Watson (2006), the pH of point of zero charge of ceria ranges from 6.4 - 8.6 (table 2.2) which suggests that the mineral exhibits a positive charge below pH 6.4 and a negative charge above pH 8.6. By examining systems of pH3, pH7 and pH10 all different scenarios with ceria being negatively charged, positively charged and close-to-neutral are accessed. Assuming a sorption process is dominated by attraction of molecules of opposite charge, the results of experiments covered a range of positive to negative binding to negative to slightly negative binding.

| <b>Mineral</b>                            | <b>pH</b> |
|---|-----------|
| <b><math>\text{Al}_2\text{O}_3</math></b> | 9.8       |
| <b><math>\text{CeO}_2</math></b>          | 6.4-8.6   |
| <b><math>\text{CuO}</math></b>            | 7.5-9.4   |
| <b><math>\text{Fe}_2\text{O}_3</math></b> | 7.3-9.5   |
| <b><math>\text{TiO}_2</math></b>          | 5.9-7.5   |

The LPS concentration used for all the cases was higher than the CMC; this was intended to represent the cell-bound form of LPS with the assumption that only the O-antigen region of the molecule is exposed for interaction with the minerals (more information in sub-section 2.1.1.1). In environmental samples, both the cell-bound and free LPS can be found in solution but in free-LPS, the lipid A moiety of the molecule is exposed which promotes strong intermolecular interactions

(Parikh and Chorover, 2008); this potentially results in no interactions with any external molecules, e.g. the nuclear-related surfaces.



Figures 2.11 – 2.13. Isotherm of LPS-Ceria interactions at pH3 (left –figure 2.11), pH7 (right- figure 2.12) and pH10 (middle-figure 2.13).

The isotherm constructed for the ceria-LPS interaction at pH3 is shown in figure 2.11. The mass adsorbed is represented by ' $Q$ ' ( $\text{mg g}^{-1}$ ). None of the sodium or calcium-containing experiments resulted in a clear adsorption profile in contrast with the water (reflecting the proton-mediated interaction) which resulted in an isotherm that reached a plateau. Calcium chloride was the electrolyte with the lowest mass of LPS adsorbed through the whole concentration range. NaCl and water seemed to behave similarly as in the pH10 case as shown in figures 2.11 and 2.13.

According to the point of zero charge of ceria, at pH3 the surface of ceria is positively charged and the surface of LPS is neutral to slightly- negatively charged. Thus, sorption would occur spontaneously due to the attraction of opposite charges, with no need for bridging ions (i.e.  $\text{Ca}^{2+}$  ions) to mediate the adhesion process. However, it has been previously suggested that high

concentrations of calcium ions disrupt LPS aggregates causing reorientation on surfaces of varying surface chemistry. There have also been observations associating calcium ions with interactions with the lipid-A component of LPS. This region of the LPS molecule has been previously studied and it was shown that it promoted intermolecular interactions, inhibiting possible adhesion processes (Parikh and Chorover, 2008).

In the case of negatively charged surface to negatively charged adsorbate, it is hypothesised that the ions in solution would contribute to the binding. Experiments conducted at high pH conditions (pH7 and pH10) represented a scenario where the ceria was negatively charged when in contact with a partly negatively charged LPS. As previously explained, the amphiphilic character of LPS enables the molecule to act differently under different pH environments. The different functional groups and the moieties present in LPS can orient according to the pH environment and as it has been previously suggested, during adhesion to negatively charged surfaces, the O-antigen of LPS is the moiety responsible for the molecule's sorption onto the surface (Parikh and Chorover, 2008).

In the cases of experiments conducted at pH7 and pH10 (figures 2.12 and 2.13 respectively), it was observed that LPS in water and LPS in NaCl behaved similarly with both cases showing a positive sorption of LPS on ceria. In the case of experiments conducted in solution containing calcium chloride, the sorption process resulted in higher mass adsorbed compared to experiments conducted in solution containing sodium chloride and water which was in agreement with previous studies on interactions of minerals with LPS in the presence of  $\text{CaCl}_2$  (Parikh and Chorover, 2008).

All the obtained results indicate a clear sorption profile at neutral to basic pH conditions with a preference for sorption to occur in solutions that contain divalent cations (specifically  $\text{Ca}^{2+}$ ). Both water and sodium chloride showed a similar sorption profile in neutral and negative environments which suggested that the two electrolytes could both mediate the interaction under specific conditions.

In acidic environments, the interaction between LPS and ceria did not result in clear sorption profiles (no clear plateau was reached). This suggested that intermolecular interactions within the LPS molecule induced a 'barrier' impeding the sorption process to occur. The term 'barrier' here is used metaphorically to describe the change of LPS conformation that inhibited the extent of sorption. That was due to bridging of LPS moieties via  $\text{Ca}^{2+}$  that resulted in limited availability of binding sites for sorption to ceria. This was not the case when only protons were present in solution under acidic conditions (water-mediated interaction). In the case of proton-mediated binding the proton is weaker and proton intermolecular forces are hence easier to break and make binding sites available for sorption with ceria.

A hypothesis arising from the above observations relates to the divalent cations which are widely available under acidic conditions due to the mobility of the ions at low pH. This increased availability of cations in solution is responsible for the inability of LPS to interact with any approaching surface as it promotes intermolecular binding which is 'bridged' by the cations. On the opposite end, divalent cations are less mobile under basic conditions due to the speciation of calcium when the pH is increasing. In this case, intermolecular binding via the cations does occur but the cations are at the same time acting as 'bridges' for sorption onto the negatively charged surface. It is therefore proposed that the conformation of LPS is not the only factor affecting the adsorption of the macromolecule onto the ceria surface. Another factor that plays a role in this interaction is the surface charge of the ceria in combination with the number of available  $\text{Ca}^{2+}$  ions under acidic or basic conditions. These two factors were found to have an effect on the availability of the surface for adsorption, as shown by the zeta potential experiments (sub-section 2.3.3.1). More details on the suggested mechanism are given in section 2.3.7.

#### **2.3.3.3.1 Equilibrium Modelling of LPS sorption onto Ceria**

In a system where LPS is approaching a surface, a series of different interactions are possible depending on the different conformations of the molecule, which are directly related to the

environmental (pH) conditions. A monolayer of adsorbed LPS would be really hard to achieve, especially due to the long chain of functional groups within the LPS molecule. This suggests that there is not just a single reaction site but multiple groups competing during an adsorption reaction.

In order to describe the sorption process, the Langmuir and the Freundlich models were used. The Langmuir isotherm is mainly used for gas adhesion onto solid surfaces and not solution to solid adhesion. Failure on fitting the data with the Langmuir model ( $R^2 < 0.6$ ) suggested the existence of a multi-site adhesion process or a more complicated situation where one or two molecules bind and the rest of the molecules are blocking the available binding sites due to their large size. The Freundlich isotherm is empirical and while the Langmuir model assumes that only a monolayer of the approaching molecule will end up on the surface, the Freundlich isotherm (equation (2.7)) is preferred when 'stacking' of adsorbed molecules onto the surface is observed.

$$\ln(Q_e) = \ln(K_f) + \frac{1}{n_f} \cdot \ln(C_e) \quad \text{equation (2.7)}$$

For better fitting, a modified version of the Freundlich model was included as shown by equation (2.8). This version of the Freundlich model provided the best  $R^2$  scores ( $R^2 > 0.95$ ).

$$\ln\left(\frac{Q_e}{C_e}\right) = \ln(K_{MF}) + \left(\frac{1}{n_{MF}} - 1\right) \ln(C_e) \quad \text{equation (2.8)}$$

The intercept of this equation is equal to  $\ln(K_{MF})$  while the slope is equal to  $\frac{1}{n_{MF}} - 1$ . After plotting  $\ln\left(\frac{Q_e}{C_e}\right)$  Vs  $\ln(C_e)$  we can therefore extract the values of  $K_{MF}$  and  $n_{MF}$ . Correlation coefficients and constant parameters calculated for the adsorption models can be found at table 2.3. A summary of all the data fitting on the modified Freundlich model for the adsorption of LPS onto ceria under varying conditions can be found in appendix 3.

**Table 2.3. Modified Freundlich model-Results of LPS adsorption on Ceria**

| ID                           | Equation  | Y                                 | X          | Intercept        | Slope                      | K <sub>MF</sub> | n <sub>MF</sub>   |
|------------------------------|---|-----------------------------------|------------|------------------|----------------------------|-----------------|-------------------|
| <b>LPS-Ceria in:</b>         | $\ln\left(\frac{Q_e}{C_e}\right) = \ln(K_{MF}) + \left(\frac{1}{n_{MF}} - 1\right)\ln(C_e)$ |                                   |            | $c = \ln K_{MF}$ | $m = \frac{1}{n_{MF}} - 1$ | $e^c$           | $\frac{1}{m + 1}$ |
| <b>NaCl pH10</b>             | $y = -0.916x + 2.486$   | $\ln\left(\frac{Q_e}{C_e}\right)$ | $\ln(C_e)$ | 2.486            | -0.916                     | 12.017          | 11.848            |
| <b>NaCl pH7</b>              | $y = -1.055x + 2.579$   |                                   |            | 2.579            | -1.055                     | 13.180          | -18.215           |
| <b>water pH7</b>             | $y = -0.580x + 0.808$   |                                   |            | 0.808            | -0.580                     | 2.244           | 2.381             |
| <b>CaCl<sub>2</sub> pH10</b> | $y = -0.948x + 3.048$   |                                   |            | 3.048            | -0.948                     | 21.082          | 19.342            |
| <b>CaCl<sub>2</sub> pH7</b>  | $y = -0.825x + 2.486$   |                                   |            | 2.486            | -0.825                     | 12.015          | 5.717             |
| <b>water pH10</b>            | $y = -0.966x + 2.845$   |                                   |            | 2.845            | -0.966                     | 17.195          | 29.674            |

Where  $C_e$ =LPS concentration at equilibrium ( $\text{mg L}^{-1}$ ),  $Q_e$ =equilibrium adsorption capacity ( $\text{mg g}^{-1}$ ),  $K_{MF}$ = Modified Freundlich constant (L/g),  $n_{MF}$  = heterogeneity factor of adsorption sites.  $R^2 > 0.95$

The standard free energy change of adsorption ( $\Delta G$ ) can be correlated with each equilibrium concentration,  $C_e$ . Different methods have been proposed during the past few years relating the isotherm constants with the free energy change of adsorption.  $K_c$  (equation (2.10)) can be replaced by constants obtained using the Langmuir isotherm, the Tempkin isotherm (Tosun, 2012), the Freundlich isotherm or by using the Khan and Singh method (Khan and Singh, 1987). Here, the method of Khan and Singh who defined the distribution coefficient  $K_d$  (equation (2.9)) was employed and used to obtain  $\Delta G$  values (equation (2.10)) where  $Q_e$ = quantity of macromolecule adsorbed at equilibrium ( $\text{mg g}^{-1}$ ),  $C_e$ =equilibrium concentration ( $\text{mg L}^{-1}$ );  $\Delta G$ = standard free energy change of adsorption,  $R$ = gas constant (0.008314 kJ/mol);  $T$ = temperature in Kelvin (K).

$$K_d = \frac{Q_e}{C_e} \quad \text{equation (2.9)}$$

$$\Delta G = -RT \ln(K_c) \quad \text{equation (2.10)}$$

$K_c$  is essentially replaced by  $K_d$  after a correction which is needed to ensure that the resulting value is dimensionless ( $K_c$  in equation (2.10) has no units thus  $K_d$  can only be used if adjusted prior to any  $\Delta G$  calculations, Milonjic, 2007; Tran *et al.*, 2016; Canzano *et al.*, 2012)). Also, the Freundlich (and modified Freundlich) constant  $K_F$  is equal to  $K_d$  as  $\ln(K_F)$  is equal to the value of  $\ln(K_d)$  at equilibrium concentration  $C_e=1 \text{ mg L}^{-1}$  (Bhatt *et al.*, 2012). That can be proved by combining the general form of the Freundlich equation (2.7) with equation (2.9). Replacing  $C_e$  with  $1 \text{ mg L}^{-1}$  in equation (2.7) results in:

$$\ln(1) = 0 \rightarrow \ln(Q_e) = \ln(K_F) \rightarrow Q_e = K_F$$

and also  $K_d = Q_e$  (when  $C_e=1 \text{ mg L}^{-1}$ ) for equation (2.9)

$$\text{Hence } K_F = K_d$$

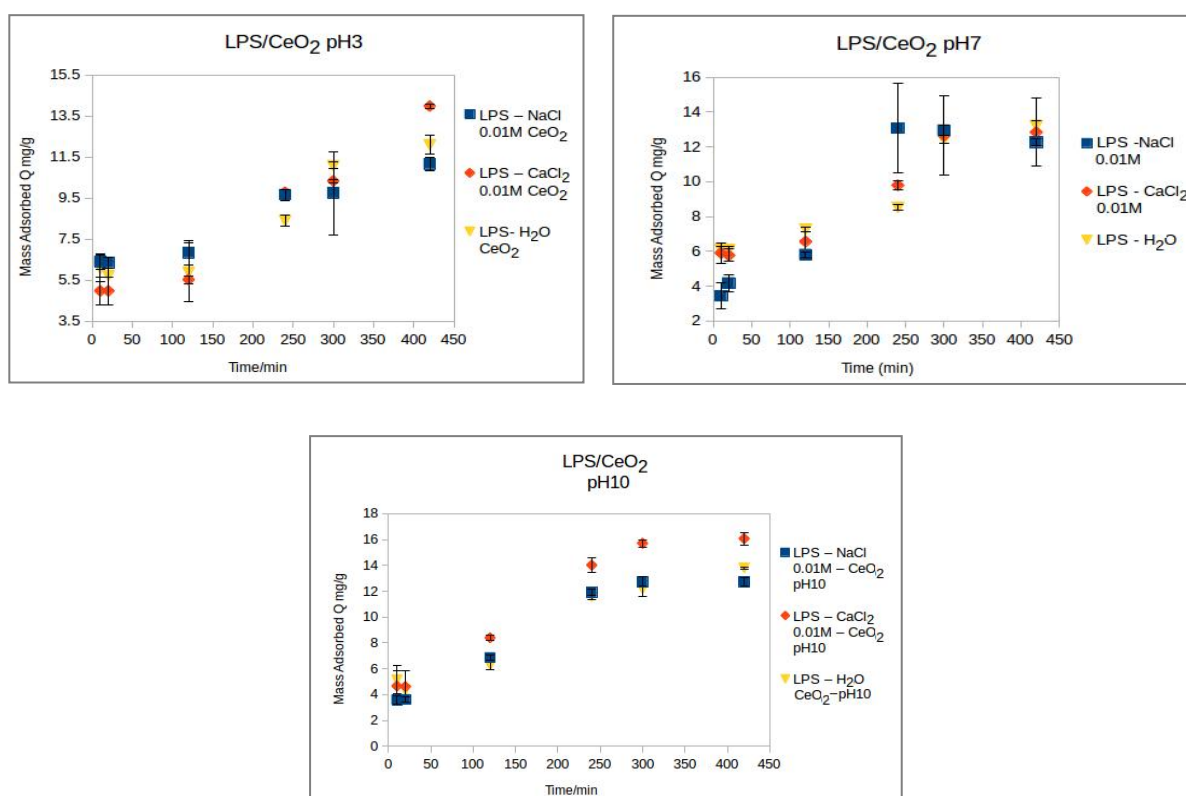
Using equations (2.9) and (2.10) results in the free energy change of adsorption which can be found at table 2.4.

| <b>ID</b>                                 | <b><math>K_{MF}</math></b> | <b><math>K_c</math></b> | <b><math>\Delta G \text{ kJ mol}^{-1}</math></b> |
|---|----------------------------|-------------------------|--|
| <b>LPS/Ceria in NaCl pH10</b>             | 12.017                     | 1201.7                  | -23.053  |
| <b>LPS/Ceria in NaCl pH7</b>              | 13.180                     | 1318                    | -23.279  |
| <b>LPS/Ceria in water pH7</b>             | 2.244                      | 2244                    | -18.935  |
| <b>LPS/Ceria in CaCl<sub>2</sub> pH10</b> | 21.081                     | 2108.1                  | -24.432  |
| <b>LPS/Ceria in CaCl<sub>2</sub> pH7</b>  | 12.015                     | 1201.5                  | -23.052  |
| <b>LPS/Ceria in water pH10</b>            | 17.195                     | 1719.5                  | -23.932  |

The negative  $\Delta G$  values indicate a spontaneous reaction between the ceria particles and the LPS molecules. It is observed that the energy values obtained for the adsorption are close numerically, ranging from  $-18 \text{ kJ mol}^{-1}$  to  $-24 \text{ kJ mol}^{-1}$ . These values are in the range of 'physisorption' ( $-40$  to  $0 \text{ kJ mol}^{-1}$  - Bhatt *et al.*, 2012), which suggests that no chemical bonding occurs between the surface and the molecule (which is known as 'chemisorption') but Van der Waals forces are causing the observed interaction instead.

### 2.3.3.4 Kinetics

The Purpald assay was used to quantify LPS at different times and constant concentration of LPS, in order to assess the kinetics of the interaction. The different kinetics of each reaction according to the corresponding pH conditions are shown in figures (2.14)-(2.16). The mass adsorbed is shown with the value  $Q$  ( $\text{mg g}^{-1}$ ).



Figures 2.14-2.16. Kinetics of LPS-Ceria interactions at pH3 (fig. 2.14-left), pH7 (fig. 2.15-right) and pH10 (fig. 2.16-middle).

From figures 2.14, 2.15 and 2.16, it can be observed that the interaction between ceria and LPS reaches a plateau after ~250 min. The process is fast, with the highest sorption reached after 420 min of interaction for all electrolyte conditions studied. At basic conditions, the inclusion of calcium chloride as the electrolyte resulted in higher LPS adsorption by the mineral compared to the acidic conditions.

NaCl followed a similar profile to that of water in all three cases. This comes in agreement with previous research on the interactions of LPS with ZnSe, GeO<sub>2</sub>, alpha-Fe<sub>2</sub>O<sub>3</sub> and alpha-Al<sub>2</sub>O<sub>3</sub> which suggested that systems with LPS in NaCl show similar surface affinity to solution phase LPS (Parikh and Chorover, 2008). This implies that Na<sup>+</sup> is such a small cation that doesn't make a difference compared to H<sup>+</sup>. Thus, Van der Waals bonding interactions can occur in the presence of both cations.

The behavior of LPS in solution is similar for both Na<sup>+</sup> and protons as the conformation of the molecule is not affected by either of the ions. Calcium on the other hand was found to affect the lipid A region of LPS due to the change of the conformation of the molecule when in solution with the ion. This also results in different sorption profiles when the molecule comes into contact with surfaces of different hydrophobicity at varying pH conditions (Parikh and Chorover, 2008).

Kinetic data was analysed using pseudo-first order and pseudo-second order models. A linear fit ( $R^2 > 0.98$ ) was obtained for a pseudo second order reaction with equation (2.11) where  $Q_e$  and  $Q_t$  = adsorption capacity at equilibrium and time  $t$  respectively ( $\text{mg g}^{-1}$ ),  $k$  = rate constant of the pseudo second order adsorption ( $\text{g mg}^{-1} \text{min}^{-1}$ ).

$$\frac{dQ}{dt} = k(Q_e - Q_t)^2 \quad \text{equation (2.11)}$$

The linear form of equation (2.11) is shown in equation (2.12) where  $k$  = rate constant of the pseudo second order adsorption ( $\text{g ml}^{-1} \text{min}^{-1}$ ).

$$\frac{t}{Q_t} = \frac{1}{kQ_e^2} + \frac{t}{Q_e} \quad \text{equation (2.12)}$$

A plot of  $\text{Time}/Q_t$  Vs Time was used to evaluate the rate constant of the interaction as shown in figure 2.17 and table 2.5.

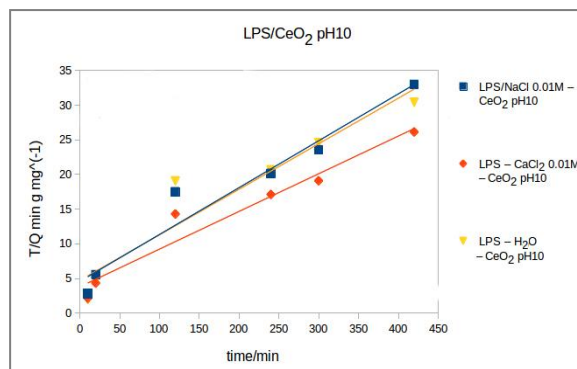


Figure 2.17. Pseudo-second order fitting of LPS-Ceria interactions.

| ID                               | Equation $y=Mx+C$ | Intercept<br>$C=1/kQ_e^2$ | Slope<br>$M=1/Q_e$ | $Q_e = 1/m$<br>$\text{mg g}^{-1}$ | $K = 1/(CQ_e^2)$<br>$*10^{-3} \text{ g mg}^{-1} \text{ min}^{-1}$ |
|----------------------------------|-------------------|---------------------------|--------------------|-----------------------------------|---|
| LPS/Ceria NaCl pH10              | $Y=0.068x+4.581$  | 4.581                     | 0.068              | 14.786                            | 0.998   |
| LPS/Ceria CaCl <sub>2</sub> pH10 | $Y=0.054x+3.797$  | 3.797                     | 0.054              | 18.388                            | 0.779   |
| LPS/Ceria water pH10             | $Y=0.066x+4.732$  | 4.732                     | 0.066              | 15.221                            | 0.912   |
| LPS/Ceria NaCl pH3               | $Y=0.088x+2.884$  | 2.884                     | 0.088              | 11.298                            | 2.717   |
| LPS/Ceria CaCl <sub>2</sub> pH3  | $Y=0.070x+5.638$  | 5.638                     | 0.070              | 14.321                            | 0.867   |
| LPS/Ceria water pH3              | $Y=0.080x+4.552$  | 4.552                     | 0.080              | 12.534                            | 1.398   |
| LPS/Ceria NaCl pH7               | $Y=0.068x+4.772$  | 4.772                     | 0.068              | 14.707                            | 0.969   |
| LPS/Ceria CaCl <sub>2</sub> pH7  | $Y=0.073x+3.952$  | 3.952                     | 0.073              | 13.760                            | 1.337   |
| LPS/Ceria water pH7              | $Y=0.074x+3.895$  | 3.895                     | 0.074              | 13.522                            | 1.404   |

The theoretical values of  $Q_e$  agreed well with the experimentally obtained values and ranged from 11 to 18 mg of LPS adsorbed per gram of mineral with LPS showing a preference (highest  $Q_e$  value) at calcium ions under basic conditions. In basic and neutral environments, a similar behavior of the sodium containing samples and the water containing samples was observed suggesting a similar sorption mechanism of the LPS in the presence of sodium ions to the solution phase LPS. The results agreed with the adsorption kinetic models obtained for the adsorption of organic compounds onto ceria-activated carbon (Alhooshani, 2015).

### 2.3.3.5 ATR-FTIR of Ceria-LPS interactions

ATR-FTIR spectroscopy was used in an attempt to confirm and characterise the interaction of ceria with LPS. Figure 2.18 shows some characteristic examples of the products of Ceria-LPS interactions under different conditions which resulted after a 400-minute interaction between the starting materials. Similar results were observed for all the samples tested and a summary of the ATR-FTIR assessment can be found in appendix 4.

Clear LPS peaks can be identified at all spectra which indicates the presence of LPS in the reaction product. A sharp peak at  $\sim 1060\text{ cm}^{-1}$  is assigned to the C-O or C-O-C band while a second one at  $1106\text{ cm}^{-1}$  shows the presence of a  $\text{PO}_2^-$  band. Hydrated  $\text{PO}_2^-$  asymmetric stretch is identified at  $1200\text{-}1225\text{ cm}^{-1}$  and the peak at  $1230\text{-}1245\text{ cm}^{-1}$  represents the metal-complexed  $\text{PO}_2^-$  asymmetric stretching vibration. The above results are in agreement with the work of Parikh and Chorover(2008) who studied the interactions of several minerals with LPS using ATR-FTIR. A list of IR assignments for LPS has been adapted from Parikh and Chorover(2008) and is shown in table 2.6.

| <b>Wavenumber <math>\text{cm}^{-1}</math></b> | <b>IR band</b>  |
|---|---|
| 2915-2923                                     | $\text{CH}_2$ asymmetric stretching vibration                   |
| 2848-2854                                     | $\text{CH}_2$ symmetric stretching vibration                    |
| 1460-1470                                     | Bending vibrations  |
| 1250-1265                                     | Metal-complexed asymmetric stretching $\text{PO}_2^-$ vibration |
| 1230-1245                                     | Complex $\text{PO}_2^-$ asymmetric stretching vibrations        |
| 1200-1225                                     | Hydrated $\text{PO}_2^-$ asymmetric stretching vibration        |
| 1106  | $\text{PO}_2^-$ stretching vibration                            |
| 1020,1050-1085                                | C-O C-O-C   |
| 960-983                                       | $\text{PO}_2^-$   |

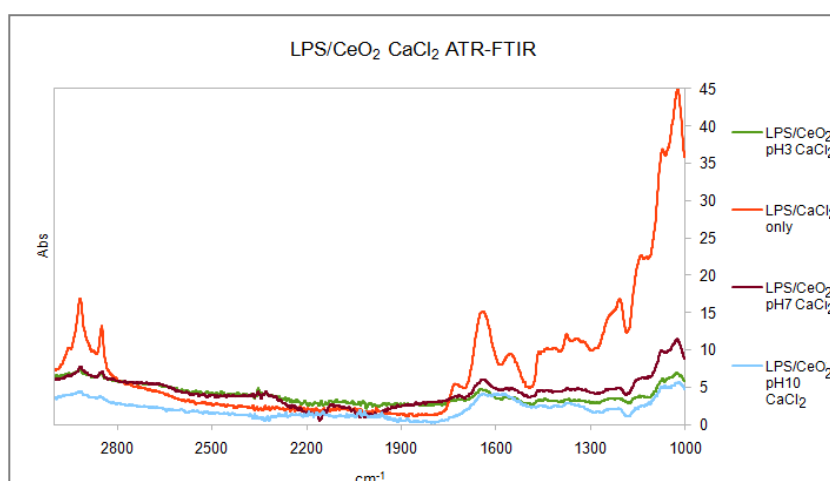


**Figure 2.18.** ATR-FTIR of LPS interacted with Ceria. ‘LPS/CaCl<sub>2</sub> only’ (red) represents the control sample while the rest are data collected under different pH conditions (green= LPS interacted with Ceria at pH3, purple= LPS interacted with Ceria at pH7 and blue= LPS interacted with Ceria at pH10) .

The results of the LPS-CeO<sub>2</sub> samples were compared to LPS controls under varying pH and electrolyte conditions (figure 2.19 shows some selected spectra of control LPS samples for clarity, the rest of the ATR-FTIR results for control LPS samples can be found in appendix 5). The difference in intensity of the peaks is associated with the quantity of materials tested.

The control spectra showed a similar range of peaks that include a very intense peak at ~1060 cm<sup>-1</sup> for the C-O or C-O-C band and a second one at 1106 cm<sup>-1</sup> for PO<sub>2</sub><sup>-</sup>. Hydrated PO<sub>2</sub><sup>-</sup> asymmetric stretch is identified at 1200-1225 cm<sup>-1</sup>. Most of the control spectra are almost identical, with a small difference at the 1300-1400 cm<sup>-1</sup> range of the LPS in CaCl<sub>2</sub> at pH10 sample which is possibly related to the different conformation of the molecule. However, most of the bands observed in the control spectra are identical, which suggests that the same functional groups are present in all samples.

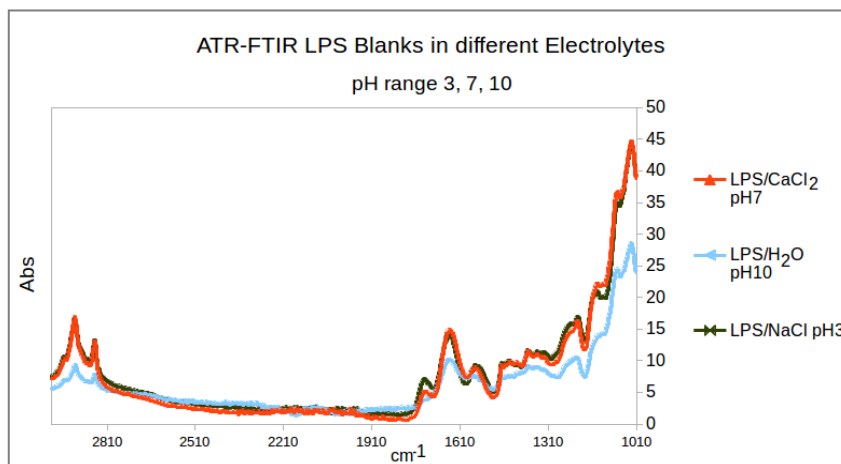


**Figure 2.19. ATR-FTIR of LPS controls under different conditions**

If we look closely at the LPS-Ceria in  $\text{CaCl}_2$  samples (figure 2.18), significant shifts can be observed, compared to the respective control LPS sample (figure 2.19). The intense peaks of the LPS vibrations at  $1640\text{ cm}^{-1}$ ,  $1070\text{ cm}^{-1}$  (C-O, C-O-C),  $1026\text{ cm}^{-1}$  are visible but not that sharp while a shift of the  $1210\text{ cm}^{-1}$  peak (hydrated  $\text{PO}_2^-$ ) and the  $1274\text{-}1376\text{ cm}^{-1}$  region are observed at all different pH conditions. A small peak at  $1245\text{ cm}^{-1}$  (metal-complexed  $\text{PO}_2^-$ ) is also observed in the LPS- $\text{CeO}_2$  samples which is not present in any of the control spectra.

Even though small differences were observed between the spectra of control LPS and LPS-Ceria interacted samples, the identified peaks cannot be used to explain how the LPS moieties have interacted with the mineral. The peak ranges where differences were observed involve C-O, C-O-C and  $\text{PO}_2^-$  functional groups which are widely available within the molecule (and especially the O-antigen region of the LPS structure), making it difficult to identify the exact LPS moieties responsible for the sorption process. Since the experiments included LPS concentrations higher than the CMC of the specific strain, it was assumed that the micelle arrangement adapted by the molecule would limit the availability of the lipid-A moieties for interaction and only the O-antigen moieties were exposed. Thus, the ATR-FTIR results can be associated with the O-antigen region, similarly with the results of Parikh and Chorover who used ATR-FTIR to examine the interaction of LPS with  $\text{FeO}_2$ . The same peaks were observed at both studies while no clear distinction relating the individual LPS moieties with the interaction could be made, with a general conclusion indicating

that the sorption of the molecule is most likely mediated by the O-antigen region and carbohydrate (C-O, C-O-C) and phosphate ( $\text{PO}_2^-$ ) groups (Parikh and Chorover, 2008).

### **2.3.3.6 Electron Microscopy**

The samples at pH 7 were considered the best samples to analyse since most interactions in the natural environment will occur around neutral pH. The results show that the ceria particles were coated with LPS (figure 2.20).

The Ce (representing the particle), C (found in LPS), P (found in LPS) and Ca (representing the electrolyte) maps taken show that all elements are present in the same locations in the sample (figure 2.20). Hence, the ceria particle is coated with both calcium ions and LPS. The EDX results confirm that only Ce is present, showing no contamination from other compounds. The results did not show specific binding sites or areas of interaction, however it is clear that LPS coats the particles thus, it is interacting with the solid. There was no excess of LPS around the particles (typical of other bacterial samples (Bjerre *et al.* 2002)) which indicates that the LPS strands stay within the particle.

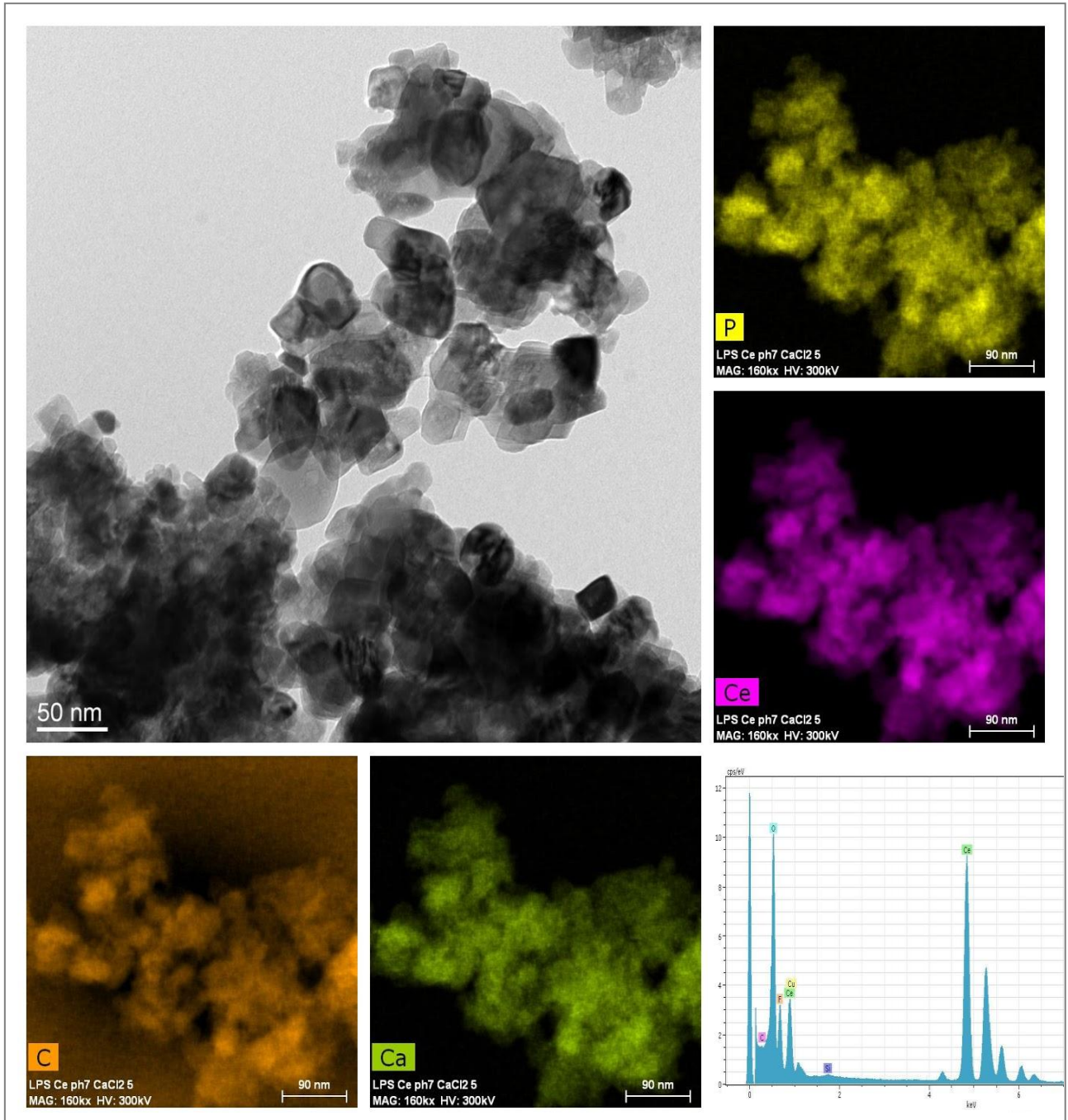


**Figure 2.20.**Transmission Electron Microscopy analysis of Ceria-LPS samples in  $\text{CaCl}_2$  at pH7. The images named P, Ce, C and Ca are the EDX maps of the corresponding elements. The Ce (representing the particle), C (found in LPS), P (found in LPS) and Ca (representing the electrolyte) maps taken show that all elements are present in the same locations in the sample. Hence, the ceria particle is coated with both calcium ions and LPS.

## **2.3.4 Adsorption of LPS onto europium oxide**

### **2.3.4.1 Quantification of LPS- Calibration curve**

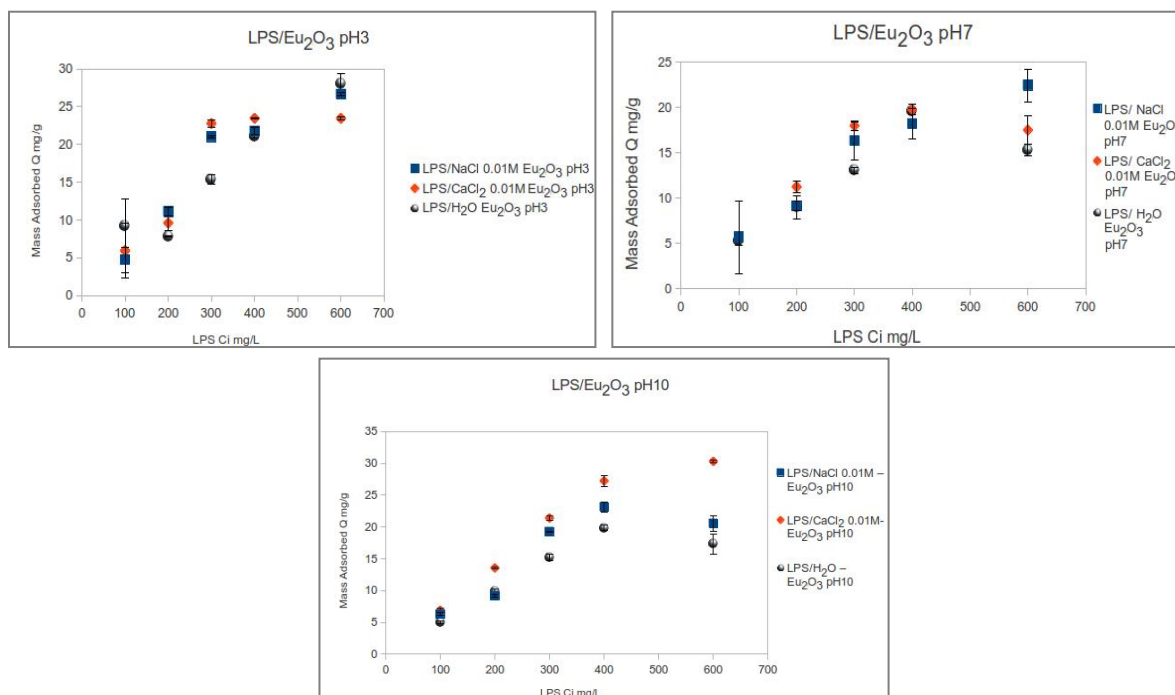
Experimental LPS uptake kinetics onto europium oxide were calculated using the Purpald assay (sub-section 2.2.4.2). The same calibration curve constructed for the quantification of LPS described in sub-section 2.3.2.2 was used.

### **2.3.4.2 Experimental Isotherms for sorption of LPS onto europium oxide**

The Purpald assay was used to quantify LPS before and after its interaction with europium oxide. Europium, as a typical nuclear fission product and a representative of the medium rare earth elements, has been one of the few elements the minerals of which have been of interest regarding the biomineralisation process (Moll *et al.*, 2014; Bayer *et al.*, 1999). Europium is also used as a chemical homologue of the radioactive Cm and Am which are hardly handled due to their high radioactivity and toxicity (Babelot, 2013). Preliminary tests on europium biomineralisation were carried out by Macaskie *et al.* (Macaskie *et al.*, 1994) while another study on europium proved the precipitation of insoluble europium complexes when growing bacteria were treated with europium ions (Bayer *et al.*, 1999).

Europium oxide ( $\text{Eu}_2\text{O}_3$ ) is a body-centered cubic oxide at low temperatures. The point of zero charge ( $p_{zc}$ ) of europium oxide is  $\text{pH}=5$  (Curtis and Tharp, 1959). The  $\text{pH}$  at point of zero charge suggests that the mineral exhibits a positive charge below  $\text{pH} 5$  and a negative charge above  $\text{pH} 5$ . By examining systems of  $\text{pH}3$ ,  $\text{pH}7$  and  $\text{pH}10$  all different situations with europium oxide being negatively, positively charged and close-to-neutral are accessed.

The LPS concentration used for all the cases was higher than the CMC; this was intended to represent the cell-bound form of LPS with the assumption that only the O-antigen region of the molecule is exposed for interaction with the minerals (more information in sub-section 2.1.1.1).



**Figures 2.21-2.23. Isotherm of LPS-Eu<sub>2</sub>O<sub>3</sub> interactions at pH3 (fig. 2.21-left), pH7 (fig. 2.22-right) and pH10 (fig. 2.23-middle)**

In the case of experiments performed at pH3 (figure 2.21), CaCl<sub>2</sub> was the electrolyte with the lowest maximum mass of LPS adsorbed. According to the zero point of charge of europium oxide, pH3 environments induce a positive charge on the surface and a neutral, slightly- negative charge on the LPS which suggests that sorption would occur spontaneously due to the attraction of opposite charges, with no need for bridging ions (i.e. Ca<sup>2+</sup> ions) to mediate the adhesion process. Additionally, it has been previously suggested that calcium ions disrupt LPS aggregates causing reorientation on surfaces of varying surface chemistry. There have also been observations associating calcium ions with interactions with the lipid-A region of LPS which does not play a

role in bound LPS-surface adhesion but intermolecular interactions instead (Parikh and Chorover, 2008).

As mentioned previously, a sorption process when no ions were included (water only) was obtained. The observed results suggest that in highly acidic environments, inclusion of ions is not necessary for a sorption process to take place and LPS cannot adsorb onto europium oxide with the same efficiency as it does at highly alkaline environments. This comes in agreement with the results obtained for sorption of LPS onto ceria, described in sub-section 2.3.3. In the case of pH7 where the surface is slightly negative (figure 2.22), NaCl resulted in the highest maximum Q with water closely following.

In the case of experiments performed at pH10 (figure 2.23), it was observed that LPS in water and LPS in NaCl behaved similarly with both cases showing a positive adsorption of LPS onto europium oxide. In the case of calcium chloride, the adsorption process resulted in the highest mass of LPS adsorbed per gram of europium oxide which is in agreement with previous research on interactions of minerals with LPS in the presence of  $\text{CaCl}_2$  (Parikh and Chorover, 2008). Experiments conducted at high pH conditions represented a scenario where the europium oxide surface was negatively charged when in contact with a negatively charged LPS.

The results were similar to that of the sorption profiles obtained for LPS interactions with ceria. All the obtained results indicate a clear sorption profile at neutral to basic pH conditions with a preference for sorption to occur in solutions that contain divalent cations (specifically  $\text{Ca}^{2+}$ ). Both water and sodium chloride showed a similar sorption profile in neutral and negative environments which suggests that the two electrolytes can also mediate the interaction under specific conditions. In the case of water, a proton-mediated process is suggested.

In acidic conditions, a clear sorption profile was obtained (clear plateau was reached) in contrast to that obtained for LPS sorption onto ceria. However, the reaction was proved challenging (no clear sorption profile could be obtained) suggesting intermolecular binding which interrupts the sorption process. Similarly with the case of ceria, a hypothesis arising from the above

observations relates to the divalent cations which are widely available under acidic conditions due to the mobility of the ions at low pH. This increased availability of cations in solution is responsible for the inability of LPS to interact with any approaching surface as it promotes intermolecular binding which is 'bridged' by the cations. On the opposite end, divalent cations are less mobile under basic conditions due to the speciation of calcium when the pH is increasing. This results in intermolecular binding via the cations but at the same time, the cations are acting as 'bridges' connecting the negatively charged surface with the negatively charged macromolecule. Since both ceria and europium oxide have similar points of zero charge, the change in surface charge according to pH is similar for both minerals which explains the similarity in sorption of LPS. More details on the suggested mechanism are given in section 2.3.7.

### **2.3.4.3 Equilibrium Modelling of LPS sorption onto Europium oxide**

In order to describe the sorption process, the Langmuir and the Freundlich isotherm models were used. The modified version of the Freundlich model, explained in sub-section 2.3.3.2.1 provided the highest  $R^2$  scores ( $R^2 > 0.98$ ) and hence, the  $K_{MF}$  and the  $n_{MF}$  values were calculated using the equation found in table 2.7. Failing to fit the data on the Langmuir model (obtained values of  $R^2 < 0.6$ ) suggests the existence of a multi-site sorption process or blocking of any available sites from a small number of LPS molecules. All the LPS-Eu<sub>2</sub>O<sub>3</sub> samples showed similar results. The plotted results can be found in appendix 6. A summary of the resulting equations and the associated constants can be found at table 2.7. The constants were calculated as explained previously (sub-section 2.3.3.2.1). Only data of  $R^2 > 0.95$  were considered.

| ID   | Equation   | Y                                 | X          | Intercept        | Slope                      | $K_{MF}$ | $n_{MF}$          |
|--|--|-----------------------------------|------------|------------------|----------------------------|----------|-------------------|
| <b>LPS-Eu<sub>2</sub>O<sub>3</sub> in:</b> | $\ln\left(\frac{Q_e}{C_e}\right) = \ln(K_{MF}) + \left(\frac{1}{n_{MF}} - 1\right) \ln(C_e)$ |                                   |            | $c = \ln K_{MF}$ | $m = \frac{1}{n_{MF}} - 1$ | $e^c$    | $\frac{1}{m + 1}$ |
| <b>NaCl pH10</b>                           | $y = -0.998x + 2.827$  | $\ln\left(\frac{Q_e}{C_e}\right)$ | $\ln(C_e)$ | 2.827            | -0.998                     | 16.900   | 503.860           |
| <b>NaCl pH7</b>                            | $y = -1.027x + 3.040$  |                                   |            | 3.040            | -1.027                     | 20.897   | -37.265           |
| <b>water pH7</b>                           | $y = -0.833x + 2.099$  |                                   |            | 2.099            | -0.833                     | 8.157    | 5.986             |
| <b>CaCl<sub>2</sub> pH10</b>               | $y = -0.875x + 2.687$  |                                   |            | 2.687            | -0.875                     | 14.689   | 8.025             |
| <b>CaCl<sub>2</sub> pH7</b>                | $y = -0.814x + 2.048$  |                                   |            | 2.048            | -0.814                     | 7.7555   | 5.368             |
| <b>water pH10</b>                          | $y = -0.939x + 2.455$  |                                   |            | 2.455            | -0.939                     | 11.649   | 16.413            |
| <b>NaCl pH3</b>                            | $y = -0.939x + 2.877$  |                                   |            | 2.877            | -0.939                     | 17.765   | 16.456            |
| <b>water pH3</b>                           | $y = -0.798x + 2.153$  |                                   |            | 2.153            | -0.798                     | 8.615    | 4.962             |
| <b>CaCl<sub>2</sub> pH3</b>                | $y = -0.989x + 3.102$  |                                   |            | 3.102            | -0.989                     | 22.242   | 93.776            |

Where  $C_e$ =LPS concentration at equilibrium ( $\text{mg L}^{-1}$ ),  $Q_e$ =equilibrium adsorption capacity ( $\text{mg g}^{-1}$ ),  $K_{MF}$ = modified Freundlich constant (L/g),  $n_{MF}$  = heterogeneity factor of adsorption sites.

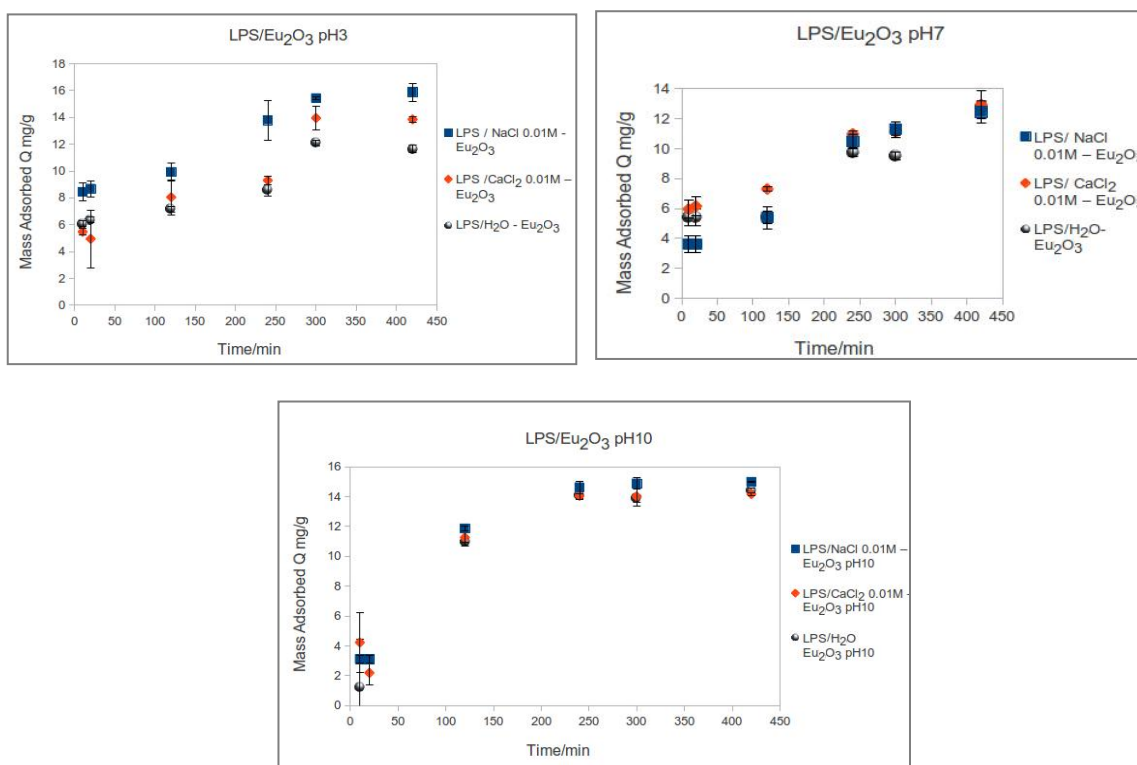
The standard free energy change of adsorption ( $\Delta G$ ) was calculated as explained previously (sub-section 2.3.3.2.1). The results can be found at table 2.8.

| ID   | $K_{MF}$ | $\Delta G \text{ kJ mol}^{-1}$ |
|--|----------|--------------------------------|
| <b>LPS/Eu<sub>2</sub>O<sub>3</sub> in NaCl pH10</b>              | 16.900   | -23.889                        |
| <b>LPS/ Eu<sub>2</sub>O<sub>3</sub> in NaCl pH7</b>              | 20.897   | -24.412                        |
| <b>LPS/ Eu<sub>2</sub>O<sub>3</sub> in water pH7</b>             | 8.157    | -22.102                        |
| <b>LPS/ Eu<sub>2</sub>O<sub>3</sub> in CaCl<sub>2</sub> pH10</b> | 14.689   | -23.545                        |
| <b>LPS/ Eu<sub>2</sub>O<sub>3</sub> in CaCl<sub>2</sub> pH7</b>  | 7.756    | -21.978                        |
| <b>LPS/ Eu<sub>2</sub>O<sub>3</sub> in water pH10</b>            | 11.649   | -22.976                        |
| <b>LPS/ Eu<sub>2</sub>O<sub>3</sub> in NaCl pH3</b>              | 17.765   | -24.012                        |
| <b>LPS/ Eu<sub>2</sub>O<sub>3</sub> in water pH3</b>             | 8.615    | -22.236                        |
| <b>LPS/ Eu<sub>2</sub>O<sub>3</sub> in CaCl<sub>2</sub> pH3</b>  | 22.242   | -24.563                        |

The negative  $\Delta G$  values indicate a spontaneous reaction between europium oxide and the LPS molecules. It is observed that the energy values obtained for the adsorption are very close numerically, ranging from  $\sim 21 \text{ kJ mol}^{-1}$  to  $\sim 24 \text{ kJ mol}^{-1}$ . These values are in the range of physisorption ( $-40$  to  $0 \text{ kJ mol}^{-1}$ ).

### 2.3.4.4 Kinetics

The Purpald assay was used to quantify LPS at different times and constant concentration of LPS, in order to assess the kinetics of the interaction. The different kinetics of each reaction according to the corresponding pH conditions are shown in figures 2.24, 2.25 and 2.26 for experiments conducted at pH3, pH7 and pH10 respectively. The mass adsorbed is shown with the value  $Q$  ( $\text{mg g}^{-1}$ ).



Figures 2.24-2.26. Kinetics of LPS-Eu<sub>2</sub>O<sub>3</sub> interactions at pH3 (fig. 2.24-left), pH7 (fig. 2.25-right) and pH10 (fig. 2.26-middle).

From figures 2.24, 2.25 and 2.26, it can be observed that all three electrolytes successfully mediated the interaction between europium oxide and LPS with a plateau reached after a ~250 min of interaction. NaCl followed a similar profile to that of water in basic and neutral conditions. This is in agreement with previous research on the interactions of LPS with ZnSe, GeO<sub>2</sub>, alpha-Fe<sub>2</sub>O<sub>3</sub> and alpha-Al<sub>2</sub>O<sub>3</sub> (Parikh and Chorover, 2008) which suggests that systems with LPS in NaCl show similar surface affinity to solution phase LPS. Similar results were obtained for LPS adsorption onto ceria. Furthermore, at acidic conditions, the use of NaCl as electrolyte resulted in higher LPS adsorption by the mineral compared to water and calcium chloride. However, if the mass of LPS adsorbed at the different pH conditions is considered numerically, the difference is very small indicating that a very similar adsorption profile has occurred for all three systems.

In order to describe the kinetic behavior, pseudo-first order and pseudo-second order models were used as previously described (sub-section 2.3.3.3). A linear fit was obtained for a pseudo-second order reaction ( $R^2 > 0.99$  -figure 2.27 and table 2.9).

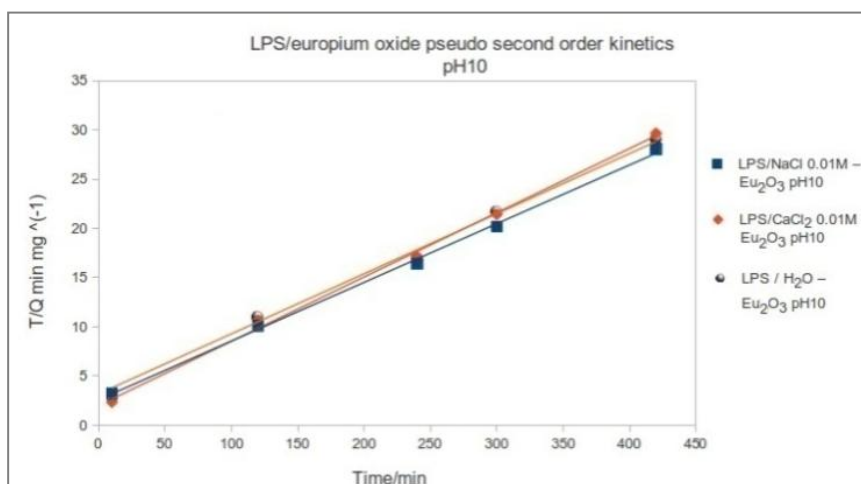


**Figure 2.27. Pseudo-second order fitting of LPS-europium oxide interactions.**

| <b>ID</b><br><b>LPS-Eu<sub>2</sub>O<sub>3</sub></b><br><b>in:</b> | <b>Equation y=Mx+C</b> | <b>Intercept</b><br><b>C=1/kQ<sub>e</sub><sup>2</sup></b> | <b>Slope</b><br><b>M=1/Q<sub>e</sub></b> | <b>Q<sub>e</sub> = 1/m</b><br><b>mg g<sup>-1</sup></b> | <b>K =1/(CQ<sub>e</sub><sup>2</sup>)</b><br><b>*10<sup>-3</sup> g mg<sup>-1</sup>min<sup>-1</sup></b> |
|---|------------------------|---|--|--|---|
| <b>NaCl pH10</b>  | Y=0.060x+2.594         | 2.594   | 0.060                                    | 16.777   | 1.370   |
| <b>CaCl<sub>2</sub> pH10</b>                                      | Y=0.065x+2.007         | 2.007   | 0.065                                    | 15.327   | 2.121   |
| <b>water pH10</b>   | Y=0.061x+3.189         | 3.189   | 0.061                                    | 16.393   | 1.167   |
| <b>NaCl pH3</b>   | Y=0.062x+1.098         | 1.098   | 0.062                                    | 16.153   | 3.489   |
| <b>CaCl<sub>2</sub> pH3</b>                                       | Y=0.065x+3.214         | 3.214   | 0.065                                    | 15.395   | 1.313   |
| <b>water pH3</b>  | Y=0.080x+2.640         | 2.640   | 0.080                                    | 12.580   | 2.393   |
| <b>NaCl pH7</b>   | Y=0.075x+3.418         | 3.418   | 0.075                                    | 13.323   | 1.648   |
| <b>CaCl<sub>2</sub> pH7</b>                                       | Y=0.078x+1.863         | 1.863   | 0.078                                    | 12.880   | 3.236   |
| <b>water pH7</b>  | Y=0.082x+2.702         | 2.702   | 0.082                                    | 12.222   | 2.477   |

The theoretical values of  $Q_e$  agree well with the experimentally obtained values and range from 12 to 16 mg of LPS adsorbed per gram of mineral with LPS showing a preference (highest  $Q_e$  value) at sodium ions under basic and acidic conditions and water under basic conditions. In basic and neutral environments, a similar behavior of the sodium containing samples and the water containing samples was observed suggesting a similar sorption mechanism of the LPS in the presence of sodium ions to the solution phase LPS. The results agreed with the adsorption kinetic models obtained for the adsorption of LPS onto Ceria.

### **2.3.4.5 ATR-FTIR of europium oxide-LPS interactions**

ATR-FTIR spectroscopy was used for the characterization of the interaction of europium oxide with LPS. Figure 2.28 shows some characteristic examples of the products of europium oxide-LPS interactions under different conditions which resulted after a 250-minute interaction

between the starting materials. Similar results were observed for all the samples tested and a summary of the ATR-FTIR assessment can be found in appendix 7.

Clear LPS peaks can be identified at all spectra which proves the presence of LPS in the reaction product. A sharp peak at  $\sim 1060\text{ cm}^{-1}$  is assigned to the C-O or C-O-C band while a second one at  $1106\text{ cm}^{-1}$  shows the presence of a  $\text{PO}_2^-$  band. Hydrated  $\text{PO}_2^-$  asymmetric stretch is identified at  $1200\text{-}1225\text{ cm}^{-1}$  and the peak at  $1230\text{-}1245\text{ cm}^{-1}$  represents the metal-complexed  $\text{PO}_2^-$  asymmetric stretching vibration. The above results come in agreement with the work by Parikh and Chorover and the LPS-Ceria complexes.

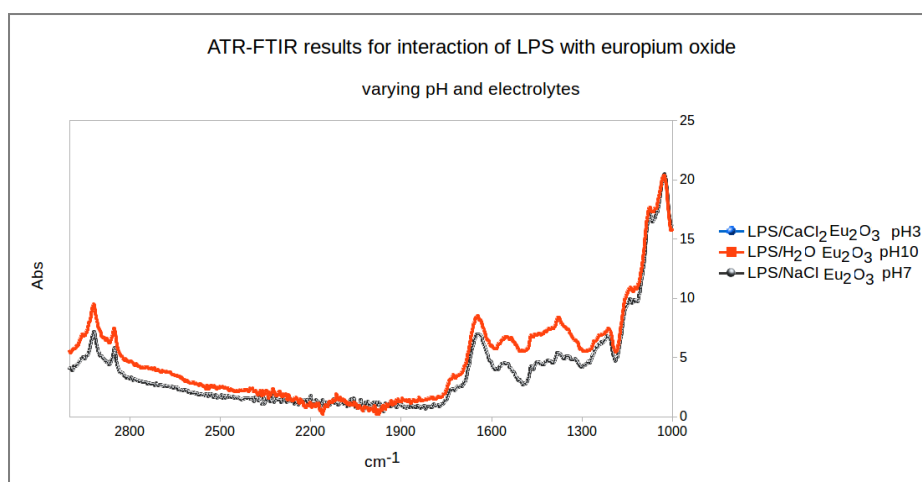


**Figure 2.28. ATR-FTIR of LPS interacted with europium oxide**

The results of the LPS-Eu<sub>2</sub>O<sub>3</sub> samples were compared to LPS controls under various pH and electrolyte conditions (figure 2.19). The LPS control spectra showed a similar range of peaks that include a very intense peak at  $\sim 1060\text{ cm}^{-1}$  for the C-O or C-O-C band and a second one at  $1106\text{ cm}^{-1}$  for  $\text{PO}_2^-$ . Hydrated  $\text{PO}_2^-$  asymmetric stretch is identified at  $1200\text{-}1225\text{ cm}^{-1}$ . Most of the spectra are almost identical. A small difference is observed at  $1300\text{-}1400\text{ cm}^{-1}$  of the LPS in CaCl<sub>2</sub> at pH10 sample which is possibly related to the different conformation of the molecule. A table of IR assignments for LPS is shown at table 2.6 sub-section 2.3.3.4.

The identified peaks cannot be used to explain how the LPS moieties have interacted with the mineral. The bands where differences were observed between LPS-control and LPS-Ceria spectra involve C-O, C-O-C and  $\text{PO}_2^-$  functional groups which are widely available within the molecule (and especially the O-antigen region of the LPS structure), making it difficult to identify the exact LPS moieties responsible for the sorption process. Similar results were also obtained for the LPS-Ceria products.

## **2.3.5 Adsorption of LPS onto thoria**

### **2.3.5.1 Quantification of LPS- Calibration curve**

Experimental LPS uptake kinetics onto thoria were calculated using the Purpald assay (*sub-section 2.2.4.2*) for quantification of LPS before and after the interaction with the minerals. The same calibration curve constructed for the quantification of LPS described in *sub-section 2.3.2.2* was used.

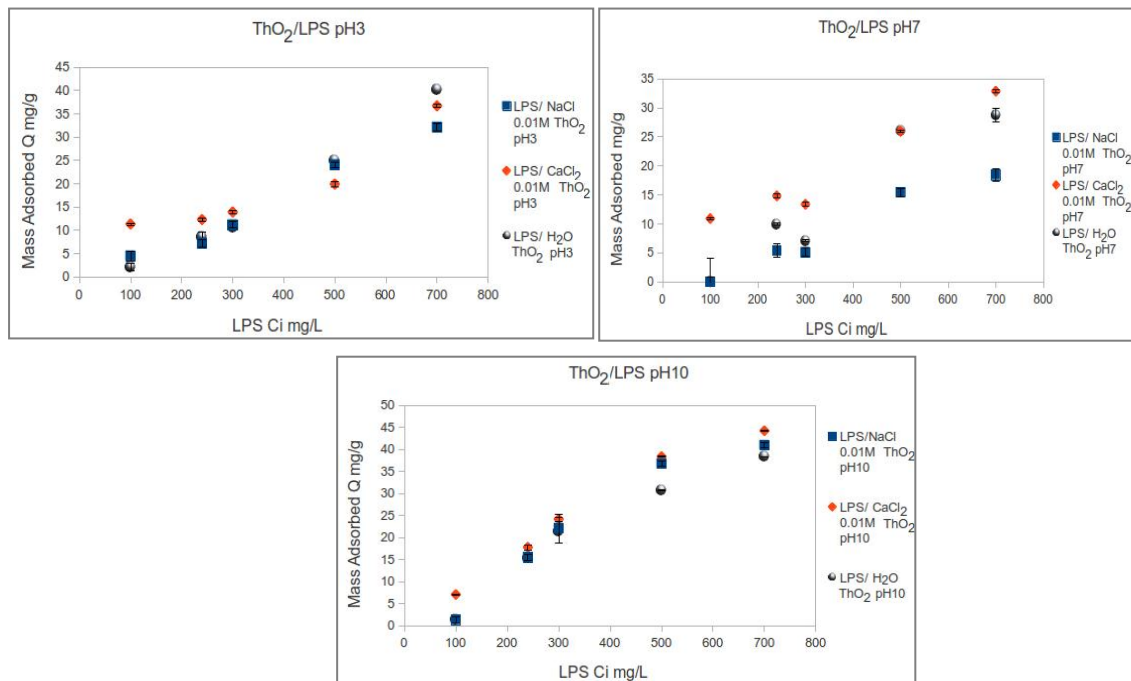
### **2.3.5.2 Experimental Isotherms for sorption of LPS onto thoria**

The Purpald Assay was used to quantify LPS before and after its interaction with the thoria. Thorium oxide, the mineral form of which is known as thoria, is a typical nuclear fission reactant and a by-product of lanthanide and uranium production. Th(IV) biosorption by *Mycobacterium smegmatis* under acidic conditions has been previously reported with values comparable to those of  $[\text{UO}_2]^{2+}$  with the same organism (Andres *et al.*, 1993). Yong and Macaskie have also reported the ability of *Mycobacterium smegmatis* to mediate the removal of Thorium as an insoluble phosphate precipitate (Young and Macaskie, 1995).

Thoria ( $\text{ThO}_2$ ) is a cubic oxide, very similar to urania (Davis, 1965). The point of zero charge ( $p_{zc}$ ) of thoria is  $\text{pH}=8$  (Olsoon *et al.*, 2002). The  $\text{pH}$  at point of zero charge suggests that

the mineral exhibits a positive charge below pH 8 and a negative charge above pH 8. By examining systems of pH3, pH7 and pH10 all different situations with thoria being negatively charged, positively charged and close-to-neutral are accessed.

The LPS concentration used for all the cases was higher than the CMC; this was intended to represent the cell-bound form of LPS with the assumption that only the O-antigen region of the molecule is exposed for interaction with the minerals (more information in sub-section 2.1.1.1). The isotherm constructed for the thoria-LPS interaction at pH3 is shown at figure 2.29. The mass adsorbed is represented by 'Q' ( $\text{mg g}^{-1}$ ).



Figures 2.29- 2.31. Isotherm of LPS- ThO<sub>2</sub> interactions at pH3 (fig. 2.29-left), pH7 (fig. 2.30-right) and pH10 (fig. 2.31-middle).

In the case of experiments conducted at pH3 (figure 2.29) water was the electrolyte with the highest maximum mass of LPS adsorbed. According to the zero point of charge of thoria, at pH3 the surface of thoria is positively charged and the surface of LPS is neutral to slightly-negatively charged. This suggests that sorption would occur spontaneously due to the attraction of opposite charges, with no need for bridging ions (i.e. Ca<sup>2+</sup> ions) to mediate the adhesion process.

In the case of experiments conducted at pH7 (figure 2.30) where the surface is positively charged, a similar behavior with the pH3 adhesion profile was observed. The results for the inclusion of NaCl in the system suggested a lower adsorption of LPS on the surface. The  $\text{Ca}^{2+}$  containing system resulted in the highest LPS adsorption with the water containing system closely following.

In the case of experiments conducted at pH10 (figure 2.31), it was observed that LPS in water, in NaCl and in  $\text{CaCl}_2$  behave similarly with all cases showing a positive adsorption of LPS onto thoria. This is in contrast with the rest of the tested surfaces (ceria and europium oxide) where a different adsorption profile was observed for the  $\text{CaCl}_2$  case. Experiments conducted at high pH conditions represented a scenario where the thoria was negatively charged when in contact with a partly negatively charged LPS.

The sorption profiles obtained for LPS interactions with thoria were slightly different from the ones obtained for ceria and europium oxide. The difference arises mainly because of the difference in surface charge coming from the different point of zero charge of the minerals. This shows that the surface charge plays a key role in the sorption processes when LPS is approaching a surface and underlines the importance of appropriate pH conditions for a successful interaction.

All the obtained results indicate a clear sorption profile at acidic, neutral and basic pH conditions with a preference for sorption to occur in solutions that contain divalent cations (specifically  $\text{Ca}^{2+}$ ) under neutral conditions. Both water and sodium chloride showed a similar sorption profile which suggests that the two electrolytes can also mediate the interaction under specific conditions. In acidic environments, all the electrolytes resulted in high LPS masses adsorbed with very small differences. This suggests that thoria attracts the macromolecule strongly and the pH dependent conformational changes of LPS do not stop sorption from happening. This is in contrast with the results obtained for ceria and europium oxide where a clear distinction between the sorption of LPS in the presence of the different electrolytes was concluded. A hypothesis arising from the above observations relates to the surface charge of thoria. Previous work on the

behavior of thorium under aqueous solutions (0.01mol/L NaCl) suggested the presence of thorium hydroxide at the extent of 20% of the XPS accessible near the surface region of the solid (Vandenborre *et al.*, 2010). This suggests that at the pH conditions tested, the adhesion of LPS was controlled by thorium hydroxides rather than the bulk crystalline ThO<sub>2</sub>.

### 2.3.5.2.1 Equilibrium Modelling of LPS sorption onto Thoria

In order to describe the isotherms, Langmuir and Freundlich models were used. The Freundlich model, explained in sub-section 2.2.4.1 provided the highest R<sup>2</sup> scores (R<sup>2</sup>>0.9) and hence the K<sub>F</sub> and the n<sub>F</sub> values were calculated using the equation found in table 2.10. The fitting can be found in appendix 8. A summary of the resulting equations and the associated constants can be found at table 2.10.

| Table 2.10. Freundlich model-Results of LPS adsorption on thoria |  |                     |                     |               |                     |                |                |
|--|--|---------------------|---------------------|---------------|---------------------|----------------|----------------|
| ID   | Equation   | Y                   | X                   | Intercept     | Slope               | K <sub>F</sub> | n <sub>F</sub> |
| <b>Freundlich Model</b>  | $\ln(Q_e) = \ln(K_F) + \left(\frac{1}{n_F}\right)\ln(C_e)$ |                     |                     | $c = \ln K_F$ | $m = \frac{1}{n_F}$ | $e^c$          | $\frac{1}{m}$  |
| LPS/ThO <sub>2</sub> in NaCl pH10                                | y=0.8585x-1.195  | ln(Q <sub>e</sub> ) | ln(C <sub>e</sub> ) | -1.195        | 0.8585              | 0.304          | 1.165          |
| LPS/ ThO <sub>2</sub> in NaCl pH7                                | y=1.103x-3.243   |                     |                     | -3.243        | 1.103               | 0.542          | 0.907          |
| LPS/ ThO <sub>2</sub> in water pH7                               | y=1.131x-3.094   |                     |                     | -3.094        | 1.131               | 0.085          | 0.884          |
| LPS/ ThO <sub>2</sub> in CaCl <sub>2</sub> pH10                  | y=0.826x-0.796   |                     |                     | -0.796        | 0.826               | 0.439          | 1.211          |
| LPS/ ThO <sub>2</sub> in CaCl <sub>2</sub> pH7                   | y=0.567x+0.205   |                     |                     | +0.205        | 0.567               | 0.039          | 1.764          |
| LPS/ ThO <sub>2</sub> in water pH10                              | y=1.089x-2.523   |                     |                     | -2.523        | 1.089               | 1.227          | 0.918          |
| LPS/ ThO <sub>2</sub> in NaCl pH3                                | y=0.565x-0.613   |                     |                     | -0.613        | 0.565               | 0.045          | 1.770          |
| LPS/ ThO <sub>2</sub> in water pH3                               | y=0.722x-0.822   |                     |                     | -0.822        | 0.722               | 0.080          | 1.385          |
| LPS/ ThO <sub>2</sub> in CaCl <sub>2</sub> pH3                   | y=0.978x-2.462   |                     |                     | -2.462        | 0.978               | 0.451          | 1.023          |

Where C<sub>e</sub>=LPS concentration at equilibrium (mg L<sup>-1</sup>), Q<sub>e</sub>=equilibrium adsorption capacity (mg g<sup>-1</sup>), K<sub>F</sub>= Freundlich constant (L/g), n<sub>F</sub> = heterogeneity factor of adsorption sites.

The standard free energy change of adsorption ( $\Delta G$ ) can be correlated with each equilibrium concentration,  $C_e$ , as explained previously (sub-section 2.3.3.2.1). The standard free energy change of adsorption can be found at table 2.11.

| <b>ID</b>                                       | <b><math>K_f</math></b> | <b><math>K_c</math></b> | <b><math>\Delta G</math> (kJ/mol)</b> |
|---|-------------------------|-------------------------|---------------------------------------|
| LPS/ ThO <sub>2</sub> in NaCl pH10              | 0.304                   | 304                     | -14.031                               |
| LPS/ ThO <sub>2</sub> in NaCl pH7               | 0.542                   | 542                     | -15.447                               |
| LPS/ ThO <sub>2</sub> in water pH7              | 0.085                   | 85                      | -10.909                               |
| LPS/ ThO <sub>2</sub> in CaCl <sub>2</sub> pH10 | 0.439                   | 439                     | -14.934                               |
| LPS/ ThO <sub>2</sub> in CaCl <sub>2</sub> pH7  | 0.039                   | 39                      | -8.994                                |
| LPS/ ThO <sub>2</sub> in water pH10             | 1.227                   | 1127                    | -17.454                               |
| LPS/ ThO <sub>2</sub> in NaCl pH3               | 0.045                   | 45                      | -9.356                                |
| LPS/ ThO <sub>2</sub> in water pH3              | 0.080                   | 80                      | -10.761                               |
| LPS/ ThO <sub>2</sub> in CaCl <sub>2</sub> pH3  | 0.451                   | 451                     | -14.998                               |

The negative  $\Delta G$  values indicate a spontaneous reaction between thoria and LPS. It is observed that the energy values obtained for the adsorption are very close numerically, ranging from  $\sim -8$  kJ mol<sup>-1</sup> to  $\sim -17$  kJ mol<sup>-1</sup> for all the systems tested. These values are in the range of physisorption ( $-40$  to  $0$  kJ mol<sup>-1</sup>) which was further examined with the  $n_F$  values obtained from the Freundlich equation.

Freundlich's parameter  $n_F$  is often used as an indication of the 'intensity' of the adsorption. A value of  $n_F$  less than 1 indicates a chemisorption,  $n_F=1$  shows a linear adsorption and  $n_F > 1$  has been related to physical processes (Bhatt *et al.*, 2012). The resulting values of  $n_F$  for this study were interesting, ranging from 0.9 to 1.7 which suggests a different adsorption process for each pH condition or electrolyte used. Chemisorption is involved in the cases where new chemical bonds are formed while physisorption involves intermolecular forces such as Van der Waals. No absolute

distinction can be made between the two and processes involving strong hydrogen bonding are considered as 'intermediate' cases (Bhatt *et al.*, 2012). This suggests that a range of processes occur which involves a synergistic interaction of both physical and chemical interactions to favor the binding of LPS to thoria. It is also hypothesised that the above results are related to thoria hydroxides that are present on the thoria surface under varying pH conditions and hence, the adhesion of LPS in some cases was controlled by the hydroxides (Vandenborre *et al.*, 2010).

### 2.3.5.3 Kinetics

The Purpald assay was used to quantify LPS at different times and constant concentration, in order to access the kinetics of the interaction. The different kinetics of each reaction according to the corresponding pH conditions are shown in figure 2.32. The results were very similar for all samples tested hence, only three samples are shown for clarity. The rest of the results can be found in appendix 9.

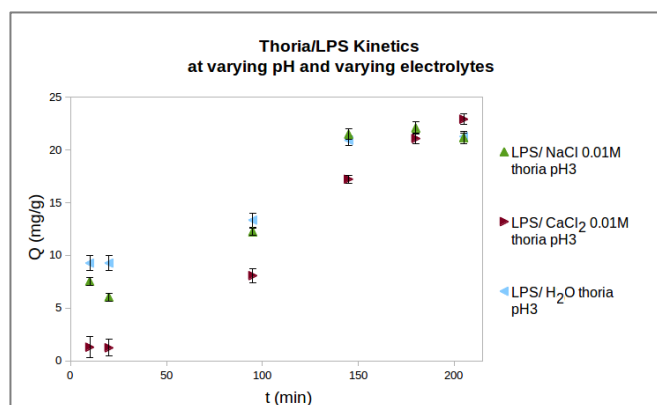


**Figure 2.32. Kinetics of LPS- thoria interactions at pH3.**

From figure 2.32, it can be observed that all three electrolytes successfully mediated the interaction between thoria and LPS with a plateau reached after a ~175 min interaction.

Kinetic data was analysed using pseudo-first order and pseudo-second order models. A linear fit ( $R^2 > 0.99$ ) was obtained for a pseudo-second order reaction as previously described (subsection 2.3.3.3). A plot of  $t/Q_t$  Vs Time was used for evaluation of the rate constant of the interaction as shown in figure 2.33 and table 2.12. The results were very similar for all cases of LPS-ThO<sub>2</sub> complexes hence, only some characteristic examples are shown for clarity. The rest of the results can be found in appendix 10.

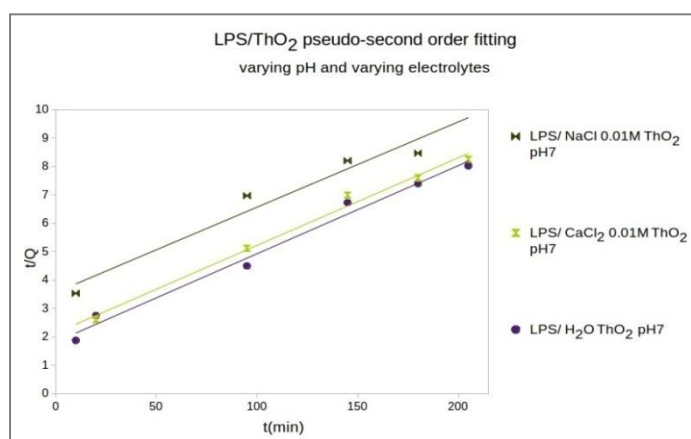


Figure 2.33. Pseudo-second order fitting of LPS- thoria interactions at pH7.

| Table 2.12. Results of kinetic analysis of LPS adsorption to thoria |                   |                        |                 |                             |  |
|---|-------------------|------------------------|-----------------|-----------------------------|--|
| ID  | Equation $y=Mx+C$ | Intercept $C=1/kQ_e^2$ | Slope $M=1/Q_e$ | $Q_e = 1/m$<br>$mg\ g^{-1}$ | $K = 1/(CQ_e^2)$<br>$*10^{-3}\ g\ mg^{-1}\ min^{-1}$ |
| LPS/ ThO <sub>2</sub> NaCl pH10                                     | $Y=0.032x+0.975$  | 0.975                  | 0.032           | 30.767                      | 1.083  |
| LPS/ ThO <sub>2</sub> CaCl <sub>2</sub> pH10                        | $Y=0.035x+0.755$  | 0.755                  | 0.035           | 28.701                      | 1.608  |
| LPS/ ThO <sub>2</sub> water pH10                                    | $Y=0.035x+0.820$  | 0.820                  | 0.035           | 28.890                      | 1.462  |
| LPS// ThO <sub>2</sub> NaCl pH3                                     | $Y=0.042x+0.839$  | 0.839                  | 0.042           | 23.930                      | 2.082  |
| LPS/ ThO <sub>2</sub> water pH3                                     | $Y=0.039x+1.004$  | 1.004                  | 0.039           | 25.633                      | 1.515  |
| LPS/ ThO <sub>2</sub> NaCl pH7                                      | $Y=0.030x+3.563$  | 3.563                  | 0.030           | 33.312                      | 0.253  |
| LPS/ ThO <sub>2</sub> CaCl <sub>2</sub> pH7                         | $Y=0.031x+2.134$  | 2.134                  | 0.031           | 32.424                      | 0.446  |
| LPS/ ThO <sub>2</sub> water pH7                                     | $Y=0.031x+1.820$  | 1.820                  | 0.031           | 32.212                      | 0.529  |

The theoretical values of  $Q_e$  were slightly higher than the experimentally obtained values and range from 23 to 33 mg of LPS adsorbed per gram of mineral with LPS, approximately  $5 \text{ mg g}^{-1}$  higher than expected. This might be arising from systematic errors done during the experimental procedures or due to incomplete construction of the kinetics profile. Nevertheless, the sorption profiles obtained for the LPS interactions with thoria suggested a strong sorption interaction under neutral conditions in the presence of calcium ions and a strong sorption interaction under acidic and basic conditions without the need of any charged ions (represented by water as the electrolyte). This is in contrast with the sorption profiles obtained for the ceria and europium oxide systems where calcium resulted in the highest adsorbed mass of LPS under basic conditions while under acidic conditions, all three minerals showed successful sorption profiles (highest adsorbed mass of LPS) when water was used as the electrolyte. A comparison of the results obtained for the three surfaces is discussed in section 2.3.7.

## **2.3.6 Adsorption of LPS onto urania**

### **2.3.6.1 Quantification of LPS- Calibration curve**

Experimental LPS uptake kinetics onto urania were calculated using the Purpald assay (sub-section 2.2.4.2) for quantification of LPS before and after the interaction. The same calibration curve constructed for the quantification of LPS described in sub-section 2.3.2.2 was used.

### **2.3.6.2 Experimental Isotherms for sorption of LPS onto urania**

The Purpald Assay was used to quantify LPS before and after its interaction with the urania surface. Urania is the most commonly used nuclear fission reactant. In addition,  $[\text{UO}_2]^{2+}$  biosorption by *Mycobacterium smegmatis* and other microorganisms has been previously reported (Andres *et al.*, 1993).

Urania ( $\text{UO}_2$ ) is a cubic oxide very similar to thoria (Sanjay-Kumar *et al.*, 2016). The point of zero charge ( $p_{zc}$ ) of urania is  $\text{pH}=4.8$  (Carlton and Laxen, 1966). The  $\text{pH}$  at point of zero charge suggests that the mineral exhibits a positive charge below  $\text{pH}$  4.8 and a negative charge above  $\text{pH}$  4.8. By examining systems of  $\text{pH}3$ ,  $\text{pH}7$  and  $\text{pH}10$  all different situations with urania being negatively charged, positively charged and close-to-neutral are accessed.

The LPS concentration used for all the cases was higher than the CMC; this was intended to represent the cell-bound form of LPS with the assumption that only the O-antigen region of the molecule is exposed for interaction with the minerals (more information in sub-section 2.1.1.1). The isotherm constructed for the urania-LPS interaction at  $\text{pH}3$  is shown at figure 2.34. The mass adsorbed is given in  $\text{mg g}^{-1}(Q_e)$ .

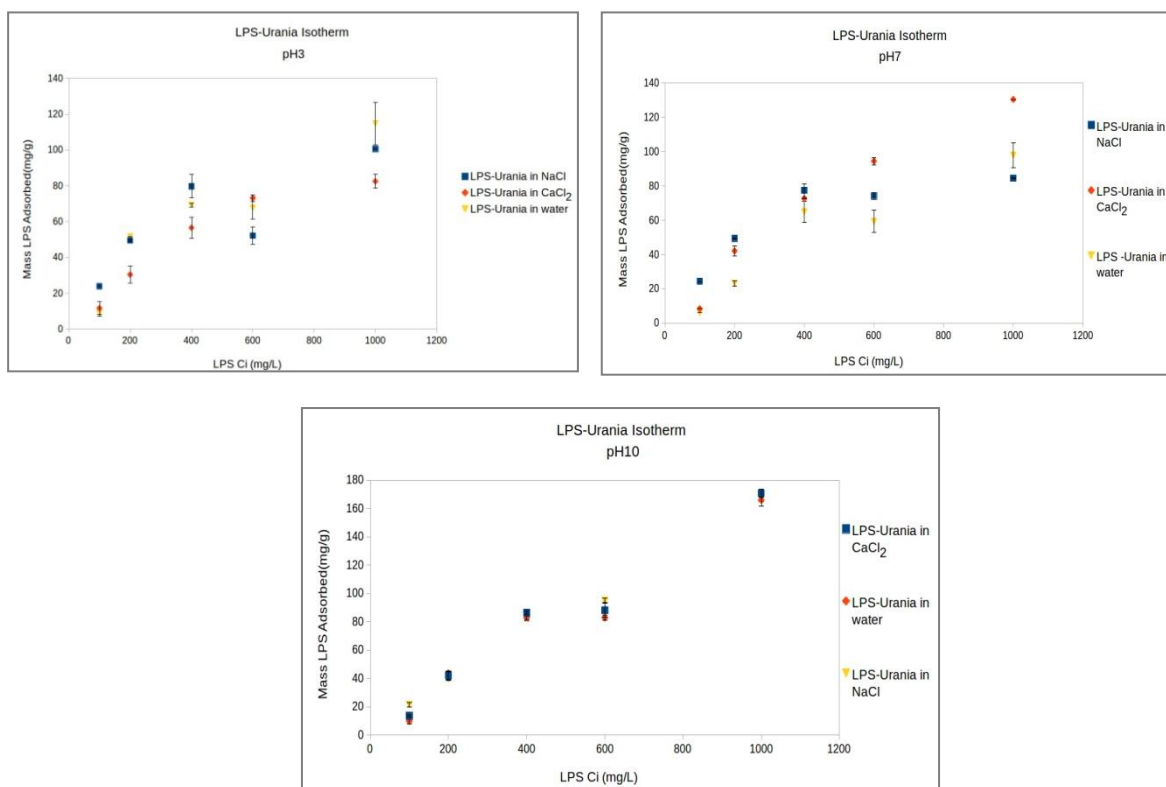


**Figure 2.34-2.36. Isotherm of LPS- urania interactions at  $\text{pH}3$  (fig. 2.34-left),  $\text{pH}7$  (fig. 2.35-right) and  $\text{pH}10$  (fig. 2.36-middle).**

Figure 2.34 summarises the results for the adsorption of LPS onto urania under acidic conditions (pH=3). In this case, water was the electrolyte with the highest maximum mass of LPS adsorbed. According to the zero point of charge of urania, at pH3 the surface of urania is positively charged and the surface of LPS is neutral to slightly- negatively charged which suggests that sorption would occur spontaneously due to the attraction of opposite charges, with no need for bridging ions (i.e.  $\text{Ca}^{2+}$  ions) to mediate the adhesion process. The observed results suggest that in highly acidic environments, inclusion of ions is not necessary for a sorption process to take place and LPS cannot adsorb onto urania with the same efficiency as it does at highly alkaline environments.

In the case of experiments conducted at pH7 where the surface is negatively charged (figure 2.35), a different behavior than the pH3 adhesion profile was observed. The results for the inclusion of NaCl in the system suggest a lower adhesion of LPS on the surface with  $\text{Ca}^{2+}$  giving the highest adsorption at the maximum concentration. Solvated LPS and LPS in the presence of  $\text{Na}^+$  showed very similar results which comes in agreement with the results obtained for the adsorption of LPS onto ceria and europium oxide.

In the case of experiments conducted at pH10 (figure 2.36), it was observed that LPS in water, in NaCl and in  $\text{CaCl}_2$  behave similarly with all cases showing a positive adsorption of LPS onto urania. This is in contrast with the results obtained for LPS adsorption onto ceria and europium oxide where a different adsorption profile was observed for the  $\text{CaCl}_2$  case. However, the results agree well with the sorption profiles obtained for LPS adsorption onto thoria. The high pH conditions here represented a negatively charged surface approached by a partly negatively charged molecule. The sorption profiles obtained for LPS interactions with urania were slightly different from the ones obtained for ceria and europium oxide but agreed well with the results obtained for thoria-LPS interactions. The difference arises mainly because of the difference in surface charge coming from the different point of zero charge of the minerals.

The interaction between LPS and urania was mediated with and without the presence of ions in solution even though a slightly higher mass of LPS per gram of urania was obtained for the case of water under acidic conditions. This suggests a strong attraction of the molecule by the surface independent of the ionic strength of the media. No preference on counter ions was observed under basic conditions, in contrast with the adsorption profiles of LPS onto ceria or europium oxide where divalent ions (calcium) were preferred. However, calcium was the counter ion that resulted in the highest LPS sorption onto urania under neutral conditions which comes in agreement with the case of LPS sorption onto thoria.

### 2.3.6.2.1 Equilibrium Modelling of LPS sorption onto Urania

In order to describe the sorption process, the Langmuir and the Freundlich isotherm models were used. The Freundlich model, explained in sub-section 2.2.4.1 provided the highest  $R^2$  scores ( $R^2 > 0.95$ ) and hence the  $K_F$  and the  $n_F$  values were calculated using the equation found in table 2.13. Characteristic examples of the fitting are found in figure 2.37. The rest of the data can be found in appendix 11. A summary of the resulting equations and the associated constants can be found at table 2.13.

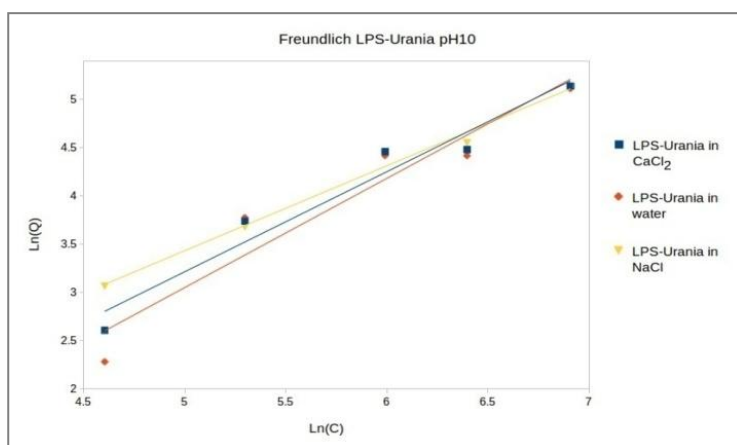


Figure 2.37. Example fitting on the Freundlich model for the adsorption of LPS onto Urania

| <b>ID</b>                                      | <b>Equation</b>   | <b>Y</b>            | <b>X</b>            | <b>Intercept</b> | <b>Slope</b>        | <b>K<sub>F</sub></b> | <b>n<sub>F</sub></b> |
|--|---|---------------------|---------------------|------------------|---------------------|----------------------|----------------------|
| <b>Freundlich Model</b>                        | $\ln(Q_e) = \ln(K_F) + \left(\frac{1}{n_F}\right) \ln(C_e)$ |                     |                     | $c = \ln K_F$    | $m = \frac{1}{n_F}$ | $e^c$                | $\frac{1}{m}$        |
| LPS/ UO <sub>2</sub> in NaCl pH10              | Y=0.880x-0.968  | ln(Q <sub>e</sub> ) | ln(C <sub>e</sub> ) | -0.968           | 0.880               | 0.380                | 1.136                |
| LPS/ UO <sub>2</sub> in NaCl pH7               | Y=0.528x+0.953  |                     |                     | +0.953           | 0.528               | 2.593                | 1.894                |
| LPS/ UO <sub>2</sub> in water pH7              | Y=1.169x-3.266  |                     |                     | -3.266           | 1.169               | 0.038                | 0.855                |
| LPS/ UO <sub>2</sub> in CaCl <sub>2</sub> pH10 | Y=1.037x-1.971  |                     |                     | -1.971           | 1.037               | 0.139                | 0.964                |
| LPS/ UO <sub>2</sub> in CaCl <sub>2</sub> pH7  | Y=1.132x-2.692  |                     |                     | -2.692           | 1.132               | 0.068                | 0.883                |
| LPS/ UO <sub>2</sub> in water pH10             | y=1.132x-2.609  |                     |                     | -2.609           | 1.132               | 0.074                | 0.883                |
| LPS/ UO <sub>2</sub> in NaCl pH3               | Y=0.533x+0.892  |                     |                     | +0.892           | 0.533               | 2.440                | 1.876                |
| LPS/ UO <sub>2</sub> in water pH3              | Y=0.973x-1.812  |                     |                     | -1.812           | 0.973               | 0.163                | 1.028                |
| LPS/ UO <sub>2</sub> in CaCl <sub>2</sub> pH3  | Y=0.857x-1.283  |                     |                     | -1.283           | 0.857               | 0.277                | 1.167                |

Where C<sub>e</sub>=LPS concentration at equilibrium (mg L<sup>-1</sup>), Q<sub>e</sub>=equilibrium adsorption capacity (mg g<sup>-1</sup>), K<sub>F</sub>= Freundlich constant (L/g), n<sub>F</sub> = heterogeneity factor of adsorption sites.

The standard free energy change of adsorption ( $\Delta G$ ) can be correlated with each equilibrium concentration, C<sub>e</sub>, as explained previously (sub-section 2.3.3.2.1). The standard free energy change of adsorption can be found at table 2.14.

| <b>Table 2.14. <math>\Delta G</math> calculations for LPS adsorption to urania</b> |                         |                         |                                       |
|--|-------------------------|-------------------------|---------------------------------------|
| <b>ID</b>  | <b><math>K_f</math></b> | <b><math>K_c</math></b> | <b><math>\Delta G</math> (kJ/mol)</b> |
| LPS/ $UO_2$ in NaCl pH10   | 0.380                   | 380                     | -8.295                                |
| LPS/ $UO_2$ in NaCl pH7  | 2.593                   | 2593                    | -13.639                               |
| LPS/ $UO_2$ in water pH7   | 0.038                   | 38                      | -3.286                                |
| LPS/ $UO_2$ in $CaCl_2$ pH10   | 0.139                   | 139                     | -6.464                                |
| LPS/ $UO_2$ in $CaCl_2$ pH7  | 0.068                   | 68                      | -4.695                                |
| LPS/ $UO_2$ in water pH10  | 0.074                   | 74                      | -4.898                                |
| LPS/ $UO_2$ in NaCl pH3  | 2.440                   | 2440                    | -13.489                               |
| LPS/ $UO_2$ in water pH3   | 0.163                   | 163                     | -6.854                                |
| LPS/ $UO_2$ in $CaCl_2$ pH3  | 0.277                   | 277                     | -8.152                                |

The negative  $\Delta G$  values indicate a spontaneous reaction between urania and LPS. It is observed that the energy values obtained for the adsorption are very close numerically, ranging from  $\sim -3$  kJ mol<sup>-1</sup> to  $\sim -13$  kJ mol<sup>-1</sup> with negative values obtained for all conditions. The negative  $\Delta G$  values are in the range of physisorption ( $-40$  to  $0$  kJ mol<sup>-1</sup>) similarly with the results obtained for the sorption of LPS to ceria.

Freundlich's parameter  $n_F$  is often used as an indication of the 'intensity' of the adsorption. A value of  $n_F$  less than 1 indicates a chemisorption,  $n_F=1$  shows a linear adsorption and  $n_F > 1$  has been related to physical processes (Bhatt *et al.*, 2012). The resulting values of  $n_F$  for this study were interesting, ranging from 0.8 to 1.8 which suggests a different adsorption process for each pH condition or electrolyte used. Chemisorption is involved in the cases where new chemical bonds are formed while physisorption involves intermolecular forces such as Van der Waals. No absolute distinction can be made between the two and processes involving strong hydrogen bonding are considered as 'intermediate' cases (Bhatt *et al.*, 2012). This suggests that a range of processes occur which involves a synergistic interaction of both physical and chemical interactions to favor the binding of LPS to urania. Previous work on the behavior of urania under aqueous solutions suggested that '*UO<sub>2</sub> will always react with water at room temperature and atmospheric pressure,*

leading to water dissociation' (Ulrich *et al.*, 2009). This suggests that water molecules near and on the surface of the mineral play a role in the adsorption processes that can take place when a biological molecule is approaching the surface. The results agree well with the sorption of LPS on Thoria as similar  $\Delta G$  and  $n_F$  values were obtained.

### 2.3.6.3 Kinetics

The Purpald assay was used to quantify LPS at different times and constant concentration of LPS, in order to assess the kinetics of the interaction. The different kinetics of each reaction according to the corresponding pH conditions are shown in figure 2.38. The mass adsorbed is shown with the value  $Q$  ( $\text{mg g}^{-1}$ ) The results were very similar for all samples tested hence, only three samples are shown for clarity. The rest of the results can be found in appendix 12.

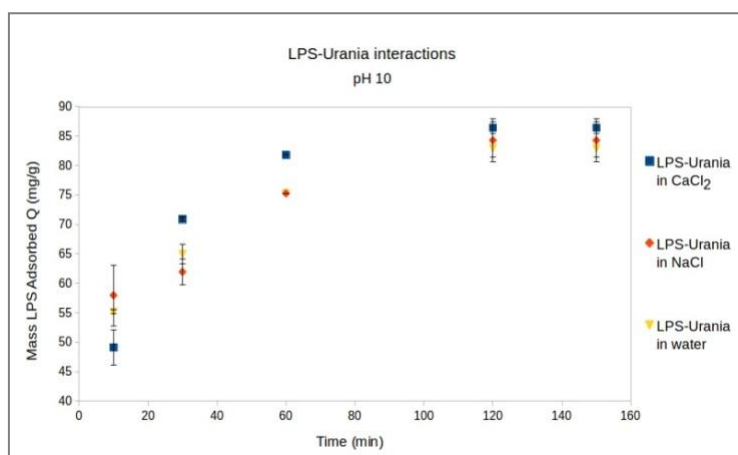


**Figure 2.38. Kinetics of LPS- urania interactions.**

From figure 2.38 it can be observed that all three electrolytes successfully mediated the interaction between urania and LPS with a plateau reached after a 120 min interaction. Kinetic data was analysed using pseudo first and pseudo-second order models. A linear fit ( $R^2 > 0.99$ ) was obtained for a pseudo-second order reaction as previously described (sub-section 2.3.3.3). A plot of  $\text{Time}/Q_t$  Vs Time was used for evaluation of the rate constant of the interaction as shown in figure

2.39 and table 2.15. The results were very similar for all cases of LPS-UO<sub>2</sub> complexes hence, only some characteristic examples are shown for clarity. The rest of the results can be found in appendix 13.

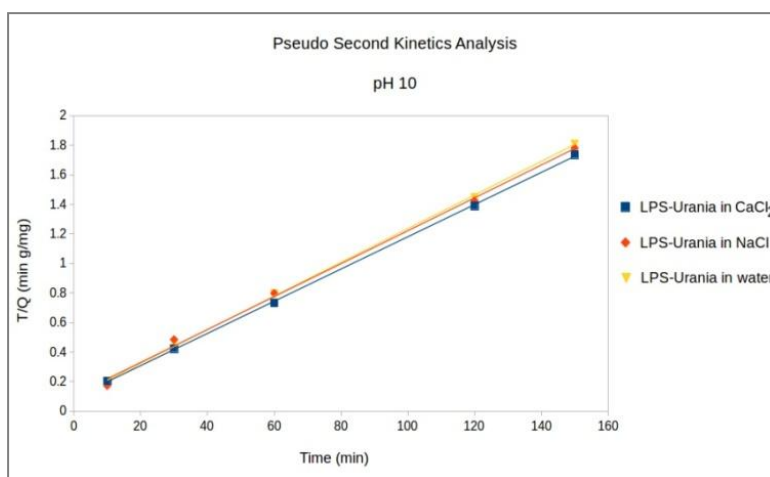


Figure 2.39. Pseudo-second order fitting of LPS- urania interactions.

| ID  | Equation $y=Mx+C$ | Intercept $C=1/kQ_e^2$ | Slope $M=1/Q_e$ | $Q_e = 1/m$<br>$mg\ g^{-1}$ | $K = 1/(CQ_e^2)$<br>$*10^{-3}\ g\ mg^{-1}\ min^{-1}$ |
|---|-------------------|------------------------|-----------------|-----------------------------|--|
| LPS/ UO <sub>2</sub> NaCl pH10              | $Y=0.011x+0.107$  | 0.107                  | 0.011           | 90.909                      | 0.001  |
| LPS/ UO <sub>2</sub> CaCl <sub>2</sub> pH10 | $Y=0.011x+0.090$  | 0.090                  | 0.011           | 90.909                      | 0.001  |
| LPS/ UO <sub>2</sub> water pH10             | $Y=0.011x+0.095$  | 0.095                  | 0.011           | 90.909                      | 0.001  |
| LPS/ UO <sub>2</sub> NaCl pH3               | $Y=0.009x+0.307$  | 0.307                  | 0.009           | 111.111                     | 0  |
| LPS/ UO <sub>2</sub> water pH3              | $Y=0.010x+0.361$  | 0.361                  | 0.010           | 100                         | 0  |
| LPS/ UO <sub>2</sub> CaCl <sub>2</sub> pH3  | $Y=0.015x+0.151$  | 0.151                  | 0.015           | 66.667                      | 0.001  |
| LPS/ UO <sub>2</sub> NaCl pH7               | $Y=0.009x+0.334$  | 0.334                  | 0.009           | 111.111                     | 0  |
| LPS/ UO <sub>2</sub> CaCl <sub>2</sub> pH7  | $Y=0.011x+0.201$  | 0.201                  | 0.011           | 90.909                      | 0.001  |
| LPS/ UO <sub>2</sub> water pH7              | $Y=0.015x+0.079$  | 0.079                  | 0.015           | 66.667                      | 0.003  |

The theoretical values of  $Q_e$  agree well with the experimentally obtained values and range from 66 to 111 mg of LPS adsorbed per gram of mineral. The sorption profiles obtained for the LPS interactions with urania suggested a strong sorption interaction under neutral conditions in the

presence of calcium ions and a strong sorption interaction under acidic conditions in the presence of  $\text{Na}^+$  and  $\text{H}^+$ .

## 2.3.7 Comparison of LPS sorption profiles

According to the point of zero charge of each surface (figure 2.40), all four surfaces were negatively charged under basic conditions (pH10) while LPS was also negative.

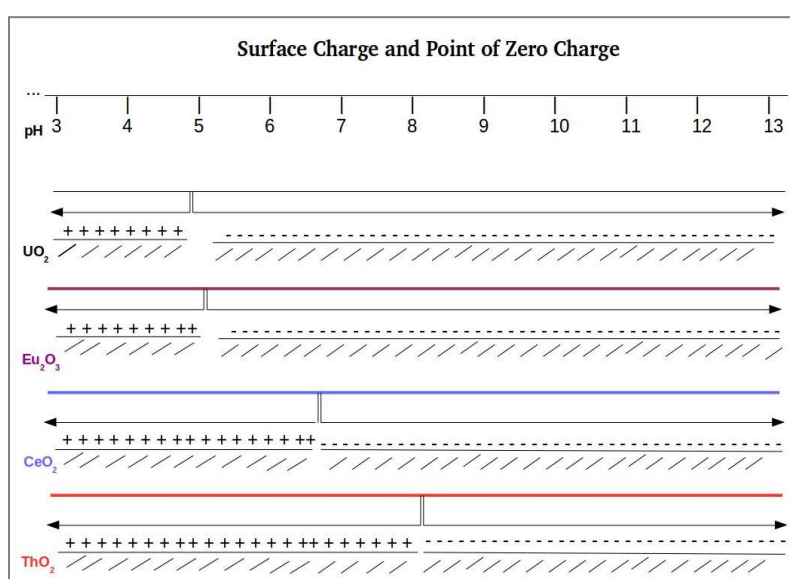
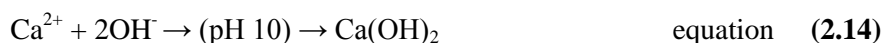


**Figure 2.40. Surface charge and point of zero charge of all minerals tested**

In the case where  $\text{Ca}^{2+}$  ions were tested for their ability to mediate the sorption of LPS onto the different surfaces under acidic conditions (figure 2.41), the systems were mainly mediated by non-ionic media (water) with the exception of ceria that showed a preference in sodium ions (even though the inclusion of sodium and water resulted in very similar sorption profiles). In acidic environments the availability of calcium ions in solution is enhanced due to the mobility of the ions that increases with increased availability of  $\text{H}^+$ . This promotes intermolecular interactions within the LPS molecules which result in inability of specific sites of the molecule to interact with the approaching minerals. It has been previously suggested that ions promote intermolecular interactions by the 'bridging' phenomenon where the cation acts as the middle charged species that

connects two similarly charged functional groups (Parikh and Chorover, 2007). It is hypothesised that due to the high availability of divalent ions that can act as the bridging agents for intermolecular binding within the LPS, the sorption onto minerals decreases with decreasing pH (and hence increasing mobility of the ions). However, the results for adsorption under basic conditions suggest that divalent ions are able to mediate the sorption process under basic conditions. All four systems with a negatively charged LPS molecule approaching a negatively charged surface resulted in a strongly adsorbed molecule when calcium ions were present in solution suggesting that charged ions are necessary for a stronger interaction (figure 2.42). The speciation of  $\text{Ca}^{2+}$  in solution under basic conditions suggests a limited availability of the ions due to limited mobility under such conditions where  $\text{OH}^-$  are present. The ion availability under such conditions is controlled by the concentration of  $\text{OH}^-$  that leads to the formation of  $\text{Ca}(\text{OH})_2$  according to equations (2.13) and (2.14).  $\text{Ca}(\text{OH})_2$  stays partly dissolved in the aqueous solution which suggests a limited availability of the divalent cations while a vast majority of the previously mobile cations is removed by  $\text{OH}^-$ .



The above observation suggests that the ions are useful for the interactions but intermolecular binding has a kinetic advantage when in acidic conditions. The fact that water showed higher sorption of LPS onto europium oxide, urania and thoria under acidic conditions supports the above statement as the absence of ions promoted the sorption process and limited intermolecular bonding due to ions. Furthermore, the presence of sodium ions in solution with LPS was previously found to result in similar conformations to that of solvated LPS. This suggests that sodium does not promote intermolecular binding in the same extent calcium does which explains why sodium resulted in the highest mass of LPS on ceria under acidic conditions. This is in agreement with previous studies that supported a similar behavior of LPS when in sodium containing solutions and water (Parikh and Chorover, 2008).

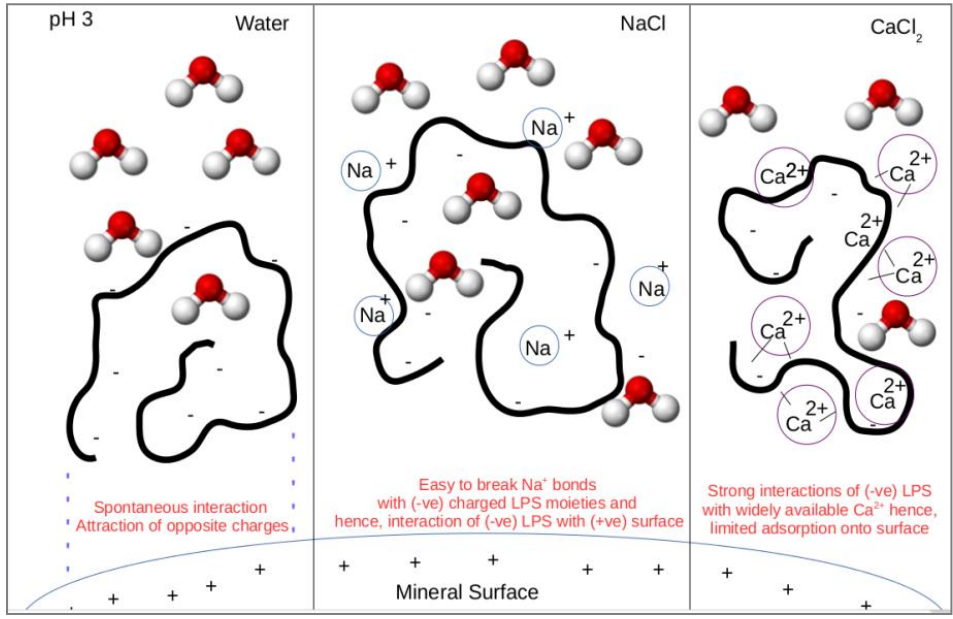


Figure 2.41. LPS sorption onto minerals under acidic conditions

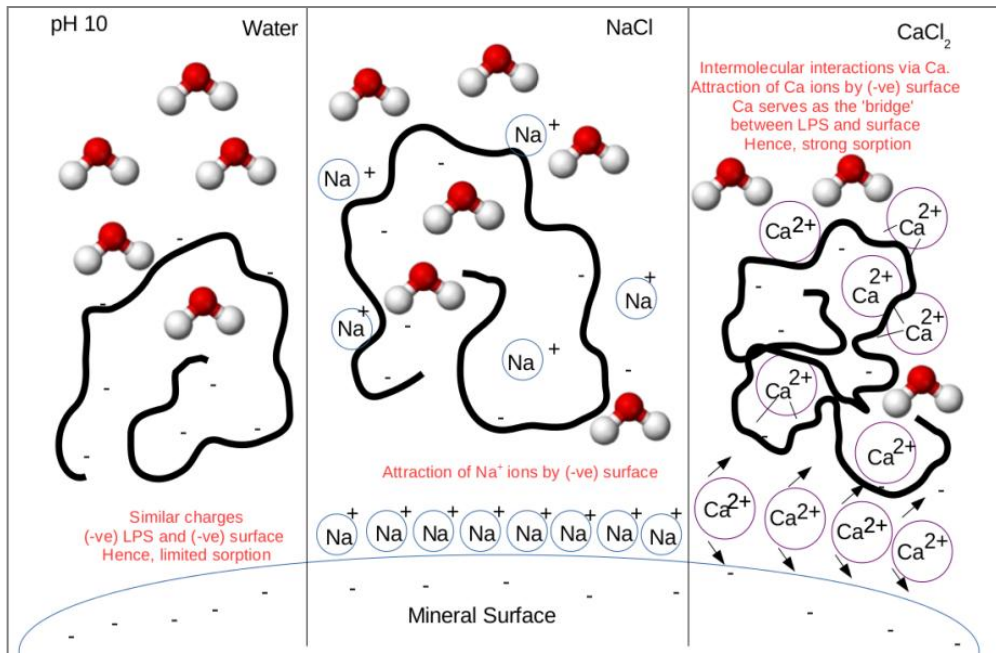


Figure 2.42. LPS sorption onto minerals under basic conditions

## 2.4 Conclusions

The observed ability of bacteria to interact with nuclear-related surfaces via different mechanisms suggests that bacteria could be used for processing and possible recovery of such matter. Here the interaction of bacterial components hypothesised to play a role in such interactions with four different nuclear-related oxides: ceria, thoria, europium oxide and urania, is considered. This work has been the first to examine the interaction of LPS as a unity with the mentioned surfaces and a review of the current literature suggests that there hasn't been any other published work similar to the one presented here.

Tests on europium oxide, ceria, urania and thoria confirmed that lipopolysaccharide, found on the outer site of Gram negative bacterial cells, follows a clear sorption mechanism in order to interact with all four surfaces under varying conditions. The Purpald assay confirmed the attachment of the biopolymers to the oxide surfaces and ATR-FTIR results showed specific involvement of C-O and PO<sub>2</sub> groups.

Lipopolysaccharides are not only found as components of live bacteria but they are also freely available in natural systems because of cell lysis and turnover. Hence, the results of LPS sorption onto minerals especially at the mineral/water interface with or without counter ions (such as calcium and sodium which are widely available in the environment) are very important not only for bacterial applications as a whole but also for LPS as a separate component.

LPS was found to behave similarly for all four surfaces (ceria, thoria, urania and europium oxide) mainly under basic conditions where the availability of cations is limited by the increased availability of OH<sup>-</sup>. Under acidic conditions, sorption of LPS onto ceria was proved quite complex. Even though experiments using thoria and europium oxide as the adsorbates showed better sorption capacities under acidic conditions compared to those resulting from ceria and urania, a general conclusion involved intermolecular binding induced by the increased mobility of cations in solution. This resulted in limited sorption of the biomolecule onto the surfaces. Sodium containing

samples were found to behave similarly to the non-ionic samples (samples containing only water) which supports previously published work that involved sorption profiles of LPS onto varying other surfaces (Parikh and Chorover, 2008). In general, water was found to mediate sorption better under acidic conditions while calcium chloride was found to mediate sorption better under basic conditions. This suggests that intermolecular binding due to enhanced availability of cations has a kinetic advantage over sorption to external minerals. Nevertheless, calcium was found to mediate the interaction under basic conditions which suggests that even though high concentrations of the cation (under acidic conditions) prevent sorption from happening, controlled concentrations of the ion (under basic conditions) can mediate the interaction more successfully than sodium ions or no ions.

# **Chapter 3**

## **Mycolic acid interactions with nuclear related materials**

## 3.1 Introduction

The findings of sorption of mycolic acid (MCA) to nuclear related materials are presented here. MCA was previously found to play a role in bacterial interactions with surfaces. More specifically, minerals synthesised during biomineralisation were found to stay located close to MCA (Lloyd *et al.*, 2002; Burgos *et al.*, 2008).

MCA is almost exclusively found in a distinct group of Gram positive bacteria that includes the genus of *Mycobacteria*, *Nocardia*, *Rhodococci* and *Corynebacteria*, known as the *Mycolates*. Since it is not found in other bacteria, MCA is an ideal candidate for the identification of any differences in the adsorption mechanisms used by the different types of microbes. In addition, the main reason to use MCA was that it is a simple molecule that contains one end carboxylic acid group, often responsible for the interactions of the molecule with its surroundings (Zhang *et al.*, 2010). These characteristics make it an ideal molecule to (a) use in a comparative

study between laboratory and computational experiments and (b) provide insight on the behavior of acid moieties from bacteria surfaces.

An example of MCA being the major component of the outer layer of the bacterial cell is *Rhodococcus* where 40% of the cell wall consists of MCA molecules (Brennan and Nikaido, 1995). Due to the highly hydrophobic character of MCAs, *Rhodococci* cells adapt an overall hydrophobic behavior which results in unique abilities such as adhesion at the oil/water interface. This hydrophobicity also allows the cells to approach and finally degrade a wide range of organic compounds including monoaromatic and polyaromatic hydrocarbons, an ability of great use in bioremediation processes (Das and Chandran, 2011). Another example of MCA containing-species is *Mycobacterium tuberculosis*. It is known as a pathogenic bacterium that was related to infectious diseases and is a highly antibiotic resistant strain. MCA was found to compose ~40% of the dry weight of the bacterium and was associated with the resistance the bacterium shows to antibiotics (Hong and Hopfinger, 2004).

MCA was firstly identified as a high-molecular weight hydroxy acid of the human *Tubercle bacillus* by Anderson in 1938 (Stodona *et al.* 1938; Anderson, 1939; Anderson, 1941; Anderson, 1943). Due to the limited structural information available at the time, the molecule was thought of as a single component of the bacterium; it was later found that there are approximately 500 chemically-related structures, identified within the different bacterial cell walls. The first extensive review on the structural and physiological characteristics of the molecule came around in 1982 by Minnikin (Minnikin, 1982).

MCAs come in various forms. Each form contains a basic  $\beta$ -hydroxy- $\alpha$ -alkyl branched structure and carbon chains of different lengths and different functional groups according to which of the various forms are distinguished. The three major MCAs known are: (a) alpha mycolates, (b) methoxy-mycolates and (c) keto-mycolates (shown in figure 3.1).

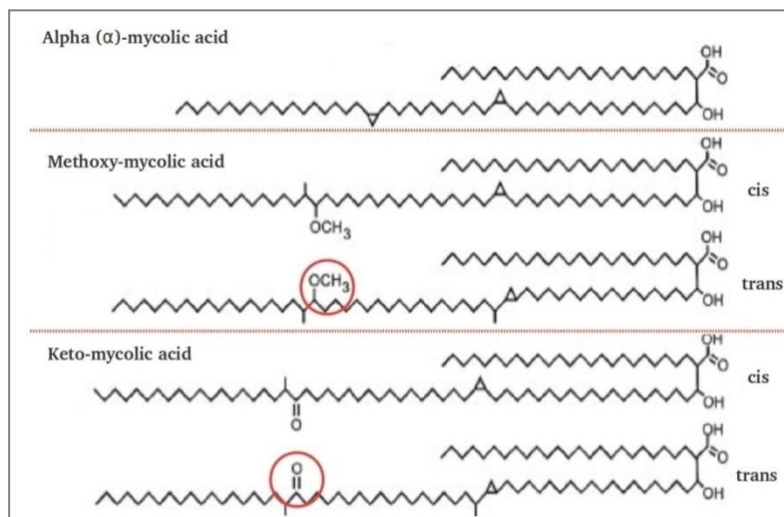


**Figure 3.1. The three major forms of MCA**

Different mycolic-containing species can be characterised according to the number of carbon atoms present in the molecule. This difference is usually assayed by reverse-phase HPLC and an example of the difference in the identified number of carbons is shown in table 3.1.

| Genus                 | Total No. of Carbons | Number of double bonds | A-branch (cont. C atoms) |
|-----------------------|----------------------|------------------------|--------------------------|
| <i>Gordona</i>        | 18-66                | 1-4                    | 16-18                    |
| <i>Mycobacteria</i>   | 60-90                | 2                      | 20-26                    |
| <i>Rhodococcus</i>    | 34-48                | 0-4                    | 12-18                    |
| <i>Nocardia</i>       | 44-60                | 0-3                    | 12-18                    |
| <i>Tsukamurella</i>   | 64-78                | 1-6                    | 20-22                    |
| <i>Corynebacteria</i> | 22-36                | 0-2                    | 14-18                    |

### 3.1.1 Adsorption of MCA onto surfaces

A recent experimental study on the adhesive and conformational behavior of MCA involving both hydrophobic and hydrophilic surfaces was conducted by Zhang *et al.* in 2010. The results indicated that the behavior of the molecule, not only depends on the polarity of the

approaching surfaces but also possess a strong relationship with the pH conditions of the surroundings. The adhesion capability of MCA was found to be controlled by the molecule's conformation at varying pH conditions with suggests that an interaction may or may not occur depending on the presence or absence of protons in solution. Water molecules were found to play a vital role in the adhesion mechanism and also the conformation adapted by the molecule which suggests that special attention should be given to the quantity of water in solution (Zhang *et al.*, 2010). Another study examining macromolecule adhesion onto surfaces involved polyacrylic acid, a polymer that contains carboxylic acid functional groups similar to that of MCA. This study included both experimental and computational results and showed a dependence of the adhesion process on the pH conditions introduced. The conformation of the molecule was once again found to play a key role in the interaction. The presence of counter ions was underlined and a point was made for the importance of flexibility of the macromolecules in the binding with surfaces (Sparks *et al.*, 2015).

Even though extensive research was carried out in order to evaluate the interactions of other biomolecules with surfaces, there is only a limited number of published works related to the sorption of MCA. A possible explanation relates to the hydrophobic character of the molecule that does not allow for any aqueous systems to be involved in the experiments. Hence, a more complex situation arises and different than the traditional techniques for evaluation of such processes are needed.

### **3.1.2 Extraction and Purification Techniques for MCA**

MCAs are found strongly bound to the cell wall or loosely-associated with the cell bound matrix (Barry *et al.*, 1998). The non-covalently bound MCAs can be easily extracted with a mixture of organic solvent and methanol while the bound molecules can be removed when the cells are treated under alkaline conditions. Purification can be accessed by Thin Layer Chromatography

(TLC) and characterization of the different forms of MCA can be accessed by Infrared Spectroscopy (IR), proton and carbon Nuclear Magnetic Resonance (NMR), various chromatographic techniques including High Performance Liquid Chromatography (HPLC) and Liquid Chromatography (LC) and also Mass Spectrometry. An example of purified MCAs from *Mycobacterium tuberculosis* is shown in figure 3.2 where the three spots represent the three forms of MCA according to increasing polarity (mycolates (a), methoxy-mycolates (M) and keto-mycolates (K)).

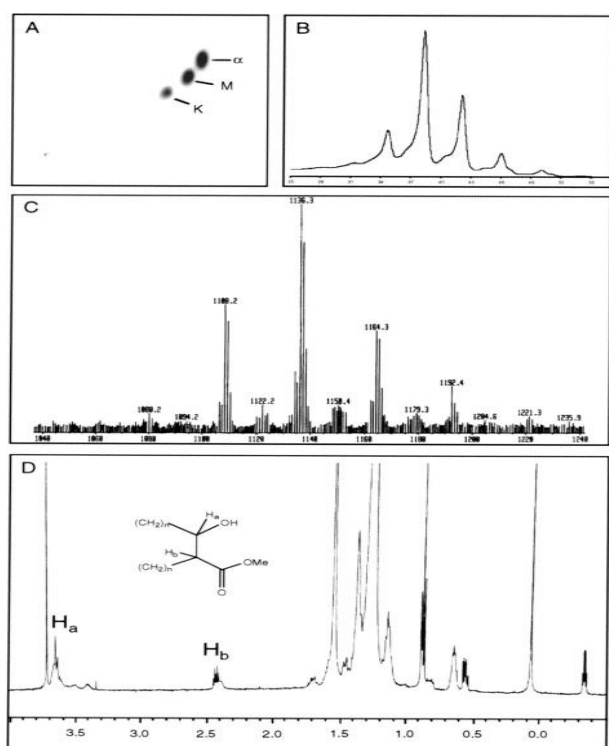


Table 3.2. MS – Characterization of the MCAs. Adapted from Cantrell *et al.*, 2012

| Mycolic Acid | Theoretical (a)* | Theoretical (b)* | Theoretical (c)* |
|--------------|------------------|------------------|------------------|
| Alpha        | 1136.1669        | 395.4            | 367.3            |
| Keto         | 1264.2870        | 395.4            | -                |
| Methoxy      | 1252.2870        | 395.4            | 367.3            |

\*Theoretical m/z from known elemental compositions

**Figure 3.2.** Basic characteristics of MCAs from *Mycobacterium tuberculosis*. (A) TLC purification – separation based on polarity (top to bottom). (B) Reverse-phase HPLC analysis of purified  $\alpha$  mycolates. (C) Mass Spectrum of  $\alpha$  mycolates shown in B. (D) Proton NMR from B. (Barry *et al.*, 1998)

Table 3.2 and figure 3.2 summarise the theoretical peaks observed when MCA is analysed with mass spectrometry (MS). The actual MCA fragments separated during MS analysis are shown in figure 3.3.

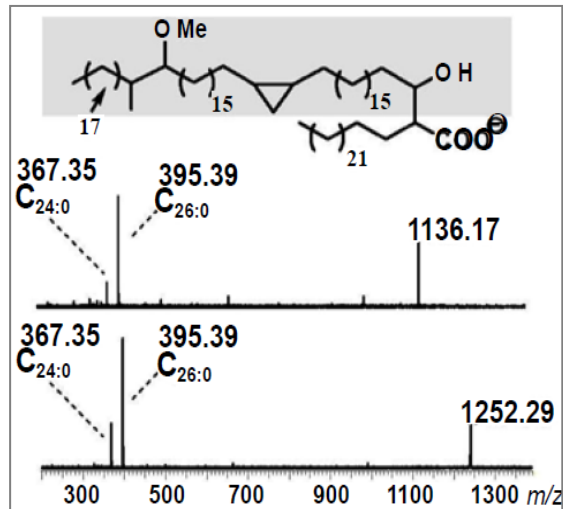


Figure 3.3. Theoretical peaks of MCA produced ions when analysed with mass spectrometry (Cantrell *et al.*, 2012). MS analysis of the alpha (m/z 1136.17; top) and methoxy (m/z 1252.29; bottom) MCAs; in each case meromycolate chain (grey portion) is lost as a neutral fragment and charge is retained on the alpha chain.

### 3.1.3 Objectives

The aim of this work was to examine the interaction of MCA with nuclear related materials at varying pH conditions and in the presence of different counter ions in order to examine whether a universal rule can be drawn for the adhesion of carboxylic acid from bacterial origin onto minerals. Non-radioactive surfaces were selected for this part of the project due to the limited availability of analytical instrumentation that allowed the analysis of radioactive materials. The surfaces chosen were: (a) ceria as the analogue of various nuclear-related minerals and (b) europium oxide as a by-product of the uranium fission process. The interaction was tested using experimental techniques (mass spectrometry and ATR-FTIR) and was further examined by computational techniques discussed in chapter 5.

## **3.2 Materials and Methods**

### **3.2.1 Chemicals**

All chemicals were purchased from Sigma-Aldrich (UK) and were of analytical grade unless stated otherwise. Double distilled water was used for all the experiments. All experiments were conducted at least in triplicate and the values reported here are average values of at least 3 results. Variation in these results is given as standard deviation and standard error values.

### **3.2.2 Macromolecules**

The only commercially available MCA came from *Mycobacterium tuberculosis* and the alternative method would require the extraction of MCAs from bacterial cells. In order to simplify the experimental procedures, mycolic acid (from *Mycobacterium tuberculosis* bovine strain), was purchased from Sigma-Aldrich and used as received. Stock solutions of MCA dissolved in a chloroform/methanol (9:1) solution in the presence of water, 0.01M NaCl or 0.01M CaCl<sub>2</sub> were

prepared before any analysis. The pH was adjusted to 3, 7 or 10 with 0.01M HCl or 0.01M NaOH. All stock solutions were vortexed, sonicated for 10 min, and stored overnight at 4 °C before re-equilibration the following day at room temperature.

### **3.2.3 MCA solubility tests**

MCA is not soluble in water and therefore solubility tests were conducted using MCA to provide essential understanding of experimental conditions. Aliquots of ~0.5 mg of MCA were transferred into 20 ml glass tubes. Addition of 100 µL volumes of the solvent (list shown in table 3.2) followed. The tubes were mixed well. When dissolution was not observed, up to 30 x additions of the solvents were introduced.

### **3.2.4 Minerals**

Two different minerals/solids were used in this study: europium oxide  $\text{Eu}_2\text{O}_3$  and ceria  $\text{CeO}_2$ . Both  $\text{Eu}_2\text{O}_3$  and  $\text{CeO}_2$  were purchased from Sigma-Aldrich (UK). X-ray Diffraction (XRD) analysis on the X'Pert<sup>3</sup> Powder by PANalytical on reflection mode for 15 minutes was used for characterization of the materials which were compared to known PDF cards from the literature (details in sub-section 2.3.2.2).

### **3.2.5 Method for MCA-Mineral Interactions**

A similar experiment to the one carried out for the LPS interactions (sub-section 2.2.4) was designed to examine the adsorption of MCA on europium oxide and ceria at different pH and ionic strength conditions including  $\text{CaCl}_2$ , NaCl and  $\text{H}_2\text{O}$ . Sample portions of  $2 \pm 0.5$  mg of ceria or

europium oxide were weighed and transferred in glass tubes with 150  $\mu\text{L}$  of 0.01M NaCl, 0.01M  $\text{CaCl}_2$  or water. The pH of the individual samples was adjusted with 0.01M HCl or 0.01M NaOH and the samples were left to equilibrate for 24 hours. After the 24-hour equilibration time, the samples were tested to ensure the pH remained the same and 150  $\mu\text{L}$  of 2mg/mL MCA dissolved in a mixture of chloroform/methanol (9:1) were added to the tubes. The only difference with the LPS experiments was that the MCAs were dissolved in a chloroform/methanol solution to increase the MCA solubility in water and mimic the hydrophobic character exhibited by the MCA fractions remaining inside the cell wall (exact mechanism is discussed in sub-section 3.3.5.3).

Kinetic analysis of the interaction of MCA with each surface was performed using the method described in sub-section 2.2.4. Samples were taken at time  $t=10$  min, 20 min, 40 min, 50 min, 60 min with constant concentration of adsorbent (MCA 2mg/mL) and adsorbate (mineral 2mg), constant pressure, temperature and pH.

A second experiment included the construction of experimental isotherms. Samples were taken at constant time, pressure, temperature and pH and varying concentration of macromolecule added to the system. The concentration of solutions of MCA used for the isotherms were 0.2 mg  $\text{ml}^{-1}$ , 0.4 mg  $\text{ml}^{-1}$ , 0.8 mg  $\text{ml}^{-1}$ , 1 mg  $\text{ml}^{-1}$  and 2 mg  $\text{ml}^{-1}$ . The amount of macromolecule adsorbed was calculated by equation (3.1).

$$Q = \frac{(C_o - C_e)V}{m} \quad \text{equation (3.1)}$$

where  $Q$  = amount of MCA adsorbed on mineral (mg  $\text{g}^{-1}$ ),  $C_o$ = initial concentration of MCA in solution (mg  $\text{L}^{-1}$ ),  $C_e$ = final concentration of MCA in solution (mg  $\text{L}^{-1}$ ),  $m$ =mass of mineral used (g) and  $V$ = volume (L).

### 3.2.5.1 Isotherm Models

In order to describe the isotherms, Langmuir and Freundlich models were used. Details on the assumptions and theory of the models can be found in sub-section 2.2.4.1. Table 3.3 shows the equations as derived from the models.

| <b>ID</b>         | <b>Equation (linear form)</b>                                    | <b>Y</b>          | <b>X</b>   | <b>Intercept</b>     | <b>Slope</b>    |
|-------------------|--|-------------------|------------|----------------------|-----------------|
| <b>Langmuir</b>   | $\frac{C_e}{Q_e} = \frac{1}{Q_m} \cdot C_e + \frac{1}{(K_l)Q_m}$ | $\frac{C_e}{Q_e}$ | $C_e$      | $\frac{1}{(Q_m)K_l}$ | $\frac{1}{Q_m}$ |
| <b>Freundlich</b> | $\ln(Q_e) = \ln(K_f) + \frac{1}{n_f} \cdot \ln(C_e)$             | $\ln(Q_e)$        | $\ln(C_e)$ | $\ln(K_f)$           | $\frac{1}{n_f}$ |

Where  $C_e$ =MCA concentration at equilibrium ( $\text{mg L}^{-1}$ ),  $Q_e$ =equilibrium adsorption capacity ( $\text{mg g}^{-1}$ ),  $K_l$ = Langmuir adsorption constant ( $\text{L/mg}$ ),  $Q_m$ =maximum adsorption capacity ( $\text{mg g}^{-1}$ ),  $K_f$ = Freundlich constant ( $\text{L/g}$ ),  $n_f$ = heterogeneity factor of adsorption sites (Bhatt *et al.* 2012)

### 3.2.6 Mass Spectrometry for Quantification of MCAs

The main experimental technique used to quantify MCA before and after its interaction with the surfaces was mass spectrometry. Known masses of MCAs were dissolved in 200  $\mu\text{L}$  chloroform/methanol (9:1) for the development of a calibration curve. The samples were analysed on a Waters LCT spectrometer with Electro-Spray Ionization and the mass spectral intensities of the ions created from the MCA fragments were plotted against concentration according to the method proposed by Cantrell *et al.* (Cantrell *et al.*, 2012). An injection volume of 200  $\mu\text{L}$  was used for each sample with a flow rate of 20  $\mu\text{L}$  per minute. Blanks of chloroform/methanol (9:1) were run between samples to avoid cross-contamination and the injection needle was rinsed with the same solvent after each run. The optimised ESI parameters were as follows: Temperature 220  $^{\circ}\text{C}$ , gas flow rate 30% (nitrogen), and ESI voltage 2.3kV. Mass spectra were recorded over the range of 200 to 1600  $m/z$  in the negative ion mode. The theoretical peaks suggested for ESI-MS are shown in table 3.2.

### **3.2.7 Attenuated Total Reflection-Fourier Transform Infrared Spectroscopy (ATR-FTIR)**

The functional groups of MCA were characterised using ATR-FTIR before and after the interaction of the macromolecules with the mineral surfaces. Similarly to the adsorption experiments, a portion of  $2 \pm 0.5$ mg of minerals was transferred into 2.5 ml glass tubes. Aliquots of 150  $\mu$ L of 0.01M NaCl solution, 0.01M CaCl<sub>2</sub> solution or H<sub>2</sub>O were then added to the tubes and the pH was adjusted to 3, 7 or 10 with 0.01M NaOH or 0.01M HCl. The contents of the tubes were mixed and left on the shaker for 24 hours at room temperature to equilibrate. The pH was then tested and 100 $\mu$ L of 1 mg ml<sup>-1</sup> macromolecules dissolved in a chloroform/methanol (9:1) solvent was then added to the equilibrated suspensions. The tubes were left to interact for 45 minutes and were then centrifuged at 5000rpm for 10 minutes. The supernatant was discarded and the sample left was freeze dried for 24 hours. ATR-FTIR spectra were collected from 400-4000cm<sup>-1</sup>, with a resolution of 4 cm<sup>-1</sup>. Background spectra of the different electrolytes, MCA stock and the mineral surfaces with no macromolecules were also collected.

## 3.3 Results and Discussion

### 3.3.1 MCA solubility tests and solvent choice

In order to examine the solubility of MCA and to identify a suitable media for the sorption experiments, basic solubility tests were run. Several organic and aqueous solvents were tested. Examples of the outcome are shown in table 3.4. Most of the organic solvents including THF, chloroform and hexane successfully dissolved the molecule showing that the organic part of the MCA is dominant and controls the molecule's dissolution (the theory behind *'like dissolves like'*) while the aqueous solvents including methanol and water resulted in undissolved particles (forming a suspension). These observations suggest that the molecule is mainly non-polar. In order to achieve complete dissolution of the molecule, a small quantity of methanol (final ratio chloroform/methanol 9:1) was added to the chloroform and the new solvent was also tested. Chloroform, chloroform/methanol and THF were found to be the best solvents (both showed a maximum MCA solubility of ~50 mg/mL of solvent) and the chloroform/methanol mixture was chosen as the most appropriate solvent for the experiments. The three main reasons for this choice were: (a) THF could not be used for mass spectrometry analysis, (b) THF is miscible with water and a solvent non-miscible with water was needed in order to mimic the natural environment where the MCAs are held in a strongly hydrophobic environment and (c) The use of a

chloroform/methanol mixture as the solvent ensured that the hydrophobic character of MCA was supported (and hence chloroform helped to mimic the natural environment) but it would also provide a miscible part (methanol) that would allow for the aqueous electrolytes and pH adjustments.

Dissolution in a non-miscible solvent ensures that the molecule is surrounded by a hydrophobic 'capsule' that protects it from any water molecules present in solution. The chloroform also serves as the strong hydrophobic agent that would lead the MCA closer to the surface since its density is higher than that of water. It was therefore hypothesised that chloroform would repel bulk water while increasing the polarity of the molecule at the carboxylic acid end groups (please see figure 3.19 for more details on this mechanism).

**Table 3.4- MCA solubility tests**

| Solvent                   | Min. Solubility | Miscible with water? | Toxic?    |
|---------------------------|-----------------|----------------------|-----------|
| THF                       | 50 mg/mL        | Yes                  | Explosive |
| Methanol                  | -               | -                    | -         |
| Chloroform                | 50 mg/mL        | No                   | Yes       |
| Chloroform/Methanol (9:1) | 50 mg/mL        | No                   | Yes       |
| Hexane                    | 10 mg/mL        | No                   | No        |
| Acetonitrile              | -               | -                    | -         |
| Dimethylformamide         | -               | -                    | -         |

### 3.3.2 Characterization of Ceria and Europium Oxide

Europium oxide and ceria were characterised using the X'Pert<sup>3</sup> Powder by PANalytical as previously described (sub-section 2.3.2.2). Both the europium oxide and ceria samples resulted in the expected peaks indicating that the surfaces used were of the purest forms with no other phases

interfering in the interactions. The size of the particles was assessed using AFM and was found to be 50-100 nm for europium oxide and <50 nm for ceria.

### 3.3.3 MCA quantification – Calibration

Mass spectrometry was used to quantify MCA in solution. The technique is based on the determination of the molecular weight of fractions of molecules once these are ionised. A calibration curve of counts per minute for each peak observed per MCA fraction was constructed in relation to the quantity of MCA used. The equations obtained for each MCA form are shown in table 3.5 and a graphical representation of the calibration curves is shown in figure 3.4.

| <b>Individual Peak</b> | <b>Equation</b>          | <b>R<sup>2</sup></b> |
|------------------------|--------------------------|----------------------|
| 395.4 m/z              | $y = 61.958x - 5248.553$ | 0.98                 |
| 367.3 m/z              | $y = 8.220x - 682.866$   | 0.98                 |
| 1136.2 m/z             | $y = 8.214x - 845.731$   | 0.95                 |
| 1252.3 m/z             | $y = 5.439x - 565.641$   | 0.95                 |
| 1264.3 m/z             | $y = 1.656x - 137.040$   | 0.98                 |

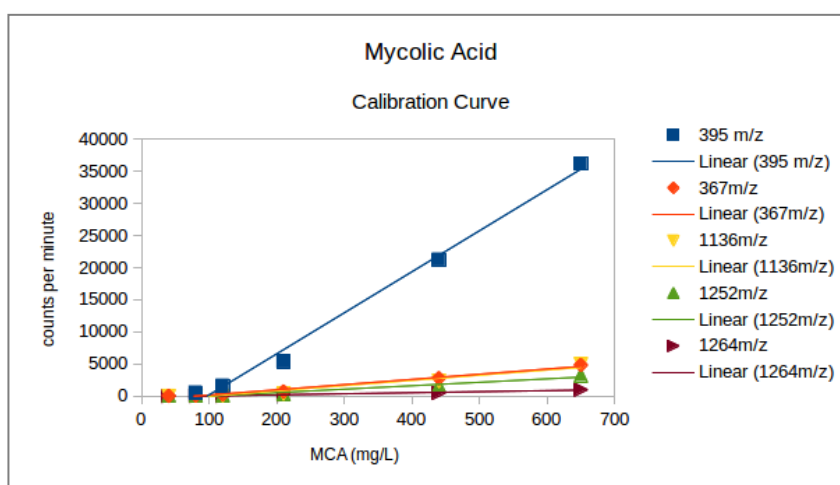


**Figure 3.4. Mass Spectrometry - calibration curve for quantification of MCA.**

The reason different calibration curves were obtained was that each part of the molecule gave out different responses due to the mixture of molecular weight fractions that may be present. The 395.4 m/z peak of the spectra was always the highest (showing that a higher amount of ions with mass 395.4 was obtained) and it was more than 5 times the height of the rest of the peaks. Examples of the spectra can be found in figure 3.5 where the 395.4 m/z peak is about 8 times the size of the 367.3 m/z peak. All calibration curves are dominated by a largely linear portion, with overall R<sup>2</sup> values close to 1 which suggested they could be used for quantification of MCA in solution. The results were comparable to those from literature (table 3.6 shows the theoretical peaks) and the peaks correspond to the different types of MCA (alpha-mycolic acid, keto-mycolic acid and methoxy-mycolic acid) (Cantrell *et al.*, 2012). The % error of the peaks obtained in order to assess the instrument's accuracy compared to published work was also calculated as shown in table 3.6. The low values of % error (ranging from ~0.0001 to 0.001%) indicated that our results were very close to the results of Cantrell *et al.* (Cantrell *et al.*, 2012).

| <b>Table 3.6. Mass spectrometry results for MCA quantification compared to literature.</b>                |                        |                     |                |
|---|------------------------|---------------------|----------------|
| The % error was calculated using: $\frac{\text{Observed} - \text{Theoretical}}{\text{Theoretical}} * 100$ |                        |                     |                |
| <b>MCA Form</b>   | <b>m/z theoretical</b> | <b>m/z observed</b> | <b>% Error</b> |
| <b>Alpha</b>  | 1136.1669              | 1136.1622           | 0.0004         |
| <b>Keto</b>   | 1264.2870              | 1264.2794           | 0.0006         |
| <b>Methoxy</b>  | 1252.2870              | 1252.2806           | 0.0005         |
| <b>neutral fragment - alpha</b>   | 367.35                 | 367.4               | 0.0140         |
| <b>neutral fragment - methoxy</b>   | 395.39                 | 395.5               | 0.0278         |

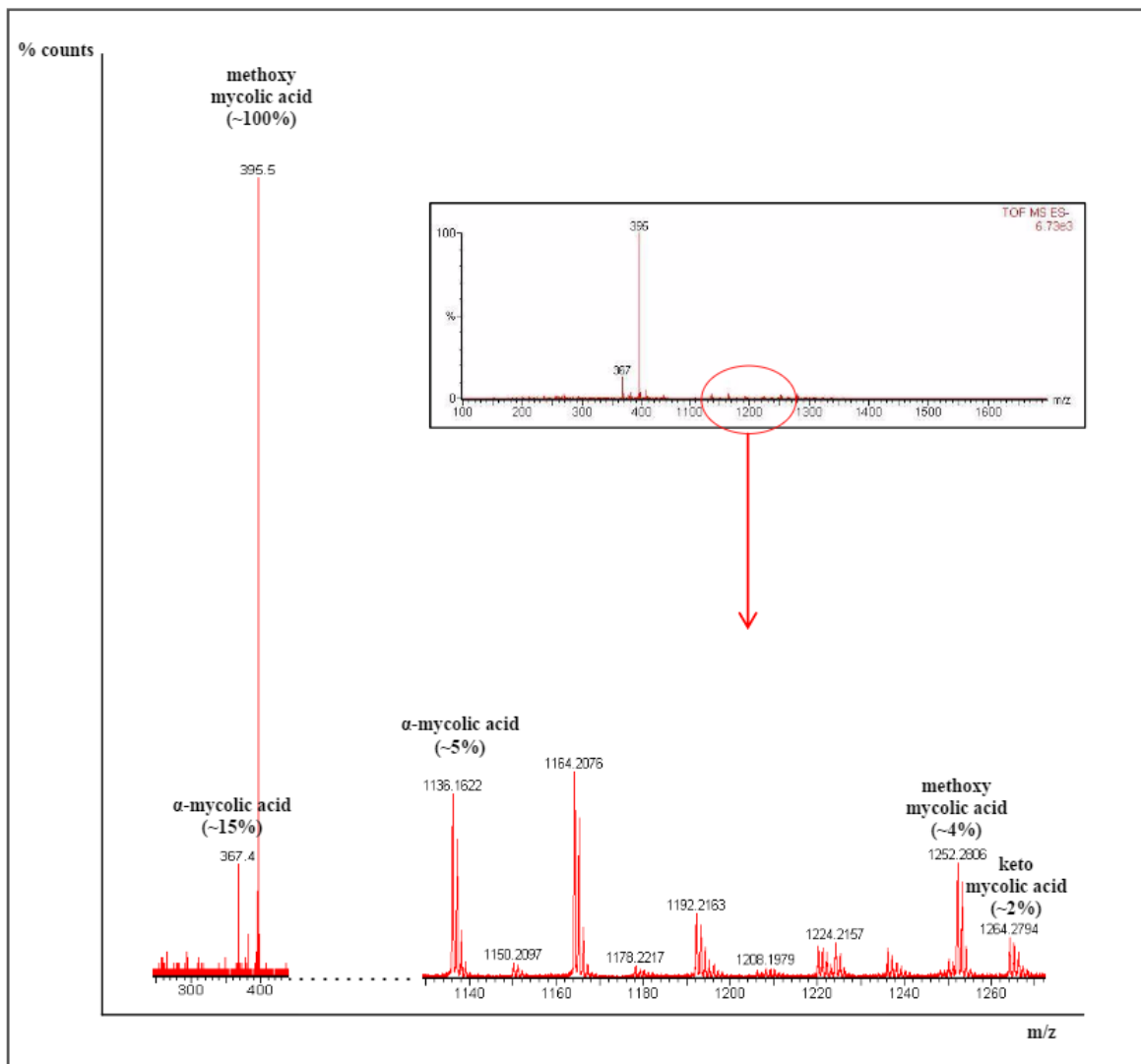


**Figure 3.5. Examples of Mass Spectrometry results for MCA identification and quantification. The 395.5 m/z peak is 8 times the size of the 367.4 m/z peak which is of similar size to the 1136.17, 1264.2 and 1252.2 m/z peaks.**

### 3.3.4 Adsorption of MCA onto Ceria

#### 3.3.4.1 MCA interactions with ceria – Kinetics

The interaction of MCA with ceria was assessed using mass spectrometry. After an equilibration time of 24 hours with small amounts of the surface in the different electrolytes, a quantity of MCA dissolved in chloroform/methanol was added and aliquots were taken at different times in order to evaluate the kinetics of the interaction. The experiments were run under acidic, neutral and basic pH conditions and different counter ions (protons, sodium and calcium) were included in order to examine if they play any role in the interaction.

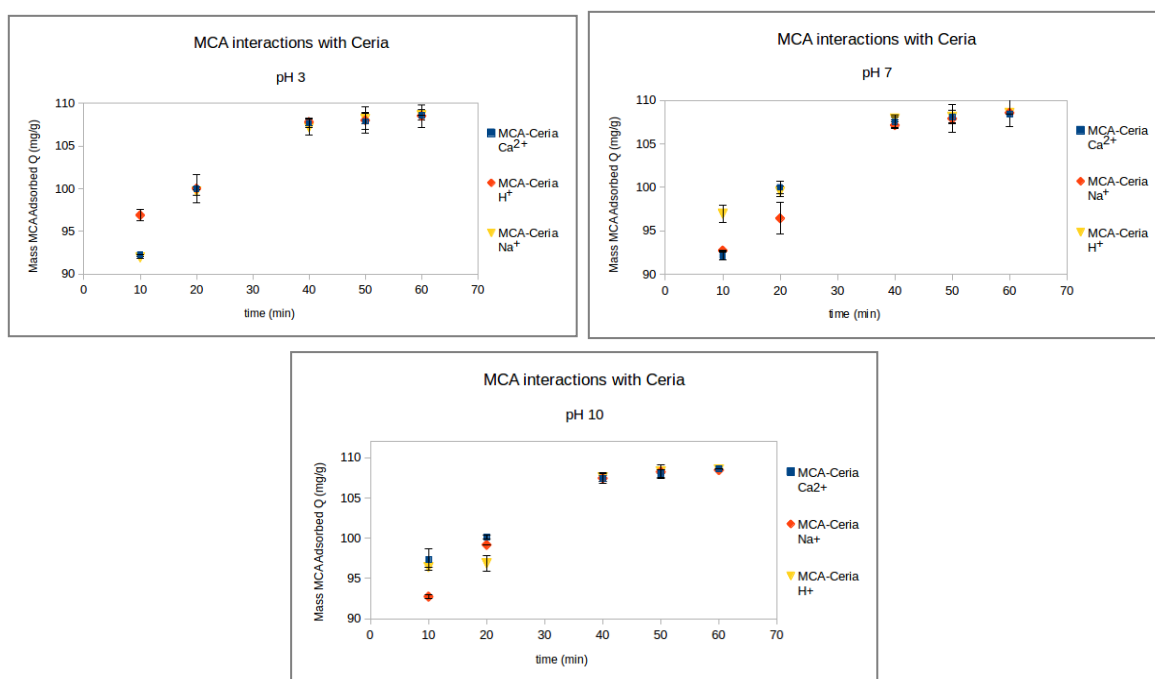


**Figure 3.6-3.8. Kinetics of adsorption of MCA-Ceria at pH3 (fig. 3.6-left), pH7 (fig. 3.7-right) and pH10 (fig. 3.8-middle).**

Figure 3.6 summarises the obtained results for the Ceria-MCA systems under acidic conditions (pH3). Very similar adsorption profiles were obtained for all systems and the highest adsorption of MCA was observed after a 40-45 minutes' interaction. Both the Na<sup>+</sup> and Ca<sup>2+</sup>-containing electrolytes started the interaction with a lower mass of MCA adsorbed onto the surface compared to that of the water-mediated interaction. This suggests that the interaction under acidic

conditions is not mediated by ion-containing electrolytes. However, even if the proton mediated interaction (represented by the water-based electrolyte) had a kinetic advantage over the ion-containing interactions, the later eventually reached the water-based system and resulted in a similar maximum adsorption capacity. Hence, all three systems showed successful sorption profiles for the MCA-Ceria interaction under acidic conditions.

The point of zero charge of ceria surface ranges from 6.4 – 8.6 (Kosmulsko, 2002; Nolan and Watson, 2006). This suggests that the mineral exhibits a positive charge below pH 6.4 and a negative charge above pH 8.6. Thus, at pH3 the ceria surface is positively charged while the MCA molecules are slightly positively charged. This is due to the carboxylic acid groups of the MCA molecules where the oxygen of the C=O groups react with protons and hence exhibit a slightly positive charge (Zhang *et al.*, 2010). This suggests that a spontaneous interaction between the two positive components would not be explained using the charges. A hypothesis explaining the behavior of the system under acidic conditions relates to the hydrophobic character of ceria (Azimi *et al.*, 2013). Due to this property, ceria is believed to avoid interactions with water molecules at the liquid/solid interface. As a result, it is possible that the hydrophobic organic layer was attracted by the ceria surface in an attempt to repel water molecules. Hence, the MCA macromolecules could eventually adsorb onto the ceria surface. It has been previously shown that adhesion on hydrophobic surfaces by bacterial cells including *Rhodococcus* and *Mycobacteria* is much better than that on hydrophilic surfaces. In addition, the ability of bacteria to adsorb onto different surfaces was directly related to the presence or absence of MCAs. In the presence of MCAs, bacteria would adsorb strongly on hydrophobic surfaces (Bendinger *et al.*, 1993). Our findings agree with the work of Bendinger *et al.* but more details are needed in order for the clear mechanism of adsorption to be revealed. Computational methods were therefore used to evaluate the interaction of MCA and ceria and are presented in chapter 5.

Figure 3.7 summarises the results for adsorption of MCA onto ceria under neutral conditions (pH7). Similarly to the acidic systems, a plateau was reached after a 40-45-minute interaction. The results were similar to that of the acidic conditions. The water-based system

showed the highest mass of MCA adsorbed at the early stages of the interaction suggesting that no ions other than protons are needed to mediate the interaction at these conditions. Examining the point of zero charge of the surface suggests that, under neutral conditions, the ceria surface was slightly positive-close to neutral while the MCA molecules were negatively charged. A spontaneous interaction was therefore possible. All three electrolytes successfully mediated the interactions and resulted in similar maximum adsorption capacities during the 60-minute period.

In the case of MCA interaction with Ceria under basic conditions (pH10-figure 3.8), no major differences were observed related to the inclusion or the absence of the different counter ions. The MCA-Ceria with calcium chloride system seemed to have a more rapid response to the adhesion process (hence, the highest adsorption of MCA onto ceria at time=10min). However, the results of the water-mediated and the calcium-mediated adsorption processes at the early stages of the experiments lay in the error bar range of one another which indicates that both processes produced similar numerical results. The Na-mediated interaction showed the slowest response. Nevertheless, all three systems eventually reached a very similar maximum capacity (thus, similar maximum adsorbed mass). The adsorption of MCA onto ceria was found to reach a plateau after a 40-45 minutes' interaction for all three electrolytes at basic conditions. The adsorption of MCA onto ceria at pH10, represents the case where a negatively charged surface is being approached by a negatively charged, highly hydrophobic macromolecule. The results suggest that the interaction between the two is mediated by the positively charged calcium ions ( $\text{Ca}^{2+}$ ) which act as 'bridges' between the two negatively charged reaction components.

It has been previously suggested that at such high pH conditions, a hydration layer between the MCA and the mineral may be observed (Zhang *et al.*, 2010). This is due to the dissociation of the carboxylic acids of the MCA macromolecules at such conditions that creates a repulsive force between the negatively charged adsorbent and the negatively charged adsorbate. This force creates a small gap between the two components which allows a number of water molecules to create a hydration layer. The introduction of the chloroform/methanol solvent as the carrier of the MCA molecules overcomes this problem. The use of an organic solvent results in removal of these bulk

water molecules due to its density which is higher than that of water. Hence, the negatively charged carboxylic acid groups can react with the negatively charged surface using an ion-mediated mechanism with  $\text{Ca}^{2+}$ ,  $\text{H}^+$  and  $\text{Na}^+$  acting as the mediators in order of the speed of reaction (with  $\text{Ca}^{2+}$  and  $\text{H}^+$  being the quickest).

Ceria was found to strongly interact with MCA at all possible surface charges and pH conditions when water was used as the electrolyte. Having the chloroform 'protecting' and 'driving' the MCA molecules, allowed us to observe the interaction when bulk water molecules (hypothetically acting as 'obstacles' for the interaction with the surfaces) were repelled. Due to the high density of chloroform, it is hypothesised that the bulk water molecules would be removed facilitating the interaction of the organic molecule with the surface. Here it should be noted that computational studies have shown that water molecules actually prevent the sorption of carboxylic acid groups onto ceria surfaces which is described in detail in chapter 5.

This system was a close approximation of the natural bacterial system where MCAs are symmetrically arranged in parallel and covalently bound to arabinogalactan, peptidoglycan and a layer of free lipids (Brennan and Nikaido, 1995). This project's hypothesis is that the hydrophobic character of MCAs is enhanced by this orderly arrangement which suggests that an increased polarity is induced in the carboxylic acid end group of the molecule. It is believed that this increased polarity results in an increased charge exhibited by the oxygens of the  $-\text{COOH}$  functional groups which mediates interactions of the carboxylic acid groups with their surroundings. It is therefore suggested that experiments should be carried out either with MCA molecules arranged in a similar manner to that observed in bacterial cell walls or by using a hydrophobic media that supports the hydrophobic nature of the molecules. To our knowledge, this is the first work to report the adsorption of MCA onto ceria using this methodology.

Kinetic data was analysed using pseudo first order and pseudo-second order models. A linear fit was obtained for a second order reaction using equation (3.2).

$$\frac{dQ}{dt} = k(Q_e - Q_t)^2 \quad \text{equation (3.2)}$$

where  $Q_e$  and  $Q_t$  =adsorption capacity at equilibrium and time  $t$  respectively ( $\text{mg g}^{-1}$ ),  $k$ = rate constant of the pseudo second order adsorption ( $\text{g mg}^{-1} \text{min}^{-1}$ ).

The equations obtained along with the  $R^2$  values are shown in table 3.7 for adsorption of MCA on ceria.

| <b>ID</b><br><b>MCA-Ceria</b><br><b>in:</b> | <b>Equation y=Mx+C</b> | <b>R<sup>2</sup></b> | <b>Intercept</b><br><b>C=1/kQ<sub>e</sub><sup>2</sup></b> | <b>Slope</b><br><b>M=1/Q<sub>e</sub></b> | <b>Q<sub>e</sub> = 1/m</b><br><b>mg g<sup>-1</sup></b> | <b>K =1/(CQ<sub>e</sub><sup>2</sup>)</b><br><b>*10<sup>-3</sup> g mg<sup>1</sup> min<sup>-1</sup></b> |
|---|------------------------|----------------------|---|--|--|---|
| <b>NaCl pH10</b>                            | Y=0.0088x + 0.0212     | 0.998                | 0.0212  | 0.0088                                   | 113.636  | 3.653   |
| <b>CaCl<sub>2</sub> pH10</b>                | Y=0.0089x + 0.0166     | 0.997                | 0.0166  | 0.0089                                   | 112.359  | 4.772   |
| <b>water pH10</b>                           | y=0.0088x + 0.0208     | 0.997                | 0.0208  | 0.0088                                   | 113.636  | 3.670   |
| <b>NaCl pH3</b>                             | Y=0.0088x + 0.0217     | 0.998                | 0.0217  | 0.0088                                   | 113.636  | 3.569   |
| <b>CaCl<sub>2</sub> pH3</b>                 | Y=0.0088x + 0.0206     | 0.998                | 0.0206  | 0.0088                                   | 113.636  | 3.759   |
| <b>water pH3</b>                            | Y=0.0089x + 0.0167     | 0.998                | 0.0167  | 0.0089                                   | 112.359  | 4.743   |
| <b>NaCl pH7</b>                             | Y=0.0088x + 0.0244     | 0.997                | 0.0244  | 0.0088                                   | 113.636  | 3.174   |
| <b>CaCl<sub>2</sub> pH7</b>                 | Y=0.0089x + 0.0206     | 0.998                | 0.0206  | 0.0089                                   | 112.359  | 3.845   |
| <b>water pH7</b>                            | Y=0.0089x + 0.0172     | 0.998                | 0.0172  | 0.0089                                   | 112.359  | 4.605   |

The high values of  $R^2$  obtained for all systems tested suggested a very good fit on the pseudo-second order model, examples of which can be found in appendix 14. In general, it was observed that the calculated  $Q_e$  values agreed well with the experimentally obtained values. A small kinetic advantage of the calcium-mediated interaction was observed for the case of basic conditions where the ceria surface is negatively charged and the MCA molecule is also negatively charged. This was attributed to the fact that the positively charged calcium ions act as bridges and mediate the interaction. On the opposite end, acidic and neutral experimental conditions resulted in a slightly positive to neutral ceria surface and a positively charged carboxylic acid group on the

MCA groups. In these cases, water-based experiments were found to mediate the interaction at the fastest reaction rate and computational modelling techniques were used in order to observe the interaction at the atomic level. Details on the actual work can be found in chapter 5.

### 3.3.4.2 Experimental Isotherms for sorption of MCA onto Ceria

In order to quantify the effect of MCA mass in solution during the sorption process, different concentrations of MCA were introduced in the systems and samples were taken at a set time. The Langmuir isotherm, the Freundlich isotherm and a combination of the two (known as the 'Langmuir-Freundlich' or the 'Sips' isotherm) were used for evaluation of the results. Tables 3.8 and 3.9 and figures 3.9 and 3.10 show examples of the fitting for Langmuir and Freundlich models and explain why the two could not be used for the tested systems. A summary of the remaining data can be found in appendix 15.

| Sample ID MCA in:                       | Equation         | R <sup>2</sup> |
|---|------------------|----------------|
| pH7 CaCl <sub>2</sub> CeO <sub>2</sub>  | Y=0.014x + 0.293 | 0.90           |
| pH7 water CeO <sub>2</sub>              | Y=0.003x + 0.862 | 0.24           |
| pH3 water CeO <sub>2</sub>              | Y=0.006x + 0.582 | 0.88           |
| pH3 NaCl CeO <sub>2</sub>               | Y=0.011x + 0.352 | 0.87           |
| pH3 CaCl <sub>2</sub> CeO <sub>2</sub>  | Y=0.012x + 0.349 | 0.87           |
| pH7 NaCl CeO <sub>2</sub>               | Y=0.004x + 0.841 | 0.50           |
| pH10 NaCl CeO <sub>2</sub>              | Y=0.004x + 0.784 | 0.57           |
| pH10 CaCl <sub>2</sub> CeO <sub>2</sub> | Y=0.007x + 0.549 | 0.63           |
| pH10 water CeO <sub>2</sub>             | Y=0.005x + 0.791 | 0.61           |

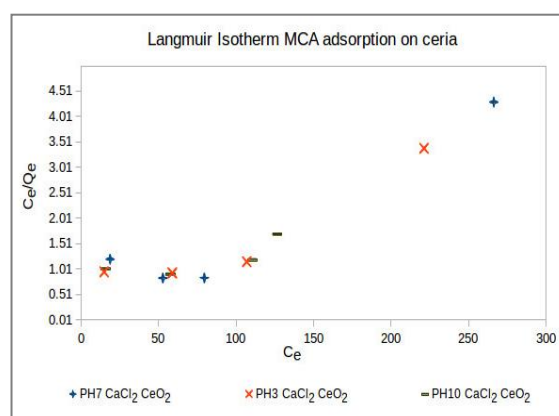


**Figure 3.9. Example fitting (Langmuir) for adsorption of MCA onto ceria where C<sub>e</sub> is in mg/L and C<sub>e</sub>/Q<sub>e</sub> is in g/L**

Figure 3.9 shows a typical result from fitting the data on the Langmuir equation. The shape of the curve shows a slight plateau at low concentrations followed by a rapid increase in capacity of the sorbent that does not exhibit saturation at high concentrations. Since the model assumes saturation at high concentration, the resulting curve does not fit the intended model. The unsuccessful data fitting on the Langmuir isotherm model and the low  $R^2$  values indicated that additional models had to be evaluated. It also suggested that the MCA adsorption onto ceria followed a complex sorption mechanism which cannot be explained by the mono-layer concept of the Langmuir isotherm.

Table 3.9 shows the equations obtained after fitting the data to the Freundlich model. The Freundlich model provided better results compared to Langmuir but the  $R^2$  values were low for some of the data considering the number of data points used. This suggested that in most cases and specifically in the systems where NaCl and water were involved, the empirical form of Freundlich was closer to describing the sorption mechanism compared to the mono-layer mechanism suggested by the Langmuir isotherm. Examples of the fitting are shown in figure 3.10 and appendix 16.

| <b>Table 3.9. Freundlich Isotherm for MCA adsorption on ceria</b> |                  |                         |
|---|------------------|-------------------------|
| <b>Sample ID MCA in:</b>  | <b>Equation</b>  | <b><math>R^2</math></b> |
| pH7 CaCl <sub>2</sub> CeO <sub>2</sub>                            | $Y=0.509x+1.751$ | 0.50                    |
| pH3 CaCl <sub>2</sub> CeO <sub>2</sub>                            | $Y=0.592x+1.409$ | 0.74                    |
| pH7 NaCl CeO <sub>2</sub>   | $Y=0.876x+0.415$ | 0.96                    |
| pH10 NaCl CeO <sub>2</sub>  | $Y=0.844x+0.545$ | 0.94                    |
| pH10 CaCl <sub>2</sub> CeO <sub>2</sub>                           | $Y=0.797x+0.827$ | 0.86                    |
| pH10 water CeO <sub>2</sub>                                       | $Y=0.822x+0.571$ | 0.93                    |
| pH3 NaClCeO <sub>2</sub>  | $Y=0.612x+1.459$ | 0.85                    |
| PH3 water CeO <sub>2</sub>  | $Y=0.934x+0.208$ | 0.93                    |
| PH7 water CeO <sub>2</sub>  | $Y=0.665x+1.203$ | 0.87                    |

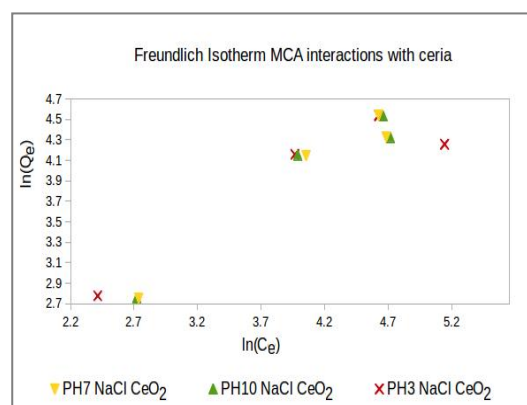


**Figure 3.10. Freundlich Isotherm Model for adsorption of MCA onto ceria**

In both cases, the Langmuir and Freundlich models did not result in good fitting of the data indicated by the low  $R^2$  values that were obtained. The Sips model was therefore used in order to evaluate the behavior the Ceria-MCA system. The Sips isotherm is known as a combination of the Langmuir and the Freundlich systems and it is used for complex interactions. The Sips linear equation model is described by equation (3.4).

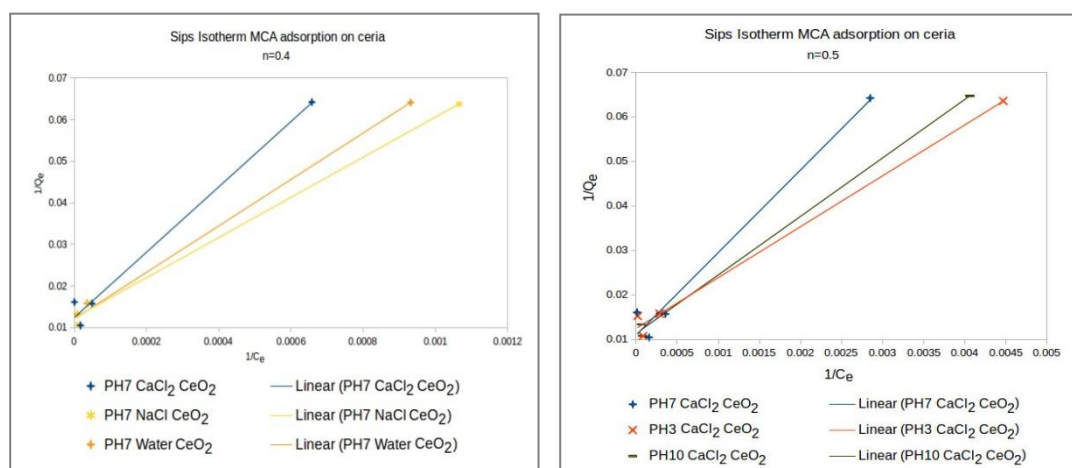
$$\frac{1}{Q_e} = \frac{1}{Q_{\max}K_s} * \left(\frac{1}{C_e}\right)^{\frac{1}{n}} + \frac{1}{Q_{\max}} \quad \text{equation(3.4)}$$

where  $K_s$  (1/mg) and  $Q_{\max}$  (mg/g) are the Sips equilibrium and maximum adsorption capacity constants, respectively.  $n$  is the dimensionless heterogeneity factor, where  $0 < n < 1$ . When approaching a low  $n$  value, the Sips isotherm reduces to Freundlich, while at high  $n$  values, it predicts the Langmuir monolayer sorption characteristics

The Sips isotherm was tested for  $n=0.1, 0.2, 0.3, 0.4, 0.5, 0.6, 0.7, 0.8, 0.9$  and  $1$ . Examples of data fitting on the Sips isotherm at  $n=0.4$  and  $n=0.5$  are shown in tables 3.10 and 3.11. Figures 3.12 and 3.13 show examples of the fitting (a summary of all the samples can be found in appendix 17).

| <b>Sample ID MCA in:</b>                | <b>Equation</b> | <b>R<sup>2</sup></b> |
|---|-----------------|----------------------|
| pH7 CaCl <sub>2</sub> CeO <sub>2</sub>  | Y=78.565x+0.012 | 0.99                 |
| pH3 CaCl <sub>2</sub> CeO <sub>2</sub>  | Y=43.601x+0.013 | 0.99                 |
| PH7 NaCl CeO <sub>2</sub>               | Y=48.309x+0.012 | 0.99                 |
| pH10 NaCl CeO <sub>2</sub>              | Y=46.436x+0.012 | 0.99                 |
| pH7 water CeO <sub>2</sub>              | Y=55.897x+0.012 | 0.99                 |
| pH3 NaClCeO <sub>2</sub>                | Y=20.650x+0.013 | 0.99                 |
| pH10 CaCl <sub>2</sub> CeO <sub>2</sub> | Y=51.076x+0.012 | 0.99                 |
| pH10 water CeO <sub>2</sub>             | Y=55.897x+0.012 | 0.99                 |
| pH3 water CeO <sub>2</sub>              | Y=17.935x+0.013 | 0.99                 |

| Table 3.11. Sips Isotherm for MCA adsorption on ceria (for n=0.5) |                 |                |
|---|-----------------|----------------|
| Sample ID MCA in:   | Equation        | R <sup>2</sup> |
| pH7 CaCl <sub>2</sub> CeO <sub>2</sub>                            | Y=18.548x+0.011 | 0.98           |
| pH3 water CeO <sub>2</sub>  | Y=5.575x+0.012  | 0.99           |
| pH3 CaCl <sub>2</sub> CeO <sub>2</sub>                            | Y=11.441x+0.012 | 0.99           |
| pH7 NaCl CeO <sub>2</sub>   | Y=12.550x+0.011 | 0.99           |
| pH10 NaCl CeO <sub>2</sub>  | Y=12.156x+0.011 | 0.99           |
| pH10 CaCl <sub>2</sub> CeO <sub>2</sub>                           | Y=13.145x+0.011 | 0.99           |
| pH7 water CeO <sub>2</sub>  | Y=14.181x+0.011 | 1              |
| pH3 NaClCeO <sub>2</sub>  | Y=6.247x+0.012  | 0.99           |
| pH10 water CeO <sub>2</sub>                                       | Y=58.020x+0.012 | 1              |



Figures 3.11-3.12. Sips Isotherm Model for adsorption of MCA onto ceria (fig. 3.11, n=0.4 - left and fig. 3.12, n=0.5 - right)

The highest R<sup>2</sup> values were obtained for n=0.4 and n=0.5. This suggests that the adsorption of MCA onto Ceria follows a complex mechanism and no clear distinction between the two main processes (monolayer or multi-site adsorption) can be made in order to describe how the molecule

approaches the surface. Since both  $n=0.4$  and  $n=0.5$  resulted in high  $R^2$  values ( $R^2 > 0.99$ ), all the Sips constants were calculated according to both, as shown in tables 3.12 and 3.13.

**Table 3.12. Sips isotherm fitting for  $n=0.4$**

| ID                                      | Equation   | Intercept               | Slope                      | $Q_{max}$               | $K_s$                         |
|---|--|-------------------------|----------------------------|-------------------------|-------------------------------|
| <b>Sips Isotherm for MCA in:</b>        | $\frac{1}{Q_e} = \frac{1}{Q_{max}K_s} * \left(\frac{1}{C_e}\right)^{0.4} + \frac{1}{Q_{max}}$ $y = \left(\frac{1}{Q_e}\right)x = \left(\frac{1}{C_e}\right)^{0.4}$ | $C = \frac{1}{Q_{max}}$ | $m = \frac{1}{Q_{max}K_s}$ | $Q_{max} = \frac{1}{C}$ | $K_s = \frac{1}{m * Q_{max}}$ |
| pH7 CaCl <sub>2</sub> CeO <sub>2</sub>  | Y=78.565x+0.012  | 0.012                   | 78.565                     | 83.333                  | 0.0001                        |
| pH3 CaCl <sub>2</sub> CeO <sub>2</sub>  | Y=43.601x+0.013  | 0.013                   | 43.601                     | 76.923                  | 0.0003                        |
| PH7 NaCl CeO <sub>2</sub>               | Y=48.309x+0.012  | 0.012                   | 48.309                     | 83.333                  | 0.0002                        |
| pH10 NaCl CeO <sub>2</sub>              | Y=46.436x+0.012  | 0.012                   | 46.436                     | 83.333                  | 0.0003                        |
| pH7 waterCeO <sub>2</sub>               | Y=55.897x+0.012  | 0.012                   | 55.897                     | 83.333                  | 0.0002                        |
| pH3 NaCl CeO <sub>2</sub>               | Y=20.650x+0.013  | 0.013                   | 20.650                     | 76.923                  | 0.0006                        |
| pH10 CaCl <sub>2</sub> CeO <sub>2</sub> | Y=51.076x+0.012  | 0.012                   | 51.076                     | 83.333                  | 0.0002                        |
| pH10 water CeO <sub>2</sub>             | Y=55.897x+0.012  | 0.012                   | 55.897                     | 83.333                  | 0.0002                        |
| pH3 water CeO <sub>2</sub>              | Y=17.935x+0.013  | 0.013                   | 17.935                     | 76.923                  | 0.0007                        |

The theoretical results obtained for the maximum Q values for all cases of Ceria-MCA adsorption were lower than the experimental values. This is due to the complexity of the system which has an effect on the resulting values. It is hypothesised that at different concentrations of MCA, the system changes from Freundlich to Langmuir and hence, from monolayer to multi-site interactions and it is not clear when that change occurs. Hence, the theoretical values of maximum Q are describing the average value between the cases of monolayer and multi-site adsorption.

| <b>ID</b>                               | <b>Equation</b>  | <b>Intercept</b>        | <b>Slope</b>               | <b>Q<sub>max</sub></b>  | <b>K<sub>s</sub></b>          |
|---|--|-------------------------|----------------------------|-------------------------|-------------------------------|
| <b>Sips Isotherm<br/>MCA in</b>         | $\frac{1}{Q_e} = \frac{1}{Q_{max}K_s} * \left(\frac{1}{C_e}\right)^{\frac{1}{0.5}} + \frac{1}{Q_{max}}$ $y = \left(\frac{1}{Q_e}\right)x = \left(\frac{1}{C_e}\right)^2$ | $C = \frac{1}{Q_{max}}$ | $m = \frac{1}{Q_{max}K_s}$ | $Q_{max} = \frac{1}{C}$ | $K_s = \frac{1}{m * Q_{max}}$ |
| pH7 CaCl <sub>2</sub> CeO <sub>2</sub>  | Y=18.548x+0.011  | 0.011                   | 18.548                     | 91.241                  | 0.001                         |
| pH3 water CeO <sub>2</sub>              | Y=5.575x+0.012   | 0.012                   | 5.575                      | 80.775                  | 0.002                         |
| pH3 CaCl <sub>2</sub> CeO <sub>2</sub>  | Y=11.441x+0.012  | 0.012                   | 11.441                     | 80.386                  | 0.001                         |
| pH7 NaCl CeO <sub>2</sub>               | Y=12.550x+0.011  | 0.011                   | 12.550                     | 89.206                  | 0.001                         |
| pH10 NaCl CeO <sub>2</sub>              | Y=12.156x+0.011  | 0.011                   | 12.156                     | 89.686                  | 0.001                         |
| pH3 NaClCeO <sub>2</sub>                | Y=6.247x+0.013   | 0.013                   | 6.246                      | 80.128                  | 0.002                         |
| pH10 CaCl <sub>2</sub> CeO <sub>2</sub> | Y=13.145x+0.011  | 0.011                   | 13.145                     | 88.106                  | 0.001                         |
| pH7 water CeO <sub>2</sub>              | Y=14.181x+0.011  | 0.011                   | 14.181                     | 92.764                  | 0.001                         |
| pH10 water CeO <sub>2</sub>             | Y=58.020x+0.012  | 0.012                   | 58.020                     | 83.333                  | 0.0002                        |

Similar observations with the n=0.4 case were made for the n=0.5 system. The theoretical values for maximum Q were lower than the experimentally obtained data due to them being averages of the mass adsorbed when in monolayer and multi-site adsorption processes. In general, it was observed that for all cases of varying *n* values, the process was favorable (higher R<sup>2</sup> values) for low *n* values. Hence, the process seemed to be closer to a Freundlich isotherm model of a multi-site adsorption process rather than the Langmuir model of monolayer adsorption. It is also possible that different mechanisms are involved depending on the electrolyte and the ions present in solution. The observation that the Freundlich isotherm could describe the systems that contained water and sodium chloride better than the calcium chloride containing systems (concluded from the higher R<sup>2</sup> values obtained when the Freundlich isotherm was tested for fitting) suggested that it could be possible that the ions play a role in the sorption process. However, no distinction between the NaCl/Water and CaCl<sub>2</sub> systems could be made when the Sips model was used.

The isotherm models used are based on the remaining mass of MCA in solution after equilibration. Quantifying the mass in this fashion does not include possible intermolecular interactions in solution before or during sorption to the surface. This may lead to a lower mass of MCA in solution that may not necessarily reflect the mass of MCA on the surface. A possible example would be a calcium mediated interaction between the C=O group found in keto-mycolic acids which could potentially interact with an OH group of another mycolic acid under specific pH conditions (for example basic conditions where the oxygen of the OH group would exhibit a negative charge and the oxygen of the C=O group would use its free pair of electrons to promote binding with Ca<sup>2+</sup> acting as the connector).

All these scenarios arising from the results suggest that the adsorption of MCA onto ceria is a complex process. The existence of long carbon chains with a limited availability of secondary functional groups could possibly allow for interactions between the MCA molecules. This suggests that no clear distinction between the ceria-mediated removal of MCA from solution or intermolecular MCA interactions in solution can be made using the constructed isotherm and a different method is needed in order to further understand the mechanism of Ceria-MCA sorption.

The standard free energy change ( $\Delta G$ ) of adsorption can be correlated with the isotherm constants as previously described (sub-section 2.3.3.2.1). In this case where the Sips isotherm was used, no constant could be used directly from the model due to it being a combination of the Langmuir and Freundlich isotherms. However, the value of  $n$  obtained from fitting the experimental data on the Sips model that resulted in the highest R<sup>2</sup> values was closer to zero ( $n=0.4$ ). It was therefore suggested that the Freundlich constant  $K_f$  should be used as the data showed a tendency to follow the Freundlich model (when  $n$  is closer to zero the Sips model changes to Freundlich and when  $n$  is closer to 1 the Sips model is following the Langmuir model). Therefore, the Freundlich isotherm (equation (3.5)) was used to calculate the standard free energy change of adsorption,  $\Delta G$ .

$$\ln(Q_e) = \ln(K_f) + \frac{1}{n_F} \cdot \ln(C_e) \quad \text{equation (3.5)}$$

As previously described (sub-section 2.3.3.2.1), the Freundlich constant can be used after a correction which is needed to ensure that the resulting value is dimensionless prior to any  $\Delta G$  calculations.

| <b>ID MCA in:</b>                       | <b><math>K_c</math></b> | <b><math>K_d</math></b> | <b><math>\Delta G</math> (kJ/mol)</b> |
|---|-------------------------|-------------------------|---------------------------------------|
| pH7 CaCl <sub>2</sub> CeO <sub>2</sub>  | 1.751                   | 1751                    | -16.981                               |
| pH3 CaCl <sub>2</sub> CeO <sub>2</sub>  | 1.459                   | 1459                    | -16.566                               |
| PH7 NaCl CeO <sub>2</sub>               | 1.408                   | 1408                    | -16.485                               |
| pH10 NaCl CeO <sub>2</sub>              | 0.571                   | 571                     | -14.433                               |
| pH3 NaClCeO <sub>2</sub>                | 1.459                   | 1459                    | -16.566                               |
| pH10 CaCl <sub>2</sub> CeO <sub>2</sub> | 0.827                   | 827                     | -15.275                               |
| pH10 water CeO <sub>2</sub>             | 0.545                   | 545                     | -14.327                               |
| pH7 water CeO <sub>2</sub>              | 1.094                   | 1094                    | -15.911                               |
| pH3 water CeO <sub>2</sub>              | 0.571                   | 571                     | -14.433                               |

The calculated standard free energy change gave negative values for all cases of basic, acidic and neutral pH conditions ranging from -14 kJ/mol to -17 kJ/mol. This suggests that the adsorption of MCA onto ceria is spontaneous at acidic and neutral pH conditions (thus, below the point of zero charge of the ceria) as well as pH conditions above the point of zero charge of the ceria surface. The results were very close numerically suggesting similar free energy changes for most of the systems involving the adsorption of MCA onto ceria. No trend was observed involving counter ions which is in contrast with previously published work on other organic macromolecule adsorption onto surfaces (Freeman *et al.*, 2009) and also the LPS adsorption onto ceria examined in chapter 2.

Note that the calculated values of  $\Delta G$  are only partly associated with the adsorption of MCA onto ceria and do not describe the overall process exclusively. The standard free energy change of adsorption was calculated using the Freundlich constant as it was concluded from the

low  $n$  value that resulted from fitting the data on the Sips isotherm. However, the conclusion that the process is closer to Freundlich should only be used to give an insight on the adsorption process and not provide strict numerical values.

The Sips model was found to give the best fit and it is therefore suggested that the interaction of MCA with ceria is a complex process that combines a monolayer and a more complex, possibly multi-site interaction (i.e. the Langmuir-Freundlich isotherm).

Due to the high toxicity of chloroform and its incompatibility with most of the instrumentation available to test sorption processes, no further examination on MCA adsorption onto ceria was tested. ATR-FTIR experiments on europium oxide-MCA complexes were used as analogues to visualise the interaction and confirm the attachment of MCA on the mineral. These can be found in sub-section 3.3.5.3.

### **3.3.5 Adsorption of MCA on europium oxide**

#### **3.3.5.1 MCA interactions with europium oxide- Kinetics**

The interaction of MCA with europium oxide was evaluated using mass spectrometry and the methods described in sub-section 3.2.5. The experiments were run under acidic, neutral and basic conditions and using different electrolytes. An example of the results obtained for the europium oxide-MCA systems under acidic conditions (pH 3) are presented in the figure 3.13.

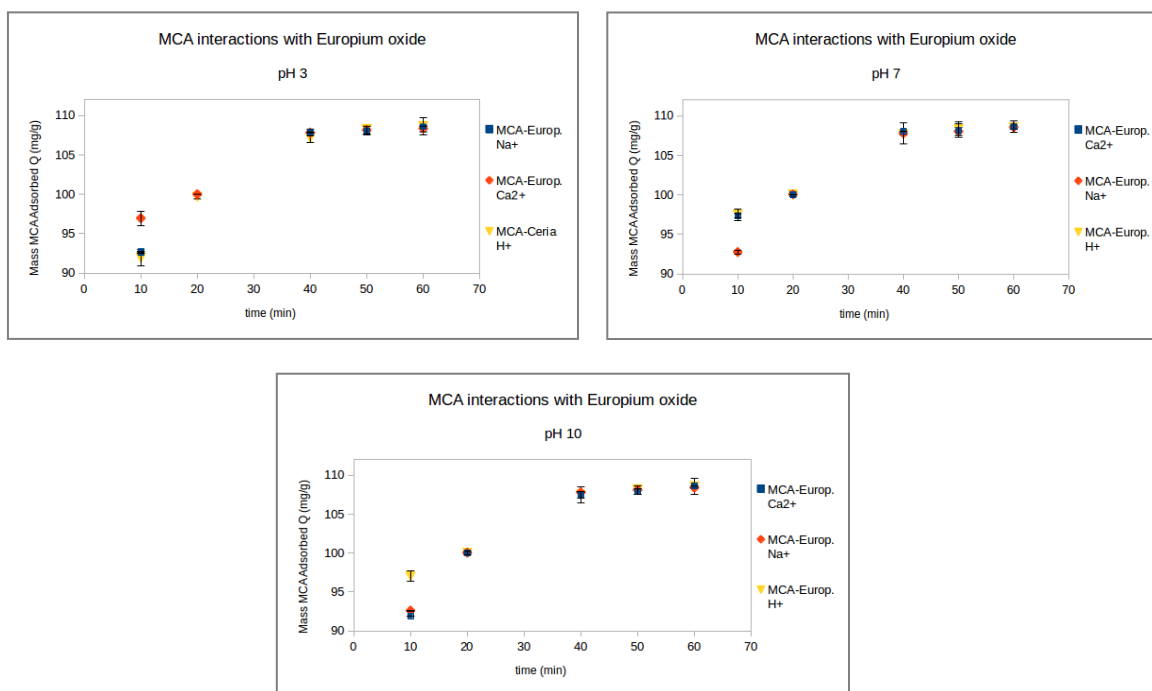


**Figure 3.13-3.15. Kinetics of adsorption of MCA-Eu<sub>2</sub>O<sub>3</sub> at pH3 (fig. 3.13- left), pH7 (fig. 3.14- right) and pH10 (fig. 3.15- middle).**

Very similar adsorption profiles were obtained for all systems and the highest adsorption of MCA was observed after a 40-45 minutes' interaction. The point of zero charge of europium oxide is pH=5. This suggests that the mineral exhibits a positive charge below pH 5 and a negative charge above pH 5. Introducing acidic conditions in the tested system suggested that a positively charged surface was being approached by a slightly positively-neutral macromolecule. This suggested that the interaction of the two similarly charged compounds would not be preferred and repulsion of the two should be observed. Interestingly, the sorption of MCA was successful and the most rapid interaction was observed when another positively charged ion was present, calcium.

A study on the acid/base properties of europium oxide examined the differences observed when ammonia or carbon dioxide were adsorbed onto the surface of europium oxide. The results indicated that europium oxide exhibits higher adsorption of CO<sub>2</sub> compared to NH<sub>3</sub> suggesting that the mineral contains more basic than acidic adsorption sites. These results were explained using the

*Sanderson electronegativity equalization* which states that bonded atoms do not exhibit the same electronegativity as free atoms (Ferreira, 1963). In fact, the electronegativity is equalised and a value can be calculated for bonded atoms if the electronegativity of each atom and the total number of atoms in the system of interest are considered. The Sanderson electronegativity of  $\text{Eu}_2\text{O}_3$  is equal to 2.05 (Shen *et al.*, 1995) while the Sanderson electronegativities of  $\text{CO}_2$  and  $\text{NH}_3$  are 3.32 and 2.73 respectively. Metal ions in aqueous solutions exhibit different electronegativities compared to ions in the gaseous phase or within molecules (bonded atoms) (Li *et al.*, 2012).  $\text{Na}^+$  in solution was found to exhibit an electronegativity of 1.063 while  $\text{Ca}^{2+}$  in solution was found to exhibit an electronegativity of 1.862 (Li *et al.*, 2012). Even though  $\text{Ca}^{2+}$  or  $\text{Na}^+$  cannot be considered acidic or basic, this difference in their electronegativity suggests that calcium ions are more likely to adsorb onto the europium oxide surface due to the higher electronegativity. Another method to evaluate this is by observing the pH of  $\text{CaCl}_2$  and  $\text{NaCl}$  aqueous solutions of similar concentrations. It is well known that  $\text{NaCl}$  results in a neutral solution of pH 7 (under clean conditions) but this is not the case for  $\text{CaCl}_2$ . According to equation (3.6) and the  $K_a$  value, a  $\text{CaCl}_2$  solution would result in a very slightly acidic solution of pH=6.4 (for 1M  $\text{CaCl}_2$ ). Even if the difference between the two is negligible, the results indicate that slightly acidic  $\text{Ca}^{2+}$  is adsorbed faster on the basic sites of the europium oxide surface while  $\text{Na}^+$  shows a slower adsorption.

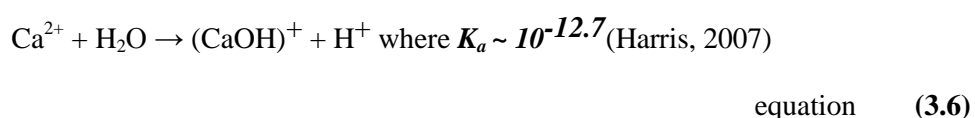


Figure 3.14 summarises the results obtained for the adsorption of MCA onto europium oxide under neutral conditions (pH7). The slower interaction between MCA and the europium oxide surface was observed for the case of  $\text{NaCl}$  while both the calcium chloride and the water-related systems showed a rapid adsorption of the macromolecule. The highest initial mass adsorbed (after a 10 minutes' interaction) was observed in the systems with calcium and water.

The adsorption of MCA onto europium oxide at pH 10, represented the case where a negatively charged surface is being approached by a negatively charged, highly hydrophobic macromolecule (figure 3.15). The results suggested that the interaction between the two was mediated by protons,  $H^+$ . Surprisingly, the larger and hence the ion that exhibited the largest positive charge compared to all the ions tested,  $Ca^{2+}$ , did not result in a rapid adsorption process. This was attributed to the limited availability of the calcium ions under basic conditions where OHs are widely available and result in complexation with calcium to form  $Ca(OH)_2$ . This was not the case observed for the MCA-ceria sorption as calcium was found to be the fastest to mediate the interaction even if sodium and protons eventually reached the leading ion.

Examining the interaction under basic conditions suggests that a negatively charged surface is being approached by a negatively charged macromolecule. Hence, the interaction could only be mediated by a positively charged compound that would act as the connector between the two negative components. The resulting rapid interaction mediated by protons came as a surprise. On the other side, calcium was expected to be the most successful ion to mediate the interaction. The fact that all three electrolytes resulted in very similar adsorption profiles suggested that the interaction was mediated by all three examined ions.

Europium oxide was found to strongly interact with MCA at all possible surface charges and all possible charges of the organic molecule. A rapid response was observed mainly when water or calcium chloride were used as the electrolytes while NaCl showed the slowest interaction rate for all pH conditions. As in the case of Ceria-MCA sorption, having the chloroform 'protecting' and 'driving' the MCA molecules, allowed us to observe the interaction when bulk water molecules (hypothetically acting as '*obstacles*' for the interaction with the surfaces) were repelled. Due to the high density of chloroform, it is hypothesised that the bulk water molecules would be removed and an easier interaction of the organic molecule with the surface would be obtained.

The experimental method used at this stage of the project could not be conclusive in regards to the mechanism used by the macromolecule in order to adsorb on a surface. The surprising results obtained for the MCA-europium oxide sorption process suggested that a different process than that of Ceria-MCA interactions was observed. It has been previously shown that the functional group that reacts with approaching surfaces is the carboxylic acid group found at the end of each MCA forms (Zhang *et al.*, 2010) but secondary functional groups are also available. An example would be the keto group found in the keto-MCA form or the OH group found closely related to the carboxylic acid group in all the MCA forms. Both groups could be potential candidates for interaction under specific conditions and intermolecular binding could also be possible. Hence, a question is raised on whether the orientation of the MCA molecule under different conditions promotes intermolecular binding but this could not be explored using this methodology.

Kinetic analysis was continued with calculation of the order of interactions. Pseudo first order and pseudo-second order models were used and a linear fit ( $R^2 > 0.99$ ) was obtained for a second order reaction (appendix 14). The equations obtained along with the  $R^2$  values are shown in table 3.15. The results agreed well with the experimentally obtained  $Q_e$ . This outcome suggested that pH conditions or ions in solution do not play a role in the interaction and that all systems showed a very similar adsorption mechanism which suggested that neither the pH conditions (and hence the surface charge of the mineral) or the presence or absence of counter ions in solution had an effect on the adsorption of MCA onto europium oxide.

**Table 3.15. Results of kinetic analysis of MCA adsorption to europium oxide**

| ID<br>MCA-Eu <sub>2</sub> O <sub>3</sub> in: | Equation y=Mx+C    | R <sup>2</sup> | Intercept<br>C=1/kQ <sub>e</sub> <sup>2</sup> | Slope<br>M=1/Q <sub>e</sub> | Q <sub>e</sub> = 1/m<br>mg g <sup>-1</sup> | K =1/(CQ <sub>e</sub> <sup>2</sup> )<br>*10 <sup>-3</sup> g mg <sup>-1</sup> min <sup>-1</sup> |
|--|--------------------|----------------|---|-----------------------------|--|--|
| NaCl pH10                                    | Y=0.0089x + 0.0201 | 0.998          | 0.0201  | 0.0089                      | 112.359                                    | 3.940  |
| CaCl <sub>2</sub> pH10                       | Y=0.0088x + 0.0211 | 0.998          | 0.0211  | 0.0088                      | 113.636                                    | 3.670  |
| water pH10                                   | Y=0.0089x + 0.0168 | 0.997          | 0.0168  | 0.0089                      | 112.359                                    | 4.715  |
| NaCl pH3                                     | Y=0.0089x + 0.0187 | 0.998          | 0.0187  | 0.0089                      | 112.359                                    | 4.236  |
| CaCl <sub>2</sub> pH3                        | Y=0.0089x + 0.0206 | 0.998          | 0.0206  | 0.0089                      | 112.359                                    | 3.845  |
| NaCl pH7                                     | Y=0.0089x + 0.0201 | 0.998          | 0.0201  | 0.0089                      | 112.359                                    | 3.941  |
| CaCl <sub>2</sub> pH7                        | Y=0.0089x + 0.0165 | 0.998          | 0.0165  | 0.0089                      | 112.359                                    | 4.800  |
| water pH7                                    | Y=0.0089x + 0.0163 | 0.996          | 0.0163  | 0.0089                      | 112.359                                    | 4.859  |
| water pH3                                    | Y=0.0089x+ 0.0149  | 0.997          | 0.0149  | 0.0089                      | 112.359                                    | 5.316  |

A kinetic advantage of the calcium and water-mediated interactions was observed for the case of neutral and basic conditions respectively, where the europium oxide surface is negatively charged and the MCA molecule is also negative. This was a surprising result especially because calcium mediated interactions did not result in high reaction rates when the basic conditions were tested. Under basic conditions, water-based experiments were found to mediate the interaction at the fastest reaction rate which suggested that a different process is observed when europium oxide is examined compared to that of ceria.

### 3.3.5.2 MCA interactions with europium oxide – Isotherms

Samples were taken at different concentrations for the isotherm analysis as previously described (sub-section 3.2.5). The Langmuir isotherm, the Freundlich isotherm and the Sips isotherm were used for evaluation of the results. Tables 3.16 and 3.17 show examples of the fitting

for Langmuir and Freundlich models and explain why the two could not be used for the tested systems (complete data set can be found in appendices 2 and 3).

The lack of fitting on the Langmuir Isotherm model and the low  $R^2$  values indicated that a monolayer adsorption process was not involved in the interaction and additional models had to be evaluated for better fitting. Table 3.17 shows the equations obtained after fitting the data on the Freundlich model.

Similarly to the fitting on the Langmuir model, the Freundlich model was proven unsuccessful in describing the adsorption of MCA onto europium oxide as shown by the low  $R^2$  values. However, the  $R^2$  values obtained from the Freundlich isotherm were higher than the ones obtained from the Langmuir fitting which suggested that Freundlich was closer to describing the adsorption process. The Sips model was the next model to be tested for fitting. Varying values of  $n$  were tested in order for the best fit to be found. Tables 3.18 and 3.19 are summarizing the equations obtained using the Sips model at  $n=1$  and  $n=0.2$ . Details on the Sips isotherm can be found in sub-section 3.3.4.2.

| <b>Table 3.16. Langmuir Isotherm for MCA adsorption on europium oxide</b> |                    |                         |
|---|--------------------|-------------------------|
| <b>Sample ID MCA in:</b>  | <b>Equation</b>    | <b><math>R^2</math></b> |
| pH3 NaCl Eu <sub>2</sub> O <sub>3</sub>                                   | $Y=0.010x + 0.455$ | 0.83                    |
| pH7 CaCl <sub>2</sub> Eu <sub>2</sub> O <sub>3</sub>                      | $Y=0.012x + 0.359$ | 0.88                    |
| pH3 CaCl <sub>2</sub> Eu <sub>2</sub> O <sub>3</sub>                      | $Y=0.011x + 0.453$ | 0.80                    |
| pH10 water Eu <sub>2</sub> O <sub>3</sub>                                 | $Y=0.005x + 0.766$ | 0.43                    |
| pH7 water Eu <sub>2</sub> O <sub>3</sub>                                  | $Y=0.080x + 0.468$ | 0.82                    |
| pH7 NaCl Eu <sub>2</sub> O <sub>3</sub>                                   | $Y=0.003x + 0.870$ | 0.17                    |
| pH10 CaCl <sub>2</sub> Eu <sub>2</sub> O <sub>3</sub>                     | $Y=0.006x + 0.691$ | 0.63                    |
| pH3 water Eu <sub>2</sub> O <sub>3</sub>                                  | $y=0.007x + 0.631$ | 0.69                    |
| pH10 NaCl Eu <sub>2</sub> O <sub>3</sub>                                  | $y=0.007x + 0.695$ | 0.60                    |

| <b>Sample ID MCA in:</b>                              | <b>Equation</b> | <b>R<sup>2</sup></b> |
|---|-----------------|----------------------|
| pH7 water Eu <sub>2</sub> O <sub>3</sub>              | Y=0.695x+1.226  | 0.94                 |
| pH10 water Eu <sub>2</sub> O <sub>3</sub>             | Y=0.868x+0.437  | 0.89                 |
| pH3 CaCl <sub>2</sub> Eu <sub>2</sub> O <sub>3</sub>  | Y=0.658x+1.206  | 0.72                 |
| pH7 CaCl <sub>2</sub> Eu <sub>2</sub> O <sub>3</sub>  | Y=0.600x+1.412  | 0.81                 |
| pH3 NaCl Eu <sub>2</sub> O <sub>3</sub>               | Y=0.724x+1.094  | 0.98                 |
| pH10 NaCl Eu <sub>2</sub> O <sub>3</sub>              | Y=0.804x+0.623  | 0.87                 |
| pH3 water Eu <sub>2</sub> O <sub>3</sub>              | Y=0.772x+0.826  | 0.91                 |
| pH10 CaCl <sub>2</sub> Eu <sub>2</sub> O <sub>3</sub> | Y=0.798x+0.726  | 0.90                 |
| pH7 NaCl Eu <sub>2</sub> O <sub>3</sub>               | Y=0.966x+0.084  | 0.88                 |

The obtained results suggested that the concept associated with the Sips model was closer to explaining the mechanism involved in the adsorption of MCA onto europium oxide. A combination of a monolayer (Langmuir) and a multi-site process was suggested even though, as explained for the MCA-Ceria systems, no clear mechanism can be extracted. It is possible that bound-MCA to free-MCA interactions were reflecting the observed removal of MCA from the solution.

| <b>Sample ID</b>                                      | <b>Equation</b> | <b>R<sup>2</sup></b> |
|---|-----------------|----------------------|
| pH7 water Eu <sub>2</sub> O <sub>3</sub>              | Y=0.573x+0.006  | 0.99                 |
| pH10 water Eu <sub>2</sub> O <sub>3</sub>             | Y=1.038x+0.001  | 0.98                 |
| pH3 CaCl <sub>2</sub> Eu <sub>2</sub> O <sub>3</sub>  | Y=0.991x+0.002  | 0.95                 |
| pH7 CaCl <sub>2</sub> Eu <sub>2</sub> O <sub>3</sub>  | Y=0.733x+0.006  | 0.98                 |
| pH7 NaCl Eu <sub>2</sub> O <sub>3</sub>               | Y=1.156x-0.002  | 0.98                 |
| pH10 CaCl <sub>2</sub> Eu <sub>2</sub> O <sub>3</sub> | Y=0.895x+0.003  | 0.98                 |
| pH3 water Eu <sub>2</sub> O <sub>3</sub>              | Y=0.837x+0.004  | 0.99                 |
| pH10 NaCl Eu <sub>2</sub> O <sub>3</sub>              | Y=1.013x+0.002  | 0.98                 |
| pH3 NaClEu <sub>2</sub> O <sub>3</sub>                | Y=0.726x+0.006  | 0.99                 |

| <b>Sample ID</b>                                      | <b>Equation</b>    | <b>R<sup>2</sup></b> |
|---|--------------------|----------------------|
| pH3 CaCl <sub>2</sub> Eu <sub>2</sub> O <sub>3</sub>  | y=62723.894x+0.013 | 0.99                 |
| pH7 NaCl Eu <sub>2</sub> O <sub>3</sub>               | Y=87788.938x+0.013 | 0.99                 |
| pH10 CaCl <sub>2</sub> Eu <sub>2</sub> O <sub>3</sub> | Y=36231.381x+0.013 | 0.99                 |
| pH3 water Eu <sub>2</sub> O <sub>3</sub>              | Y=27981.305x+0.013 | 0.99                 |
| pH10 NaCl Eu <sub>2</sub> O <sub>3</sub>              | Y=62793.946x+0.014 | 0.99                 |
| pH3 NaClEu <sub>2</sub> O <sub>3</sub>                | Y=16849.001x+0.013 | 0.99                 |
| pH7 CaCl <sub>2</sub> Eu <sub>2</sub> O <sub>3</sub>  | Y=19216.338x+0.014 | 0.99                 |
| pH7 water Eu <sub>2</sub> O <sub>3</sub>              | Y=5476.202x+0.013  | 0.99                 |
| pH10 water Eu <sub>2</sub> O <sub>3</sub>             | Y=63084.472x+0.013 | 0.99                 |

The fitting obtained for n=0.2 resulted in the highest R<sup>2</sup> values and hence the equations resulting from the fit were used to calculate the varying constants associated with the isotherm (table 3.20).

| <b>ID</b>   | <b>Equation</b>   | <b>Intercept</b>         | <b>Slope</b>                | <b>Q<sub>max</sub></b>   | <b>K<sub>s</sub><br/>x 10<sup>-3</sup></b> |
|---|---|--------------------------|-----------------------------|--------------------------|--|
| <b>Sips Isotherm<br/>MCA in:</b>                      | $\frac{1}{Q_e} = \frac{1}{Q_{\max}K_s} * \left(\frac{1}{C_e}\right)^{\frac{1}{n}} + \frac{1}{Q_{\max}}$ | $C = \frac{1}{Q_{\max}}$ | $m = \frac{1}{Q_{\max}K_s}$ | $Q_{\max} = \frac{1}{C}$ | $K_s = \frac{1}{m * Q_{\max}}$             |
| pH3 CaCl <sub>2</sub> Eu <sub>2</sub> O <sub>3</sub>  | y=62723.894x+0.013  | 0.013                    | 62723.894                   | 76.923                   | 0.0002                                     |
| pH7 NaCl Eu <sub>2</sub> O <sub>3</sub>               | Y=87788.938x+0.013  | 0.013                    | 87788.938                   | 76.923                   | 0.0001                                     |
| pH10 CaCl <sub>2</sub> Eu <sub>2</sub> O <sub>3</sub> | Y=36231.381x+0.013  | 0.013                    | 36231.381                   | 76.923                   | 0.0005                                     |
| pH3 water Eu <sub>2</sub> O <sub>3</sub>              | Y=27981.305x+0.013  | 0.013                    | 27981.305                   | 76.923                   | 0.0002                                     |
| pH10 NaCl Eu <sub>2</sub> O <sub>3</sub>              | Y=62793.946x+0.014  | 0.014                    | 62793.946                   | 71.429                   | 0.0008                                     |
| pH3 NaClEu <sub>2</sub> O <sub>3</sub>                | Y=16849.001x+0.013  | 0.013                    | 16849.001                   | 76.923                   | 0.0007                                     |
| pH7 CaCl <sub>2</sub> Eu <sub>2</sub> O <sub>3</sub>  | Y=19216.338x+0.014  | 0.014                    | 19216.338                   | 71.429                   | 0.002                                      |
| pH7 water Eu <sub>2</sub> O <sub>3</sub>              | Y=5476.202x+0.013   | 0.013                    | 5476.202                    | 76.923                   | 0.0002                                     |
| pH10 water Eu <sub>2</sub> O <sub>3</sub>             | Y=63084.472x+0.013  | 0.013                    | 63084.472                   | 76.923                   | 0.0002                                     |

As in the case of MCA adsorption onto ceria, the value of  $n$  obtained from fitting the experimental data on the Sips model that resulted in the highest  $R^2$  values is closer to zero ( $n=0.2$ ). It was therefore suggested that the Freundlich constant  $K_f$  could be used to calculate the standard free energy change,  $\Delta G$  as the data showed a tendency to follow the Freundlich model (more details in sub-section 2.3.3.2.1). Table 3.21 summarises the results of the calculated free energy change of adsorption using the Freundlich constant after the appropriate adjustments to ensure that the requirements related to the units of the constants were met.

| <b>Table 3.21. <math>\Delta G</math> calculations for MCA adsorption to europium oxide according to Freundlich Isotherm</b> |                         |                         |                                       |
|---|-------------------------|-------------------------|---------------------------------------|
| <b>ID</b>   | <b><math>K_f</math></b> | <b><math>K_c</math></b> | <b><math>\Delta G</math> (kJ/mol)</b> |
| pH3 CaCl <sub>2</sub> Eu <sub>2</sub> O <sub>3</sub>  | 1.206                   | 1206                    | -16.133                               |
| pH7 NaCl Eu <sub>2</sub> O <sub>3</sub>   | 0.084                   | 84                      | -10.075                               |
| pH10 CaCl <sub>2</sub> Eu <sub>2</sub> O <sub>3</sub>   | 0.726                   | 726                     | -14.979                               |
| pH3 water Eu <sub>2</sub> O <sub>3</sub>  | 0.827                   | 827                     | -15.275                               |
| pH10 NaCl Eu <sub>2</sub> O <sub>3</sub>  | 0.623                   | 623                     | -14.631                               |
| pH3 NaClEu <sub>2</sub> O <sub>3</sub>  | 1.203                   | 1203                    | -16.128                               |
| pH7 CaCl <sub>2</sub> Eu <sub>2</sub> O <sub>3</sub>  | 1.412                   | 1412                    | -16.491                               |
| pH7 water Eu <sub>2</sub> O <sub>3</sub>  | 1.226                   | 1226                    | -16.171                               |
| pH10 water Eu <sub>2</sub> O <sub>3</sub>   | 0.437                   | 437                     | -13.825                               |

Negative values of the free energy change were obtained for all the cases of MCA sorption onto europium oxide. The calculated results suggested that at low  $n$  values and hence, following the Freundlich isotherm model of multi-site molecule adsorption, MCA spontaneously adsorbed onto europium oxide under all different pH conditions.

As in the case of ceria-MCA adsorption, it should be noted that the calculated values of  $\Delta G$  are only partly associated with the adsorption of MCA onto europium oxide and do not describe the overall process exclusively. The free energy change of adsorption was calculated using the Freundlich constant as it was concluded from the low  $n$  value that resulted from fitting the data on the Sips isotherm. However, the conclusion that the process is closer to Freundlich should only be used to give an insight on the adsorption process and not provide strict numerical values. Compared to the Ceria-MCA systems, the value of  $n$  that obtained the best fit for the europium oxide-MCA interactions was even closer to zero. This suggested that the europium oxide-MCA systems are more likely to follow the Freundlich model of adsorption compared to the ceria-MCA systems. Nevertheless, the Sips model was found to give the best fit and it is therefore suggested that the interaction of MCA with both ceria and europium oxide is a complex process

that combines a monolayer and a more complex, possibly multi-site interaction (i.e. the Langmuir-Freundlich isotherms).

### 3.3.5.3 ATR-FTIR of Europium Oxide - MCA interactions

IR spectroscopy was used to characterise the europium oxide-MCA complex. Figure 3.16 shows an example of the resulting spectra. Clear MCA peaks can be identified at all spectra which proves the presence of MCA in the reaction product. No europium oxide control is shown due to the lack of peaks associated to the compound in the 1000-2400  $\text{cm}^{-1}$  range.

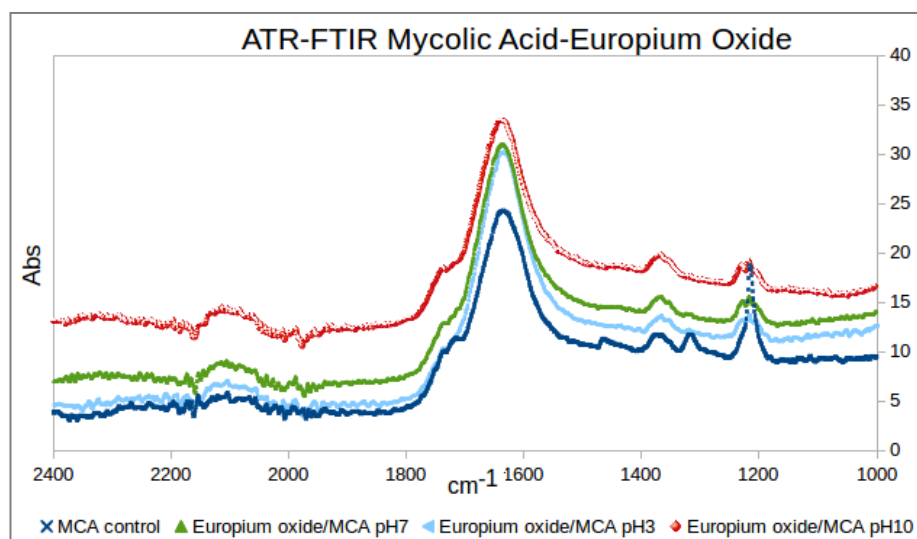


**Figure 3.16.**ATR-FTIR spectra of MCA adsorption onto europium oxide. The peak at  $\sim 1680 \text{ cm}^{-1}$  represents the C=O stretch and the peak at  $1375 \text{ cm}^{-1}$  suggests the presence of -C-H (bending).

A large peak at  $\sim 1680 \text{ cm}^{-1}$  is assigned to the C=O stretch while a second one at  $1375 \text{ cm}^{-1}$  shows the presence of -C-H (bending). A sharp peak representing the C-O functional group of the blank material (MCA control) is observed at  $1210 \text{ cm}^{-1}$ . A small shift of that at the three interacted samples ( $\sim 1250 \text{ cm}^{-1}$ ) shows that the C-O group has been involved in the interaction with the mineral.

### 3.3.6 Comparison between Ceria-MCA and Europium Oxide-MCA interactions

MCA was examined for its sorption behavior onto ceria and europium oxide under acidic, neutral and basic conditions. All systems resulted in a rapid adsorption of the organic molecule onto the minerals when water was used as the electrolyte suggesting that proton ions mediate the interaction. Water was found to increase the sorption at the early stages of the process which suggested a kinetic advantage compared to the other ion-containing cases. Nevertheless, all tested electrolytes contributed to the adsorption of MCA onto both mineral surfaces. Overall, pH does not seem to affect the sorption process to surfaces. The results were surprising especially because usually, pH conditions are a key component of adsorption processes that involve pH sensitive functional groups, such as carboxylic acids. One of the reasons why both surfaces resulted in similar adsorption isotherms was attributed to the fact that the point of zero charge of both surfaces was very close (figure 3.17).

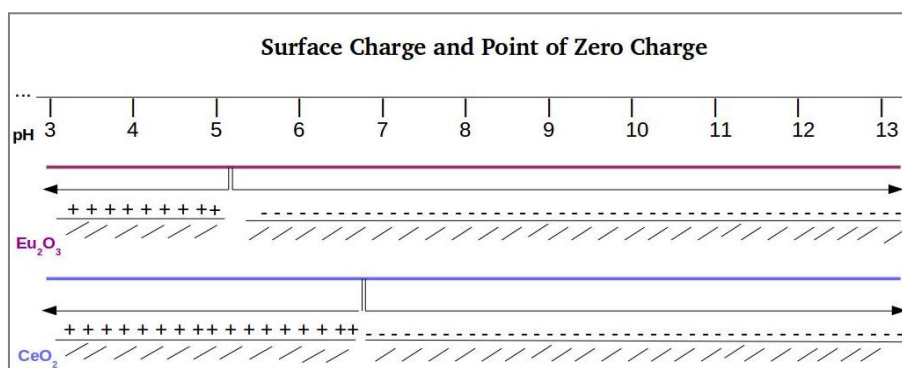


Figure 3.17. Theoretical surface charge of ceria and europium oxide

It could be assumed that since ceria and europium oxide exhibit similar changes on their surface charge depending on pH conditions, a common adhesion behavior would be expected. Surprisingly, even though both the two minerals have similar maximum adsorption capacities, the initial stages of the interactions revealed two different processes. It is believed that the property of the two surfaces that resulted in the different sorption of MCA was their relationship with water.

Europium oxide is a hydrophilic surface that absorbs water while ceria is hydrophobic (Shen *et al.*, 1995; Azimi *et al.*, 2013). This suggests that while europium oxide interacts with water molecules at the solid/liquid interface, ceria inhibits such interactions. As a result, water may promote or inhibit the interaction of organic molecules with the minerals.

Zhang *et al.*(2010) showed that water molecules affected the interaction observed when MCAs were deposited on hydrophilic or hydrophobic surfaces. Hydration layers were observed between the tested hydrophilic surface and the macromolecules. On the other end, no hydration layers were observed when hydrophobic surfaces were tested. Thus, the assumption that water may play a role in the adsorption of MCA depending on the hydrophobicity exhibited by the surface may be the answer to why the ceria and europium oxide surfaces showed different adsorption profiles at least for the early interaction stages. An attempt to examine how water is involved in the interaction with ceria was completed with computational methods (chapter 5).

The use of chloroform as the solvent to dissolve the macromolecules resulted in different observations from those of Zhang *et al.* (2010). The introduction of the organic phase in an aqueous electrolyte resulted in a two-layer system between the aqueous phase and the organic macromolecules. Due to the density of chloroform which is higher than that of water, the organic layer was removing the bulk water molecules. Hence, the organic layer was easily located on top of the tested surfaces. Additionally, the use of chloroform increased the solubility of the MCA carboxylic end in water. That is due to the increased polarity exhibited by the molecule when the organic solvent was introduced. This enhanced polarity resulted in an increased availability of the carboxylic -OH groups which could now undergo hydrogen bonding. The addition of  $\text{Ca}^{2+}$  and  $\text{Na}^+$  further increased the hydrophilicity of the carboxylic end due to the higher charge carried by the salt ions. Hence, the carboxylic oxygens became more negative which promoted the interaction of the carboxylic end groups with water molecules and eventually the mineral surface. A graphical representation of the above explanation is shown in figure 3.18.

This experimental set-up was intended to mimic the natural system. Within bacterial cell walls, MCAs are tightly bound in an orderly arrangement, forming a highly hydrophobic organic layer (represented by the chloroform component in the experimental system) with a layer of enhanced polarity formed by the exposed carboxylic end groups. It is therefore suggested that comparing the results with experiments that do not include an organic solvent will result in major differences.

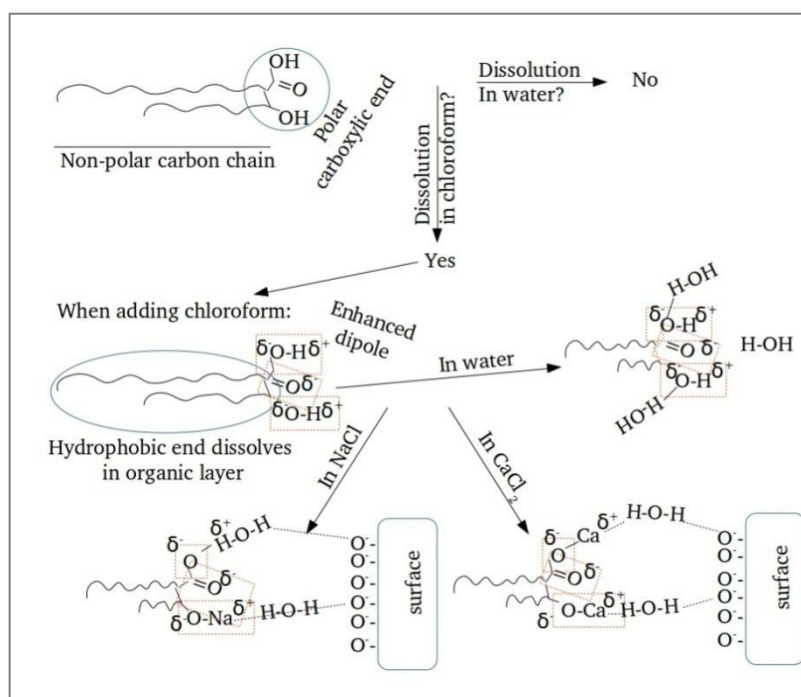


**Figure 3.18.**The effect of chloroform in the solubility of MCA. When using chloroform as solvent, an enhanced dipole at the end of the carbon chain of the MCA (at the  $\text{-COOH}$  functional group) provides the charge difference necessary to mediate interactions with water molecules and other ions (i.e.  $\text{Ca}^{2+}$ ).

The work of Moll *et al.* (2013) summarises the observed mechanisms when bacterial isolates from Mont Terri Opalinus Clay were interacted with a series of actinide and lanthanide ions. Those included  $\text{UO}_2^{2+}$ ,  $\text{Cm}^{3+}$ ,  $\text{Eu}^{3+}$  and  $\text{Pu}^{2+}$  and the identified bacterium was *Sporomusa sp.*, a Gram positive bacterium. Even though this work did not involve any mycolic acids, the results indicated that adsorption processes were mediated by carboxylic acid functional groups. A strong adsorption of uranyl ions on the surface of the cell was observed as a function of pH. Phosphoryl and carboxyl bacterial sites were found to be the major contributors of this process as

complexation resulted from the adsorption process, producing  $R\text{-COO-UO}_2^{2+}$  and  $R\text{-O-PO}_3\text{-UO}_2$  complexes of various forms (Moll *et al.*, 2013). Complexation after reduction of europium ions was also observed by the same species, with the same functional groups acting as the major contributors in the complexation process (Moll *et al.* 2014). A summary of the results as proposed by Moll *et al.*(2013) is shown in figure 3.19. The results suggested that bacterial carboxyl and phosphoric groups are essential for the removal of lanthanide and actinide ions in solution. Even though our work did not involve ion complexation, it is important to note that  $\text{-COOH}$  from bacterial origin can promote biosorption and complexation of highly mobile and toxic species. Our ATR-FTIR results showed that sorption of MCA onto europium oxide involved the C-O group of the bacterial macromolecule. Hence, similarly to the work of Moll *et al.*, our results supported that the functional group involved in the sorption process was the  $\text{-C=O}$  carboxyl component.

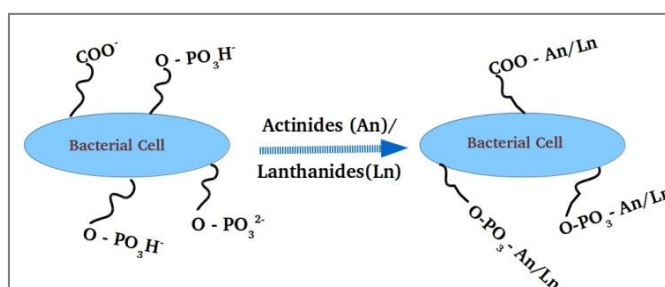


**Figure 3.19. Sorption of An and Ln onto bacterial cells mediated by  $\text{-COOH}$  functional groups. (Moll *et al.*, 2013)**

The interaction of MCA with ceria was further examined with computational methods, explained in chapter 5. A comparison between the two methods is analysed in detail there.

## 3.4 Conclusions

Here the interaction of MCA from bacterial origin with two different nuclear-related oxides, ceria and europium oxide is considered. This work has been the first to examine the interaction of MCA with the mentioned surfaces as no other published work similar to that presented here could be identified in the literature.

Tests on europium oxide and ceria confirmed that MCA, found on the outer layer of gram-positive bacterial cells, interacts with each surface under varying pH and electrolyte conditions. Mass spectrometry and ATR-FTIR confirmed the attachment of the biopolymers to the oxide surfaces after a 1-hour interaction. The results indicated the involvement of the -COOH functional group of MCA in the sorption process and agreed with previously published data. Calcium, sodium and protons tested in solution showed similar effects on the adsorption of MCA on both surfaces except when the systems were tested under acidic conditions. In this case, MCA adsorption to ceria was better when the adsorption process was mediated by protons while MCA adsorption to europium oxide was better for calcium-mediated processes. This difference was attributed to the difference in hydrophobicity of the two surfaces. Ceria is a hydrophobic surface which would attract the organic layer containing MCA molecules in order to repel water molecules found in solution while europium oxide is a hydrophilic surface that has basic adsorption sites. Those are more likely to adsorb calcium ions due to their slightly acidic character. Nevertheless, the adsorption of MCA onto both the ceria and europium surface was successfully mediated in all reaction conditions and the carboxylic end group of MCA was found to be the major contributor to the adsorption process.

This work has shown that MCAs from bacterial origin can mediate bacterial adhesion onto different surfaces via their -COOH end functional group. This indicates that carboxylic groups from bacterial origin can sustain different mechanisms for the removal of highly toxic, nuclear-related particles. Ceria was used as the analogue of urania and thoria in order to examine whether

MCA could adsorb onto the surface. The adsorption was proved successful suggesting that MCA-like polymeric substances could be used for binding and removal of particles from solution in bioremediation processes. This knowledge, in combination with studies that showed sorption and complexation of uranyl and other lanthanide/actinide ions by -COOH bacterial groups, could be used to produce a polymeric substance similar to MCA that will promote treatment of nuclear waste as well as biomining processes.



# **Chapter 4**

## **Peptidoglycan Interactions with Nuclear Related Materials**

## 4.1 Introduction

The preliminary findings of sorption of peptidoglycan (PGN) to nuclear related materials are presented here. PGN is a polymer of sugars and amino acids that forms a layer at the outer side of Gram positive bacteria and the cell wall of Gram negative bacteria. It is found in both Gram positive and negative species making it an ideal candidate to examine sorption mechanisms used by bacteria.

One of the limitations of working with PGN is that extraction methods from bacterial cells result in a PGN containing impurities that require rigorous purification. Preliminary results indicated that commercially available PGN contains proteins which may cause major interference in sorption studies, making it difficult to interpret sorption data. This is a limitation of this study, where the number of experiments and replications performed was constrained by the amount of pure PGN available for the experiments. Thus, the results included in this chapter are only

preliminary and are intended as a comparison to other molecules studied. Although further experimentation is needed to obtain more accurate conclusions, the results presented are encouraging and contribute to provide an overall picture of the processes at cell wall level.

Similarly to lipopolysaccharides, PGN is a complex molecule with a range of functional groups and a series of possible adhesions processes may arise (Van Hee *et al.*, 2004). In the absence of a protective outer membrane in Gram positive bacterial cells, the main role of PGN is to provide rigidity to the cell structure. Gram positive bacterial cells were found to contain about 40 layers of PGN (30%-70% of the cell wall dry weight) (Schleifer and Kandler, 1972). PGN is also found in about 10%-30% of the cell wall dry weight as the inner layer of the Gram negative bacterial cell wall (figure 4.1). PGN maintains the shape of the cell and allows bacterial cells to withstand media of low osmotic pressure. Additionally, in contrast to LPS, PGN is one of the best targets for antibacterial drugs (Crick *et al.*, 2001).

The basic structure of PGN contains alternative units of N-acetylglucosamine and N-acetylmuramic acid (figure 4.2). Attached to each of the N-acetylmuramic acid units is a series of amino acids forming a tetrapeptide.

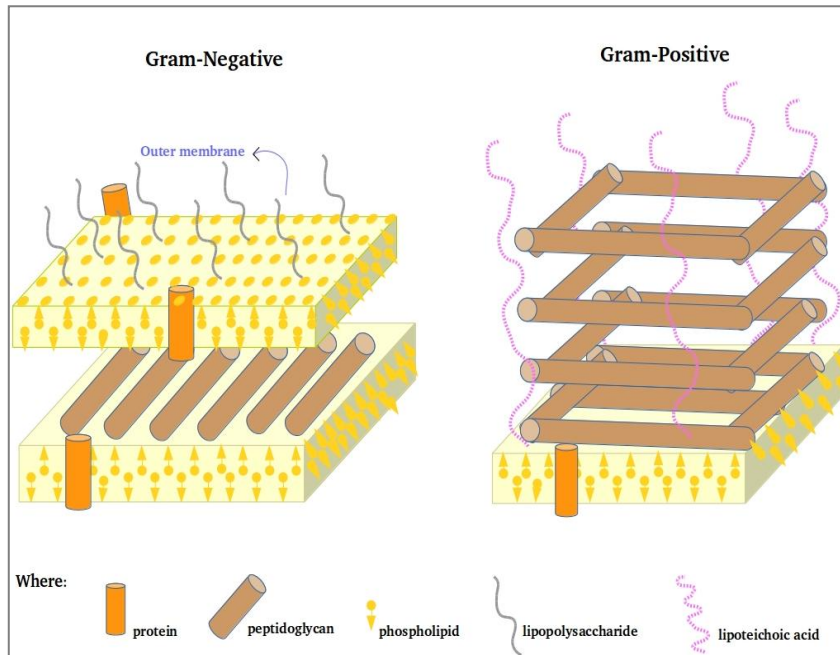


**Figure 4.1. PGN in Gram negative and Gram positive bacterial cell walls.**

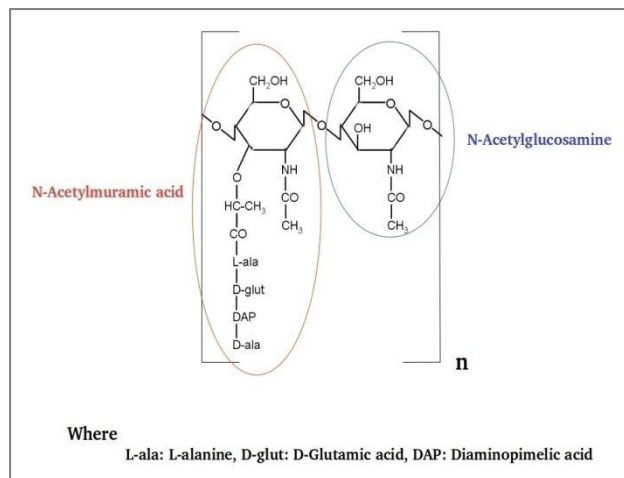


**Figure 4.2. Structure of the repeating unit of PGN**

## 4.1.1 Quantification of PGN

PGN has been established as a successful biomarker for the identification of bacteria. Its quantification is therefore essential and a range of quantification methods is now available in the

literature. High Performance Liquid Chromatography (HPLC), Mass Spectroscopy (MS) and Colorimetric techniques have been used to determine the amount of PGN present in bacterial samples. Since no technique is able to quantify the whole of the molecule, its quantification has been achieved by targeting a part of the molecule. For example, the muramic acid component (figure 4.3) can be identified using the muramic acid assay as described by Hadžija in 1974 (Hadžija, 1974). This simple and rapid method involves the degradation of muramic acid into acetaldehyde. The latter can be quantified colorimetrically with a range of possible complexation techniques including the use of p-hydroxydiphenyl (PHD) with copper solutions. Since there is only one muramic acid group per molecule, the amount of muramic acid can be related to the original amount of PGN in the sample.

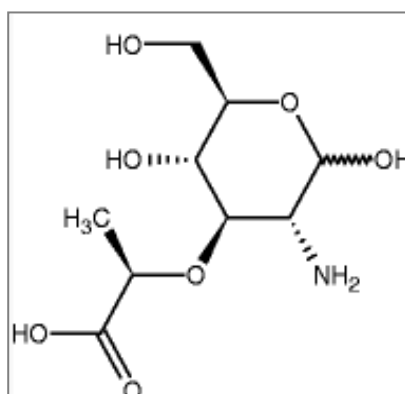


**Figure 4.3. The muramic acid structure**

Another technique used for quantification of PGN involves the quantification of D-lactic acid, resulting from treatment of PGN moieties. Enzymatic bioanalysis of D-lactic Acid-L-lactic acid was explored by Tipper (Tipper, 1968) and a linear relationship between the amount of PGN in solution and the product of the enzymatic analysis was established. A high number of the methods developed for quantification of either the muramic acid moiety or the D-lactic acid moiety coming from a PGN origin were based on these two first methods(Hoijer *et al.*, 1995; Schrijver *et al.*, 1999; Van Hee *et al.*, 2004).

## 4.1.2 PGN interactions with surfaces

Several studies have examined the adsorption of heavy metal oxides and other toxic ions including  $\text{UO}_2^{2+}$ ,  $\text{Pd}^{2+}$ ,  $\text{Cd}^{2+}$  onto PGN layers from Gram positive or Gram negative bacterial cells (Barkleit *et al.*, 2009; Johnson *et al.*, 2006). Several complexation sites were identified including carboxylic sites of glutamic acid and diaminopimelic acid, as well as hydroxyl and amino groups (Barkleit *et al.*, 2009). The identification of mechanisms involving strong complexation after adhesion processes suggested that bacterial PGN is a possible candidate for bioremediation processes.

Strong adsorption of PGN onto kaolinite was also reported (Spencer and Kelleher, 2012). The results indicated that the complexes resulting from such interactions remained dominant after acid hydrolysis. As the authors explained, acid hydrolysis is possibly one of the worst environmental conditions such complexes will ever experience which suggested that a very strong bond between the PGN and the mineral was formed (Spencer and Kelleher, 2012).

Sorption of non-biogenic Fe oxides was studied on *Shewanella putrefaciens*, in order to examine if minerals other than these formed within the bacterial cells during biomineralisation can adsorb onto the bacterial surface. Ferrihydrite (hydrous ferric oxide), goethite ( $\alpha\text{-FeOOH}$ ) and haematite ( $\alpha\text{-Fe}_2\text{O}_3$ ) were found to adhere strongly on the surface. In some cases, the minerals had even penetrated the outer membrane and reached the PGN layer of the cell, suggesting that an adsorption process may be possible between the PGN components and the iron-related minerals (Glasauer *et al.*, 2001).

Polysaccharides share similar chemical composition to peptidoglycan and therefore, their behavior may be comparable to the PGN. Strong adsorption of bacterial polysaccharides was described by Natarajan and Namita who studied the sorption profiles and the changes in surface charge involved in binding between several minerals with the biomolecules (Natarajan and Namita, 2001). Calcite, quartz, corundum and haematite were all assessed for their ability to bind with

bacterial polysaccharides and ATR-FTIR showed specific binding related to -COOH, -NH<sub>2</sub> and -OH groups. Zeta potential analysis showed changes in the surface charge of the minerals after interaction with bacterial polysaccharides and a clear distinction between two different processes was obtained relating the hydrophilic or hydrophobic character of the mineral with the change in surface charge (Natarajan and Namita, 2001).

### **4.1.3 Objectives**

The aim of this work was to examine the interaction of PGN with nuclear related materials at varying pH conditions and in the presence of different counter ions in order to examine whether a universal rule can be drawn for the adhesion of PGN from bacterial origin onto minerals. Non-radioactive surfaces were selected due to the limited availability of analytical instrumentation for the analysis of radioactive materials. The surfaces chosen were: (a) ceria as the analogue of various nuclear-related minerals and (b) europium oxide as a by-product of the uranium fission process. The interaction was tested using experimental techniques (colorimetry and ATR-FTIR).

## 4.2 Materials and Methods

### 4.2.1 Chemicals

All chemicals were purchased from Sigma-Aldrich (UK) and were of analytical grade unless stated otherwise. Double distilled water was used for all the experiments. The peptidoglycan was extracted from *Staphylococcus aureus* and obtained from the Krebs Institute, Department of Molecular Biology and Biotechnology, University of Sheffield led by Dr Stephane Mesnage. The results described in this chapter were performed as batch experiments and only one measurement was taken per system since the total mass available of PGN was ~5 mg.

## 4.2.2 Macromolecules

Chemically produced muramic acid (MA) was purchased from Sigma-Aldrich. Commercially available Peptidoglycan (from *Staphylococcus aureus*) was also purchased from Sigma-Aldrich in order to examine the purity of the product and compare with the purified PGN sample obtained from the Krebs Institute. Stock solutions of purified PGN, non-purified PGN and MA dissolved in water, 0.01M NaCl or 0.01M CaCl<sub>2</sub> were prepared. The pH was adjusted to 3, 7 or 10 with 0.01M HCl or 0.01M NaOH. All stock solutions were vortexed, sonicated for 10 min, and stored overnight at 4 °C before re-equilibration the following day at room temperature.

### 4.2.2.1 Purification of PGN

It has been previously shown that proteins may be covalently bound to commercially available PGN samples (Atrih *et al.*, 1999; Kühner *et al.*, 2014; Trevassos *et al.*, 2004; Guillot *et al.*, 2006). Hence, PGN was purified to avoid any interference of protein moieties with the tested materials (Kühner *et al.*, 2014). The samples were heated with hot 4% sodium dodecyl sulfate (SDS) solution for 15 minutes and were then washed 6 times with distilled water. The washed pellets were then re-suspended in 50mM Tris-HCl (pH7) in the presence of 3mg/ml of pronase and were incubated at 60 °C for 90 minutes. The samples were then washed once with distilled water and were re-suspended in concentrated hydrofluoric acid (HF). The suspensions were incubated at 4 °C for 24 hours after which they were washed with cold distilled water. The supernatant was disposed of and the remaining protein-free PGN was kept at -20 °C until further use. The purity of the samples was tested with High Performance Liquid Chromatography (sub-section 4.2.2.1.1).

#### 4.2.2.1.1 Analysis of peptidoglycan purity using HPLC

The purity of the treated- PGN samples was tested using the method of Atrih *et al.*(1999). High Performance Liquid Chromatography with UV detection was used to separate muuropeptides from the resulting protein-free PGN and assess its purity. The muuropeptides were separated by reverse-phase HPLC (RP-HPLC) on a Hypersil C<sub>18</sub> column (3 µm, 2.1 by 200 mm; ThermoFisher Scientific) coupled to an Agilent 6500 Series Q-TOF LC/MS System. The elution buffers were as follows: A, 10 mM ammonium phosphate (pH 5.5); B, 10 mM ammonium phosphate containing 30% (vol/vol) methanol. The column was equilibrated at 45 °C with buffer A at a flow rate of 0.3 ml/min for 5 min. The sample was then run using a linear gradient of 0 to 75% buffer B over a period of 45 min. The gradient of elution of buffer B was then increased to 100% over a period of 10 minutes (to reach a total of 55 minutes). The flow rate was constant at 0.3 ml/min and the eluted compounds were detected by monitoring the absorbance at 202 nm (Atrih *et al.*, 1999). The results showed clear peaks for the purified PGN muuropeptides with no contamination from proteins or extracellular materials. Figure 4.4 summarises the results of the HPLC analysis analysed by Dr Stephane Mesnage.

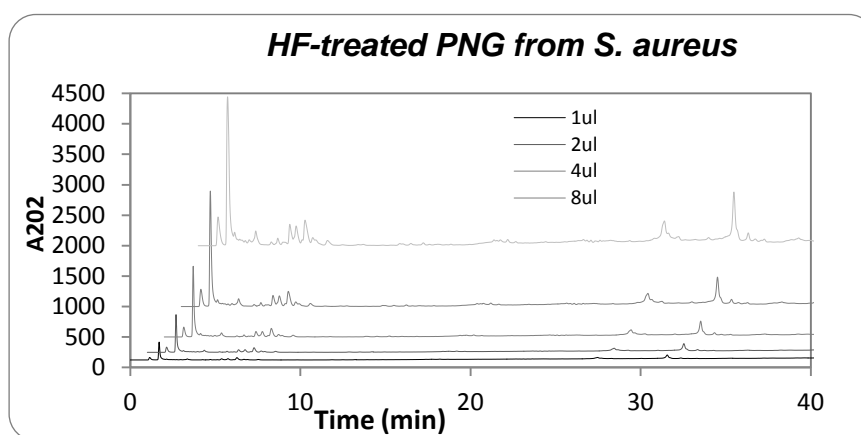


**Figure 4.4.** HPLC results for purity of PGN-treated. The peaks represent the individual muuropeptides extracted from peptidoglycan. (Dr Stephane Mesnage, Univ. of Sheffield, pers. comm.)

### 4.2.3 Minerals

Two different minerals were used in this study: europium oxide  $\text{Eu}_2\text{O}_3$  and ceria  $\text{CeO}_2$ . Both  $\text{Eu}_2\text{O}_3$  and  $\text{CeO}_2$  were purchased from Sigma-Aldrich (UK). X-ray Diffraction (XRD) analysis on the X'Pert<sup>3</sup> Powder by PANalytical on reflection mode for 15 minutes was used for characterization of the materials which were compared to known PDF cards from the literature (details in sub-section 2.3.2.2).

### 4.2.4 Method for PGN and Surface Interactions

The method followed to observe the interactions of PGN with surfaces was similar to the method described before. Two mg of ceria or europium oxide were weighed and transferred in glass tubes with 100  $\mu\text{L}$  of NaCl 0.01M,  $\text{CaCl}_2$  0.01M or water. The pH of the individual samples was adjusted with 0.01M HCl or 0.01M NaOH. The samples were left to equilibrate for 24 hours and the pH was tested. Aliquots of 100  $\mu\text{L}$  of purified- PGN (previously prepared as described in sub-section 4.2.2.1) were added to the tubes.

Kinetic analysis of the interaction of PGN with ceria was performed using the method described in sub-section 2.2.4. Samples were taken at time  $t=1$  min, 5 min, 10 min, 50 min, 90 min and 160 min with constant concentration of adsorbent (PGN 0.2mg/mL) and adsorbate (surface 2mg), constant pressure, temperature and pH.

A second experiment included the construction of experimental isotherms. Samples were taken at constant time, pressure, temperature and pH and varying concentrations of macromolecule added to the system. The concentration of solutions of PGN used for the isotherms were 0.005  $\text{mg ml}^{-1}$ , 0.01  $\text{mg ml}^{-1}$ , 0.012  $\text{mg ml}^{-1}$ , 0.015  $\text{mg ml}^{-1}$  and 0.02  $\text{mg ml}^{-1}$ . The amount of macromolecule adsorbed was calculated by equation (1).

$$Q = \frac{(C_o - C_e)V}{m} \quad \text{equation (4.1)}$$

where Q = amount of PGN adsorbed on mineral (mg g<sup>-1</sup>), C<sub>o</sub>= initial concentration of PGN in solution (mg L<sup>-1</sup>), C<sub>e</sub>= final concentration of PGN in solution (mg L<sup>-1</sup>), m=mass of mineral used (g) and V= volume (L).

#### 4.2.4.1 Isotherm Models

In order to describe the sorption behavior, Langmuir and Freundlich models were used. The assumptions and theory related to each isotherm can be found in sub-section 2.2.4.1. Table 4.1 shows the equations as derived from the models.

| ID         | Equation (linear form)   | Y                   | X                   | Intercept            | Slope           |
|------------|--|---------------------|---------------------|----------------------|-----------------|
| Langmuir   | $\frac{C_e}{Q_e} = \frac{1}{Q_m} \cdot C_e + \frac{1}{(K_l)Q_m}$ | $\frac{C_e}{Q_e}$   | C <sub>e</sub>      | $\frac{1}{(Q_m)K_l}$ | $\frac{1}{Q_m}$ |
| Freundlich | $\ln(Q_e) = \ln(K_f) + \frac{1}{n_f} \cdot \ln(C_e)$             | ln(Q <sub>e</sub> ) | ln(C <sub>e</sub> ) | ln(K <sub>f</sub> )  | $\frac{1}{n_f}$ |

Where C<sub>e</sub>=PGN concentration at equilibrium (mg L<sup>-1</sup>), Q<sub>e</sub>=equilibrium adsorption capacity (mg g<sup>-1</sup>), K<sub>l</sub>= Langmuir adsorption constant (L/mg), Q<sub>m</sub>=maximum adsorption capacity (mg g<sup>-1</sup>), K<sub>f</sub>= Freundlich constant (L/g), n<sub>f</sub>= heterogeneity factor of adsorption sites.

#### 4.2.5 Quantification of PGN – Colorimetric Method

The amount of muramic acid in the samples after the interaction with the minerals was determined using the Hadžija method (Hadžija, 1974) with some modifications (Schrijver *et al.*, 1999 and Hoijer *et al.*, 1995). One hundred μL of the samples were heated for 2 hours at 90°C with 100 μL of 5 M H<sub>2</sub>SO<sub>4</sub>, (hydrolysis). The samples were then neutralized with 100 μL of 10 M NaOH and incubated with an additional 50 μL of 1 M NaOH at 37°C for 30 min. Addition of 100 μL of conc. H<sub>2</sub>SO<sub>4</sub> followed and the samples were heated for 3.5 min at 100°C in a water-bath.

Rapid cooling in ice followed, and the samples were mixed with 10  $\mu\text{L}$  of 4% (w/v)  $\text{CuSO}_4 \cdot 5\text{H}_2\text{O}$  in  $\text{H}_2\text{O}$  and 20  $\mu\text{L}$  1.5% p-hydroxydiphenyl in 96% ethanol. After incubation for 30 min at  $30^\circ\text{C}$ , the absorbance at 560 nm was determined. Controls including purified-PGN (non-reacted) and non-reacted ceria were used. Solutions containing 0–50  $\mu\text{g}/\text{mL}$  of muramic acid in  $\text{H}_2\text{O}$  were used as standards. This method required the development of a calibration curve with standard solutions of muramic acid (MA) and purified PGN concentrations. That was constructed according to the Beer-Lambert Law where absorbance ( $A$ ) is directly related to the analyte concentration and is equal to the absorptivity coefficient ( $\epsilon$ ) multiplied by the analyte concentration ( $C$ ) and the path length ( $l$ ) (equation 4.2).

$$A = \epsilon \cdot C \cdot l \quad \text{equation (4.2)}$$

The Purpald assay to measure the absorbance was performed in transparent 96-well plates (Fisher Scientific) and a Biotek Plate Reader to measure absorbance. The data were analysed using the Gen5 software.

## 4.2.6 Attenuated Total Reflection-Fourier Transform Infrared Spectroscopy (ATR-FTIR)

The functional groups of PGN were characterised using ATR-FTIR before and after the interaction of the macromolecules with the mineral surfaces. An amount of  $2 \pm 0.5\text{mg}$  of minerals was transferred into 2.5 ml glass tubes. Aliquots of 100  $\mu\text{L}$  of 0.01M NaCl solution, 0.01M  $\text{CaCl}_2$  solution or  $\text{H}_2\text{O}$  were then added to the tubes and the pH was adjusted with 0.01M NaOH or 0.01M HCl. The contents of the tubes were mixed and left in the shaker for 24 hours at room temperature to equilibrate. The pH of the equilibrated suspensions was then tested and adjusted if required and 100 $\mu\text{L}$  of 0.1 mg/ml PGN dissolved in water, 0.01M NaCl or 0.01M  $\text{CaCl}_2$  and purified as described before was then added. The tubes were left to interact for 60 minutes and were then centrifuged at 5000rpm for 10 minutes. The supernatant was discarded and the samples left were

freeze dried for 24 hours. FTIR spectra were collected from 400-4000 $\text{cm}^{-1}$ , with a resolution of 4  $\text{cm}^{-1}$ .

### **4.2.7 Zeta Potential Analysis**

Information on the surface charge of PGN and minerals was obtained by measuring the zeta potential using a Zeta Potential Analyzer (ZetaPALS by Brookhaven Instruments Corporation). The zeta potential was also measured to confirm the adsorption of macromolecules onto the mineral surfaces. Suspensions of 0.25  $\text{mg L}^{-1}$  mineral in 0.01M  $\text{CaCl}_2$ , 0.01M  $\text{NaCl}$  solution or  $\text{H}_2\text{O}$  and at different pH (3,7,10 adjusted with 0.01M  $\text{NaOH}$  and 0.01M  $\text{HCl}$ ) were prepared in 250 ml tubes and left to equilibrate for 24 hours before zeta potential measurement. Approximately 1 ml of the cell suspension was transferred to a glass cuvette and the zeta potential was obtained from the average of 10 measurements, presented at a 95% confidence level. The same procedure was followed after the addition of 25 $\mu\text{L}$  of 0.2 $\text{mg ml}^{-1}$  PGN stock solutions at the corresponding pH conditions and after 24 hours of equilibration.

## 4.3 Results and Discussion

### 4.3.1 Adsorption of PGN onto Ceria

#### 4.3.1.1 Zeta Potential of PGN – Ceria interactions

Surface charge is a key component describing the surface behavior of micro-organisms. Therefore, the behavior of their bio-components such as PGN can be used to access important information regarding cell interactions. The observed charge is a result of an increase in net charge at the molecule surface. This affects the distribution of ions in the close surrounding region which results in the formation of a double layer. More details on the double layer can be found in subsection 2.3.3.1.

Figure 4.5 summarises the results of zeta potential of ceria-PGN as a function of pH. Control PGN showed a negative potential at neutral and basic conditions with a slightly positive zeta potential under acidic pH conditions. This result agrees with previously published work on zeta potential of bacterial polysaccharides (Natarajan and Namita, 2001) and also the work of Jiang *et al.*, 2013 who showed that bacterial cells have a low point of zero charge in close-to-neutral aqueous environments (Jiang *et al.*, 2013). The same was shown for both *P. fluorescens* biofilms,

the zeta potential of which is primarily controlled by LPS and PGN moieties (Takenaka *et al.*, 2007).

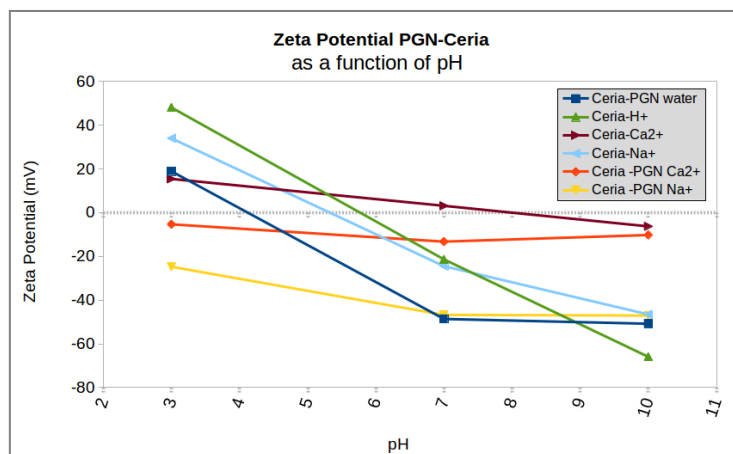


**Figure 4.5.** Zeta potential as a function of pH for ceria before and after the interaction with PGN in the presence of different electrolytes.

Slightly positive zeta-potential is expected for acidic solutions due to the added protons found in the samples which are directly related to zeta potential measurements (Yukselen-Aksoy and Kaya, 2011). Hence, control PGN at pH3 is slightly positive (~5mV – not shown). Similarly, ceria control samples (Ceria-H<sup>+</sup>, Ceria-Na<sup>+</sup>, Ceria-Ca<sup>2+</sup>) under acidic conditions resulted in positive zeta potential while neutral and basic conditions resulted in negative zeta potential measurements (with the exception of Ceria-Ca<sup>2+</sup> at pH 7 which was slightly positive, ~2mV). The small pH-dependent changes in zeta potential values obtained for the Ceria-Ca<sup>2+</sup> controls indicate that intermolecular binding with calcium ions reduces the surface charge and increases molecule aggregation, most likely due to conformational changes exhibited by the PGN macromolecules. This result agreed with reported differences in FTIR spectra of PGN dissolved in water and PGN dissolved in other electrolytes (Naumann *et al.*, 1982). The spectrum obtained for PGN dissolved in electrolytes showed significant peak broadening which was justified as the effect of intermolecular binding mediated by the ions in solution.

The results for the Ceria-PGN systems (figure 4.5) showed a change in zeta potential. The zeta potential of PGN-Ceria at acidic conditions in the presence of water, CaCl<sub>2</sub> and NaCl was 18.94, -5.32 and -24.75 mV respectively. The zeta potential of the Ceria controls at pH3 (indicated in figure 4.5 as Ceria-H<sup>+</sup> for ceria in water, Ceria-Na<sup>+</sup> for ceria in NaCl and Ceria-Ca<sup>2+</sup> for Ceria in CaCl<sub>2</sub>) was always higher than 0 mV. This decrease in zeta potential and the change from positive to negative values when the macromolecule is added in the system indicates that the surface charge has changed, most likely due to sorption of the molecule to the surface. Similarly, the zeta potential of PGN-Ceria at neutral conditions in the presence of water, CaCl<sub>2</sub> and NaCl was -48.62, -13.25 and -46.77 mV respectively. Lastly, the zeta potential of PGN-Ceria at basic conditions in the presence of water, CaCl<sub>2</sub> and NaCl was -50.81, -10.21 and -47.06 mV respectively. In general, it was observed that in all acidic and neutral Ceria-PGN samples, the zeta potential was lower than the zeta potential of the Ceria controls while the basic systems showed a slight decrease in the measured zeta-potential values when the macromolecule was added to the system. These results agreed with the observed reduction in zeta potential with increasing hydrophobicity of hydrocarbon adsorption onto *Staphylococcus aureus* (Wilson *et al.*, 2001) and suggested that an adsorption process has taken place. Similar observations were reported by Natarajan and Namita who examined the interactions of several surfaces including calcite, quartz, kaolinite, haematite and corundum with bacterial polysaccharides and bacterial proteins (Natarajan and Namita, 2001). The results presented here agreed well with the reported values of zeta potential changes associated with bacterial polysaccharide interactions with haematite and corundum. The measured zeta potentials of the surfaces were observed to shift towards more negative values when those were treated with bacterial polysaccharides. For example, the isoelectric point (IEP) for corundum before the interaction was close to pH 7 while after the sorption experiment it shifted to a lower pH of about 2.8. The work described here did not include enough data points in order to examine the true IEP values of ceria before and after interaction with the bacterial compound. However, a general shift towards more negative values is observed when the zeta potential of the surface was tested in the range 3<pH<7 where all the ceria controls started with a high zeta potential while the

Ceria-PGN samples were moving towards negative zeta potential. Thus, this change in zeta potential after the addition of PGN in ceria samples indicated a successful sorption process.

### 4.3.1.2 Muramic Acid Assay-Calibration Curve

The muramic acid assay as proposed by Hadžija (Hadžija, 1974) with some modifications (Schrijver *et al.*, 1999 and Hoijer *et al.*,1995) was chosen as the quantification method of PGN before and after its interaction with ceria. A calibration curve was constructed in accordance to the Beer-Lambert law. A series of tests was run to establish whether ions in solution had an effect on the assay but no trends were observed. This led to the conclusion that a single calibration curve would be sufficient for the quantification of PGN when each of the different electrolytes were included in the reaction system. A summary of the results can be found in figure 4.6. A linear relationship was observed describing the absorption of light at 560 nm and the concentration of muramic acid (shown as  $\mu\text{g/mL}$ ) in the presence of  $\text{Ca}^{2+}$ ,  $\text{Na}^{+}$  and  $\text{H}^{+}$ . The results were comparable to that of Hadžija (Hadžija, 1974) where similar curves were obtained. The curve was also evaluated by examining standard samples of commercially available muramic acid against PGN-derived muramic acid.

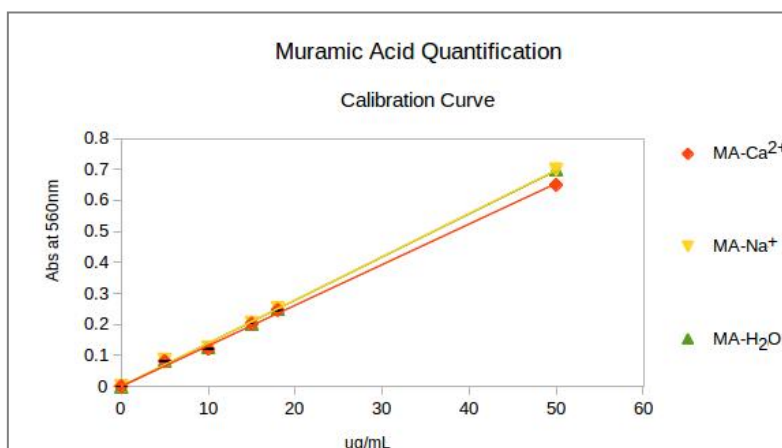


Figure 4.6. Calibration curve for muramic acid quantification with varying electrolytes

It has been previously shown that commercially available PGN contained proteins that were strongly bound to the PGN molecules. Hence, the samples containing non-purified PGN could have been contaminated with proteins. Samples involving purified- PGN produced results in accordance to the calibration curve constructed using the muramic acid assay. However, when non-purified PGN samples were tested, the absorption at 560nm was higher than expected. This indicated that proteins were present in the tested samples and were interfering with the measurement. As a result, it was decided that the calibration curve was not suitable for such samples and only purified PGN samples were to be tested for sorption onto ceria.

### **4.3.1.3 Adsorption of PGN onto Ceria-Kinetics**

The interaction of PGN with ceria was assessed using the muramic acid assay. After an equilibration time of 24 hours with small amounts of the mineral in the different electrolytes, a quantity of purified PGN was added and aliquots were taken at different times in order to evaluate the kinetics of the interaction. The experiments were run under neutral pH conditions and different counter ions (proton, sodium and calcium) were included in order to examine if they play any role in the interaction. An example of the results obtained for the Ceria- PGN systems is presented in figure 4.7.

No major differences were observed related to the inclusion or the absence of the different counter ions. The PGN-Ceria with water system seemed to have a more rapid response to the process (hence, the highest adsorption of PGN onto ceria at time=1min). The Na-mediated interaction showed the slowest response. Nevertheless, all three systems eventually reached a very similar maximum sorption capacity. The adsorption of PGN onto ceria was found to reach a plateau after a 100-120 minutes' interaction for all three electrolytes at neutral conditions.

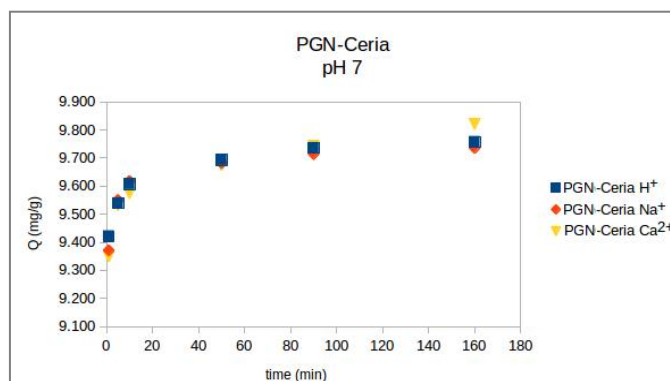


**Figure 4.7. Kinetics of adsorption of PGN with Ceria -pH7.**

The point of zero charge of ceria ranges from 6.4 – 8.6 (Kosmulsko, 2002; Nolan and Watson, 2006). This suggests that the mineral exhibits a positive charge below pH 6.4 and a negative charge above pH 8.6. The adsorption of PGN onto ceria at pH 7, represents the case where a slightly positive, close to neutral surface is being approached by an overall negatively charged macromolecule. The protonation state of the main functional groups associated with PGN is shown in table 4.2. According to the pKa values obtained by potentiometric titrations, carboxylic groups from PGN at neutral conditions are negatively charged while amine and hydroxyl groups are positively charged (Tofail, 2012). A spontaneous interaction was therefore expected involving the slightly positively charged surface and the negatively charged -COOH sites. The fact that no trends were associated with the inclusion or exclusion of ions in solution further supports the signs of a spontaneous interaction between two oppositely charged compounds. At this stage, the kinetics analysis only showed signs of the possible adsorption mechanism with different possible scenarios arising from the results. Further investigation using more suitable methods was needed in order to distinguish between the different PGN moieties that were possible candidates to serve as sorption sites. This was achieved using ATR-FTIR which is described in sub-section 4.2.6.

In general, all three electrolytes successfully mediated the interactions and resulted in similar adsorption profiles. The high Q values suggested that even though ions were present in solution with the purified PGN, they did not interfere with the sorption process and the PGN

interaction with ceria had a kinetic advantage over possible intermolecular reactions involving charged PGN sites and the ions in solution.

| <b>pK<sub>a</sub></b> | <b>Sites</b>                      | <b>Charge at pH 7</b> | <b>Reaction</b>  |
|-----------------------|-----------------------------------|-----------------------|--|
| 4.55 +/- 0.02         | Carboxyl<br>(glutamic acid)       | -                     | R-COOH → R-COO <sup>-</sup> + H <sup>+</sup>   |
| 6.31 +/- 0.01         | Carboxyl<br>(diaminopimelic acid) | -                     | R-COOH → R-COO <sup>-</sup> + H <sup>+</sup>   |
| 9.56 +/- 0.03         | Amine/Hydroxyl                    | +                     | R-NH <sub>3</sub> <sup>+</sup> → R-NH <sub>2</sub> + H <sup>+</sup><br>or R-OH → R-O <sup>-</sup> + H <sup>+</sup> |

Kinetic data was analysed using pseudo first order and pseudo-second order models. A linear fit was obtained for a second order reaction using equation (4.3).

$$\frac{dQ}{dt} = k(Q_e - Q_t)^2 \quad \text{equation (4.3)}$$

where  $Q_e$  and  $Q_t$  =adsorption capacity at equilibrium and time  $t$  respectively ( $\text{mg g}^{-1}$ ),  $k$ = rate constant of the pseudo second order adsorption ( $\text{g mg}^{-1} \text{min}^{-1}$ ).

The linear form of equation (4.3) is shown in equation (4.4). The equations obtained along with the  $R^2$  values are shown in table 4.3.

$$\frac{t}{Q_t} = \frac{1}{kQ_e^2} + \frac{t}{Q_e} \quad \text{equation (4.4)}$$

where  $k$ =rate constant of the pseudo second order adsorption ( $\text{g ml}^{-1} \text{min}^{-1}$ )

| <b>ID<br/>PGN in:</b>                  | <b>Equation<br/><math>y=Mx+C</math></b> | <b><math>R^2</math></b> | <b>Intercept<br/><math>C=1/kQ_e^2</math></b> | <b>Slope<br/><math>M=1/Q_e</math></b> | <b><math>Q_e = 1/m</math><br/><math>mg\ g^{-1}</math></b> | <b><math>K = 1/(CQ_e^2)</math><br/><math>g\ mg^{-1}\ min^{-1}</math></b> |
|--|---|-------------------------|--|---------------------------------------|---|--|
| pH7 CaCl <sub>2</sub> CeO <sub>2</sub> | Y=0.102x + 0.032                        | 1                       | 0.032  | 0.102                                 | 9.804   | 0.325  |
| pH7 water CeO <sub>2</sub>             | Y=0.102x + 0.016                        | 1                       | 0.016  | 0.102                                 | 9.804   | 0.652  |
| PH7 NaCl CeO <sub>2</sub>              | y=0.103x + 0.014                        | 1                       | 0.014  | 0.103                                 | 9.709   | 0.758  |

The high values of  $R^2$  obtained for all systems tested suggested a very good fit on the pseudo-second order model, examples of which can be found in figure 4.8. In general, it was observed that the calculated  $Q_e$  values agreed well with the experimentally obtained values.

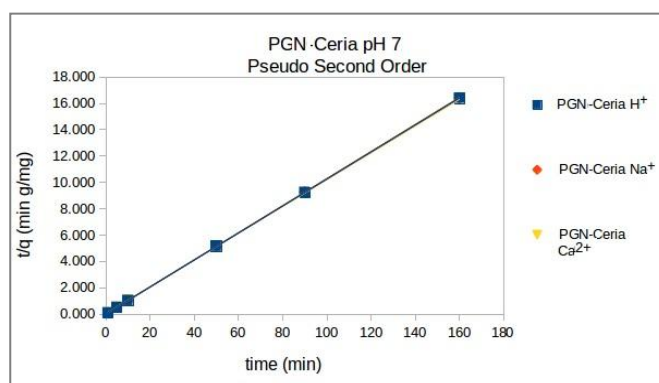


**Figure 4.8. Pseudo second order kinetics for PGN-Ceria at pH 7**

#### **4.3.1.4 Adsorption of PGN onto Ceria-Isotherm**

The adsorption of PGN onto ceria was tested using the muramic acid assay as described in sub-section 4.2.5. Due to the limited availability of purified PGN as the starting compound, batch experiments were run. The experiments were only carried out once hence no error bars could be included in the analysis. The experiment included the measurement of remaining PGN in solution after its interaction with the surface in the presence of different electrolytes and at neutral pH conditions. Neutral pH conditions were chosen in order to examine the interaction close to

environmental conditions and hence, observe the interaction at the conditions bacteria are usually found (Tofail, 2012).

The remaining PGN was quantified using the muramic assay. The calculated value of  $Q_e$  (mg of muramic acid adsorbed per gram of ceria) was then plotted against the concentration of muramic acid at equilibrium in order for the best isotherm to be chosen. The Langmuir, the Freundlich, a modified version of the Freundlich and the Sips isotherms were all tested for comparison purposes. The Langmuir isotherm resulted in the best fit giving the highest  $R^2$  values. Examples of data fitting on the Langmuir isotherm are shown in figure 4.9 and table 4.4.

| Sample ID                              | Equation         | $R^2$ |
|--|------------------|-------|
| pH7 CaCl <sub>2</sub> CeO <sub>2</sub> | $Y=0.373x+0.017$ | 0.99  |
| pH7 water CeO <sub>2</sub>             | $Y=0.384x+0.032$ | 0.92  |
| PH7 NaCl CeO <sub>2</sub>              | $Y=0.443x+0.015$ | 0.85  |

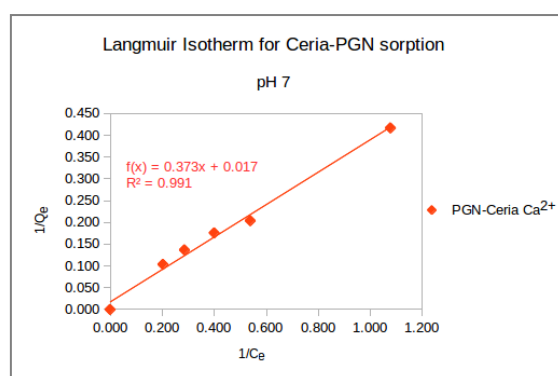


Figure 4.9. Fitting on the Langmuir isotherm of Ceria-PGN with CaCl<sub>2</sub>

The highest  $R^2$  values were obtained using the Langmuir isotherm for the cases of calcium mediated interaction and water mediated interaction. The sodium-mediated interaction resulted in a lower  $R^2$  value of 0.85. The results suggested that the adsorption of PGN onto Ceria follows a monolayer process as described by the Langmuir isotherm. The high  $R^2$  values obtained, especially

for the calcium-mediated interaction suggested a linear adsorption of PGN onto the ceria surface. The isotherm constants were calculated as previously described. A summary of the results is shown in table 4.5.

| <b>ID</b>                              | <b>Equation</b>  | <b>Intercept</b>        | <b>Slope</b>               | <b>Q<sub>max</sub></b>  | <b>K<sub>1</sub></b>          |
|--|--|-------------------------|----------------------------|-------------------------|-------------------------------|
| <b>Langmuir Isotherm</b>               | $\frac{1}{Q_e} = \frac{1}{Q_{max}K_1} * \left(\frac{1}{C_e}\right) + \frac{1}{Q_{max}}$ $y = \left(\frac{1}{Q_e}\right)x = \left(\frac{1}{C_e}\right)$ | $C = \frac{1}{Q_{max}}$ | $m = \frac{1}{Q_{max}K_1}$ | $Q_{max} = \frac{1}{C}$ | $K_1 = \frac{1}{m * Q_{max}}$ |
| pH7 CaCl <sub>2</sub> CeO <sub>2</sub> | Y=0.373x+0.017   | 0.017                   | 0.373                      | 66.667                  | 0.034                         |
| pH7 water CeO <sub>2</sub>             | Y=0.384x+0.032   | 0.032                   | 0.384                      | 58.824                  | 0.046                         |
| PH7 NaCl CeO <sub>2</sub>              | Y=0.443x+0.015   | 0.015                   | 0.443                      | 31.250                  | 0.083                         |

The theoretical results obtained for the maximum Q values showed a higher maximum adsorption capacity for the calcium-mediated interaction. That was further supported by the kinetics results were the calcium-mediated interaction resulted in a slightly higher mass of PGN adsorbed onto the surface during the 60-minute period.

Isotherm models are often used to extract thermodynamic parameters as previously described (sub-section 2.3.3.2.1). Since fitting to the Langmuir isotherm produced the higher R<sup>2</sup> values for the sorption of PGN on ceria, the K<sub>1</sub> constants obtained from the isotherm, were used to calculate the free energy change of adsorption, ΔG. A small adjustment to produce dimensionless values was needed to meet the requirements for ΔG calculations (equation (4.5) where K<sub>1</sub> is in L g<sup>-1</sup> and 1 L = 1000mL or g since the solution density is ~1 g ml<sup>-1</sup>).

$$K_d = 1000K_1 \quad \text{equation (4.5)}$$

| <b>ID</b>                              | <b><math>K_1</math></b> | <b><math>K_d</math></b> | <b><math>\Delta G</math> (kJ/mol)</b> |
|--|-------------------------|-------------------------|---------------------------------------|
| pH7 CaCl <sub>2</sub> CeO <sub>2</sub> | 0.034                   | 34                      | -8.000                                |
| pH7 NaCl CeO <sub>2</sub>              | 0.046                   | 46                      | -8.674                                |
| pH7 water CeO <sub>2</sub>             | 0.083                   | 83                      | -10.044                               |

The resulting negative  $\Delta G$  values (table 4.6) suggest a spontaneous reaction at neutral conditions when all the electrolytes were used. The results were in the range of physisorption (-40 to 0 kJ/mol) (Bhatt *et al.*, 2012). This supports the hypothesis that PGN structures adsorb onto ceria surfaces and a further investigation is needed in order to identify the active chemical sites that allow PGN to interact with approaching minerals.

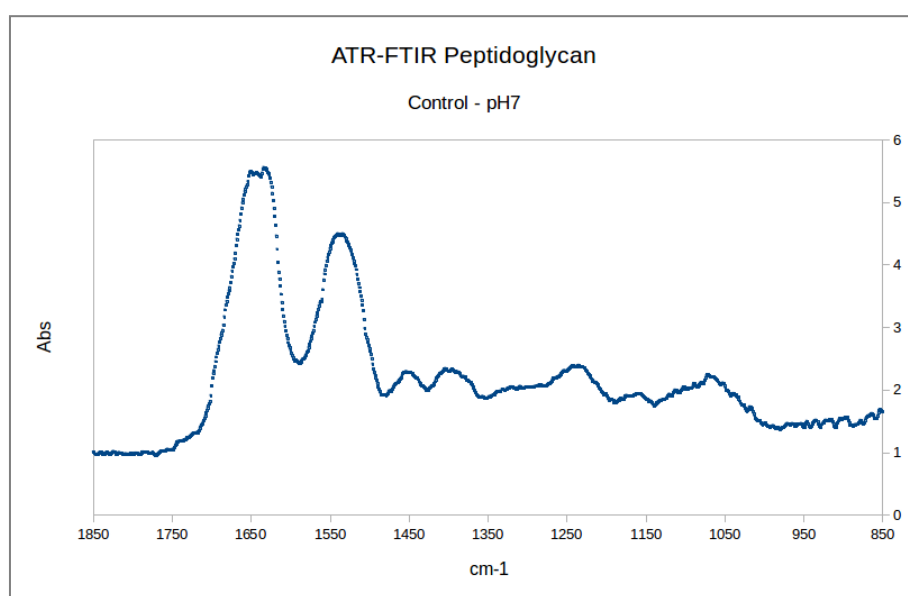
#### **4.3.1.5 ATR-FTIR of Ceria - PGN interactions**

It has been previously suggested that the -COOH groups found in PGN moieties are responsible for the observed adsorption of minerals (Naumann *et al.*, 1982). In order to examine whether this was true for the ceria adsorption processes, ATR-FTIR was used to investigate the functional groups found in interacted and non-interacted samples and to examine if any differences in the FTIR spectra of the two could provide information on the functional groups involved in the interaction.

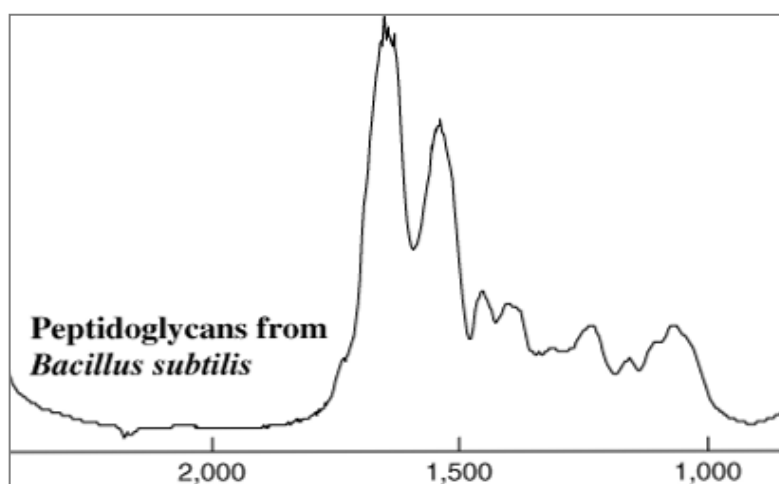
IR spectroscopy was used to characterise the Ceria-PGN complex. Evaluation of the interaction in a range of pH conditions in order to examine the effect of surface charge on binding is usually carried out for such processes. Due to the limited availability of purified PGN, tests were run only at pH7.

Figure 4.10 shows an example of the resulting spectra of a control PGN sample. Clear sharp peaks were obtained at 1600-1650 cm<sup>-1</sup>, 1540-1550 cm<sup>-1</sup>, 1450 cm<sup>-1</sup>, 1400 cm<sup>-1</sup>, 1230-1240

$\text{cm}^{-1}$ ,  $1060 \text{ cm}^{-1}$  representing mainly amide and carboxylic functional groups. The observed peaks correspond to C=O stretching vibrations from carboxylic and amide groups, N-H bending vibration and C-N stretching vibration from the amide groups, C-H stretch, C-H bend or C-N and C-O-C respectively. The results were compared to the work of Leenheer and Rostad (figure 4.11) and similar peaks were observed in the  $900\text{-}2000 \text{ cm}^{-1}$  range. All the peaks in the range  $2500\text{-}3500 \text{ cm}^{-1}$  have been ignored due to interference by water. A ceria control sample was also tested and no peaks were observed in the range  $900\text{-}2500 \text{ cm}^{-1}$ .



**Figure 4.10. ATR-FTIR spectra of PGN control**



**Figure 4.11. FT-IR spectra of PGN at pH7 measuring absorbance (Leenheer and Rostad, 2004)**

Figure 4.12 shows examples of the Ceria-PGN complexes. A different spectrum from that of control PGN samples was obtained. A small peak at  $\sim 1650\text{ cm}^{-1}$  confirmed the presence of C=O bonds in the sample while a large shift of the  $1450\text{ cm}^{-1}$  peak to  $1430\text{ cm}^{-1}$  corresponds to the adsorption of the PGN onto ceria via a combination of carboxylic and amide groups. While PGN control spectra show small and sharp peaks, it has been previously shown that FTIR analysis of PGN in salts results in a band broadening of typical carboxylate bands in the  $1600$  and  $1400\text{ cm}^{-1}$  regions (Naumann *et al.*, 1982). That is believed to be due to intermolecular binding mediated by the ions in solution (i.e. calcium) which increases the vibration and stretching exhibited by the amine and carboxyl-related bonds. This broadening is strongly observed at the  $1440\text{ cm}^{-1}$  region where a combination of the amide ( $1534\text{ cm}^{-1}$ ), the symmetric C-H ( $1450\text{ cm}^{-1}$ ) and the symmetric C=O of  $-\text{COO}-$  ( $1400\text{ cm}^{-1}$ ) is observed. The peak is very broad which suggests that the mentioned bands were covered within the one peak observed in the spectra. The peak at  $880\text{ cm}^{-1}$  confirms the presence of reacted  $\text{CeO}_2$  which has been covered by  $\text{NO}_3^-$  (with a small shift from the  $834\text{ cm}^{-1}$  usually observed for the asymmetric stretching mode of the nitrate group (Vivek *et al.*, 2016)).

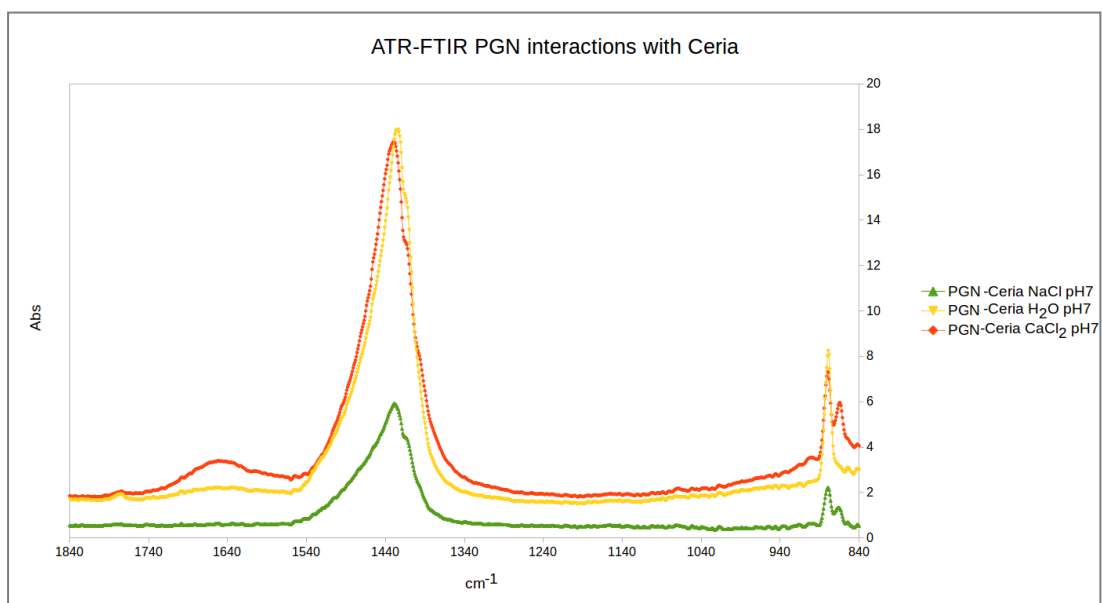


**Figure 4.12. ATR-FTIR spectra of Ceria- PGN**

Peaks were observed in the range of 1050-1200  $\text{cm}^{-1}$  which are not visible in figure 4.12 due to the large absorption difference at 1430  $\text{cm}^{-1}$ . The same peaks at 1050, 1070 and 1150  $\text{cm}^{-1}$ , related to complex sugar ring modes are observed in all control and Ceria-PGN systems confirming the presence of PGN-related functional groups in the PGN-Ceria complexes.

The shift in the -COOH and amide related bands confirms the binding via the carboxylic and amide groups which was previously proposed by several research groups. This indicates that under environmental conditions where the pH is close to 7, interactions between the  $-\text{COO}^-$  or the N-C=O groups and the positively charged-close to neutral ceria surface would take place.

## 4.3.2 Adsorption of PGN onto europium oxide

### 4.3.2.1 ATR-FTIR of europium oxide - PGN interactions

Due to the limited availability of purified PGN starting material, only IR spectroscopy was used to characterise the europium oxide- PGN complex.

According to the point of zero charge of europium oxide (pH=5), the mineral is negatively charged under neutral conditions. At the same time, PGN has both negatively and positively charged moieties as proposed by the  $pK_a$  values obtained for -COOH and amide from bacterial origin.

Figure 4.10 shows an example of the resulting spectra of a control PGN sample. Clear sharp peaks were obtained at  $1600-1650\text{ cm}^{-1}$ ,  $1540-1550\text{ cm}^{-1}$ ,  $1450\text{ cm}^{-1}$ ,  $1400\text{ cm}^{-1}$ ,  $1230-1240\text{ cm}^{-1}$ ,  $1060\text{ cm}^{-1}$  representing mainly amide and carboxylic bands. The observed peaks correspond to C=O stretching vibrations from carboxylic and amide groups, N-H bending vibration and C-N stretching vibration from the amide groups, C-H stretch, C-H bend or C-N and C-O-C respectively. The results were compared to the work of Leenheer and Rostad (figure 4.11) and similar peaks were observed in the  $900-2000\text{ cm}^{-1}$  range. All the peaks in the range  $2500-3500\text{ cm}^{-1}$  have been ignored due to interference by water. A europium oxide control sample was also tested and no peaks were observed in the range  $900-2500\text{ cm}^{-1}$ .

Figure 4.13 shows an example of the europium oxide-PGN complexes. A different spectrum from that of control PGN samples was obtained. A small peak at  $\sim 1650\text{ cm}^{-1}$  confirms the presence of C=O bonds while a large shift of the  $1450\text{ cm}^{-1}$  peak to  $1430\text{ cm}^{-1}$  corresponds to the adsorption of the PGN onto europium oxide via a combination of carboxylic and amide groups. FTIR analysis of PGN in salts results in a band broadening of typical carboxylate bands in the  $1600$  and  $1400\text{ cm}^{-1}$  regions (Naumann *et al.*, 1982). This broadening is observed at the  $1440\text{ cm}^{-1}$  region where a combination of the amide ( $1534\text{ cm}^{-1}$ ), the symmetric C-H ( $1450\text{ cm}^{-1}$ ) and the symmetric C=O of -COO- ( $1400\text{ cm}^{-1}$ ) is observed. The peak is very broad which suggests that the mentioned bands were covered within the one peak observed in the spectra. The shift from  $1640\text{ cm}^{-1}$  to  $1650\text{ cm}^{-1}$  confirms the presence and involvement in the sorption process of C=O groups while the peak at  $\sim 880\text{ cm}^{-1}$  confirms the presence of reacted  $\text{Eu}_2\text{O}_3$  covered with  $\text{NO}_3^-$  (with a small shift from the  $834\text{ cm}^{-1}$  usually observed for the asymmetric stretching mode of the nitrate group (Vivek *et al.*, 2016)).

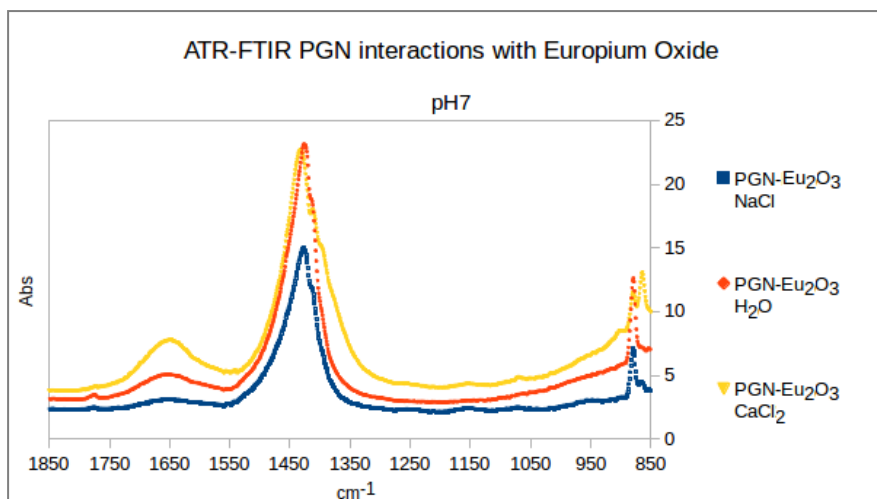


**Figure 4.13.ATR-FTIR spectra of Europium oxide- PGN at pH7**

The results are almost identical to the FTIR spectra of ceria-PGN complexes. This is due to the absence of any ceria or europium-related bands which are usually found below the  $900\text{ cm}^{-1}$  range. Thus, no real distinction between the systems can be made using the spectra but the presence of PGN-related peaks in both spectra in combination with the results obtained from zeta potential analysis and sorption behavior indicate that an adsorption process has taken place. Additionally, the broad peak in the  $1450\text{ cm}^{-1}$  range is indicative of intermolecular binding involving -COOH and amide groups present in PGN. This is further supported by the small pH-dependent changes in zeta potential values obtained for the Ceria- $\text{Ca}^{2+}$  controls. The results indicated that intermolecular binding with calcium ions reduces the surface charge and increases molecule aggregation, most likely due to conformational changes exhibited by the PGN macromolecules. Combining the two results, a question arises on whether -COOH groups are available for binding when calcium ions are present in solution. This cannot be answered by examining the spectra but the successful sorption behavior and the linear fit obtained using the Langmuir isotherm indicates that sorption did take place and the limited availability of -COOH in combination with amide groups present in PGN were able to promote binding on the minerals. Therefore, it is proposed that the presence of calcium ions contributes to modifications of the PGN

surface making it available for sorption to ceria. This behavior is similar to the sorption profiles of LPS, where the calcium ions seem to mediate the sorption of the mineral surfaces studied.

Peaks were observed in the range of 1050-1200  $\text{cm}^{-1}$  which are not visible in figure 4.13 due to the large peak observed at 1430  $\text{cm}^{-1}$ . As in the case of Ceria- PGN complexes, the same peaks at 1050, 1070 and 1150  $\text{cm}^{-1}$  were observed in all cases confirming the presence of PGN-related functional groups in the PGN-  $\text{Eu}_2\text{O}_3$  complexes.

At pH 7 (environmental conditions), PGN possesses negatively charged -COOH groups which would enable electrostatic interaction with positively charged minerals with point of zero charge ( $p_{zc}$ ) higher than pH 7, such as ceria and thoria ( $p_{zc}=8$ ). However, such an electrostatic interaction is unlikely for minerals with  $p_{zc}<7$  like europium oxide or urania ( $p_{zc}=5$ ) which suggests that the PGN moieties used an alternative mechanism for adhesion compared to the one used for bonding on ceria. Shifts relating both -COOH and C-NH<sub>2</sub> groups suggest a synergistic effect of the two functional groups that mediated the sorption of PGN onto europium oxide.

## 4.4 Conclusions

Here the interaction of PGN from bacterial origin with two different nuclear-related oxides: ceria and europium oxide is considered. This work has been the first to examine the interaction of PGN with the mentioned surfaces and a review of the current literature suggests that there has not been any other published work similar to the one presented here.

Tests on ceria confirmed that PGN interacts with the surface under varying electrolyte conditions and neutral pH. Colorimetry confirmed the attachment of the biopolymers to the oxide surface after a 160-minute interaction. The results indicated the involvement of two different functional groups in the sorption process: -COOH and amide. Previous studies have related these groups with the -COOH functional group of diaminopimelic acid, the -COOH functional group of glutamic acid and the amide groups found in the peptide component of the PGN molecule. Our results agreed with previously published data that showed specific adsorption mediated by the three functional groups (Tofail, 2012). Sodium and protons (represented by water) tested in solution showed similar effect on the adsorption of PGN on ceria when those were tested under neutral conditions. Additionally, zeta potential results showed intermolecular binding mediated by calcium ions. The Langmuir model was used to examine the sorption behavior of PGN and a linear fit was obtained, suggesting a mono-layer adsorption of the molecule on ceria under neutral conditions. These results further supported the successful binding of PGN on the surfaces even if the FTIR spectra could not be used to examine the possibility of intermolecular binding inhibiting the sorption process by limiting the available -COOH groups.

Ceria was used as the analogue of urania and thoria in order to examine whether PGN could adsorb onto the surface. The adsorption was proved successful suggesting that PGN-like polymeric substances could be used for binding and removal of particles from solution in bioremediation processes. These results were similar to those obtained from mycolic acid (MCA) interactions with minerals which suggests that -COOH holding molecules could be used to promote treatment of nuclear waste as well as biomining processes.

Even though only a small amount of PGN was available and could only be used to obtain preliminary results on the sorption profile of the molecule, the presented findings agreed with the work of others and could be used to explain observations that were not previously understood. One such example is the observed penetration of ions in Gram negative bacteria up to the PGN layers (Glasauer *et al.*, 2001) which is now believed to be controlled by interactions with the PGN moieties. The fact that all our tests on PGN sorption on ceria agreed and provided a single profile for the sorption process provides the confidence that the results reported here are very close to the true values. However, this work should be continued and more repetitions should be carried out in order to confirm the results and show that the sorption of PGN on ceria can be described with accuracy and in detail.

# **Chapter 5**

## **Computational Simulation of Mycolic Acid Adsorption onto Ceria**

## **5.1 Introduction**

The previous chapters have described the experimental studies carried out during this project to measure biomolecule adsorption onto mineral surfaces. This chapter covers the modelling work that was carried out in order to explore such phenomena at the atomic level. Experimental and computational results are compared and reasons on possible differences are explored. This chapter is a continuation of the studies exploring the adsorption of mycolic acid onto ceria (chapter 3).

### **5.1.1 Simulations of Mineral-Organics systems**

Molecular Dynamics and other computational techniques have been used to describe biomineralisation processes. Even though this specific project is not examining the biomineralisation process itself, techniques used for such cases were proven extremely useful as usually the biomineralisation process includes an organic-inorganic interface.

### 5.1.1.1 Simulation of Biomineralisation Processes

The *Chemical Reviews* article by J.H. Harding *et al.* in 2008 summarises a series of studies on computational techniques used for the organic-inorganic interface and specifically biologically controlled biomineralisation (Harding *et al.*, 2008). Many studies were included in the review with some of them being closely related to this project. The interactions of polysaccharides with calcite by Perry *et al.* (Perry *et al.*, 2007) and the simulation studies of adsorption of peptides on titania by Sushko *et al.* (Sushko *et al.*, 2006) both looked at the interaction of inorganic surfaces with organic molecules of similar sizes with the ones examined in this project. According to the authors, an important question in cases of large organic molecules that contain more than one functional group is whether the interaction depends on the types of functional groups present, their sequence or their density. Another question that was raised was how the inclusion of water affects the simulations, especially when those are compared to real systems. The importance of water models was underlined as it has been previously proved that water layers can affect molecular bonding to the surface and the dynamics of the system (Harding *et al.*, 2008). In many cases, hydrogen bonding and hence water molecules may not allow the interaction between the mineral surface and the approaching organic molecule. This was not taken into account in a few published studies (Harding *et al.*, 2008). The differences between excluding and including water in the system were studied by Yu *et al.* who proved that the presence of water molecules can alter the behavior of the organic molecules in the system (Yu *et al.*, 2003). Freeman and Harding also described the entropy associated with the binding of mannose and methanoic acid onto calcite surfaces in the presence of water (Freeman and Harding, 2014). The number of water molecules included in a simulation was a key element of the interaction for most of the cases, something that was shown again by Kerisit *et al.* who studied hematite and calcite surfaces in contact with an aqueous solution (Kerisit *et al.*, 2005). The behavior of the surfaces and the role of water was extensively described. Spagnoli *et al.* also showed that water molecules control the distribution of ions close to inorganic surfaces, suggesting a change of the resulting energetics when ions are introduced in the system (Spagnoli *et al.*, 2006).

Another important point that was raised was how efficient the force fields chosen in relation to the individual studies are, as Harding *et al.* pointed out that several cases of studies on the organic-mineral interface included inadequate force fields (Harding *et al.*, 2008). This is one of the most important issues that researchers have to overcome as the existing force fields can only be used for a range of applications and new force fields have to be developed for more complex systems.

Computational studies on biomineralisation have been quite general and mainly depended on the individual researcher or research group that was undertaking the study as no general method existed for such processes. The use of existing potentials for each component taking part in the interaction to produce a 'cross-term' was suggested as a generic method for investigation of the biomineralisation process through computational methods (Freeman *et al.*, 2007). In addition, the simulation of a surface of calcite interacting with an ovocleidin protein in several different configurations by Freeman *et al.* could be taken as an analogue of the simulation of the nuclear-related material tested in this project and one of the biological macromolecules of concern (Freeman *et al.*, 2011).

Two recent papers published on simulations of interactive mechanisms between uranyl ions and matter are (a) the work of Sebbari *et al.* who showed that temperature affects the nature of the surface species and the interaction of uranyl ions with TiO<sub>2</sub> surfaces, a very important observation when it comes to nuclear waste disposal routes and deep geological repositories (Sebbari *et al.*, 2012) and (b) the work of Leung and Nenoff on hydration structures of U[III] and U [IV] ions. The outcome of this last work was that inclusion of hydrolysis effects when U[III] and [IV] are studied is vital, as it was proved that the extend of hydrolysis plays an essential role in interactions including either species (Leung and Nenoff, 2012).

## 5.1.2 Simulation of Inorganic surfaces

Ceria,  $\text{CeO}_2$  is one of the most frequently used analogues for plutonium and uranium oxides due to its fluorite structure and the range of oxidation states it can adopt. Hence, many experimental studies have involved ceria instead of any of the radioactive analogues to make the procedure safer for the researchers. Due to the large amount of experimental data available, ceria has been frequently studied using computational techniques for comparison purposes (Yang *et al.*, 2010). There is a variety of articles available in literature involving ceria including the work of Baudin *et al.* who described the molecular dynamics of 20-30 Å thick ceria slabs for the (111), (011) and (001) surfaces (Baudin *et al.*, 2000). Sayle *et al.* studied the behavior of ceria particles in water using molecular dynamics and compared that with the behavior of the particles in vacuum. The authors concluded that the reactivity of ceria varies depending on the environment the particles are tested in (Sayle *et al.*, 2013). This underlines once again how important it is to include models of water molecules in the simulations, especially when an attempt is made to mimic environmental systems. The potentials used in the last article can be used to simulate surfaces with water molecules and an organic molecule to represent the macromolecules examined in this study.

Urania,  $\text{UO}_2$  has also been studied using computational techniques, especially for investigation of oxygen and hydrogen diffusion in the structure. This came as a result of the extensive usage of the mineral in nuclear power reactors in the form of rods (nuclear fuel). Extended research has been carried out especially from computational sciences as knowledge on the characteristics of urania was proved essential in terms of safety and reactivity related to nuclear power. Chen *et al.* in 2010 studied the hyper-stoichiometric form of  $\text{UO}_{2+x}$ , which is observed due to possible diffusion of oxygen in urania (Chen *et al.*, 2010). In the same year, Fayek *et al.* examined not only oxygen but also hydrogen diffusion in urania and described the two most likely diffusion mechanisms associated with each element (Fayek *et al.*, 2010). Another publication by Skomurski *et al.* also reported the observed oxygen diffusion in hyper-stoichiometric uranium oxide. (Skomurski *et al.*, 2007).

### 5.1.3 Objectives

The aim of the modelling work was to examine the interaction between Ceria as a nuclear related material and mycolic acid at pH 7 in the presence of  $\text{Na}^+$ . This system is considered a good representation of the potential surface interactions between the biomolecule and the system. Other pH and ionic strength values were not included due to limitations on time available for these calculations. The results obtained are compared to the experimental systems presented in Chapter 3.

The reason mycolic acid was chosen was due to the size of the molecule and the number of functional groups that the molecule contains which is ideal when the interaction is examined at the atomic level. Mycolic acid contains one main carboxylic acid group. Compared to LPS and peptidoglycan that are both complex molecules with a large number of functional groups, the simulation of mycolic acid is much simpler and does not require long simulation times and high computational costs to examine.

The initial thought was to examine the interaction of urania with mycolic acid because due to the radioactivity of the mineral, no experiments could be carried out to test the interaction. Unfortunately, no modelling work was identified with a suitable force field for the inclusion of water interactions in a urania model. This suggested that ceria would serve better the purposes of this project. Since ceria was also used for the experimental part of this work, modelling of the same systems would fit well with those results.

## 5.2 Materials and Methods<sup>1</sup>

In order to mimic the natural system, MD simulations were performed on modelling sets that included a block of (110) ceria slabs, one pseudo - mycolic acid molecule of acidic pH and 2100 TIP3P water molecules.

---

<sup>1</sup> All the input files for the modelling runs were created by Dr Shaun Hall and Dr Colin Freeman under the supervision of Prof John Harding. The simulations were run and the results analysed by Lygia Eleftheriou under the supervision of Dr Colin Freeman and Prof John Harding.

## 5.2.1 Ceria modeling

The ceria slabs were constructed using the method of Sayle *et al.* (Sayle *et al.*, 2013) and the starting model is shown in figure 5.1. The initial potentials as suggested by Sayle *et al.* were based upon the Born model where the energy of the system,  $U$ , is given by equation (5.1).

$$U(r_{ij}) = \frac{1}{2} \sum \left[ \frac{(Q_i)(Q_j)}{(4(\epsilon_0)\pi r_{ij})} \right] + \frac{1}{2} \sum A \exp\left(\frac{-r_{ij}}{\rho}\right) - Cr_{ij}^{(-6)} \quad \text{equation (5.1)}$$

The first summation represents the Coulombic interactions between ions  $i$  and  $j$  (that are carrying charges  $Q_i$  and  $Q_j$  respectively) which are distance  $r_{ij}$  apart. The second summation represents the short-range interactions using the Buckingham potential which is often used for ionic solids. The potentials suggested by Sayle *et al.* are shown in table 5.1.

| <i>Atom i</i> | <i>Atom j</i> | <i>A (eV)</i>     | <i>P (Å)</i> | <i>C (eV Å)</i>   | <i>Cut-off (Å)</i> |
|---------------|---------------|-------------------|--------------|-------------------|--------------------|
| O             | O             | 22764.3           | 0.149        | 27.89             | 10.0               |
| O             | Ce (IV)       | 1986.83           | 0.351        | 20.40             | 10.0               |
| O             | Ce(III)       | 1731.62           | .364         | 14.43             | 10.0               |
| <i>Atom</i>   |               | <i>Mass (amu)</i> |              | <i>Charge (e)</i> |                    |
| O             |               | 16.00             |              | -2                |                    |
| Ce (IV)       |               | 140.12            |              | +4                |                    |
| Ce (III)      |               | 140.12            |              | +3                |                    |

Since the ceria was intended to exist in a system with one organic molecule and a high number of water molecules, new potentials were needed to account for the interactions between the cerium atoms (Ce), the oxygen of the ceria (Oc) and the organic atoms (C for carbon, Oh for oxygen attached to organics, Hc for hydrogen attached to organics) as well as the ions (NA for Na<sup>+</sup>

ion in solution) and the water atoms (OW and HW for oxygen and hydrogen respectively). In order to deal with this, a generic method to produce cross term potentials was used as described by Freeman *et al.* (Freeman *et al.*, 2007). More precisely, the Schröder method was performed using the existing potentials for the Ceria mineral (Sayle *et al.*, 2013) and a Ce-Oh cross-term potential was scaled according to the method described by Freeman *et al.*(Freeman *et al.*, 2007).A 12-6 Lennard-Jones potential was fitted to the values given in the Sayle work to create cross potentials of the Oc to organics interaction and lastly, the ceria potentials as given by Sayle *et al.* were scaled to accommodate the NA-Oc interactions. All the final potentials are given in appendix 18.

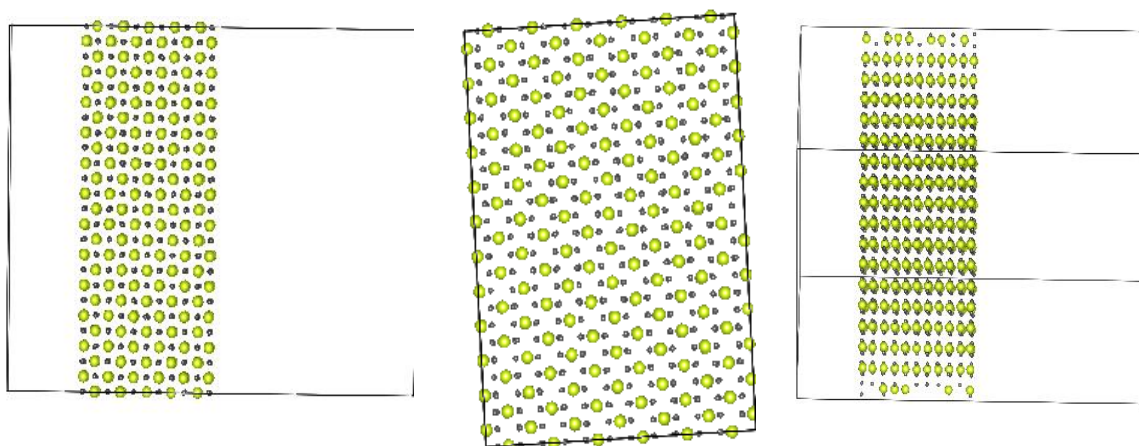
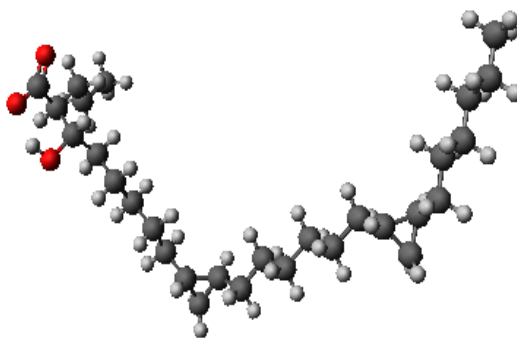


Figure 5.1.The Ceria model shown from different angles.

## 5.2.2 Mycolic acid modeling

In order to avoid long simulation times and high computational costs, a ‘pseudo’ (shorter) form of the natural biomolecule(mycolic acid) was constructed (Milano *et al.*, 2013; Lyubartsev and Rabinovich, 2010; Muller, Katsov and Schick, 2006; Riniker, Allison and van Gunsteren, 2012). Since the molecule consists of long carbon chains and very few functional groups, the structure was cut at the sides in order to limit the number of carbons present but kept all the functional groups in a configuration as close to the original molecule as possible (figure 5.2). The

final structure was similar to that used by Hong and Hopfinger who constructed and presented a model of the *Mycobacterium tuberculosis* cell walls and included a shorter form of mycolic acids (Hong and Hopfinger, 2004). The structure consisted of 30 carbon atoms with their respective hydrogens, the carboxylic acid end group along with a hydroxyl group at the same positions these are found within the original molecule (figure 5.2). The modelled molecule was constructed using the AVOGADRO (Hanwell *et al.*, 2012) and VESTA (Momma and Izumi, 2011) programs and all atomic charges were calculated using AMBER Antechamber (Weiner *et al.*, 1984). The molecule was energy-minimised and the pH was set to 7 in order to examine an interaction where the molecule is charged [(pKa of -COOH groups varies between 1.73 and 4 (Bray, 2012)]. A Na<sup>+</sup> ion was added to ensure that the simulation cell had an overall charge of zero and to test whether the inclusion of positively charged ions affects the interaction.



**Figure 5.2.** The model of (pseudo-)mycolic acid constructed with shorted carbon chains (grey) but retaining the -COOH and -OH (red) functional groups of the original molecule.

The organic and water molecules along with a Na<sup>+</sup> ion were packed together randomly using the Packmol code (Martinez *et al.*, 2009) and placed on top of a ceria slab with a surface area of 32.83 Å x 44.63 Å and 20 Å depth. The dimensions of the box were chosen so that the organic molecule would have just enough space to stretch (even though it wasn't expected to ever adopt a perfectly linear configuration) and to ensure a density of water of 0.99 g cm<sup>-3</sup>. In order to understand the energetics of the system, several simulations were run including: (i) all components in a box, (ii) only ceria and water, (iii) only organic and water. Two separate simulations that

included all components in a box were also run: (a) with the -COOH functional group of the organic molecule being in a distance of  $< 3 \text{ \AA}$  from the surface (*close*) and (b) with the -COOH functional group of the organic molecule pointing upwards with a distance  $>5 \text{ \AA}$  from the surface (*far*). Simulations were also tested for the  $\text{Na}^+$  being away or close to the -COOH functional group or the surface for an evaluation of the role of ions in solution.

### 5.2.3 Simulation Parameters

The Molecular Dynamics package DL\_POLY Classic (Todorov *et al.*, 2006) was used for all simulations. All systems were firstly equilibrated to allow for a smooth production run for 1.0 ns with a time step of 0.2 fs, using an NVT ensemble with a Berendsen thermostat (relaxation time of 0.1 ps) at a temperature of 300 K. After the equilibration, a production run took place for 1 ns and data were collected to obtain the adsorption energies at 300 K. A cut-off at  $12 \text{ \AA}$  was also used and the results were processed with the program DL\_Analyser\_1.2 (Yong, 2014).

## 5.3 Results and Discussion

### 5.3.1 Structure of Ceria

The bulk ceria slab was in good agreement with the ceria slabs constructed by Sayle *et al.* (Sayle *et al.*, 2013). The RDFs obtained for both the solvated and the non-solvated ceria were almost identical indicating that water did not disrupt the structure of ceria (figure 5.3). The Ce–Ce, Ce–O and O–O radial distribution functions were used to assess the long-range order of the particle (only Ce–Ce shown here).

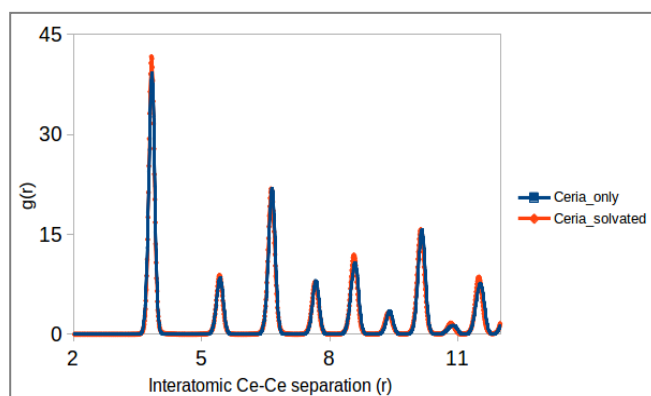


**Figure 5.3.** Ce–Ce Radial Distribution Functions calculated for solvated ceria (red) compared to the vacuum simulation of the same slabs (blue). Interatomic separations are shown in Å.

### 5.3.2 Simulation binding energies

The adsorption energies of the pseudo- mycolic acid onto the ceria surface were calculated with respect to the water solvated slab and the water-solvated-pseudo-mycolic acid simulations where:

$$U_{\text{binding}} = U_{\text{water+ceria+mycolic acid}} - [U_{\text{water+ceria}} + U_{\text{water+mycolic acid}}] + U_{\text{water}}$$

equation (5.2)

and  $U$  refers to the total configurational energy of each solvated system. This method is widely used in studies involving adsorption of organic molecules to surfaces and the results are often compared to experimental results, such as energy/force calculations carried out with Atomic Force Microscopy (AFM) or Scanning Electron Microscopy (SEM). The adsorption energies as calculated with Molecular Dynamics are shown in table 5.2.

**Table 5.2** Calculated values for the energy of adsorption ( $U_{\text{binding}}$ ) of pseudo-mycolic acid onto the surface of (110) ceria.

| System ID   | $U_{\text{binding}}$ (kJ/mol) |
|---|-------------------------------|
| $U_{\text{water+Ceria+mycolic acid (close)}} - (U_{\text{ceria-water}} + U_{\text{water+mycolic acid}}) + U_{\text{water}}$ | -11.598                       |
| $U_{\text{water+Ceria+mycolic acid (far)}} - (U_{\text{ceria-water}} + U_{\text{water+mycolic acid}}) + U_{\text{water}}$   | 61.32                         |

Interestingly, when the starting configuration locates the -COOH group of the biomolecule closer to the ceria surface (case *close*), a strong attraction between the ceria slab and the molecule is observed, which could be explained by the fact that the molecule no longer has to overcome the layers of water that are present in the first example (case *far*). In order to start with a short distance between the surface and the molecule and avoid disruption by the water, a vacuum simulation was run with the surface and the molecule before the inclusion of water. That ensured that the molecule

would have the time and energy to approach the surface without energy barriers.

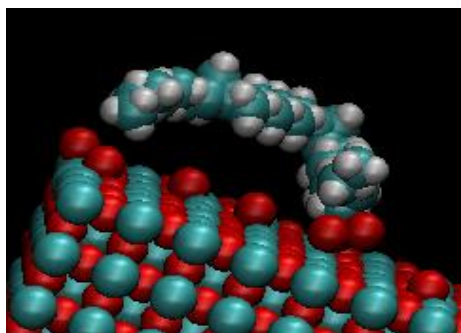


**Figure 5.4.**The binding of mycolic acid onto ceria when starting at  $<3\text{\AA}$  away from surface.

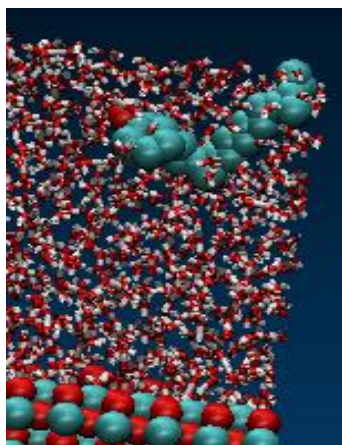


**Figure 5.5.** Repulsion of mycolic acid from surface when starting  $>5\text{\AA}$  from surface

The effect of the tightly-bound water can clearly be seen in the two configurations observed. As shown in figures 5.4 and 5.5, the  $-\text{COOH}$  group of the pseudo-mycolic acid can only adsorb onto the ceria surface when its starting position is closer to the surface while the opposite situation results in repulsion of the molecule. This calculation includes only the enthalpic contribution (strictly speaking the configurational energy contribution) and ignores the entropic contribution of the system. However, as the macromolecule is approaching the surface, the highly ordered water layers are disrupted which suggests that there will be a non-negligible entropy contribution. This contribution has been estimated by Freeman and Harding for the case of binding of mannose and methanoic acid onto the (104) calcite surface. According to the authors, the entropy of binding for surface water molecules is  $\sim 6\text{ J per mol per K}$  (Freeman and Harding, 2014). The possible effects of this term are further discussed in sections 5.4 and 5.4.1.

The force field used for this project did not include any hydroxylation of the surface but a very strong attraction of the water molecules by the surface was observed. This attraction explains why the pseudo-mycolic acid was unable to overcome the water layers when the molecule's starting distance from the surface is higher than  $3\text{\AA}$  and a repulsion of the  $-\text{COOH}$  group from the ceria slab is observed (figure 5.7-far).

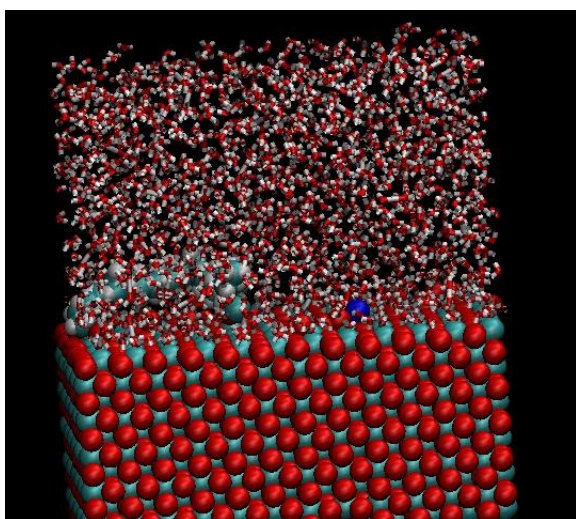


(fig. 5.6) Starting configuration with -COOH functional group of pseudo-MCA  $< 3 \text{ \AA}$  away from surface with/without H<sub>2</sub>O. (close)

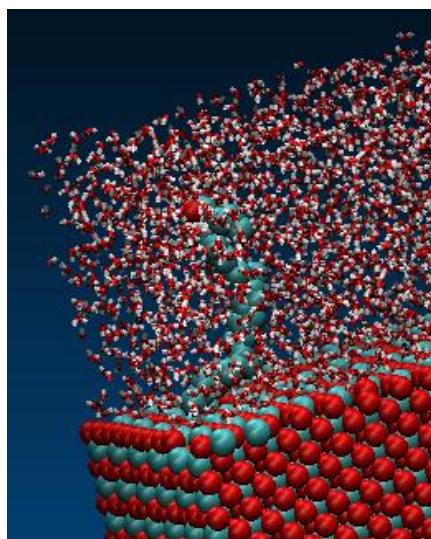


(fig. 5.7) Starting configuration of -COOH functional group of pseudo-MCA  $> 3 \text{ \AA}$  away from surface. (far)

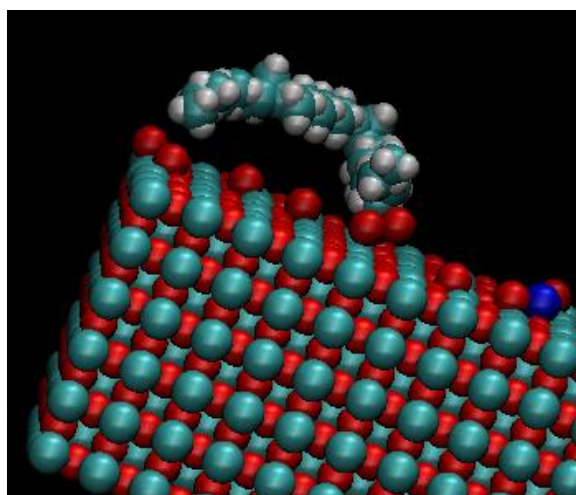


(fig. 5.8) Final configuration of pseudo-MCA  $< 3 \text{ \AA}$  away from surface without H<sub>2</sub>O.

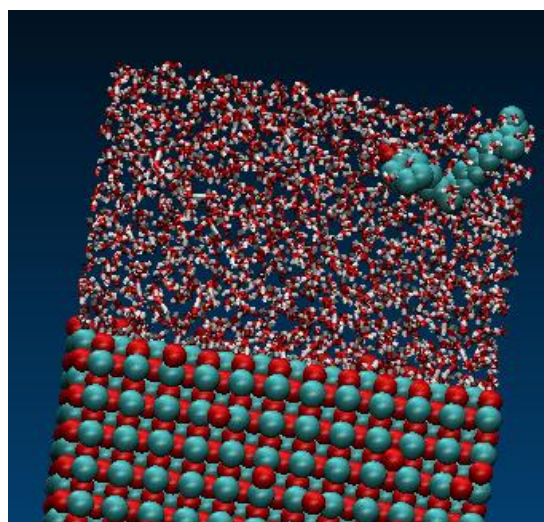


(fig 5.9): Final configuration of -COOH functional group of pseudo-MCA  $> 3 \text{ \AA}$  away from surface.

Figures 5.6-5.9. Starting and final simulation configurations Ceria-pseudo-MCA- water

### 5.3.3 Effect of ions in binding

The  $\text{Na}^+$  ion used in the simulation to examine a non-charged system was also chosen in order to evaluate whether or not the inclusion of ions plays a role in the interaction and how that affects the overall binding process. The results indicated that the inclusion of the ion did not play an important role (figure 5.10).

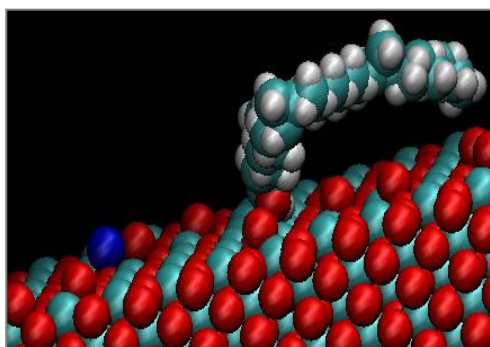


**Figure 5.10.**The role of Na ion. The ion (blue) is found away from the -COOH group of the organic molecule and strongly bound on the surface of ceria.

The final position of the ion suggests a strong interaction with the surface but not with the -COOH of the molecule. This result was quite surprising as similar interactions were previously found to involve the 'bridging' of the molecule to the surface via a charged ion as shown in figure 5.11.

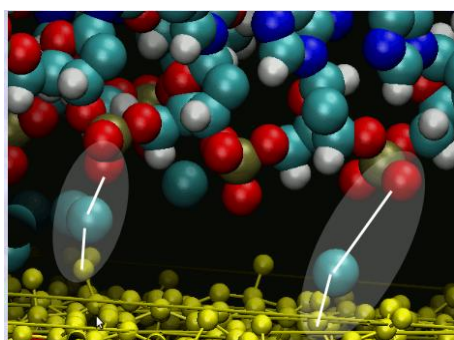


**Figure 5.11.**The bringing effect of  $\text{Ca}^{2+}$  ions in the binding of DNA to Silica. Ca cations act as bridges between O (silica) and O (phosphate-DNA). (Colin Freeman, Univ. of Sheffield, pers. comm.)

### 5.3.4 Comparison to experimental results

The experimental set-up designed to examine the interaction between ceria and mycolic acid (chapter 3) included the introduction of mycolic acid dissolved in chloroform in a solvated sample of ceria that had been previously left to equilibrate for 24 hours. Due to the density of chloroform being higher than that of water, the organic layer was removing the bulk water molecules. Hence, the organic layer was easily located on top of the tested surfaces. Additionally, the use of chloroform increased the solubility of the MCA carboxylic end in water. That is due to the increased polarity exhibited by the molecule when the organic solvent was introduced. This enhanced polarity resulted in an increased availability of the carboxylic -OH groups which could now undergo hydrogen bonding.

The simulated system was also equilibrated to allow for a close comparison with the experimental system but chloroform was not included in the simulation due to difficulties that arise from the addition of large numbers of atoms in the simulation box. High computational costs and expenses related to the extra molecules (Milano *et al.*, 2013; Lyubartsev and Rabinovich, 2010; Muller, Katsov and Schick, 2006; Riniker, Allison and van Gunsteren, 2012) did not allow for the addition of other than the ceria, sodium ion, water and pseudo mycolic acid models in the simulation box but a different approach was chosen to examine what happens in the presence of chloroform.

In order to mimic the behavior of chloroform without any additional molecules in the simulation box, two different simulations were tested. In the first simulation box, the interaction between the organic molecule and the approaching surface was tested with a small starting distance between the organic molecule and the surface (to mimic the inclusion of chloroform that repels bulk water) and in the second simulation box, the organic molecule and the ceria were put far away from each other (to mimic the exclusion of chloroform and hence, the presence of bulk water molecules between the surface and the organics).

As described in chapter 3, the Langmuir, Freundlich and the Sips models were used to evaluate the behavior of the mycolic acid binding onto ceria and other surfaces. According to the  $R^2$  values the Sips isotherm which represents a combination of the Langmuir and the Freundlich models produced the most accurate fit. The standard free energy change for each system was therefore calculated using the Sips isotherm which when approaching a low  $n$  value reduces to Freundlich, while at high  $n$  values, it predicts the Langmuir monolayer sorption characteristics (details on equations in chapter 3). The standard free energy change of adsorption of each system as calculated from the experimental methods is presented in table 5.3. The comparison is closest between theory and experiment for the results at pH 7 in the presence of  $\text{Na}^+$  ions. The simulation binding energy is -11.598 kJ/mole whereas experiment gives -16.485kJ/mole. This comparison seems reasonable since for both theory (pH 7) and experiment (pH 7) the mycolic acid will be ionised (Brey, 2012). However, there are a number of issues with making such a comparison that require discussion.

| <b>ID</b>                           | <b><math>K_c</math></b> | <b><math>\Delta G</math> (kJ/mol)</b> |
|-------------------------------------|-------------------------|---------------------------------------|
| pH7 $\text{CaCl}_2$ $\text{CeO}_2$  | 1.751                   | -16.981                               |
| pH3 $\text{CaCl}_2$ $\text{CeO}_2$  | 1.459                   | -16.566                               |
| PH7 $\text{NaCl}$ $\text{CeO}_2$    | 1.408                   | -16.485                               |
| pH10 $\text{NaCl}$ $\text{CeO}_2$   | 0.571                   | -14.433                               |
| pH3 $\text{NaClCeO}_2$              | 1.459                   | -16.566                               |
| pH10 $\text{CaCl}_2$ $\text{CeO}_2$ | 0.827                   | -15.275                               |
| pH10 water $\text{CeO}_2$           | 0.545                   | -14.327                               |
| pH7 water $\text{CeO}_2$            | 1.094                   | -15.911                               |

The first issue is the nature of the surface of ceria. For computational simplicity, the (110) surface was studied (attempts were made to study the (111) surface but encountered technical difficulties). Even though the (110) surface was chosen for computational reasons, it was expected to be significantly more reactive than the more stable (111) surface. Hence, the binding energy of the simulation was expected to be different than the experimental energy. An example of a study showing the difference in reactivity of the ceria surfaces came by Meißner *et al.* (2015) who tested the interaction of all (100), (110) and (111) ceria surfaces with silane molecules. The organic molecules were found to exhibit stronger sorption onto the (111) ceria surface compared to the (110) surface which supports the hypothesis that the different surfaces would result in different adsorption of organic molecules (Meißner *et al.*, 2015).

In order to examine the stability of the (100) and (110) ceria surfaces, Zhou *et al.* (2007) synthesised and studied a single crystalline ceria nanorod with higher than the usual percentage of the (100) and (110) surfaces through a solution based hydrothermal method. These are more reactive than the (111) surface but both (100) and (110) surfaces were rapidly deactivated. This was ascribed to hydroxylation resulting from interaction of the surfaces with the reaction products (Zhou *et al.*, 2007). This assertion is supported by two sets of *ab initio* simulations. Molinari *et al.* (2012) showed that water 'spontaneously' splits and the resulting H and OH are found strongly bound to the ceria (110) surface at which the dissociated state of water is the most stable. This suggests that once the water molecule is broken, the surface will no longer be chemically active as a very stable hydroxylated surface is formed (Molinari *et al.*, 2012). Freunte *et al.* supported the above observation and calculated an adsorption energy of 4.57 eV for the water-ceria (110) interaction. As the authors explain, the '*high surface activity can be attributed to the specific position that O and Ce atoms occupy on this surface*' (Fuente *et al.* 2012). The results of Molinari *et al.* were quite different from those of Fuente *et al.* as the calculated adsorption energy of water was found to be -1.12 eV (Molinari) compared to -4.57 eV (Fuente). Even though the ceria models of the two calculations were different in geometry (with Fuente using a larger surface and fewer layers) the difference in adsorption energy is quite high and suggests that at least one calculation is

exaggerating the effect. In addition, none of the two studies considered the interaction of bulk water with the surface. Nevertheless, the calculations of Molinari *et al.*(2012) showed a strong dependence of the dissociated state on coverage and resulted in an estimate of the energy of adsorption of water molecules (non-dissociated). These were -0.85 eV for the isolated case and -0.76 eV for the 1ML case (where 1ML coverage equals 4.69 H<sub>2</sub>O/nm<sup>2</sup>). These calculations underline once again that (110) surface hydroxylation is quite likely and the dissociation of water molecules should always be considered when the (110) surface is to be tested. Great attention should also be given to calculations related to non-dissociated water molecules because they are likely to over-estimate binding onto ceria.

Small differences in the resulting energies from computational versus experimental works were also associated with the fact that the entropic contribution has been ignored in the modelling work while the experimental free energy describes the total energy calculated from the isotherms. In order to calculate the associated energy, the disruption of water molecules needs to be taken into account by calculating the Helmholtz free energy, A, according to equation (5.3).

$$A=U-TnS \quad \text{equation (5.3)}$$

**where U is the energy of adsorption ( $U_{\text{binding}}$ ), T is the temperature, n is the number of water molecules displaced from the surface by the adsorbate and S is the entropy.**

It should also be remembered that the simulations were performed on smaller molecules than the experiment. In order to avoid long simulation runs in terms of time and money, a shorter version of the organic molecule was constructed and tested while the actual experiment involved the full length molecule. The simulated model included a much smaller number of atoms which were involved in the binding to the mineral. For the experimental systems, where a much larger polymer is involved, more parts of the macromolecule were available to interact with the mineral. Here, it is also important to consider the existence of all three different types of mycolic acids which are made up of different functional groups that may play a role in the molecule's interactions. The simulation included a version of the alpha mycolic acid which is the most

commonly found form while only a small percentage of the rest of the forms can be found in a natural mycolic acid sample. The three major mycolic acids known are: (a) alpha mycolates, (b) methoxy-mycolates and (c) keto-mycolates (shown in figure 5.12). Each form of mycolic acid contains the -COOH functional group tested in the simulation but the methoxy and the keto mycolic acid forms also include a -OCH<sub>3</sub> and a C=O (keto) groups respectively that are possibly contributing in interactions of the molecule with approaching surfaces due to the existence of the highly reactive oxygen atoms.

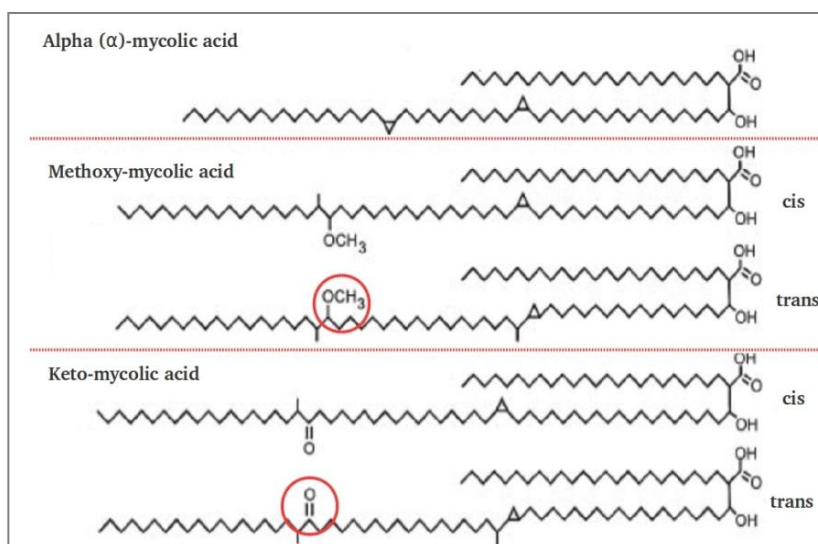


**Figure 5.12. The three different forms of mycolic acid**

It is also known that polymers can adapt different configurations while in solution depending on the conditions, the pH and the adsorption mechanism. According to Gurumoorth and Khan (Gurumoorth and Khan, 2011), polymers can adapt three different configurations while adsorbing onto a surface as shown in figure 5.13. Depending on the functional groups available, the polymer can either form a tail, with only one functional group approaching the surface and the rest of the molecule floating in solution or make a 'loop' and a train where the molecule is

approaching the surface through different functional groups and hence is being attached at multiple sites.

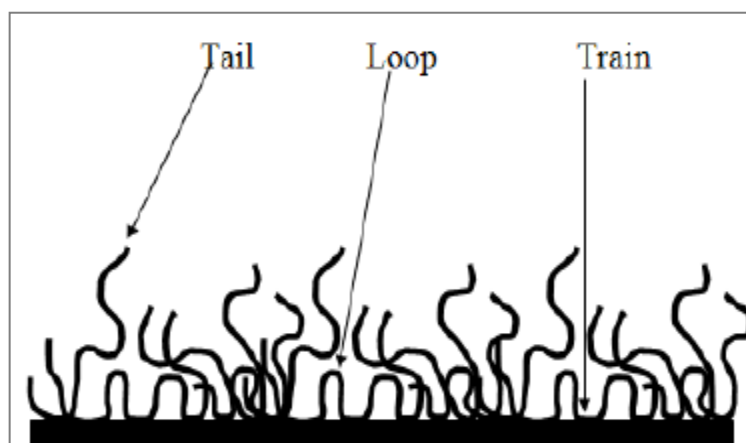


**Figure 5.13** The different modes of polymer adsorption onto surfaces ( Gurumoorth and Khan, 2011).

The longer mycolic acid included in the experimental isotherms will exhibit these modes of adsorption upon approaching the ceria surface, whereas the shorter pseudo-mycolic acid used in the modelling studies will not be able to adopt all these conformations. Hence, the computational models will only reflect part of the adsorption of the molecule and this will result in different energy estimation.

Furthermore, one of the main conclusions drawn from the comparison between experimental and computational results was that both systems showed no preference on the ions included which suggests that the interaction is not mediated by ions in solution, thus the presence of ions does not influence the process. This is particularly important in highly saline conditions such as salt rock or marine conditions which will not affect the reaction.

To summarise the comparison between the experimental and computational results, it was evident from both that the interaction between the ceria surface and the mycolic acid would take place mainly under acidic or near neutral conditions, with no effect of the ions present. The computational results suggest that the interaction will only take place if water molecules can be

removed before the binding with the organic molecule or if the water molecules are inserted in the system after the binding of the organics with the surface. As shown with the simulation where the -COOH group of the mycolic acid was more than 3 Å far from the surface, the molecule was unable to overcome the water layers located between the -COOH and the ceria and hence, no bonding could occur. On the experimental set-up, the inclusion of chloroform for the dissolution of the mycolic acid prior to its injection to the ceria samples ensured that a hydrophobic 'capsule' was holding the organic molecule. This chloroform 'capsule' was protecting the organics from the bulk water molecules present in the system and allowed the interaction with the ceria by removing the water layers sitting on top of the surface. This suggests that the simulations were actually a representation of the experimental systems with and without the inclusion of chloroform: the simulation marked as 'close' represented the case where chloroform was used and the simulation marked as 'far' represented the case where chloroform was not used (or was unable to overcome the water layers).

## 5.4 Conclusions

This chapter covered the modelling work that was carried out in order to explore the binding of mycolic acid onto ceria at the atomic level. Experimental and computational results were compared and reasons explaining the observed differences were explored. It was found that binding of mycolic acid onto the surface of ceria is favorable when simulations are started with less than 3 Å distance between the organic molecule and the surface. Na<sup>+</sup> ions were found located away from the -COOH group of the acid suggesting no role in the binding between the organic molecule and the surface. The -COOH group of the organic molecule was found to be the functional group responsible for the observed binding. The above observation was absent when the molecule started at a distance higher than 3 Å from the surface. In that case, the molecule was moving away from the surface, mainly due to water layers between the organics and the surface that do not allow the adsorption of the organics on ceria. This suggests an energetic barrier induced by the water molecules that control the binding of the hydrophobic mycolic acid on the surface of ceria.

In terms of natural systems, the hydrophobicity of the organic part and the overall non-polar character of the molecule suggest that mycolic acids are not the biomolecules responsible for the sorption processes involving bacteria and minerals. Water molecules are widely available in environmental samples which suggests that mycolic acids would have to overcome the energetic barrier induced by the water layers, something that would not be easily achieved as shown by the results of the calculations. Also, in order for a sorption process to occur, the -COOH functional group of mycolic acids would have to be available for interactions which is only true for free mycolic acids due to cell lysis. This however, is not the case for bound mycolic acids within the bacterial cell wall of the *Mycolata* members as those are strongly attached to peptidoglycan through arabinogalactan moieties and hence, unavailable for interactions with approaching minerals. Further discussion on the natural systems and the mycolic acid interactions is found in the next sections.

# General Discussion

It is generally admitted that the main factor affecting the mobility of uranium in the environment is its oxidation state. Micro-organisms catalyse both the oxidation and reduction of uranium and other elements which is an important ability, especially because it can be used in cases of accidental release of ions in the environment such as radioactive species in water streams. A release of radioactive particles in water results in a rapid and usually uncontrolled spread of contamination which suggests that microbial-induced precipitation after a reduction process would limit the mobility of the species and hence the extent of contamination.

This work considers the basic principles of bacterial interactions with nuclear-related minerals after the reduction process. We are particularly interested in the recovery stage where the precipitated minerals should be collected with the minimum human involvement possible, to avoid unnecessary exposure to radiation. This suggested that an investigation on the interactions between the mineral phases produced as a result of the microbial involvement with potential polymeric substances that could be used for the agglomeration of such matter was needed. To simplify the work, macromolecules of bacterial origin that could serve as 'attraction centres' for the reduced complexes were used.

Tests on europium oxide, ceria, urania and thoria confirmed that lipopolysaccharide, found on the outer layer of gram-negative bacterial cells, adsorbs on all four surfaces under varying conditions with  $\Delta G$  values in the range of physisorption (-3 to -25 kJ/mol) for all systems. Lipopolysaccharides are not only found as components of live bacteria but they are also freely available in natural systems because of cell lysis. Hence, the results of LPS sorption onto minerals especially at the mineral/water interface are very important not only for bacterial applications as a whole but also for LPS as a separate component.

LPS was found to behave similarly for all four surfaces (ceria, thoria, urania and europium oxide) mainly under basic conditions where the availability of cations is limited by the increased availability of OH<sup>-</sup>. Under acidic conditions, sorption of LPS onto ceria was proven quite complex. A general conclusion involved intermolecular binding induced by the increased mobility of cations in solution. Hence, environmental sites of acidic conditions and high ionic strength such as mining sites (where the pH is usually low promoting metal solubility) would not favor an interaction between bacterial LPS and minerals.

Sodium containing samples behaved similarly to the samples in water as a solvent with both water and sodium mediating sorption better under acidic conditions. This suggests that sites of low calcium content but high sodium and proton content would promote LPS adsorption onto minerals. Examples of such conditions found in nature are mining sites, acidic lakes or acidic soil. However, calcium and sodium ions are usually found closely related in nature which suggests that acidic conditions in the presence of only sodium are more likely to be obtained under clean laboratory conditions.

Calcium was found to mediate sorption better under basic conditions. This suggests that even though high concentrations of the cation (under acidic conditions) prevent the sorption from happening, controlled concentrations of the ion (under basic conditions) can mediate the interaction more successfully than sodium ions or protons. An example found in nature related to such alkaline conditions is seawater where calcium is widely available mainly due to dissolution from rocks. Hence, LPS-driven bacteria or free LPS found in water or other aqueous environments of alkaline conditions can promote sorption processes and hence, binding on mineral surfaces. Similarly, bacteria and specifically bacterial LPS in groundwater repositories of high alkalinity can be considered as sorption sites for nuclear-related minerals. This is important for cases of radioactive release in water streams and aqueous media where bacterial LPS or similar moieties could be used to limit the contamination by capturing the particles through sorption processes.

Tests on europium oxide and ceria confirmed that MCA, found on the outer layer of bacterial cells of the genus *Mycolata*, interacts with each surface under varying pH and electrolyte conditions with  $\Delta G$  values in the physisorption range (-10 to -17 kJ/mol) for all systems. The results indicated the involvement of the -COOH functional group of MCA in the sorption process which suggests that carboxylic-containing moieties can adsorb onto nuclear-related surfaces under acidic, neutral and basic conditions. Calcium, sodium and protons tested in solution showed similar effect on the adsorption of MCA on both surfaces which suggests that pH or ionic strength conditions do not have an effect on the interaction and all conditions can promote the removal of radioactive particles. Hence, MCA-related moieties (i.e. organic molecules with carboxylic acid functional groups) could be used as attraction centres for the collection of nuclear related particles. Acid lakes and mining sites would be ideal locations for such processes especially for binding of hydrophilic surfaces such as europium complexes found as products of the uranium fission cycle.

Our experiments were intended to mimic the natural systems where MCA is found closely bound in an orderly arrangement that induces a strong polar bond at the carboxylic end. It was proven that this arrangement is essential for the adsorption mechanism. Hence, MCA-like polymeric substances could be used for binding and removal of particles from solution in bioremediation processes if they are arranged in a similar manner. Supporting results were obtained from the computational studies of MCA adsorption onto ceria. The calculated binding energy from molecular dynamics simulations ( $E_{\text{binding}} = -11.598$  kJ/mol for simulation representing a ceria slab at pH7 in the presence of  $\text{Na}^+$ ) agreed well with the experimental results for the corresponding system (-16.485 kJ/mol). Additionally, it was found that an energetic barrier induced by water molecules controls the binding of the hydrophobic mycolic acid on the surface of ceria. In terms of natural systems, the orderly arrangement of mycolic acids within the outer layer of the bacterial cell wall suggests that MCA will not attach to nuclear-related minerals. The structure of the bacterial cell wall inhibits this kind of interaction due to the active site of the MCA molecule (the carboxylic acid end group) being strongly bound to the rest of the bacterial cell wall and thus, being unavailable to interact with external compounds such as minerals. Thus, the results

presented here suggest that MCA in bacterial cells is not promoting adsorption of the cell on the different minerals. In the case of free MCA molecules (mainly available due to cell lysis), the biomolecule will not adsorb onto nuclear related surfaces unless they are within a highly hydrophobic capsule that increases the polarity of the carboxylic bond and drives the molecules close to the intended surface depending on physical properties (for example density of solvent). Such conditions are not often found in environmental sites but clean laboratory conditions would be required instead.

Preliminary results from ceria interactions with peptidoglycan showed that PGN, found on both Gram positive and Gram negative bacterial cell walls, interacts with the mineral under varying electrolyte conditions and neutral pH with  $\Delta G$  values in the physisorption range (-8 to -10 kJ/mol). The results suggested the involvement of two different functional groups in the sorption process: -COOH and amide. Calcium, sodium and protons tested in solution showed similar effects on the adsorption capacity. This suggests that carboxylic and amide groups from bacterial origin can sustain successful mechanisms for the binding of highly toxic, nuclear-related particles. PGN-like polymeric substances could be used for binding and removal of particles from solution in bioremediation processes. These results were similar to those obtained from MCA interactions with mineral surfaces which suggests that -COOH holding molecules could be used to promote treatment of nuclear waste as well as biomining processes.

Most tested interactions showed a clear preference in calcium containing media which suggests that calcium 'uses' its charge to act as a 'bridge' and connects the functional groups with the mineral surface. This suggests that calcium ions could be used in bioremediation processes to speed the reaction rates of interactions between bacterial components and mineral surfaces (for example during treatment of nuclear waste mediated by bacteria). The use of complex molecules such as LPS is not advised for such processes even if the molecule has shown sorption capacity related to the tested surfaces. This is due to the increased intermolecular binding observed when the biomolecule was treated with electrolytes especially under acidic conditions where speciation theory suggests high mobility and hence availability of the salt ions. On the other end, long carbon

chain molecules with only a limited number of carboxylic acid end groups (MCA) showed a tendency to adsorb strongly on the mineral surfaces when in organic solvents. This suggests that in order for highly hydrophobic biomolecules to undergo sorption onto surfaces, an organic carrier (or solvent) is required. This is in great agreement with the natural systems where the mycolic acids are orderly arranged in parallel with the carboxylic acid groups facing towards the lipid components and the hydrophobic carbon chains facing towards the arabinogalactan. This arrangement supports the hydrophobic character of the MCA carbon chains but at the same time it triggers the polarity of the carboxylic acid end groups which are now available to interact with the rest of the cell wall molecules.

In an intermediate state in terms of complexity and size, PGN contains more functional groups than MCA but it has a lower molecular weight than LPS. The PGN functional groups are similar to those of MCA and the preliminary results showed a successful adsorption of the molecule onto ceria mediated by the carboxylic and amide groups. The PGN molecule is mainly hydrophilic thus, in contrast to MCA, no organic carrier is needed to promote the sorption interactions. However, calcium mediated intermolecular interactions were observed, similar to those analysed for LPS samples. It can therefore be concluded that, in terms of free biomolecules, each one (i.e. LPS, MCA and PGN) may undergo sorption onto mineral oxides dependent on pH conditions, hydrophobicity of adsorbent and adsorbate, electrolyte concentration and media used. When whole bacterial cells are considered, a general conclusion relates to ion specific sorption processes undertaken by the external LPS biomolecules. These processes are further supported by the PGN moieties if the minerals manage to enter the cell wall or if the minerals are formed within the cell wall. MCA was not related to the sorption process due to its active functional groups (-COOH) being strongly bound on the rest of the cell wall which suggests limited availability of the molecule for interactions with other than the cell's moieties. These conclusions are further supported by earlier scientific reports showing a specific localisation of biogenic or non-biogenic minerals within the cell wall of bacteria or closely related to extracellular moieties. Work on non-biogenic iron oxides and their interactions with bacteria indicated that the minerals were able to

penetrate the cell wall of Gram positive bacteria (Glasauer *et al.*, 2001). The final position of the mineral was the PGN layer which suggested a possible interaction of the PGN functional groups with the oxide. The work presented within this thesis showed that PGN is able to bind on similar minerals suggesting that the oxide particles tested in the mentioned work were most likely stopped by the PGN moieties by a sorption process mediated by the -COOH and amide groups. Furthermore, specific localisation of uranium-related minerals formed due to bacterial involvement was also reported with the mineral being located close to biomolecules in both intracellular and extracellular sites. The results suggest that LPS could be the main biomolecule responsible for the observed localisation of biogenic urania at the extracellular sites while PGN was possibly the biomolecule responsible for the intracellular localisation of the mineral.

It is hypothesised that similar interactions to the ones described in this project will occur between the bacterial macromolecules with minerals of similar characteristics to the ones examined. For example, ceria was used as the analogue of thoria and urania, both found as natural oxides in the earth's crust, as well as oxides of americium (such as AmO<sub>2</sub>), found in nuclear waste. The four minerals share similar structural characteristics, such as the Fluorite crystal structure indicating similar coordination geometry. Thus, the biomolecules would undergo sorption processes depended on their protonation and deprotonation states as well as the charge exhibited by the mineral's surface, mainly controlled by the mineral's oxygen atoms. Differences are expected due to the different point of zero charge exhibited by the minerals. However, when the sorption profiles are compared for similarly charged surfaces, similar adsorption mechanisms are expected. Additionally, similar observations to the ones described here were reported for interactions of bacterial biomolecules with minerals other than the nuclear oxides such as hematite (iron oxide), corundum (aluminium oxide) and calcite, suggesting that similar sorption mechanisms may be possible with more minerals. This is particularly important for biomining processes that rely on the ability of bacteria to process and bind on a range of minerals. Additionally, the ability for sorption of biomolecules onto nuclear related surfaces is particularly important for nuclear waste treatment.

The current practices of bacterial involvement in nuclear waste treatment include the reduction and precipitation of metal ions. This application benefits from the limited involvement of humans in nuclear-related tasks but due to the small size of microbes, long reaction times and enormous quantities of required biomass render this as a secondary nuclear waste practice. If reduction was induced by other means (e.g. chemical substances), recovery of the produced oxides could be obtained via polymeric substances similar to the ones tested in this project. The adsorption capacity of the biomolecules showed that when permitted by pH and other conditions, the biomolecules can accomplish strong adsorption onto the mineral particles. It is therefore suggested that further sorption experiments are needed to evaluate whether polymeric substances (possibly synthetic) that contain multiple numbers of the basic functional groups identified in this project (i.e. -COOH and amide) can increase the adsorption capacity and hence the binding of the polymers on the oxides. An immediate application of such a successful polymer would be the recovery of oxide minerals from nuclear wastes and potential uses would include the recovery process during biomining processes and the recovery process during decontamination after reduction of aqueous sites such as lakes contaminated with radionuclides.



# General Conclusions

The research objectives described in the first chapter of this thesis have all been met. The starting hypothesis questioning the ability of individual bacterial macromolecules to interact with minerals was examined after the observation that biogenic minerals were often found located at the bacterial cell wall. The results indicated that the macromolecules tested during this project were able to interact with  $UO_2$  and other chemogenic minerals including thoria, ceria and europium oxide. Thus, it was shown that non-biogenic minerals were also affected by the biomolecules. The energy associated with the interactions between the biominerals and the bacterial components was calculated with experimental and computational techniques. Negative standard free energy values were obtained for all systems suggesting successful sorption of the biomolecules on the minerals.

Ion and pH dependent sorption was proposed for the case of a lipopolysaccharide which showed successful sorption profiles under all experimental conditions. Under neutral conditions and thus, in natural systems, the lipopolysaccharide was found to interact strongly with the minerals suggesting that free lipopolysaccharides due to cell lysis as well as bound lipopolysaccharides at the surface of bacterial cells will undergo sorption on mineral oxides. It was also demonstrated that the sorption of bacterial cells on minerals is controlled by the pH and ion-dependent sorption of lipopolysaccharides as these are the biomolecules at the external layer of the bacterial cell wall and thus, the first biocomponents that an approaching mineral will meet.

The dependence of mycolic acid adsorption on the hydrophobicity of the solvent present during the interaction was also demonstrated. Ion and pH effects were not observed for the case of mycolic acid interactions but a strong negative effect was observed when water molecules were present in the system of interest. Computational methods were used to examine the ability of mycolic acid to interact with ceria and the results suggested that the biomolecule will only interact with the mineral if water molecules are not present in solution (or if the water molecules are introduced in the system after the interaction of the biomolecule with the ceria surface). It was also shown through experimental techniques that mycolic acid will only interact with oxide minerals if

an organic layer is introduced in the system in order for it to repel any bulk water molecules and mediate the interaction with the surface. These results suggest that sorption of bacterial cells with minerals is not mediated by mycolic acids as the conditions required for such processes to take place are not met in natural systems. The orderly arrangement of mycolic acids within the bacterial cell wall also suggested that the active sites of mycolic acids (i.e. the carboxylic acid functional groups) are not available for interaction with external molecules because they are strongly attached to lipids, arabinogalactan and peptidoglycan. Thus, it is proposed that mycolic acids do not participate in the interaction of bacterial cells with minerals.

Ion dependent sorption was proposed for the preliminary tests of peptidoglycan interactions with minerals. According to the results, peptidoglycans can mediate sorption processes with oxides at natural systems through carboxylic and amide moieties. The interaction was ion-dependent as it was proposed by the ATR-FTIR results that showed intermolecular binding mediated by calcium ions. However, linear sorption profiles were constructed suggesting that intermolecular binding is not inhibiting the interaction of peptidoglycans with the oxides. Thus it was proposed that peptidoglycans are also participating in the sorption process with lipopolysaccharides.

The above results can be used to establish a universal rule for the sorption of bacterial cells with mineral oxides. Lipopolysaccharides and peptidoglycans are two of the components responsible for the observed localisation of minerals within the bacterial cell wall or closely related to the cell structure. Mycolic acid does not interact with the minerals as explained by its position and orientation within the cell wall. Thus it is proposed that two of the main bacterial biocomponents involved in bacterial sorption are lipopolysaccharides and peptidoglycans.

## **Future Work**

### ***Lipopolysaccharides***

In order to suggest a general mechanism that LPS uses for its interactions when approaching a surface, continuation of this work with experiments on the sorption of LPS onto

more minerals is required. The above work has shown the solution chemistry underlying the sorption that occurs under varying pH conditions and changing ionic strength. However, no work was done at the atomic level in order to visualise the exact functional groups present in LPS that are active during sorption. Available sites and functional groups are quite hard to identify due to the large size of the molecule but there are a few possible techniques that could support this work including Scanning Electron Microscopy and Atomic Force Microscopy. Modelling of a shorter version of the molecule could also examine the different available for interaction sites at the atomic level. This, however, would not be possible for the whole molecule due to the high computational costs and the computational time needed for such systems (Milano *et al.*, 2013; Lyubartsev and Rabinovich, 2010; Muller, Katsov and Schick, 2006; Riniker, Allison and van Gunsteren, 2012). In general, this work has shown signs of a general mechanism LPS was found to follow for sorption on the four surfaces tested but more surfaces with a wider range of surface charges should be tested as well. Another suggestion is the usage of the individual LPS moieties in the interactions in order to find the exact functional groups responsible for the observed sorption.

### ***Mycolic acid***

The observation of mycolic acid interactions with minerals through Force Microscopy or Scanning Electron Microscopy would be ideal for the visualisation of the interactions describe during this project. These techniques could provide the actual forces involved in the interaction and the results could be compared to that of computational techniques (chapter 5). Unfortunately, no previous work has been identified describing the interaction of MCAs with any minerals or other surfaces involving the techniques described here. Hence, no comparison with other systems could be made. In general, this work has shown signs of a general mechanism MCA follows for sorption on the two surfaces tested but more surfaces with a wider range of surface charges should be tested as well. The hydrophobicity induced by the long carbon chain of the molecules suggests that experimental set-ups cannot easily mimic the bacterial cells. Thus, more interactions of monolayer of mycolic acid or interactions involving live bacterial cells should be used in order for the natural system to be observed. Scanning Electron Microscopy could be a potential technique to evaluate

such interactions even though limitations will be encountered if live bacterial cells are to be considered.

## ***Peptidoglycan***

The preliminary results described in chapter 4 have shown successful sorption profiles for the interaction of peptidoglycan with ceria as the analogue of thoria and urania under neutral conditions. It is clear that more replicates of the experiments are needed to assess the accuracy of the reported data but the agreement of our results with previously published work as well as the nicely fitted profile obtained via the different methods used provide the confidence that the results reported here will be verified.

## ***Simulations***

It is clear that more computational work is needed for a complete data set describing the adsorption of mycolic acid onto ceria. First of all, simulations including more surfaces of ceria should be completed with (100) and (111) ceria being of great importance especially because the (111) ceria is the dominant surface found in nature. This work will have to overcome the 'dipole' problem observed when running simulations that include the (100) surface and a suitable force field will be needed. Different methods can be used to avoid this problem such as the standard method of Tasker (Tasker, 1979) which includes the rearrangement of ions from the top layer of the surface to the bottom layer which will quench the dipole and at the same time introduce defects into the surface.

Hydroxylation of the surface and dissociation of water for all surfaces, especially for the case of ceria (110) and (100) should also be considered with a suitable force field. The additional surfaces will have to be tested with different forms of the organic molecule, including different charging states corresponding to different pH conditions. The inclusion of different ions (for example  $\text{Ca}^{2+}$  instead of  $\text{Na}^+$ ) should also be considered as the experimental results suggested that

both ions can mediate the interaction. A larger version of the acid could also be considered, probably with a coarse grained molecule that would explore the full potential of the molecule.

As a last note, the entropic contribution of water displacement by the organics from the ceria should be studied. This is currently quite difficult due to the high affinity of the water molecules on the surface. A special method will be needed to overcome the problems arising from the spontaneous dissociation of water close to the surface as previously discussed as well.

### ***Evaluation/Errors and possible improvements***

Even though every possible attempt was made to keep the systems tested under controlled conditions, human and instrumental errors are always possible when it comes to experimental setups. Weighing losses, transport losses and instrumental errors are usually unavoidable and affect the experimental work carried out by researchers. To limit these effects, multiple measurements were taken per system and at least three replicates were reported. The error associated with the measurements was reported as standard error and standard deviation while data obtained using published methods were compared to the published results to account for theoretical errors (for example the theoretical peaks of MS analysis for MCA which were compared to the published results and a % error was reported). Error bars indicating standard deviation results were introduced in most of the graphs reported except the cases where preliminary results were obtained (for example PGN analysis). Instrumentation-related quality checks were also carried out in an attempt to make sure all data collected was of the highest accuracy. Calibration curves with standard materials were verified regularly before the use of the instruments for analysis of samples. In several cases the method of 'spike' addition (i.e. standard addition) was followed to make sure the measured values were not affected by the detection limit of the instrument.

Slight changes of temperature and pressure could lead to small changes in the experimental results. These slight changes though are expected in natural environments and the systems tested in this project were intended to mimic the natural system of LPS, MCA and PGN approaching the different minerals. In nature, such systems are open to more environmental changes which suggests

the possible availability of more ions and hence more possible interactions. An attempt was made to mimic this 'openness' of the natural systems as closely as possible and the samples tested were not introduced into clean conditions but were left open to the atmosphere instead. This suggests that other than calcium and sodium ions that were intended to support the interaction could possibly disrupt the overall process. An example is the presence of carbonates that are widely available in the atmosphere and are usually attracted by water molecules and  $\text{OH}^-$  in basic solutions. This case would lead to further precipitation of the calcium ions in solution due to interaction with carbonates that would also limit the availability of free calcium ions in solution. This scenario suggests that even though conclusions can be drawn from the experimental results for the systems tested, more parameters should be taken into consideration when constructing a general mechanism for the sorption process of macromolecules onto minerals. Natural systems are much more complex than the clean experimental setups tested in laboratory which suggests that no quick conclusions should be drawn from laboratory-based experiments referring to natural environments.





# References

- Akob, D.M., Mills, H.J., Kostka, J.E. (2007). Metabolically active microbial communities in uranium-contaminated subsurface sediments, *FEMS Microbiol Ecol.*, 59, 95-107
- Al-Anber, M. A. *Thermodynamics Approach in the Adsorption of Heavy Metals*. Retrieved from <http://www.intechopen.com/books/thermodynamics-interaction-studies-solids-liquids-and-gases/thermo>
- Alessi, D. S., Uster, B., Veeramani, H., Suvorova, E. I., Lezama-Pacheco, J. S., Stubbs, J. E., . . . Bernier-Latmani, R. (2012). Quantitative Separation of Monomeric U(IV) from UO<sub>2</sub> in Products of U(VI) Reduction. *Environmental Science & Technology*, 46(11).doi:10.1021/es204123z
- Alhooshani, K. R. (2015). Adsorption of chlorinated organic compounds from water with cerium oxide-activated carbon composite. *Arabian Journal of Chemistry*. doi:10.1016/j.arabjc.2015.04.013
- Allen, M. P. (2004). Introduction to Molecular Dynamics Simulation (Vol. 23, pp. 1-28): John von Neumann Institute for Computing.
- Amadasi, A., moi, F., Cozzini, P., Abraham, D. J., Kellogg, G. E., & Mozzarelli, A. (2006). Mapping the energetics of water-protein and water-ligand interactions with the "natural" HINT forcefield: Predictive tools for characterizing the roles of water in biomolecules. *Journal of Molecular Biology*, 358(1). doi:10.1016/j.jmb.2006.01.053
- Ananthi, T., Emmanuel, E.S., Anandkumar, B. and Maruthamuthu, S. (2012). Accumulation of rare earth elements by siderophore-forming *Arthrobacter luteolus* isolated from rare earth environment of Chavara, India, *J Biosci.*, 37, 25-31
- Anderson, R.J. (1939) The chemistry of the lipids of the tubercle bacillus and certain other microorganisms *Fortschritte. Chem. Org. Naturst.*, 3, pp. 145–202
- Anderson, R.J. (1941) Structural peculiarities of acid-fast bacterial lipids *Chem. Rev.*, 29, pp. 225–243
- Anderson, R. J. (1943). The Chemistry of the Lipids of the Tubercle Bacillus. *The Yale Journal of Biology and Medicine*, 15(3), 311–345.
- Anderson, R. T., & Lovley, D. R. (2002). Interactions of microorganisms with Radionuclides-Microbial redox interactions with uranium: an environmental perspective. Chapter 7 of *Interactions of Microorganisms with Radionuclides*, Miranda J. Keith-Roach and Francis R. Livens (Editors), 2002 Elsevier Science Ltd.
- Andres, Y., MacCordick, H. J., & Hubert, J. C. (1993). Adsorption of several actinides (Th, U) and lanthanide (La, Eu, Yb) ions by mycobacterium smegmatis. *Applied Microbiology and Biotechnology*, 39(3).

- Andres, Y., MacCordick, H.J. and Hubert, J.-C.(1994), Binding sites of sorbed uranyl ion in the cell wall of *Mycobacterium smegmatis*.*FEMS Microbiology Letters*, 115: 27–32. doi:10.1111/j.1574-6968.1994.tb06609.x
- Antia, A. L., and C. T. Lee.(1963). Studies on the determination and differential analysis of dissolved carbohydrate in sea-water.*Fish.Res. Board Can. Manuscript Rep. Ser.* 168.
- Asano, S., Arvapalli, R., Manne, N., Maheshwari, M., Ma, B., Rice, K., . . . Blough, E. (2015). Cerium oxide nanoparticle treatment ameliorates peritonitis-induced diaphragm dysfunction. *International journal of Nanomedicine*, 10(1), 11. doi:10.2147/IJN.S89783
- Atrih, A, Bacher, G, Allmaier, G, Williamson, M P, Foster, S J, (1999) Analysis of peptidoglycan structure from vegetative cells of *Bacillus subtilis* 168 and role of PBP 5 in peptidoglycan maturation, *Journal of bacteriology*, Vol.181(13), pp.3956-66
- Aurell, C. A., & Wistrom, A. O. (1998).Critical Aggregation Concentrations of Gram-Negative Bacterial Lipopolysaccharides (LPS).*Biochemical and Biophysical Research Communications*, 253(1), 119-123. doi:http://dx.doi.org/10.1006/bbrc.1998.9773
- Azimi, G., Dhiman, R., Kwon, H.-M., Paxson, A. T., & Varanasi, K. K. (2013). Hydrophobicity of rare-earth oxide ceramics.*Nat Mater*, 12(4), 315-320.
- Babelot, C. (2013) *Monazite-type ceramics for conditioning of Minor actinides: Structural characterization and properties*, Doktorin der Ingenieurwissenschaften, 153 pages
- Bailey, B. W. and Rankin, J. M. (1971), New Spectrophotometric Method for Determination of Formaldehyde, *Analytical Chemistry*, 43(6), 782-784
- Bargar, J.R., Bernier-Latmani, R., Giammar, D.E., Mehta, A., Schofield, E., Sharp, J.O., Suvorova, E.I., Ulrich, K., Veeramani, H. (2009)*Goldschmidr Conference Abstracts*, A87
- Barkan, D., Hedhli, D., Yan, H. G., Huygen, K., & Glickman, M. S. (2012). *Mycobacterium tuberculosis* lacking all mycolic acid cyclopropanation is viable but highly attenuated and hyperinflammatory in mice. *Infect Immun*, 80(6), 1958-1968. doi:10.1128/IAI.00021-12
- Barkleit, A., Moll, H., & Bernhard, G. (2009). Complexation of uranium(vi) with peptidoglycan. *Dalton Transactions* (27), 5379-5385.doi:10.1039/B818702A
- Barry Iii, C. E., Lee, R. E., Mdluli, K., Sampson, A. E., Schroeder, B. G., Slayden, R. A., & Yuan, Y. (1998). Mycolic acids: structure, biosynthesis and physiological functions. *Progress in Lipid Research*, 37(2–3), 143-179. doi:10.1016/S0163-7827(98)00008-3
- Bartha, F., Molnar, B., Foldi, P., Benedict, M.G. (2003). Time evolution in the Morse potential using supersymmetry: Dissociation of the NO molecule. *EPL (Europhysics Letters)*,61(4), 445

- Basso, L. A., da Silva, L. H. P., Fett-Neto, A. G., de Azevedo, W. F., Jr., Moreira, I. d. S., Palma, M. S., . . . Santos, D. S. (2005). The use of biodiversity as source of new chemical entities against defined molecular targets for treatment of malaria, tuberculosis, and T-cell mediated diseases--a review. *Memorias do Instituto Oswaldo Cruz*, 100(6).
- Baudin, M., Wójcik, M., & Hermansson, K. (2000). Dynamics, structure and energetics of the (111), (011) and (001) surfaces of ceria. *Surface Science*, 468(1-3), 51-61. doi:http://dx.doi.org/10.1016/S0039-6028(00)00766-4
- Bayer, M E, Bayer, M H,(1991), Lanthanide accumulation in the periplasmic space of Escherichia coli B, *Journal of bacteriology*, Vol.173(1), pp.141-9
- Beekes, M., Lasch, P., & Naumann, D. (2007). Analytical applications of Fourier transform-infrared (FT-IR) spectroscopy in microbiology and prion research. *Veterinary Microbiology*, 123(4), 305-319. doi:10.1016/j.vetmic.2007.04.010
- Bendinger, B., Rijnaarts, H. H. M., Altendorf, K., & Zehnder, A. J. B. (1993). Physicochemical Cell Surface and Adhesive Properties of Coryneform Bacteria Related to the Presence and Chain Length of Mycolic Acids. *Applied and Environmental Microbiology*, 59(11), 3973-3977.
- Benzerara, K., Miot, J., Morin, G., Ona-Nguema, G., Skouri-Panet, F., & Ferard, C. (2011).Significance, mechanisms and environmental implications of microbial biomineralisation. *Comptes Rendus Geoscience*, 343(2-3). doi:10.1016/j.crte.2010.09.002
- Benzerara, K., Miot, J., Morin, G., Kappler, A., Bernanrd, S., Obst, M., Ferard, C., Skouri, F., Guigner, J.M., Posth, N., Galvez, M., Brown, G.E., and Guyot, F. (2009)Ironbiomineralisation by anaerobic neutrophilic iron-oxidizing bacteria, *Geochimica et Cosmochimica Acta*, 73, 696-711
- Beveridge, T.J. (1999), *J Bacteriol.*, 16 p. 4725-4733
- Beveridge, D. L., & DiCapua, F. M. (1989). Free Energy Via Molecular Simulation: Applications to Chemical and Biomolecular Systems. *Annual Review of Biophysics and Biophysical Chemistry*, 18(1), 431-492. doi:10.1146/annurev.bb.18.060189.002243
- Bhatt, A. S., Sakaria, P. L., Vasudevan, M., Pawar, R. R., Sudheesh, N., Bajaj, H. C., & Mody, H. M. (2012). Adsorption of an anionic dye from aqueous medium by organoclays: equilibrium modeling, kinetic and thermodynamic exploration. *RSC Advances*, 2(23), 8663-8671. doi:10.1039/C2RA20347B
- Bjerre, A., Brusletto, B., Mollnes, T. E., Fritzsønn, E., Rosenqvist, E., Wedege, E., . . . Brandtzaeg, P. (2002). Complement activation induced by purified Neisseria meningitidis lipopolysaccharide (LPS), outer membrane vesicles, whole bacteria, and an LPS-free mutant. *J Infect Dis*, 185(2), 220-228. doi:10.1086/338269
- Boice, J. (2006). Thyroid Disease 60 Years After Hiroshima and 20 Years After Chernobyl. *JAMA: The Journal of the American Medical Association*, 9(295), 3.

- Boyanov, M. I., Fletcher, K. E., Kwon, M. J., Rui, X., O'Loughlin, E. J., Loeffler, F. E., & Kemner, K. M. (2011). Solution and Microbial Controls on the Formation of Reduced U(IV) Species. *Environmental Science & Technology*, 45(19).doi:10.1021/es2014049
- Boyanov, M. I., O'Loughlin, E. J., Roden, E. E., Fein, J. B., & Kemner, K. M. (2007). Adsorption of Fe(II) and U(VI) to carboxyl-functionalized microspheres: The influence of speciation on uranyl reduction studied by titration and XAFS. *Geochimica Et Cosmochimica Acta*, 71(8). doi:10.1016/j.gca.2007.01.025
- Boyarchenkov, A. S., Potashnikov, S. I., Nekrasov, K. A., & Kupryazhkin, A. Y. (2012). Molecular dynamics simulation of UO<sub>2</sub> nanocrystals melting under isolated and periodic boundary conditions. *Journal of Nuclear Materials*, 427(1-3). doi:10.1016/j.jnucmat.2012.05.023
- Bray, B. L., (2003) Large-scale manufacture of peptide therapeutics by chemical synthesis *Nat. Rev. Drug Discovery* 2, 587–593.
- Brennan, P.J. and Nikaido, H.(1995), The envelope of Mycobacteria, *Ann. Rev. Biochem.*, 64, 29-63
- Brennecka, G. A., Borg, L. E., Hutcheon, I. D., Sharp, M. A., & Anbar, A. D. (2010). Natural variations in uranium isotope ratios of uranium ore concentrates: Understanding the U-238/U-235 fractionation mechanism. *Earth and Planetary Science Letters*, 291(1-4). doi:10.1016/j.epsl.2010.01.023
- Burgos, W.D., McDonough, J.T., Senko, J.M., Zhang, G., Dohnakova, A.C., Kelly, S.D., Gorby, Y., Kemner, K.M. (2008), *Geochimica et Cosmochimica Acta*, 72, p. 4901
- Butler, W.R. and Guthertz, L.S.(2001), Mycolic acid analysis by High Performance Liquid Chromatography for Identification of Mycobacterium Species, *Clin. Microbiol.Rev.*, 14, 704-726
- Butler, W.R. and Kilburn, J.O. (1988) 'Identification of major slowly growing pathogenic mycobacteria and mycobacterium gordonae by high-performance liquid chromatography of their mycolic acids', *J Clin Microbiol.*, 26, 50-53
- Cantrell, S. A., Leavell, M. D., Marjanovic, O., T.lavarone, A., Leary, J. A., & Riley, L. W. (2012). Regulated Alteration of Mycolic Acid Structure in the Cell Wall of Mycobacterium Tuberculosis. *Mycobac Dis.*, 2(3), 6. doi:10.4172/2161-1068.1000108
- Canzano, S., Iovino, P., Salvestrini, S., Capasso, S., (2012), Comment on 'Removal of ionic dye Congo red from aqueous solution by raw pine and acid-treated pine cone powder as adsorbent: Equilibrium, thermodynamics, kinetics, mechanism and process design', *Water Research*, 46(13), 4314-4315
- Carlton, C. J. E., & Laxen, P. A. (1966). *The Zero Point of Charge of Uranium Dioxide and Uraninite*. Technical Report, *National Inst. for Metallurgy*
- Central Michigan University, Retrieved from <http://isaacs.sourceforge.net/phys/psc.html> [last checked: 20/08/16]
- Chaplin, M.,(2016)Water Structure Retrieved from: [http://www1.lsbu.ac.uk/water/water\\_models.html](http://www1.lsbu.ac.uk/water/water_models.html) [last checked: 20/08/16]

- Char, N. L., & Csik, B. J. (1987). Nuclear power development: History and outlook. *IAEA BULLETIN*(3),7.
- Chen, Y., Geng, H.Y., Kaneta, Y., Kinoshita, M. and Iwata, S. (2010), First principles modelling of stability mechanism of nonstoichiometric uranium dioxide, *Computational Materials Science*, 49, S364-S368
- Chicote, E., Moreno, D., Garcia, A., Sarro, I., Lorenzo, P., & Montero, F. (2004). Biofouling on the walls of a spent nuclear fuel pool with radioactive ultrapure water. *Biofouling*, 20(1).doi:10.1080/08927010410001662670
- Ciopec, M., Negrea, A., Lupa, L., Davidescu, C. M., & Negrea, P. (2014). Studies regarding as(V) adsorption from underground water by Fe-XAD8-DEHPA impregnated resin. equilibrium sorption and fixed-bed column tests. *Molecules*, 19(10), 16082-16101. doi:10.3390/molecules191016082
- Clifton, L.A., Skoda, M.W.A., Daulton, E.L., Hughes, A.V., Le Brun, A.P., Lakey, J.H. and Holt, S.A. (2013) Asymmetric phospholipid: lipopolysaccharide bilayers; a Gram-negative bacterial outer membrane mimic *J. R. Soc. Interface* 2013 10 20130810; DOI: 10.1098/rsif.2013.0810.
- Cornell, W. D., Cieplak, P., Bayly, C. I., Gould, I. R., Merz, K. M., Ferguson, D. M., Kollman, P. A. (1995). A Second Generation Force Field for the Simulation of Proteins, Nucleic Acids, and Organic Molecules. *Journal of the American Chemical Society*, 117(19), 5179-5197. doi:10.1021/ja00124a002
- Cotton, S. (2006). Lanthanide and Actinide Chemistry, John Wiley & Sons, 280 pages.
- Crick, D.C., Mahapatra, S., and Brennan, P.J., (2001), Biosynthesis of the arabinogalactan-peptidoglycan complex of Mycobacterium tuberculosis, *Glycobiology*, 11, 107R-118R
- Curtis, C. E., & Tharp, A. G. (1959). Ceramic Properties of Europium Oxide. *Journal of the American Ceramic Society*, 42(3), 6.
- Das Nilanjana and Chandran Preethy, (2011), Microbial Degradation of Petroleum Hydrocarbon Contaminants: An Overview, *Biotechnology Research International*, vol. 2011, 13 pages.
- Davidson, L.A., Draper, P. and Minnikin, D.E. (1982), Studies on the mycolic acids from the walls of Mycobacterium microti, *J Gen Microbiol*. 128, 823–828
- Davis, B. H. (1965). *Preparation and adsorptive properties of thorium oxide*. (Doctor of Philosophy), University of Florida, Florida.
- Denecke, M. A. (2006). Actinide speciation using X-ray absorption fine structure spectroscopy. *Coordination Chemistry Reviews*, 250(7-8). doi:10.1016/j.ccr.2005.09.004
- Durst, H. D., Milano, M., Kikta, E. J., Connelly, Jr. S. A. and Grushka, E., (1975), Phenacyl Esters of Fatty Acids via Crown Ether Catalysts for Enhanced Ultraviolet Detection in Liquid Chromatography, *Analytical Chemistry*, 47, 1797-1801
- Edmondson, P. D., Zhang, Y., Moll, S., Namavar, F., & Weber, W. J. (2012). Irradiation effects on microstructure change in nanocrystalline ceria –Phase, lattice stress, grain size and boundaries. *Acta Materialia*, Vol.60(15)

- Evans, J. E., Jungjohann, K. L., Wong, P. C. K., Chiu, P.-L., Dutrow, G. H., Arslan, I., & Browning, N. D. (2012). Visualizing macromolecular complexes with in situ liquid scanning transmission electron microscopy. *Micron*, 43(11). doi:10.1016/j.micron.2012.01.018
- Fayek, M., Anovitz, L. M., Cole, D. R., & Bostick, D. A. (2010). O and H diffusion in uraninite: Implications for fluid-uraninite interactions and nuclear forensics. *Geochimica Et Cosmochimica Acta*, 74(12).
- Ferreira, R. (1963). Principle of electronegativity equalization. Part 1.-Bond moments and force constants. *Transactions of the Faraday Society*, 59(0), 1064-1074. doi:10.1039/TF9635901064
- Finneran, K. T., Anderson, R. T., Nevin, K. P., & Lovley, D. R. (2002). Potential for Bioremediation of Uranium-contaminated aquifers with microbial U(VI) reduction. *Soil and Sediment Contamination*, 11(3), 20.
- Fonseca, C., Araneda, C., Yazdani-Pedram, M., Borrmann, T., Basualto, C., Sapag, J., & Valenzuela, F. (2010). Microencapsulation of trioctylamine in polymeric matrices for removing Zn(II) AND Cu(II) from chloride aqueous solutions. *Journal of the Chilean Chemical Society*, 55, 6.
- Freeman, C. L., Asteriadis, I., Yang, M., & Harding, J. H. (2009). Interactions of Organic Molecules with Calcite and Magnesite Surfaces. *The Journal of Physical Chemistry C*, 113(9), 3666-3673. doi:10.1021/jp807051u
- Freeman, C. L., & Harding, J. H. (2014). Entropy of Molecular Binding at Solvated Mineral Surfaces. *The Journal of Physical Chemistry C*, 118(3), 1506-1514. doi:10.1021/jp407122u
- Freeman, C. L., Harding, J. H., Cooke, D. J., Elliott, J. A., Lardge, J. S., & Duffy, D. M. (2007). New Forcefields for Modelling Biomineralisation Processes. *The Journal of Physical Chemistry C*, 111(32), 11943-11951. doi:10.1021/jp071887p
- Freeman, C. L., Harding, J. H., Quigley, D., & Rodger, P. M. (2011). Simulations of Ovocleidin-17 Binding to Calcite Surfaces and Its Implications for Eggshell Formation. *The Journal of Physical Chemistry C*, 115(16), 8175-8183. doi:10.1021/jp200145m
- Frenkel, D. and Smit, B (2002) *Understanding molecular simulation: from algorithms to application*, Academic Press, 638 pages.
- Fuente, S., Branda, M. M., & Illas, F. (2012). Role of step sites on water dissociation on stoichiometric ceria surfaces. *Theoretical Chemistry Accounts*, 131(3), 1-7. doi:10.1007/s00214-012-1190-2
- Fujiwara, Y. and Fukukawa, K. A (2012), Practical Method to Solve Cut-off Coulomb Problems in the Momentum Space Application to the Lippmann-Schwinger Resonating-Group Method and the pd Elastic Scattering *Prog.Theor.Phys.* 128, 301-347
- Gaberle, J., Gao, D. Z., Watkins, M. B., & Shluger, A. L. (2016). Calculating the Entropy Loss on Adsorption of Organic Molecules at Insulating Surfaces. *The Journal of Physical Chemistry C*, 120(7), 3913-3921. doi:10.1021/acs.jpcc.5b12028

- Gavrilescu, M., Pavel, L. V., & Cretescu, I. (2009). Characterization and remediation of soils contaminated with uranium. *Journal of Hazardous Materials*, 163(2-3). doi:10.1016/j.jhazmat.2008.07.103
- Giménez, J., de Pablo, J., Casas, I., Martínez-Lladó, X., Rovira, M., & Martínez Torrents, A. (2014). Solubility study and point of zero charge of studtite (UO<sub>2</sub>O<sub>2</sub>·4H<sub>2</sub>O). *Applied Geochemistry*, 49, 42-45. doi:10.1016/j.apgeochem.2014.07.004
- Glasauer, S., Langley, S., & Beveridge, T. J. (2001). Sorption of Fe (Hydr)Oxides to the Surface of *Shewanella putrefaciens*: Cell-Bound Fine-Grained Minerals Are Not Always Formed De Novo. *Applied and Environmental Microbiology*, 67(12), 5544-5550. doi:10.1128/AEM.67.12.5544-5550.2001
- Gojova, A., Lee, J.-T., Jung, H. S., Guo, B., Barakat, A. I., & Kennedy, I. M. (2009). Effect of cerium oxide nanoparticles on inflammation in vascular endothelial cells. *Inhalation toxicology*, 21(Suppl 1), 123-130. doi:10.1080/08958370902942582
- Gomez, P., Garralon, A., Buil, B., Turrero, M.J., Sanchez, L., and de la Cruz, B., (2006), Modelling of geochemical processes related to uranium mobilization in the groundwater of a uranium mine, *Science of the Total Environment*, 2006, 366, 295-309
- Gray, G. R., Wong, M. Y. H., & Danielson, S. J. (1982). The major mycolic acids of *Mycobacterium smegmatis*, *Progress in Lipid Research*, 21(2). doi:10.1016/0163-7827(82)90001-7
- Guillot, A., Courtin, F.P., Mezange, C., Domakova, E., Kulakauskas, S., Miranda, G., Chapot-Chartier, M.P., (2006), Peptidoglycan Structure Analysis of *Lactococcus lactis* Reveals the Presence of an L,D-Carboxypeptidase Involved in Peptidoglycan Maturation', *Journal of Bacteriology*, p. 5293–5298 Vol. 188, No. 14
- Gurumoorthy, V. P., & Khan, K. H. (2011). Polymers at interfaces: biological and non-biological Applications. *Rec. Res. Sci. Tech*, 3(2), 6.
- Hadžija, O. (1974). A simple method for the quantitative determination of muramic acid. *Analytical Biochemistry*, 60(2), 512-517. doi:10.1016/0003-2697(74)90261-9
- Hagen, S.R., and Thompson, J.D. (1995), Analysis of mycolic acids by high-performance liquid chromatography and fluorimetric detection. Implications for the identification of mycobacteria in clinical samples, *J. Chromatogr A.*, 692, 167-172
- Hanwell, M.D., Curtis, D.E., Lonie, D.C., Vandermeersch, T., Zurek, E., and Hutchison, G.R. (2012) Avogadro: An advanced semantic chemical editor, visualization, and analysis platform *Journal of Cheminformatics* 4:17.
- Harding, J. H., Duffy, D. M., Sushko, M. L., Rodger, P. M., Quigley, D., & Elliott, J. A. (2008). Computational Techniques at the Organic–Inorganic Interface in Biomineralisation. *Chemical Reviews*, 108(11), 4823-4854. doi:10.1021/cr078278y

- Harris, G.D. (2007) *Quantitative Chemical Analysis*, W. H. Freeman and Company, 828 pages
- Hazenberg, M. P., & de Visser, H. (1992). Assay for N-acetylmuramyl-L-alanine amidase in serum by determination of muramic acid released from the peptidoglycan of *Brevibacterium divaricatum*. *Eur J Clin Chem Clin Biochem*, 30(3), 141-144.
- Herbowski, L., & Gurgul, H. (1970). The Structure of the Electric Double Layer of Macromolecules Suspended in Human Cerebrospinal Fluid. *Journal of Neurology & Neurophysiology*. doi:10.4172/2155-9562.1000108
- Ho, Y. S., & McKay, G. (1999). Pseudo-second order model for sorption processes. *Process Biochemistry*, 34(5), 451-465. doi:10.1016/S0032-9592(98)00112-5
- Hoijer, M. A., Melief, M. J., van Helden-Meeuwsen, C. G., Eulerink, F., & Hazenberg, M. P. (1995). Detection of muramic acid in a carbohydrate fraction of human spleen. *Infection and Immunity*, 63(5), 1652-1657.
- Hong, X., & Hopfinger, A. J. (2004). Construction, Molecular Modelling, and Simulation of Mycobacterium tuberculosis Cell Walls. *Biomacromolecules*, 5(3), 1052-1065. doi:10.1021/bm034514c
- Housecroft, C.E. & Constable, E.C. (2006), *Chemistry: An Introduction to Organic, Inorganic and Physical Chemistry*, Pearson, 1517 pages
- Iwase, A., Ohno, H., Ishikawa, N., Baba, Y., Hirao, N., Sonoda, T., & Kinoshita, M. (2009). Study on the behaviour of oxygen atoms in swift heavy ion irradiated CeO<sub>2</sub> by means of synchrotron radiation X-ray photoelectron spectroscopy. *Nuclear Instruments and Methods in Physics Research Section B: Beam Interactions with Materials and Atoms*, 267(6), 969-972. doi:10.1016/j.nimb.2009.02.035
- Jann B., Reske, K., Jann, K., (1975) Heterogeneity of lipopolysaccharides. Analysis of polysaccharide chain lengths by sodium dodecylsulfate-polyacrylamide gel electrophoresis. *European Journal of Biochemistry* 12(01)
- Jiang, W., Ghosh, S., Song, L., Vachet, R. W., & Xing, B. (2013). Effect of Al<sub>2</sub>O<sub>3</sub> nanoparticles on bacterial membrane amphiphilic biomolecules. *Colloids and Surfaces B: Biointerfaces*, 102, 292-299. doi:10.1016/j.colsurfb.2012.08.043
- Jing, H., Mezgebe, B., Aly Hassan, A., Sahle-Demessie, E., Sorial, G. A., & Bennett-Stamper, C. (2014). Experimental and modeling studies of sorption of ceria nanoparticle on microbial biofilms. *Bioresour Technol*, 161, 109-117. doi:10.1016/j.biortech.2014.03.015
- Johnson, D. B. (2014). Biomining-biotechnologies for extracting and recovering metals from ores and waste materials. *Curr Opin Biotechnol*, 30, 24-31. doi:10.1016/j.copbio.2014.04.008
- Johnson, S. B., Brown, G. E., Healy, T. W., & Scales, P. J. (2005). Adsorption of Organic Matter at Mineral/Water Interfaces. 6. Effect of Inner-Sphere versus Outer-Sphere Adsorption on Colloidal Stability. *Langmuir*, 21(14), 6356-6365. doi:10.1021/la047030q

- Johnson, K. J., Cygan, R.T., Fein, J.B. (2006) Molecular simulations of metal adsorption to bacterial surfaces. *Geochimica et Cosmochimica Acta* 70, 5075–5088
- Jucker, B. A., Harms, H., Hug, S. J., & Zehnder, A. J. B. (1997). Adsorption of bacterial surface polysaccharides on mineral oxides is mediated by hydrogen bonds. *Colloids and Surfaces B: Biointerfaces*, 9(6), 331-343. doi:[http://dx.doi.org/10.1016/S0927-7765\(97\)00038-6](http://dx.doi.org/10.1016/S0927-7765(97)00038-6)
- Jucker, B. A., Harms, H., & Zehnder, A. J. B. (1998). Polymer interactions between five gram-negative bacteria and glass investigated using LPS micelles and vesicles as model systems. *Colloids and Surfaces B: Biointerfaces*, 11(1–2), 33-45. doi:10.1016/S0927-7765(98)00029-0
- Karkhanis, Y. D., Zeltner, J. Y., Jackson, J. J., & Carlo, D. J. (1978). A new and improved microassay to determine 2-keto-3-deoxyoctonate in lipopolysaccharide of gram-negative bacteria. *Analytical Biochemistry*, 85(2), 595-601. doi:[http://dx.doi.org/10.1016/0003-2697\(78\)90260-9](http://dx.doi.org/10.1016/0003-2697(78)90260-9)
- Kelly, S. D., Kemner, K. M., Fein, J. B., Fowle, D. A., Boyanov, M. I., Bunker, B. A., & Yee, N. (2002). X-ray absorption fine structure determination of pH-dependent U-bacterial cell wall interactions. *Geochimica Et Cosmochimica Acta*, 66(22). doi:10.1016/s0016-7037(02)00947-x
- Kerisit, S., Cooke, D. J., Spagnoli, D., & Parker, S. C. (2005). Molecular dynamics simulations of the interactions between water and inorganic solids. *Journal of Materials Chemistry*, 15(14), 1454-1462. doi:10.1039/B415633C
- Khan, A.A.; Singh, R.P. (1987) Adsorption thermodynamics of carbofuran on Sn (IV) arsenosilicate in H<sup>+</sup>, Na<sup>+</sup> and Ca<sup>2+</sup> forms. *Colloids Surf.* 24, 33–42.
- King, J. D., and White, D. C. (1977), Muramic acid as a measure of microbial biomass in estuarine and marine samples, *Appl Environ Microbiol.*, 33(4), 777-83
- Kinoshita, M., Yasunaga, K., Sonoda, T., Iwase, A., Ishikawa, N., Sataka, M., . . . Matzke, H. (2009). Recovery and restructuring induced by fission energy ions in high burnup nuclear fuel. *Nuclear Instruments and Methods in Physics Research Section B: Beam Interactions with Materials and Atoms*, 267(6), 960-963. doi:10.1016/j.nimb.2009.02.022
- Kosmulski, M. (2002). The pH-Dependent Surface Charging and the Points of Zero Charge. *Journal of Colloid and Interface Science*, 253(1), 77-87. doi:<http://dx.doi.org/10.1006/jcis.2002.8490>
- Komarov, P. V., Zherenkova, L. V., & Khalatur, P. G. (2008). Computer simulation of the assembly of gold nanoparticles on DNA fragments via electrostatic interaction. *The Journal of Chemical Physics*, 128(12). doi:10.1063/1.2842070
- Kosog, B., La Pierre, H. S., Denecke, M. A., Heinemann, F. W., & Meyert, K. (2012). Oxidation State Delineation via U L-III-Edge XANES in a Series of Isostructural Uranium Coordination Complexes. *Inorganic Chemistry*, 51(14). doi:10.1021/ic3011234

- Kumar, P. S., Vincent, C., Kirthika, K., & Kumar, K. S. (2010). Kinetics and equilibrium studies of Pb<sup>2+</sup> in removal from aqueous solutions by use of nano-silversol-coated activated carbon. *Brazilian Journal of Chemical Engineering*, 27, 7.
- Kumara, N. T. R. N., Hamdan, N., Petra, M. I., Tennakoon, K. U., & Ekanayake, P. (2014). Equilibrium Isotherm Studies of Adsorption of Pigments Extracted from Kuduk-kuduk (*Melastoma malabathricum* L.) Pulp onto TiO<sub>2</sub> Nanoparticles. *Journal of Chemistry*, 6. doi:10.1155/2014/468975
- Kühner, D., Stahl, M., Demircioglu, D. D., & Bertsche, U. (2014). From cells to muropeptide structures in 24 h: Peptidoglycan mapping by UPLC-MS. *Scientific Reports*, 4, 7494. doi:10.1038/srep07494
- Lay, H. C., Spencer, M. J. S., Evans, E. J., & Yarovsky, I. (2003). Molecular Simulation Study of Polymer Interactions with Silica Particles in Aqueous Solution. *The Journal of Physical Chemistry B*, 107(36), 9681-9691. doi:10.1021/jp034572s
- Leach, A.R. (2001), *Molecular Modelling: Principles and Applications (2nd Edition)* Pearson, 784 pages
- Lee, C.H. and Tsai, C.M. (1999), Quantification of Bacterial Lipopolysaccharides by the Purpald Assay: Measuring Formaldehyde Generated from 2-keto-3-deoxyoctonate and Heptose at the Inner Core by Periodate Oxidation, *Analytical Biochemistry*, 267, 161-168
- Leenheer, J. A. (2004). Fractionation and characterization of organic matter in wastewater from a swine waste-retention basin. In C. E. Rostad (Ed.). Reston, Va.: U.S. Dept. of the Interior, U.S. Geological Survey.
- Leenheer, J. A., and Rostad, C. E. (2004). Fractioning and Characterization of Organic Matter in wastewater from a Swine Waste-Retention Basin.
- Retrieved from <http://pubs.usgs.gov/sir/2004/5217/pdf/sir2004-5217.pdf>
- Leung, K., & Nenoff, T. M. (2012). Hydration structures of U(III) and U(IV) ions from ab initio molecular dynamics simulations. *Journal of Chemical Physics*, 137(7). doi:10.1063/1.4742754
- Li, K., Li, M., & Xue, D. (2012). Solution-Phase Electronegativity Scale: Insight into the Chemical Behaviors of Metal Ions in Solution. *The Journal of Physical Chemistry A*, 116(16), 4192-4198. doi:10.1021/jp300603f
- Liang, C., Read, H. W., & Balser, T. C. (2009). Reliability of Muramic Acid as a Bacterial Biomarker is Influenced by Methodological Artifacts from Streptomycin. *Microbial Ecology*, 57(3), 494-500. doi:10.1007/s00248-008-9406-7
- Lin, S., Chen, J.-L., HLeungang, L.-S., & Lin, H.-W. (2005). Measurements of the forces in protein interactions with atomic force microscopy. *Current Proteomics*, 2(1). doi:10.2174/1570164053507754
- Lin, Z., Zhou, C., Wu, J., Cheng, H., Liu, B., Ni, Z., . . . Fu, J. (2002). Adsorption and reduction of palladium (Pd<sup>2+</sup>) by *Bacillus licheniformis* R08. *Chinese Science Bulletin*, 47(15), 1262-1266. doi:10.1360/02tb9279

- Liu, X.Y., Wang, L.H., Zheng, Z., Kang, M.L., Li, Ci. and Liu, C.L. (2013), Molecular Dynamics simulation of the diffusion of uranium species in clay pores', *J Hazard Mater.*, 15, 244-245
- Liu, D., P. T. S. Wong, and B. J. Dutka.(1973), Determination of carbohydrates in the lake sediment by a modified phenol-sulfuric acid method.*Water Res.* 7:741-746.
- Livens, F. R., Al-Bokari, M., Fomina, M., Gadd, G. M., Geissler, A., Lloyd, J. R., . . . Vaughan, D. J. (2010).*Microbial transformations of actinides in the environment*. Paper presented at the Actinides Conference, San Francisco, CA.
- Lloyd, J.R., Chesnes, J., Glasauer, S., Bunker, D.J., Livens, F.R., Lovley, D.R., (2002), *Geomicrobiol. J.*, 19, p. 103
- Lloyd, J. R., & Renshaw, J. C. (2005). Bioremediation of radioactive waste: radionuclide-microbe interactions in laboratory and field-scale studies. *Current Opinion in Biotechnology*, 16(3). doi:10.1016/j.copbio.2005.04.012
- Lloyd, J R; Sole, V A; Van Praagh, C V; Lovley, D R, (2000), Direct and Fe(II)-mediated reduction of technetium by Fe(III)-reducing bacteria, *Applied and environmental microbiology*, Vol.66(9), pp.3743-9
- Lu, Q., Wang, J., Faghihnejad, A., Zeng, H., & Liu, Y. (2011). Understanding the molecular interactions of lipopolysaccharides during E. coli initial adhesion with a surface forces apparatus.*Soft Matter*, 7(19), 9366-9379. doi:10.1039/C1SM05554B
- Macaskie, L. E., Jeong, B. C., Tolley, M. R., (1994), Enzymically accelerated biomineralisation of heavy metals: Application to the removal of americium and plutonium from aqueous flows, *FEMS Microbiology Reviews*, 1994, Vol.14(4), pp.351-367
- Marchetti, R., Canales, A., Lanzetta, R., Nilsson, I., Vogel, C., Reed, D. E., . . . Silipo, A. (2013). Unraveling the Interaction between the LPS O-Antigen of Burkholderia anthina and the 5D8 Monoclonal Antibody by Using a Multidisciplinary Chemical Approach, with Synthesis, NMR, and Molecular Modeling Methods.*ChemBioChem*, 14(12), 8.
- Markai, S., Montavon, G., Andres, Y., and Grambow, B. (2013), Transfer of Eu (III) associated with polymaleic acid to Bacillus subtilis, *Appl Radiat Isot.*, 2003, 58, 161-168
- Martínez, L., Andrade, R., Birgin, E.G., Martínez, J.M. (2009) Packmol: A package for building initial configurations for molecular dynamics simulations.*Journal of Computational Chemistry*, 30(13):2157-2164
- Mashall, M. J., Beliaev, A. S., Dohnalkova, A. C., Kennedy, D. W., Shi, L., Wang, Z., Boyanov, M. I., Lai, B., K. M. Kemner, J. S. McLean, S. B. Reed, S.E. Culley, V. L. Bailey, C. J. Simonson, D. A. Saffarini, M. F. Romine, J. M. Zachara, J. K. Fredrickson, (2006), *PLoS Biology*, 4p.268
- Marx, J. L. (1989). *A Revolution in biotechnology*: Cambridge University Press, 238 pages

- Meißner, R., Wei, G., & Ciacchi, L. C. (2015). Estimation of the free energy of adsorption of a polypeptide on amorphous SiO<sub>2</sub> from molecular dynamics simulations and force spectroscopy experiments. *Soft Matter*, 11(31), 6254-6265. doi:10.1039/C5SM01444A
- Merroun, M. L., Nedelkova, M., Ojeda, J. J., Reitz, T., Lopez Fernandez, M., Arias, J. M., . . . Selenska-Pobell, S. (2011). Bio-precipitation of uranium by two bacterial isolates recovered from extreme environments as estimated by potentiometric titration, TEM and X-ray absorption spectroscopic analyses. *Journal of Hazardous Materials*, 197. doi:10.1016/j.jhazmat.2011.09.049
- Merroun, M. L., & Selenska-Pobell, S. (2008). Bacterial interactions with uranium: An environmental perspective. *Journal of Contaminant Hydrology*, 102(3-4). doi:10.1016/j.jconhyd.2008.09.019
- Miller, R. W. (1995). Delayed Effects of External Radiation Exposure: A Brief History. *Radiation Research*, 144(2), 9.
- Milonjic, S. K. (2007). A consideration of the correct calculation of thermodynamic parameters of adsorption. *Journal of the Serbian chemical society*, 72(12), 6.
- Minnikin, D. E., (1982) *The Biology of the Mycobacteria*, Vol. 1, eds C. Ratledge and J. Standford. Academic Press, London, pp. 95-184
- Molinari, M., Parker, S. C., Sayle, D. C., & Islam, M. S. (2012). Water Adsorption and Its Effect on the Stability of Low Index Stoichiometric and Reduced Surfaces of Ceria. *The Journal of Physical Chemistry C*, 116(12), 7073-7082. doi:10.1021/jp300576b
- Moll, H. et al. (2013), Microbial diversity in Opalinus Clay and interaction of dominant microbial strains with actinides, *Final Report BMWi-Project 02E10618*, HZDR-036, 2013.
- Moll, H., Lütke, L., Bachvarova, V., Cherkouk, A., Selenska-Pobell, S., & Bernhard, G. (2014). Interactions of the Mont Terri Opalinus Clay Isolate *Sporomusa* sp. MT-2.99 with Curium(III) and Europium(III). *Geomicrobiology Journal*, 31(8), 682-696. doi:10.1080/01490451.2014.889975
- Momma, K. and Izumi, F. (2011) VESTA 3 for three-dimensional visualization of crystal, volumetric and morphology data, *J. Appl. Crystallogr.*, 44, 1272-1276.
- Montavon, G., Rabung, T., Geckeis, H., Grambow, B. (2004), Interaction of Eu(III)/Cm(III) with alumina-bound poly (acrylic acid): sorption, desorption, and spectroscopic studies, *Environmental science & technology*, Vol.38(16), pp.4312-8
- Morris, J. C., Storandt, M., Miller, J. P., McKeel, D. W., Price, J. L., Rubin, E. H., & Berg, L. (2001). Mild cognitive impairment represents early-stage Alzheimer disease. *Arch Neurol*, 58(3), 397-405.
- Mudunkotuwa, I. A., Minshid, A. A., & Grassian, V. H. (2014). ATR-FTIR spectroscopy as a tool to probe surface adsorption on nanoparticles at the liquid-solid interface in environmentally and biologically relevant media. *Analyst*, 139(5), 870-881. doi:10.1039/C3AN01684F
- Murray, P.R, Rosenthal, K.S., Kobayashi, G.S., Pfaller, M.A. (2010), *Medical Microbiology*, 4<sup>th</sup> edition

- Nagao, M., & Morimoto, T. (1969). Differential heat of adsorption and entropy of water adsorbed on zinc oxide surface. *The Journal of Physical Chemistry*, 73(11), 3809-3814. doi:10.1021/j100845a040
- Namjesnik, D., Mutka, S., Iveković, D., Gajović, A., Willinger, M., & Preočanin, T. (2016). Application of the surface potential data to elucidate interfacial equilibrium at ceria/aqueous electrolyte interface. *Adsorption*, 22(4), 825-837. doi:10.1007/s10450-016-9785-x
- Natarajan, K. A., & Namita, D. (2001). Role of bacterial interaction and bioreagents in iron ore flotation. *International Journal of Mineral Processing*, 62(1-4), 143-157. doi:10.1016/S0301-7516(00)00049-1
- Naumann, D., Barnickel, G., Bradaczek, H., Labischinski, H., & Giesbrecht, P. (1982). Infrared spectroscopy, a tool for probing bacterial peptidoglycan. Potentialities of infrared spectroscopy for cell wall analytical studies and rejection of models based on crystalline chitin. *Eur J Biochem*, 125(3), 505-515.
- Neu, M. P., Boukhalfa, H., & Merroun, M. L. (2010). Biomineralisation and biotransformations of actinide materials. *Mrs Bulletin*, 35(11). doi:10.1557/mrs2010.711
- Newsome, L., Morris, K., Trivedi, D., Atherton, N., & Lloyd, J. R. (2014). Microbial reduction of uranium(VI) in sediments of different lithologies collected from Sellafield. *Applied Geochemistry*, 51, 55-64. doi:10.1016/j.apgeochem.2014.09.008
- Nolan, M., & Watson, G. W. (2006). The Surface Dependence of CO Adsorption on Ceria. *The Journal of Physical Chemistry B*, 110(33), 16600-16606. doi:10.1021/jp062499a
- Olsoon, M., Jakobsson, A.-M., & Albinsson, Y. (2002). Surface Charge Densities of Two Actinide(IV) Oxides: UO<sub>2</sub> and ThO<sub>2</sub>. *Journal of Colloid and Interface Science*, 256(2), 5.
- Osborn, M. J., Gander, J. E., Paris, E., and Carson, J. (1972) *J. Biol. Chem.* 247, 3962-3972.
- Panagiotopoulos, C., & Sempere, R. (2005). Analytical methods for the determination of sugars in marine samples: A historical perspective and future directions. *Limnology and Oceanography*, 3(10), 35. doi:10.4319/lom.2005.3.419
- Parikh, S. J., & Chorover, J. (2008). ATR-FTIR study of lipopolysaccharides at mineral surfaces. *Colloids and Surfaces B: Biointerfaces*, 62(2), 188-198. doi:10.1016/j.colsurfb.2007.10.002
- Parikh, S. J., & Chorover, J. (2007). Infrared spectroscopy studies of cation effects on lipopolysaccharides in aqueous solution. *Colloids and Surfaces B: Biointerfaces*, 55(2), 241-250. doi:http://dx.doi.org/10.1016/j.colsurfb.2006.12.014
- Paterson-Beedle, M., Jeong, B. C., Lee, C. H., Jee, K. Y., Kim, W. H., Renshaw, J. C., & Macaskie, L. E. (2012). Radiotolerance of phosphatases of a *Serratia* sp.: Potential for the use of this organism in the biomineralisation of wastes containing radionuclides. *Biotechnology and Bioengineering*, 109(8). doi:10.1002/bit.24467

- Perry Iv, T. D., Cygan, R. T., & Mitchell, R. (2007). Molecular models of a hydrated calcite mineral surface. *Geochimica et Cosmochimica Acta*, 71(24), 5876-5887.
- Peterson, S., Adams, R.E., Douglas, D.A., (1965) *Properties of Thorium, its alloys and its compounds*, 32
- Rawlings, D. E. (1997). *Biomining: theory, microbes, and industrial processes*. Berlin; London: Springer.
- Rawlings, D. E., Dew, D., & du Plessis, C. (2003). Biomineralisation of metal-containing ores and concentrates. *Trends Biotechnol*, 21(1), 38-44.
- Reddy, C. A. (2007). *Methods for general and molecular microbiology* (3rd ed. ed.). Washington, D.C.: ASM ; Oxford : Blackwell [distributor].
- Reifsteck, F., Wee, S., & Wilkinson, B. J. (1987). Hydrophobicity-hydrophilicity of staphylococci. *J Med Microbiol*, 24(1), 65-73. doi:10.1099/00222615-24-1-65
- Renshaw, J. C., Lloyd, J. R., & Livens, F. R. (2007). Microbial interactions with actinides and long-lived fission products. *Comptes Rendus Chimie*, 10(10-11). doi:10.1016/j.crci.2007.02.013
- Rieß, F.G., Elflein, M., Benk, M., Schiffler, B., Benz, R., Garton, N., and Sutcliffe, I., (2003), The cell wall of the pathogenic bacterium *Rhodococcus equi* contains two channel-forming proteins with different properties, *J. Bacteriol.*, 2003, 185, 2952-2960
- Rietschel, E. T., Kirikae, T., Schade, F. U., Mamat, U., Schmidt, G., Loppnow, H., . . . Di Padova, F. (1994). Bacterial endotoxin: molecular relationships of structure to activity and function. *FASEB J*, 8(2), 217-225.
- Roeser, S., Hillerbrand, R., Sandrin, P., Peterson, M. (2012), *Handbook of Risk Theory: Epistemology, Decisión Theory, Ethics and Social Implications of Risk* Volume 1, 600
- Romero-González, J., Peralta-Videa, J. R., Rodríguez, E., Ramirez, S. L., & Gardea-Torresdey, J. L. (2005). Determination of thermodynamic parameters of Cr(VI) adsorption from aqueous solution onto *Agave lechuguilla* biomass. *The Journal of Chemical Thermodynamics*, 37(4), 343-347. doi:10.1016/j.jct.2004.09.013
- Rosenfeld, Y., Shai, Y. (2006) Lipopolysaccharide)-host defense antibacterial peptides interactions: Role in bacterial resistance and prevention of sepsis, *Biochimica et Biophysica Acta*, 1758(9), 1513-1522
- Sanjay Kumar, D., Ananthasivan, K., Venkata Krishnan, R., Amirthapandian, S., & Dasgupta, A. (2016). Bulk synthesis of nanocrystalline urania powders by citrate gel-combustion method. *Journal of Nuclear Materials*, 468, 178-193. doi:10.1016/j.jnucmat.2015.10.054
- Santos, N. C., Silva, A. C., Castanho, M. A., Martins-Silva, J., & Saldanha, C. (2003). Evaluation of lipopolysaccharide aggregation by light scattering spectroscopy. *ChemBiochem*, 4(1), 96-100. doi:10.1002/cbic.200390020
- Sayar, A. A., Sayar, N. A., Selcen, D.-S., & Gizay, O. (1970). Biosorption of Co(II) by *Schizosaccharomyces pombe*: Kinetic and Thermodynamic Studies for Process Design. *Journal of Bioprocessing & Biotechniques*, 3.

- Sayle, T. X., Molinari, M., Das, S., Bhatta, U. M., Möbus, G., Parker, S. C., . . . Sayle, D. C. (2013). Environment-mediated structure, surface redox activity and reactivity of ceria nanoparticles. *Nanoscale*, 5(13), 6063-6073. doi:10.1039/c3nr00917c
- Sayle, T. X. T., Sayle, L. W. L., & Sayle, D. C. (2015). Liquid crystal seed nucleates liquid-solid phase change in ceria nanoparticles. *Physical Chemistry Chemical Physics*, 17(6), 4441-4447. doi:10.1039/C4CP05499G
- Schippers, A., Hedrich, S., Vasters, J., Drobe, M., Sand, W., & Willscher, S. (2014). Biomining: metal recovery from ores with microorganisms. *Adv Biochem Eng Biotechnol*, 141, 1-47. doi:10.1007/10\_2013\_216
- Schleifer, K.H., Kandler, O. (1972) Peptidoglycan types of bacterial cell walls and their taxonomic implications. *Bacteriol Rev*; 36: 407-77.
- Schravendijk, W. J. (2007). Computational Modeling of Surface Interactions. (Doktor der Naturwissenschaften), Johannes Gutenberg-Universität Mainz, Amsterdam.
- Schrijver, I. A., Melief, M.-J., Eulderink, F., Hazenberg, M. P., & Laman, J. D. (1999). Bacterial Peptidoglycan Polysaccharides in Sterile Human Spleen Induce Proinflammatory Cytokine Production by Human Blood Cells. *Journal of Infectious Diseases*, 179(6), 1459-1468. doi:10.1086/314761
- Sebbari, K., Roques, J., Simoni, E., Domain, C., Perron, H., & Catalette, H. (2012). First-principles molecular dynamics simulations of uranyl ion interaction at the water/rutile TiO<sub>2</sub>(110) interface. *Surface Science*, 606(15-16). doi:10.1016/j.susc.2012.01.023
- Shahryari, Z., Soltani Goharrizi, A., & Azadi, M. (2010). Experimental study of methylene blue adsorption from aqueous solutions onto carbon nano tubes. *International Journal of Water Resources and Environmental Engineering*, 2(2), 12.
- Shen, J., Lochhead, M. J., Bray, K. L., Chen, Y., & Dumesic, J. A. (1995). Structural and Acid/Base Properties of Supported Europium Oxides. *J. Phys. Chem.*, 99, 8.
- Shen, L., Johnson, T. L., Clugston, S., Huang, H., Butenhof, K. J., & Stanton, R. V. (2011). Molecular Dynamics Simulation and Binding Energy Calculation for Estimation of Oligonucleotide Duplex Thermostability in RNA-Based Therapeutics. *Journal of Chemical Information and Modeling*, 51(8), 1957-1965. doi:10.1021/ci200141j
- Shu, L., Obagbemi, I. J., Liyanaarachchi, S., Navaratna, D., Parthasarathy, R., Aim, R. B., & Jegatheesan, V. (2016) Why does pH increase with CaCl<sub>2</sub> as draw solution during forward osmosis filtration. *Process Safety and Environmental Protection*. doi:10.1016/j.psep.2016.06.007
- Siddiqui, M. H., Kumar, A., Kumar, K. K., & Arif, J. M. (2009). Biomining - A Useful Approach Toward Metal Extraction. *American-Eurasian Journal of Agronomy*, 2(2), 4.

- Sigel, A., Sigel, H., & Sigel, R. K. O. (2005). *Metal Ions In Biological Systems, Volume 44: Biogeochemistry, Availability, and Transport of Metals in the Environment* (Vol. 44): CRC Press.
- Silhavy, T.J., Kahne, D., and Walker, S. (2010), The bacterial cell envelope, *Cold Spring Harb Perspect Biol*; 2: a000414
- Skomurski, F., Becker, U., & Ewing, R. (2007). *Computational investigation of the formation of hyperstoichiometric uranium dioxide (UO<sub>2+x</sub>)*. Paper presented at the 30th Symposium on Scientific Basis for Nuclear Waste Management, Boston, MA.
- Smith, B. C., (1995), *Fundamentals of Fourier Transform Infrared Spectroscopy*, by CRC Press, 207 Pages
- Smith, T.W., Forester, T.R. and Todorov, I.T. (2010), DL POLY Classic 1.9 manual, pp. 1–326
- Somani, B. L., Khanade, J., Sinha, R. (1987) A modified anthrone-sulfuric acid method for the determination of fructose in the presence of certain proteins, *Analytical Biochemistry*, 167(2), 327-330
- Spagnoli, D., Kerisit, S., & Parker, S. C. (2006). Atomistic simulation of the free energies of dissolution of ions from flat and stepped calcite surfaces. *Journal of Crystal Growth*, 294(1), 103-110. doi:<http://dx.doi.org/10.1016/j.jcrysgro.2006.05.030>
- Sparks, D. J., Romero-González, M. E., El-Taboni, E., Freeman, C. L., Hall, S. A., Kakonyi, G., . . . Harding, J. H. (2015). Adsorption of poly acrylic acid onto the surface of calcite: an experimental and simulation study. *Physical Chemistry Chemical Physics*, 17(41), 27357-27365. doi:10.1039/C5CP00945F
- Spence, A. and Kelleher, B. P. (2012). FT-IR spectroscopic analysis of kaolinite–microbial interactions. *Vibrational Spectroscopy*, 61, 151-155. doi:10.1016/j.vibspec.2012.02.019
- Stennett, M. C., Corkhill, C. L., Marshall, L. A., & Hyatt, N. C. (2013). Preparation, characterisation and dissolution of a CeO<sub>2</sub> analogue for UO<sub>2</sub> nuclear fuel. *Journal of Nuclear Materials*, 432(1–3), 182-188. doi:10.1016/j.jnucmat.2012.07.038
- Stodola, F.H., Lesuk, A. and Anderson, R.J. (1938) The chemistry of the lipids of tubercle bacilli. LIV. The isolation and properties of mycolic acid *J. Biol. Chem.*, 126, pp. 505–513
- Strauss, J., Burnham, N. A., & Camesano, T. A. (2009). Atomic force microscopy study of the role of LPS O-antigen on adhesion of *E. coli*. *J Mol Recognit*, 22(5), 347-355. doi:10.1002/jmr.955
- Sushko, M. L., Gal, A. Y., & Shluger, A. L. (2006). Interaction of organic molecules with the TiO<sub>2</sub> (110) surface: ab initio calculations and classical force fields. *J Phys Chem B*, 110(10), 4853-4862. doi:10.1021/jp055486q
- Sutcliffe, I. (1998), Cell envelope composition and organisation in the genus *Rhodococcus*, *Antoine van Leeuwenhoek*, 74, 49-58

- Sutradhar, N., Pahari, S. K., Jayachandran, M., Stephan, A. M., Nair, J. R., Subramanian, B., . . . Panda, A. B. (2013). Organic free low temperature direct synthesis of hierarchical protonated layered titanates/anatase TiO<sub>2</sub> hollow spheres and their task-specific applications. *Journal of Materials Chemistry A*, 1(32), 9122-9131. doi:10.1039/C3TA11628J
- Szewczyk, R., Kowalski, K., Janiszewska-Drobinska, B., & Druszczyńska, M. (2013). Rapid method for Mycobacterium tuberculosis identification using electrospray ionization tandem mass spectrometry analysis of mycolic acids. *Diagnostic Microbiology and Infectious Disease*, 76(3), 298-305. doi:10.1016/j.diagmicrobio.2013.03.025
- Takenaka, Y., Saito, T., Nagasaki, S., Tanaka, S., Kozai, N., & Ohnuki, T. (2007). Metal Sorption to Pseudomonas fluorescens: Influence of pH, Ionic Strength and Metal Concentrations. *Geomicrobiology Journal*, 24(3-4), 205-210. doi:10.1080/01490450701457337
- Tan, Y. H., Terrill, S. E., Paranjape, G. S., Stine, K. J., & Nichols, M. R. (2014). The influence of gold surface texture on microglia morphology and activation. *Biomaterials Science*, 2(1), 110-120. doi:10.1039/C3BM60096C
- Tasker, P. W. (1979) The stability of ionic crystal surfaces, *Journal of Physics C: Solid State Physics*, Volume 12, Number 22, pp4977
- Taylor, K. A. C. C. (1996). A simple colorimetric assay for muramic acid and lactic acid. *Applied Biochemistry and Biotechnology*, 56(1), 49-58. doi:10.1007/BF02787869
- Tipper, D. J. (1968). Alkali-catalyzed elimination of D -lactic acid from muramic acid and its derivatives and the determination of muramic acid. *Biochemistry* 7:1441–1449
- Tkatchenko, A., Romaner, L., Hofmann, O. T., Zojer, E., Ambrosch-Draxl, C., & Scheffler, M. (2010). Van der Waals interactions between organic adsorbates and at organic/inorganic interfaces. *MRS Bulletin*, 35, 8.
- Todorov, I.T., Smith, W. S, Trachenko, K. and Dove, M.T. (2006) *Journal of Materials Chemistry*, 16 , 1911-1918
- Tofail, S. A. M. (2012). *Biological interactions with surface charge in biomaterials*. Cambridge: RSC Publishing. Print publication date: 14 Nov 2011 Copyright: 2012
- Tomioka, N., Uchiyama, H., & Yagi, O. (1992). Isolation and characterization of cesium-accumulating bacteria. *Applied and Environmental Microbiology*, 58(3).
- Tosun, I. (2012) Ammonium Removal from Aqueous Solutions by Clinoptilolite: Determination of Isotherm and Thermodynamic Parameters and Comparison of Kinetics by the Double Exponential Model and Conventional Kinetic Models, *Int. J. Environ. Res. Public Health*, 9,970-984
- Tran, H.N., You, S.J., Chao, H.P. (2016), Thermodynamic parameters of cadmium adsorption onto orange peel calculated from various methods: A comparison study, *Journal of Environmental Chemical Engineering*, 4(3), 2671-2682

- Travassos, L.H., Girardin, S.E., Philpott, D.J., Blanot, D., Nahori, M.A., Werts, C., Boneca, I.G., (2004), Toll-like receptor 2-dependent bacterial sensing does not occur via peptidoglycan recognition, *EMBO reports*, Vol.5(10), p.1000
- Trujillo, M. E., Velazquez, E., Kroppenstedt, R. M., Schumann, P., Rivas, R., Mateos, P. F., & Martinez-Molina, E. (2004). *Mycobacterium psychrotolerans* sp nov., isolated from pond water near a uranium mine. *International Journal of Systematic and Evolutionary Microbiology*, 54. doi:10.1099/ijs.0.02938-0
- Trumbo, T. A., Schultz, E., Borland, M.G., Pugh, M.E. (2013). Applied Spectrophotometry: Analysis of a Biochemical Mixture. *Biochemistry and Molecular Biology Education*, 242. doi: 10.1002/bmb.20694
- Ulrich, K.-U., Ilton, E. S., Veeramani, H., Sharp, J. O., Bernier-Latmani, R., Schofield, E. J., . . . Giammar, D. E. (2009). Comparative dissolution kinetics of biogenic and chemogenic uraninite under oxidizing conditions in the presence of carbonate. *Geochimica Et Cosmochimica Acta*, 73(20). doi:10.1016/j.gca.2009.07.012
- Ulrich, K.-U., Singh, A., Schofield, E. J., Bargar, J. R., Veeramani, H., Sharp, J. O., . . . Giammar, D. E. (2008). Dissolution of biogenic and synthetic UO<sub>2</sub> under varied reducing conditions. *Environmental Science & Technology*, 42(15). doi:10.1021/es800647u
- Ulrich, K. A. I., Singh, A., Schofield, E. J., Bargar, J. R., Veeramani, H., Sharp, J. O., . . . Giammar, D. E. (2008). Dissolution of Biogenic and Synthetic UO<sub>2</sub> under Varied Reducing Conditions. *Environmental science & technology*, 42(15), 5600-5606. doi:10.1021/es800647u
- U.S. Department of Health and Human Services, Public Health Service, 1996, 'Standardized Method for HPLC Identification of Mycobacteria'
- Van Hee, P., Middelberg, A. P. J., Van der Lans, R. G. J. M., Wielen, L. A. (2004). Quantification of solid cell material by detection of membrane-associated proteins and peptidoglycan. *Journal of Chromatography B*, 807(1), 111-119. doi:10.1016/j.jchromb.2004.01.052
- Vandenborre, J., Grambow, B., & Abdelouas, A. (2010). Discrepancies in Thorium Oxide Solubility Values: Study of Attachment/Detachment Processes at the Solid/Solution Interface. *Inorganic Chemistry*, 49(19), 8736-8748. doi:10.1021/ic100756f
- Vanderkooi, J. M., Dashnau, J. L., & Zelent, B. (2005). Temperature excursion infrared (TEIR) spectroscopy used to study hydrogen bonding between water and biomolecules. *Biochimica Et Biophysica Acta-Proteins and Proteomics*, 1749(2). doi:10.1016/j.bbapap.2005.03.008
- Vivek, S., Arunkumar, P., & Babu, K. S. (2016). In situ generated nickel on cerium oxide nanoparticle for efficient catalytic reduction of 4-nitrophenol. *RSC Advances*, 6(51), 45947-45956. doi:10.1039/C6RA04120E
- Von Hippel, F. (2011), The radiological and psychological consequences of the Fukushima Daiichi accident', *Bulletin of the Atomic Scientists*, 67, 5

- Wang, L., Li, F. T., & Zhou, Q. (2006). Contribution of cell-surface components to Cu<sup>2+</sup> adsorption by *Pseudomonas putida* 5-x. *Applied Biochemistry and Biotechnology*, 128(1), 33-46. doi:10.1385/ABAB:128:1:033
- Watkinson, E.J., Whiting, C.E., Barklay, C.D., Ambrosi, R.M., Williams, H.R., Reece, M., Ning, H., Weston, D., Sarsfield, M., Tinsley, T., Kramer, D.P., (2015), Sintering trials of ceria as an analogue of americium-241, *NETS-2015*
- Weber, M., & Andrae, K. (2010). A simple method for the estimation of entropy differences. *MATCH Commun. Math. Comput. Chem.*, 63, 13.
- Weck, P. F., Kim, E., Jove-Colon, C. F., & Sassani, D. C. (2012). Structures of uranyl peroxide hydrates: a first-principles study of studtite and metastudtite. *Dalton Transactions*, 41(32), 9748-9752. doi:10.1039/C2DT31242E
- Weil, B. (2012). *Uranium Mining and Extraction from Ore*. Prof. Robert B. Laughlin courses, Department of Physics Stanford University, <http://large.stanford.edu/courses/>
- Weiner, S. J., Kollman, P. A., Case, D. A., Singh, U. C., Ghio, C., Alagona, G., . . . Weiner, P. (1984). A new force field for molecular mechanical simulation of nucleic acids and proteins. *Journal of the American Chemical Society*, 106(3), 765-784. doi:10.1021/ja00315a051
- Wickham, J. R., & Rice, C. V. (2008). Solid-state NMR studies of bacterial lipoteichoic acid adsorption on different surfaces. *Solid State Nuclear Magnetic Resonance*, 34(3), 154-161. doi:10.1016/j.ssnmr.2008.06.001
- Wilson, (2007) The Winning Weapon? Rethinking Nuclear Weapons in Light of Hiroshima, *International Security*, 31, 18
- Wilson, W. W., Wade, M. M., Holman, S. C., & Champlin, F. R. (2001). Status of methods for assessing bacterial cell surface charge properties based on zeta potential measurements. *Journal of Microbiological Methods*, 43(3), 153-164. doi:http://dx.doi.org/10.1016/S0167-7012(00)00224-4
- Yagi, T., Mahapatra, S., Mikusova, K., Crick, D., and Brennan, P.J. (2003) Polymerization of Mycobacterial Arabinogalactan and Ligation of Peptidoglycan, *The Journal of Biological Chemistry*, 278, 26497-26504
- Yang, Y., Shen, Y., Liu, H., & Yao, X. (2011). Molecular Dynamics Simulation and Free Energy Calculation Studies of the Binding Mechanism of Allosteric Inhibitors with p38 $\alpha$  MAP Kinase. *Journal of Chemical Information and Modeling*, 51(12), 3235-3246. doi:10.1021/ci200159g
- Yang, Z., Wang, Q., Wei, S., Ma, D., & Sun, Q. (2010). The Effect of Environment on the Reaction of Water on the Ceria(111) Surface: A DFT+U Study. *The Journal of Physical Chemistry C*, 114(35), 14891-14899. doi:10.1021/jp101057a
- Yong, C.W. (2014), [http://www.ccp5.ac.uk/DL\\_ANALYSER/](http://www.ccp5.ac.uk/DL_ANALYSER/)

- Young P, Macaskie LE (1995) Removal of tetravalent actinide thorium from solution by a biocatalytic system. *J. Chem. Tech. Biotechnol.* **64**: 87-95.
- Yu, C.-H., Newton, S. Q., Norman, M. A., Schäfer, L., & Miller, D. M. (2003). Molecular Dynamics Simulations of Adsorption of Organic Compounds at the Clay Mineral/Aqueous Solution Interface. *Structural Chemistry*, *14*(2), 175-185. doi:10.1023/A:1022190416038
- Yuji A., Sparks D.L. , (2001) ATR–FTIR Spectroscopic Investigation on Phosphate Adsorption Mechanisms at the Ferrihydrite–Water Interface, *Journal of Colloid and Interface Science*, Volume 241, Issue 2, Pages 317-326, ISSN 0021-9797, <http://dx.doi.org/10.1006/jcis.2001.7773>.
- Yukselen-Aksoy, Y., & Kaya, A. (2011). A study of factors affecting on the zeta potential of kaolinite and quartz powder. *Environmental Earth Sciences*, *62*(4), 697-705. doi:10.1007/s12665-010-0556-9
- Zein-Eldin, Z. P., and B. Z. May. (1958). Improved n-ethylcarbazole determination of carbohydrates with emphasis on sea water samples. *Anal. Chem.* *30*:1935-1941.
- Zhang, H.-p., Lu, X., Leng, Y., Watari, F., Weng, J., Feng, B., & Qu, S. (2011). Effects of aqueous environment and surface defects on Arg-Gly-Asp peptide adsorption on titanium oxide surfaces investigated by molecular dynamics simulation. *Journal of Biomedical Materials*, *96A*(2), 10. doi:10.1002/jbm.a.33003
- Zhang, Z., Pen, Y., Edyvean, R. G., Banwart, S. A., Dalglish, R. M., & Geoghegan, M. (2010). Adhesive and conformational behaviour of mycolic acid monolayers. *Biochimica Et Biophysica Acta-Biomembranes*, *1798*(9). doi:10.1016/j.bbamem.2010.05.024
- Zhou, L., Srisatjaluk, R., Justus, D. E., & Doyle, R. J. (1998). On the origin of membrane vesicles in Gram-negative bacteria. *FEMS Microbiology Letters*, *163*(2), 5.
- Zhou KB, Yang ZQ, Yang S. (2007) Highly Reducible CeO<sub>2</sub> Nanotubes. *Chem Mater*; *19*:1215–1217





# Appendices

## Appendix 1

### X-ray Diffraction Analysis

Configuration=Reflection-Transmission Spinner,

Goniometer=PW3050/60 (Theta/Theta); Minimum step size 2Theta:0.001; Minimum step size Omega:0.001

Sample stage=Reflection-Transmission Spinner PW3064/60; Minimum step size Phi:0.1

Diffractometer system: XPERT-3

Anode material: Cu

K-Alpha1 wavelength : 1.540598

K-Alpha2 wavelength : 1.544426

Ratio K-Alpha2/K-Alpha1: 0.5

Divergence slit: Fixed

Monochromator used: NO

Generator voltage: 45

Scan axis: Gonio

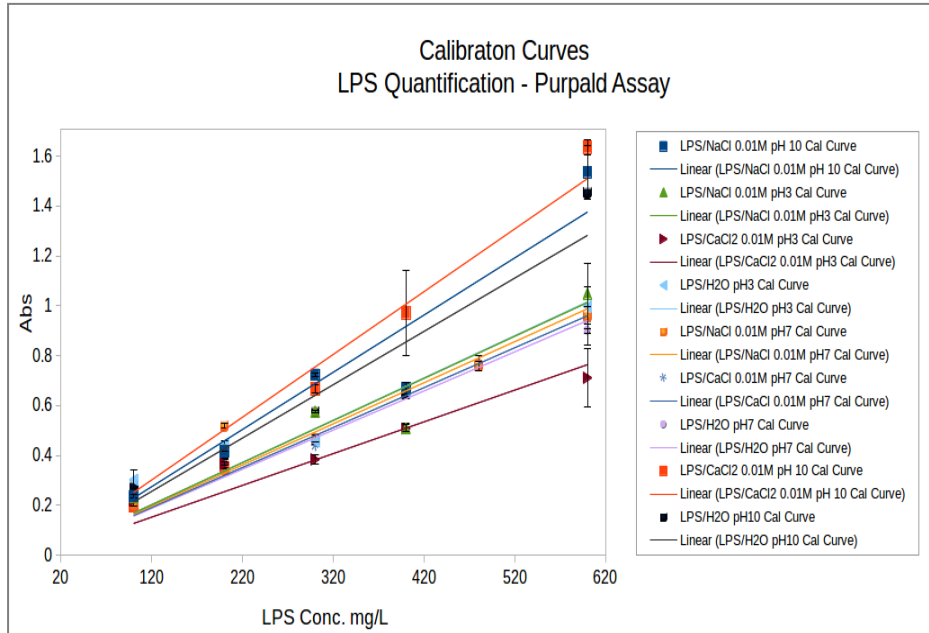
Scan type: CONTINUOUS

Phi: 328.7

Time per step: 25.245

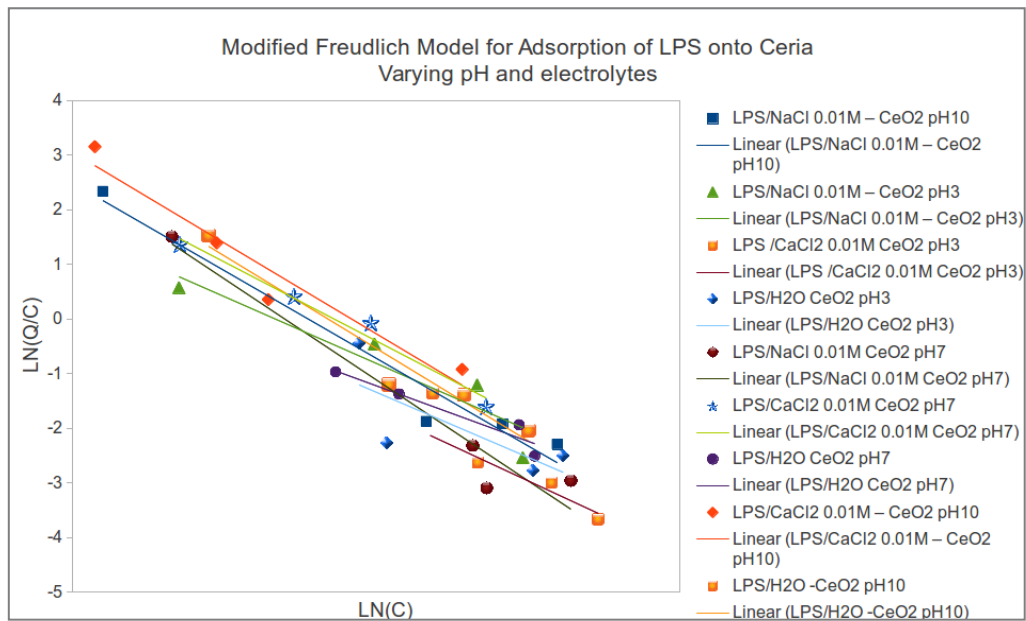
## Appendix 2

### The calibration curves constructed for LPS under varying conditions



## Appendix 3

### Modified Freundlich model for LPS adsorption onto Ceria



The modified Freundlich equations for pH10 were:

$$y = -0.9155970085x + 2.4863446448 \text{ for NaCl,}$$

$$y = -0.9483514237x + 3.0484002931 \text{ for CaCl}_2 \text{ and}$$

$$y = -0.9662651153x + 2.8446334307 \text{ for water.}$$

The modified Freundlich equations for the pH3 systems were:

$$y = -0.6969020143x + 1.6272832424 \text{ for NaCl,}$$

$$y = -0.7357654971x + 0.9029786006 \text{ for CaCl}_2 \text{ and}$$

$$y = -0.6800044041x + 1.0403429451 \text{ for water.}$$

The modified Freundlich equations obtained for the pH7 systems were:

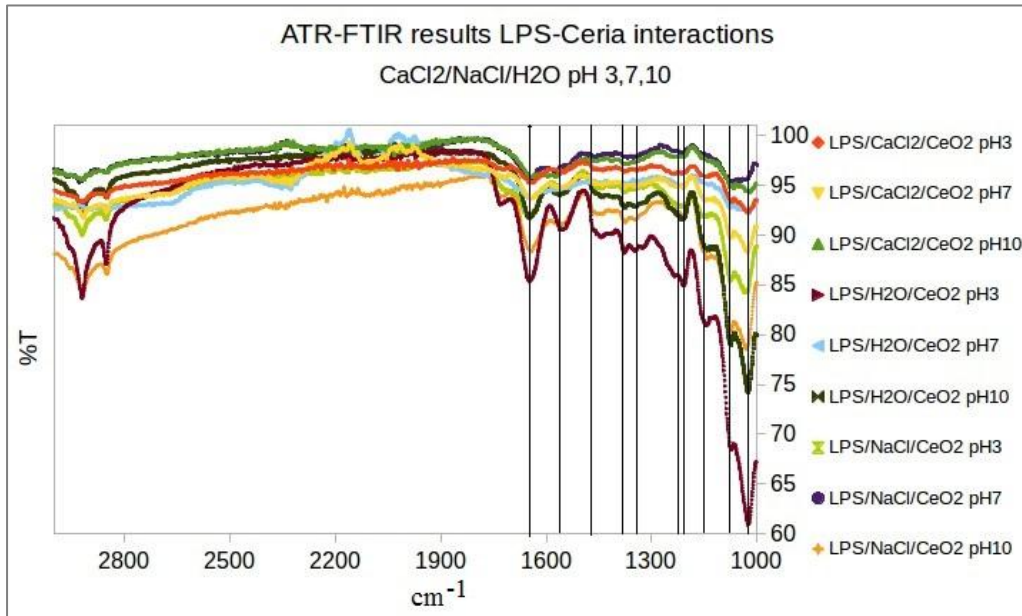
$$y = -1.0548564277x + 2.5786764769 \text{ for NaCl,}$$

$$y = -0.8251291446x + 2.4861393636 \text{ for CaCl}_2 \text{ and}$$

$$y = -0.5800922385x + 0.8083207664 \text{ for water.}$$

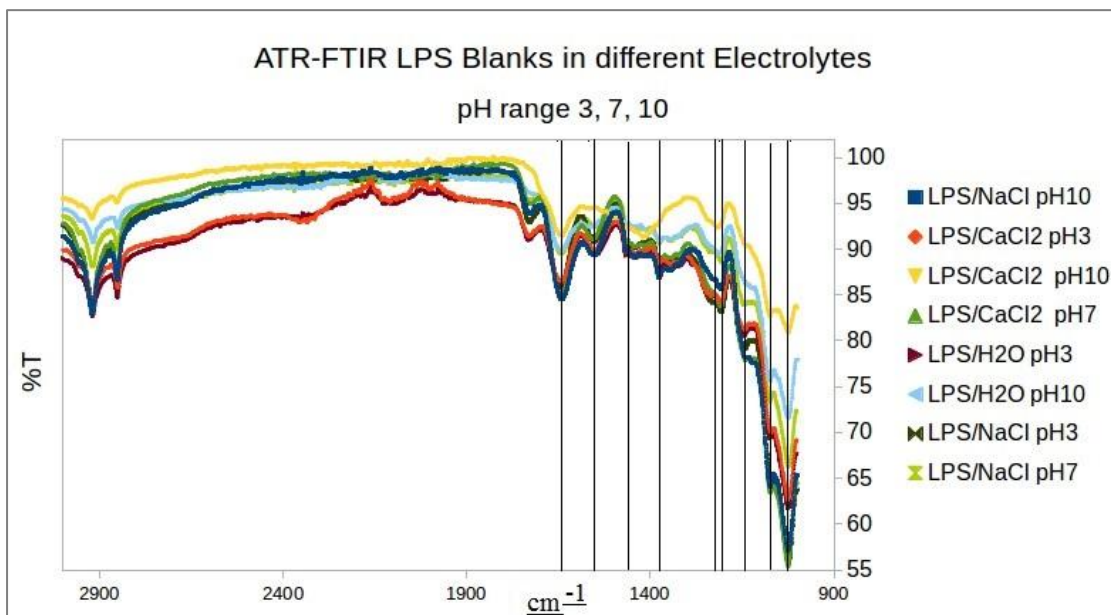
## Appendix 4

### ATR-FTIR results for LPS-Ceria complexes



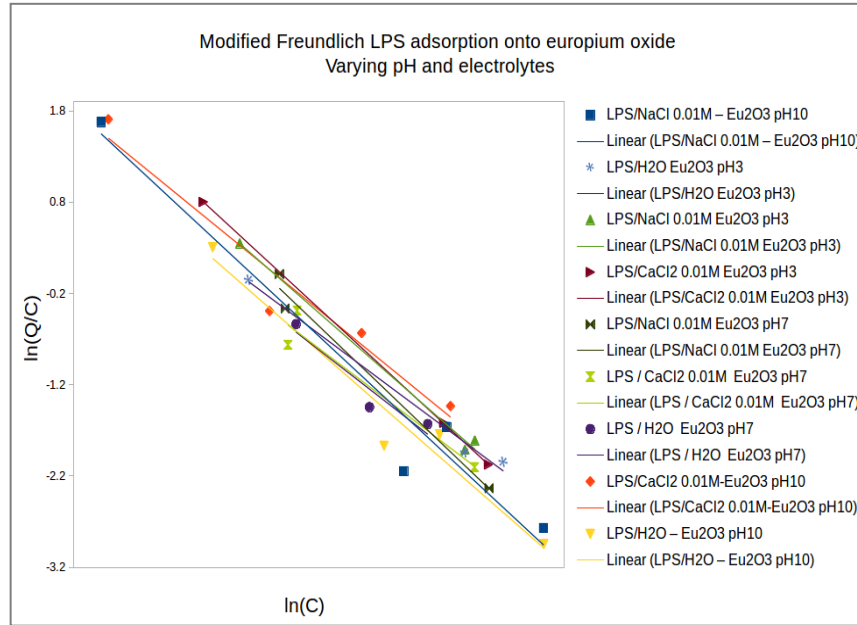
## Appendix 5

### ATR-FTIR data of LPS controls under varying conditions



## Appendix 6

### Modified Freundlich model for LPS adsorption onto $\text{Eu}_2\text{O}_3$ under varying conditions



The modified Freundlich equations for pH10 were:

$$y = -0.9980153209x + 2.8273208609 \text{ for NaCl,}$$

$$y = -0.8753813112x + 2.6871283977 \text{ for CaCl}_2 \text{ and}$$

$$y = -0.9390719097x + 2.455249308 \text{ for water.}$$

The modified Freundlich equations obtained for the pH3 systems were:

$$y = -0.9392324952x + 2.8772247755 \text{ for NaCl,}$$

$$y = -0.9893362905x + 3.1019854866 \text{ for CaCl}_2 \text{ and}$$

$$y = -0.798450837x + 2.1534862879 \text{ for water.}$$

The modified Freundlich equations obtained for the pH7 systems were:

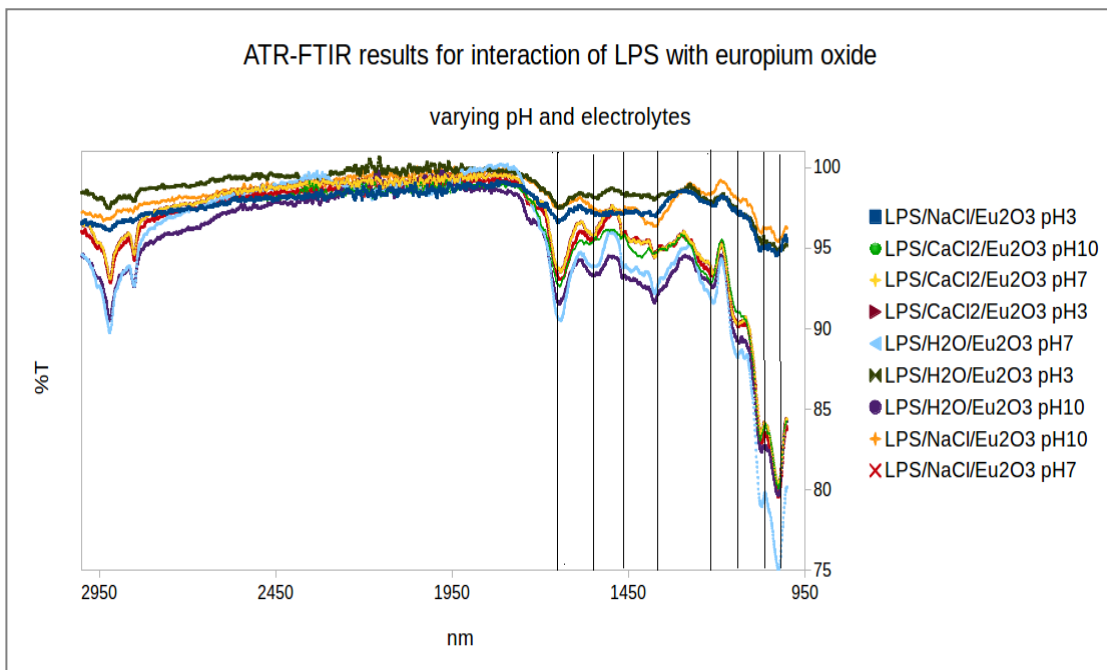
$$y = -1.0268351127x + 3.0395984502 \text{ for NaCl,}$$

$$y = -0.8137184849x + 2.0484016239 \text{ for CaCl}_2 \text{ and}$$

$$y = -0.8329469725x + 2.0989332509 \text{ for water.}$$

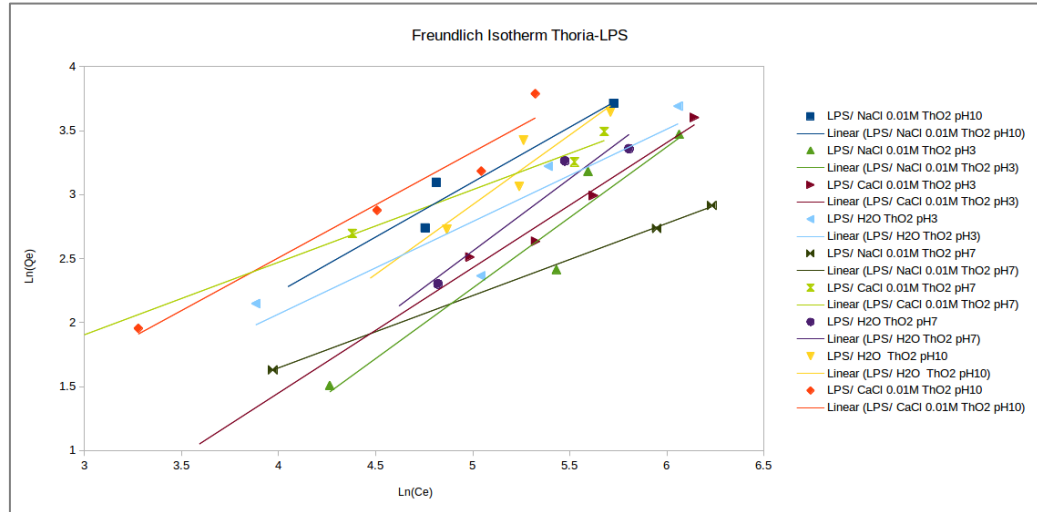
## Appendix 7

### ATR-FTIR results for LPS-Eu<sub>2</sub>O<sub>3</sub> complexes



## Appendix 8

### Freundlich model fitting for Thoria-LPS sorption



The Freundlich equations for pH10 were:

$$y=2.6179099815x - 11.7351119351 \text{ for NaCl,}$$

$$y=1.0620112025x - 7.5849609724 \text{ for CaCl}_2 \text{ and}$$

$$y=1.7394588619x - 7.5849609724 \text{ for water.}$$

The Freundlich equations obtained for the pH3 systems were:

$$y=1.0178784784x - 3.1735993491 \text{ for NaCl,}$$

$$y=0.6625261312x - 1.1286122547 \text{ for CaCl}_2 \text{ and}$$

$$y=1.2272946913x - 4.3716669381 \text{ for water.}$$

The Freundlich equations obtained for the pH7 systems were:

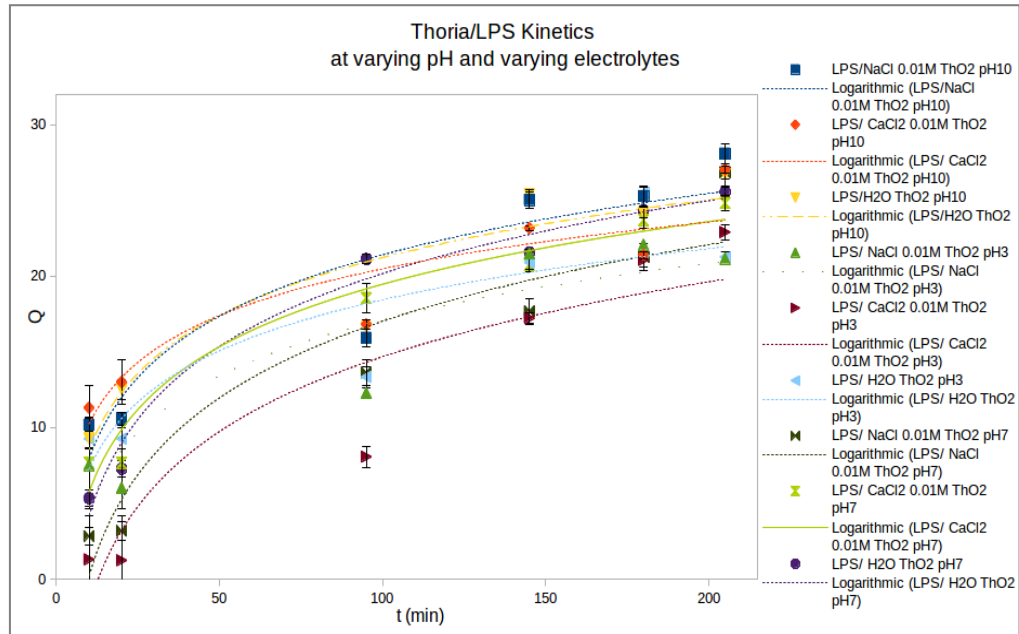
$$y=0.668547145x - 1.4435052028 \text{ for NaCl,}$$

$$y=0.5760596109x - 0.3317315463 \text{ for } CaCl_2 \text{ and}$$

$$y=3.1035785466x - 15.9104177476 \text{ for water.}$$

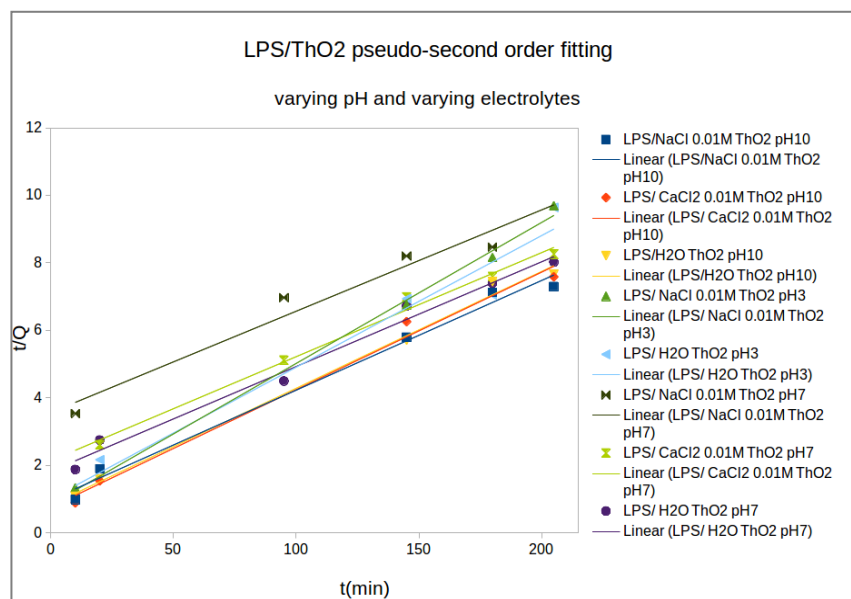
## Appendix 9

### Thoria-LPS kinetics analysis for varying conditions



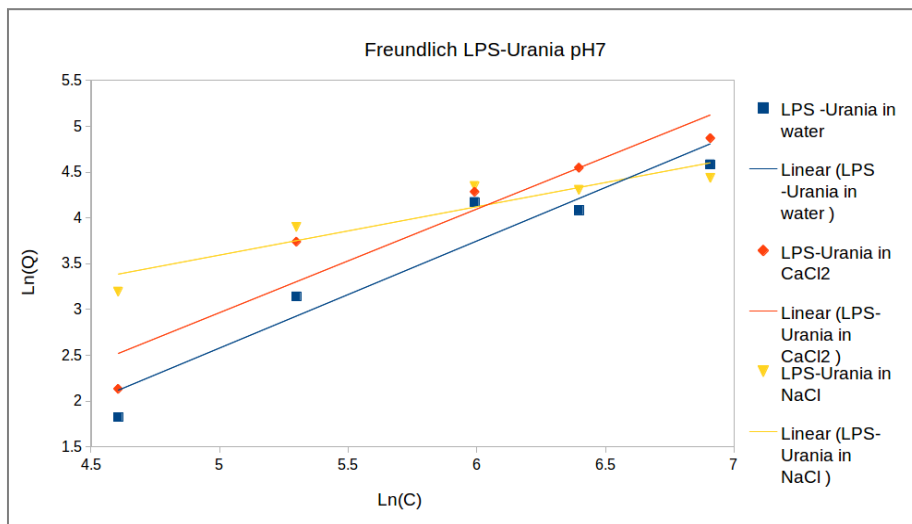
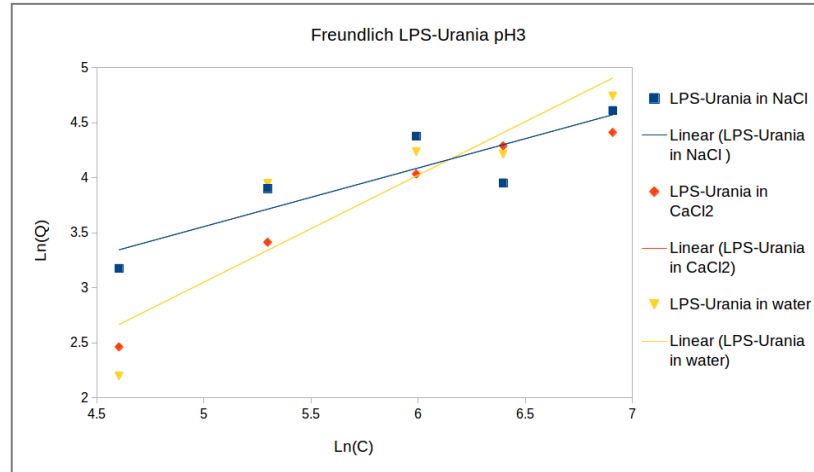
## Appendix 10

### LPS-Thoria Pseudo-Second Order fitting for varying conditions



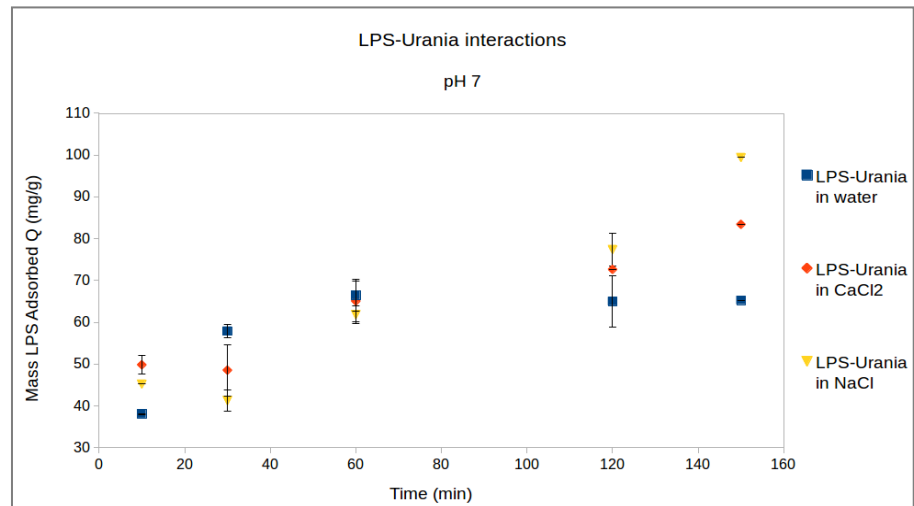
## Appendix 11

### LPS-Urania Freundlich Modelling



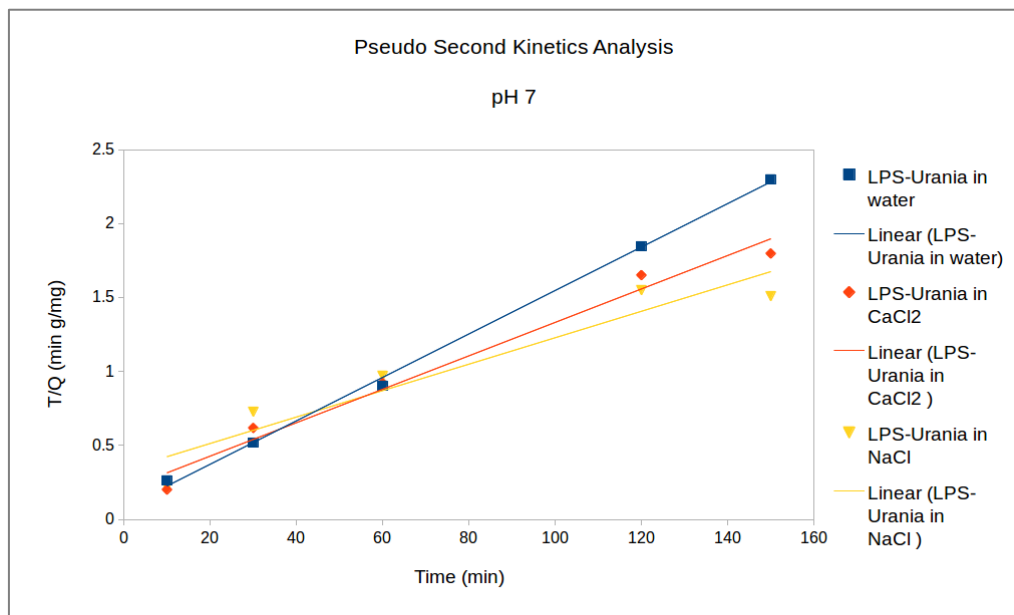
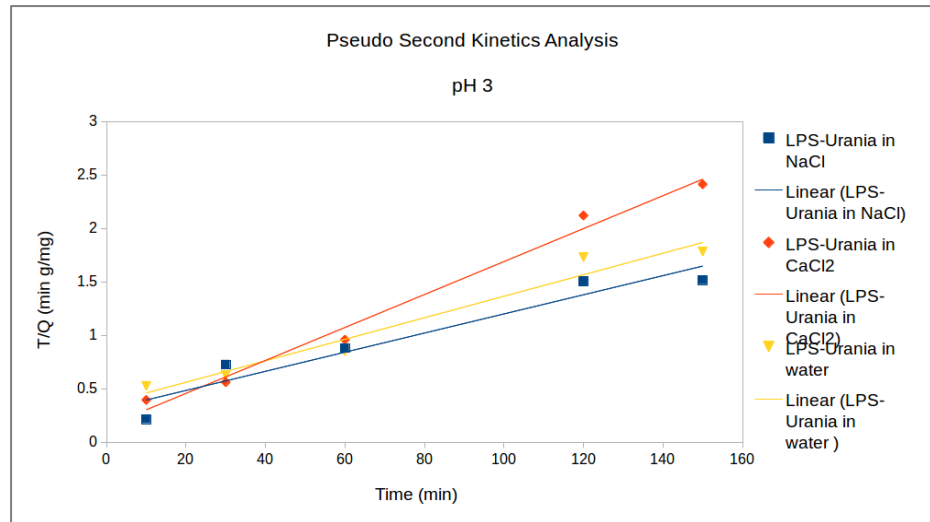
## Appendix 12

### LPS-Urania interactions



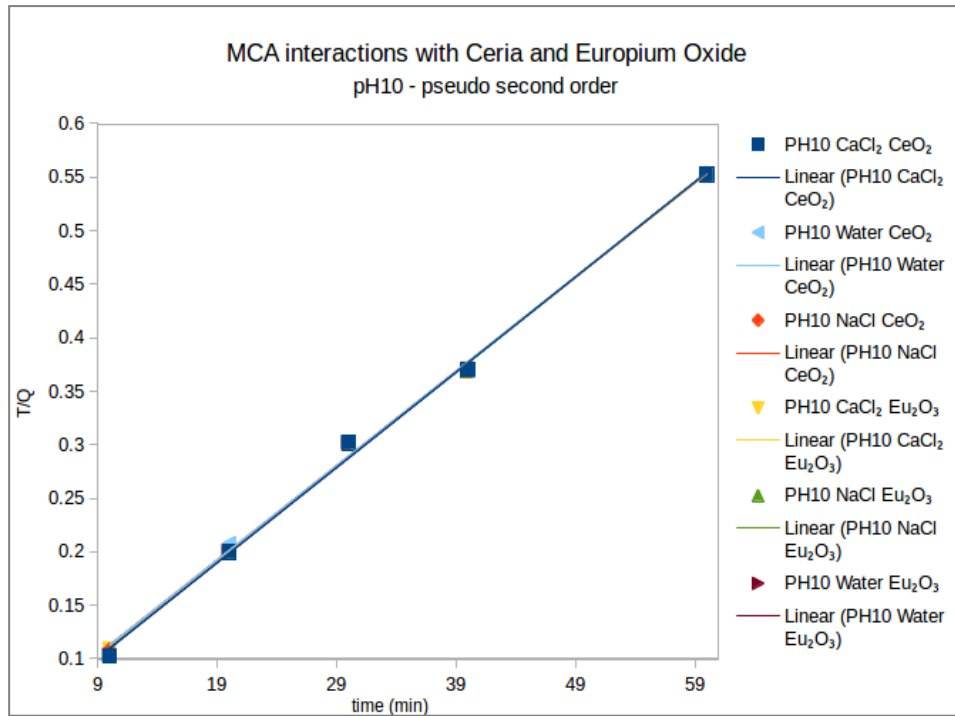
## Appendix 13

### Pseudo second kinetics analysis for Urania-LPS interactions

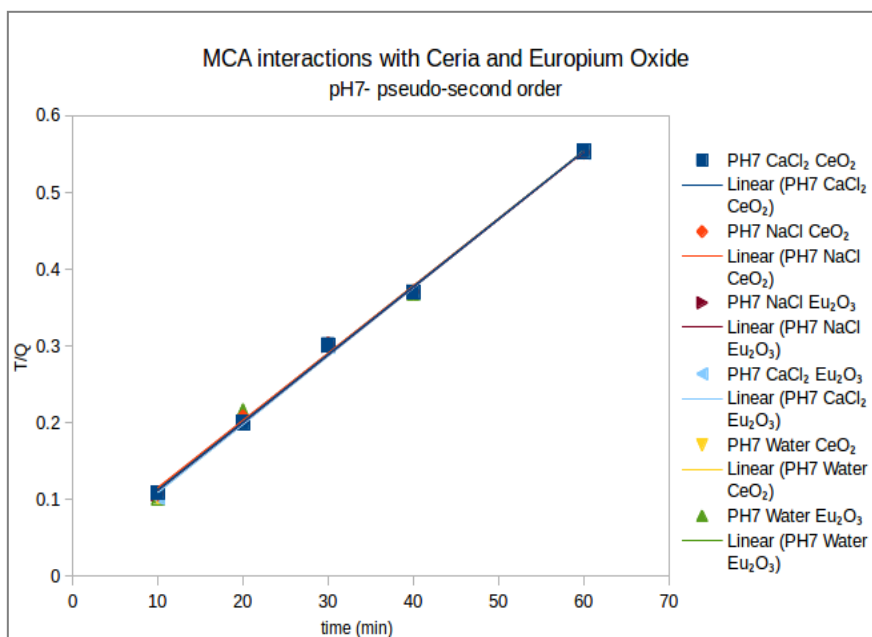


## Appendix 14

### (a) Pseudo-second Order Kinetics MCA adsorption to ceria and europium oxide pH10

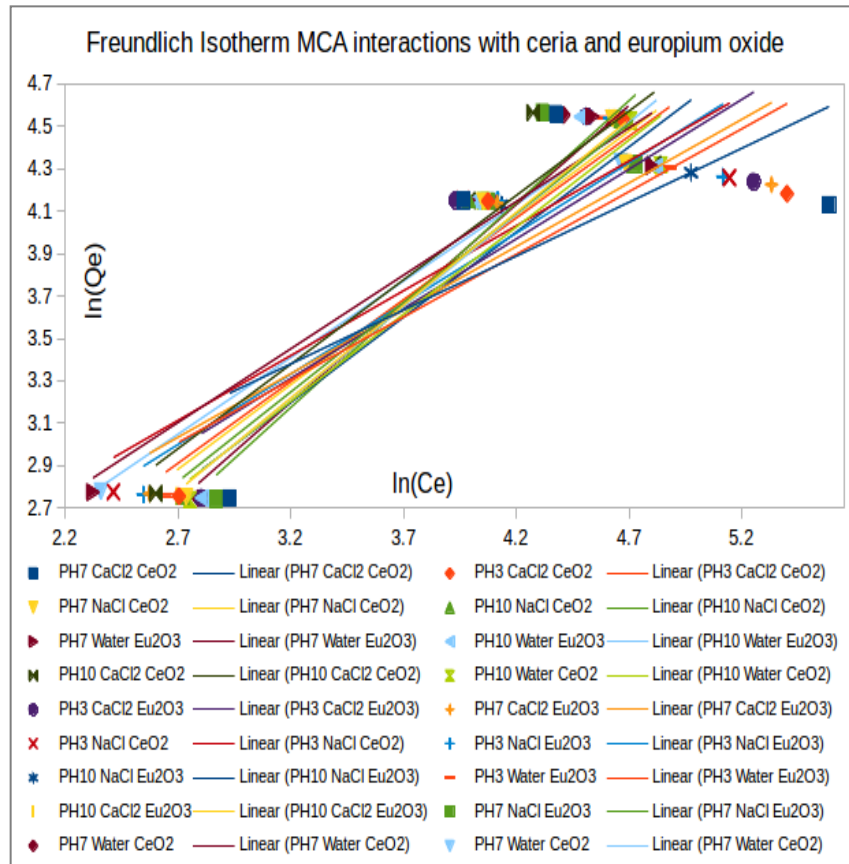


### (b) Pseudo-second Order Kinetics MCA adsorption to ceria and europium oxide pH7

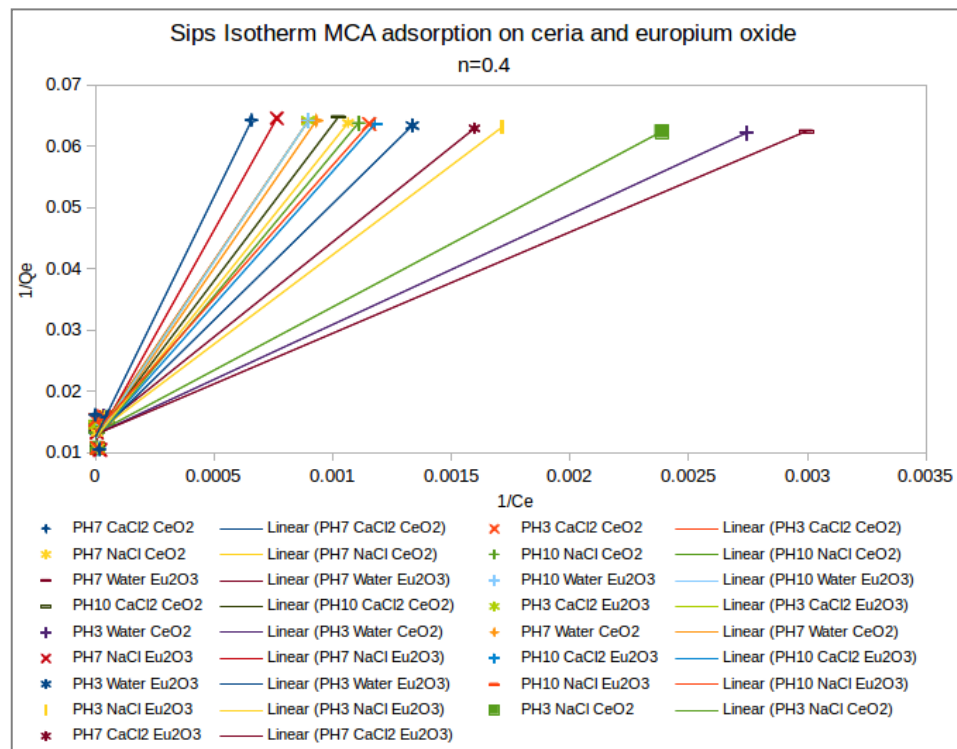




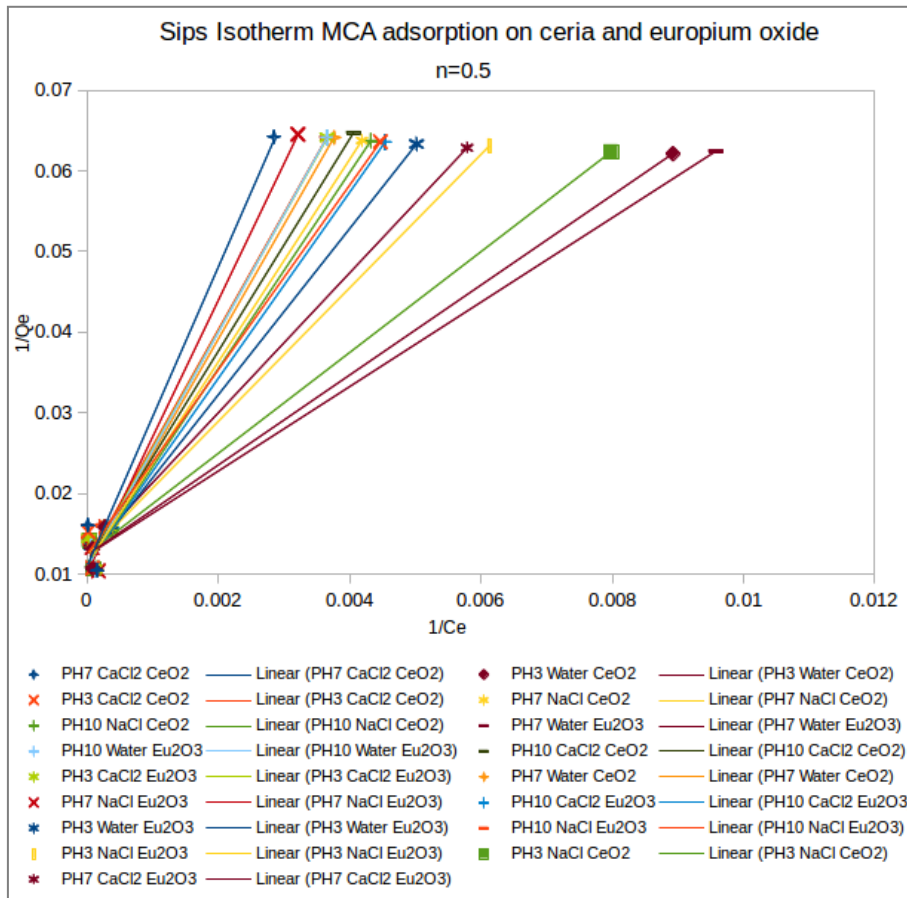
## Appendix 16



## Appendix 17a



Appendix 17b



## Appendix 18

### Computational Parameters for interactions of Ceria (110) with pseudo-mycolic acid

#### Simulation ID: Ceria (110)-Mycolic Acid-Water and Na+

Units kJ/mol

Characters included: 5

##### *Character 1: Cerium*

Number of atoms in simulation: 792

| <b>ID</b> | <b>Mass (amu)</b> | <b>Charge (e)</b> |
|-----------|-------------------|-------------------|
| Ce        | 140.116000        | 2.400000          |

##### *Character 2: Oxygen*

Number of atoms in simulation: 1584

| <b>ID</b> | <b>Mass (amu)</b> | <b>Charge (e)</b> |
|-----------|-------------------|-------------------|
| Oc        | 16.000000         | -1.200000         |

##### *Character 3: pseudo-Mycolic Acid*

Number of atoms in simulation: 1 MCA of 85 atoms in total

| <b>ID</b> | <b>Mass (amu)</b> | <b>Charge (e)</b> |
|-----------|-------------------|-------------------|
| c3        | 12.011000         | -0.2050000000     |
| c3        | 12.011000         | -0.1600000000     |
| c3        | 12.011000         | -0.1480000000     |
| c3        | 12.011000         | -0.2090000000     |
| c3        | 12.011000         | 0.0670000000      |
| oh        | 15.999000         | -0.3890000000     |
| c3        | 12.011000         | -0.1580000000     |
| c3        | 12.011000         | -0.1560000000     |
| c3        | 12.011000         | -0.1570000000     |
| c3        | 12.011000         | -0.1550000000     |
| c3        | 12.011000         | -0.1320000000     |
| cx        | 12.011000         | -0.1490000000     |

|    |           |               |
|----|-----------|---------------|
| cx | 12.011000 | -0.2160000000 |
| cx | 12.011000 | -0.1620000000 |
| c3 | 12.011000 | -0.1280000000 |
| c3 | 12.011000 | -0.1580000000 |
| c3 | 12.011000 | -0.1560000000 |
| c3 | 12.011000 | -0.1600000000 |
| c3 | 12.011000 | -0.1540000000 |
| c3 | 12.011000 | -0.1330000000 |
| cx | 12.011000 | -0.1540000000 |
| cx | 12.011000 | -0.2120000000 |
| cx | 12.011000 | -0.1610000000 |
| c3 | 12.011000 | -0.1290000000 |
| c3 | 12.011000 | -0.1570000000 |
| c3 | 12.011000 | -0.1570000000 |
| c3 | 12.011000 | -0.1590000000 |
| c3 | 12.011000 | -0.1580000000 |
| c3 | 12.011000 | -0.2110000000 |
| c  | 12.011000 | 0.3290000000  |
| o  | 15.999000 | -0.5590000000 |
| o  | 15.999000 | -0.5930000000 |
| hc | 1.007940  | 0.0470000000  |
| hc | 1.007940  | 0.0600000000  |
| hc | 1.007940  | 0.0700000000  |
| hc | 1.007940  | 0.0640000000  |
| hc | 1.007940  | 0.0730000000  |
| hc | 1.007940  | 0.1210000000  |
| hc | 1.007940  | 0.0590000000  |
| hc | 1.007940  | 0.0860000000  |

|    |          |              |
|----|----------|--------------|
| h1 | 1.007940 | 0.0630000000 |
| ho | 1.007940 | 0.2540000000 |
| hc | 1.007940 | 0.0730000000 |
| hc | 1.007940 | 0.0770000000 |
| hc | 1.007940 | 0.1000000000 |
| hc | 1.007940 | 0.0710000000 |
| hc | 1.007940 | 0.0690000000 |
| hc | 1.007940 | 0.0740000000 |
| hc | 1.007940 | 0.0790000000 |
| hc | 1.007940 | 0.0790000000 |
| hc | 1.007940 | 0.0770000000 |
| hc | 1.007940 | 0.0800000000 |
| hc | 1.007940 | 0.1180000000 |
| hc | 1.007940 | 0.1060000000 |
| hc | 1.007940 | 0.1020000000 |
| hc | 1.007940 | 0.1200000000 |
| hc | 1.007940 | 0.0750000000 |
| hc | 1.007940 | 0.0770000000 |
| hc | 1.007940 | 0.0920000000 |
| hc | 1.007940 | 0.0800000000 |
| hc | 1.007940 | 0.0730000000 |
| hc | 1.007940 | 0.0770000000 |
| hc | 1.007940 | 0.0870000000 |
| hc | 1.007940 | 0.0800000000 |
| hc | 1.007940 | 0.0770000000 |
| hc | 1.007940 | 0.0770000000 |
| hc | 1.007940 | 0.0890000000 |
| hc | 1.007940 | 0.0810000000 |

|    |          |              |
|----|----------|--------------|
| hc | 1.007940 | 0.1170000000 |
| hc | 1.007940 | 0.1080000000 |
| hc | 1.007940 | 0.1040000000 |
| hc | 1.007940 | 0.1200000000 |
| hc | 1.007940 | 0.0790000000 |
| hc | 1.007940 | 0.0770000000 |
| hc | 1.007940 | 0.0860000000 |
| hc | 1.007940 | 0.0810000000 |
| hc | 1.007940 | 0.0750000000 |
| hc | 1.007940 | 0.0760000000 |
| hc | 1.007940 | 0.0830000000 |
| hc | 1.007940 | 0.0810000000 |
| hc | 1.007940 | 0.0750000000 |
| hc | 1.007940 | 0.0750000000 |
| hc | 1.007940 | 0.0730000000 |
| hc | 1.007940 | 0.0680000000 |
| hc | 1.007940 | 0.0740000000 |

*Character 4: Sodium*

Number of atoms in simulation: 1

| <b>ID</b> | <b>Mass (amu)</b> | <b>Charge (e)</b> |
|-----------|-------------------|-------------------|
| NA        | 22.990000         | 1.000000          |

*Character 5: Water*

Number of atoms in simulation: 2100 H2O of 3 atoms each

| <b>ID</b> | <b>Mass (amu)</b> | <b>Charge (e)</b> |
|-----------|-------------------|-------------------|
| OW        | 16.000000         | -0.834000         |
| HW        | 1.000800          | 0.417000          |
| HW        | 1.000800          | 0.417000          |

### **Potentials**

Where: 12-6 is 
$$U(r) = \frac{A}{r_{ij}^{12}} - \frac{B}{r_{ij}^6}$$

### **Mycolic Acid Intermolecular**

*Note: Only the pair-pair potentials are provided.*

| <b>Bond ID</b> | <b>Type</b> | <b>A</b>       | <b>B</b>    |
|----------------|-------------|----------------|-------------|
| c3-c3          | 12-6        | 4364247.685263 | 2826.761643 |
| oh-oh          | 12-6        | 2434264.710887 | 2927.740652 |
| cx-cx          | 12-6        | 3430761.434484 | 2222.134382 |
| c-c            | 12-6        | 3430761.434484 | 2222.134382 |
| o-o            | 12-6        | 1589402.851422 | 2363.482956 |
| hc-hc          | 12-6        | 31447.266311   | 90.900675   |
| h1-h1          | 12-6        | 13638.569122   | 59.863219   |
| ho-ho          | 12-6        | 0.000000       | 0.000000    |

### **Water-Mycolic Acid**

|       |      |                 |              |
|-------|------|-----------------|--------------|
| OW-OW | 12-6 | 2436397.3742000 | 2490.8297993 |
| OW-c3 | 12-6 | 3289273.4990970 | 2664.8170359 |
| OW-oh | 12-6 | 2438006.5108107 | 2701.7466431 |
| OW-cx | 12-6 | 2916356.0898970 | 2362.6966243 |
| OW-c  | 12-6 | 2916356.0898970 | 2362.6966243 |
| OW-o  | 12-6 | 1979379.5567584 | 2433.2461229 |
| OW-hc | 12-6 | 289523.8460518  | 486.6162868  |
| OW-h1 | 12-6 | 199102.0292556  | 403.5377113  |

### **Na<sup>+</sup> - Water and Na<sup>+</sup> - Mycolic Acid**

|       |      |               |            |
|-------|------|---------------|------------|
| NA-NA | 12-6 | 85694.678860  | 63.0193716 |
| OW-NA | 12-6 | 458853.403817 | 397.024565 |
| c3-NA | 12-6 | 611961.427332 | 422.242681 |
| oh-NA | 12-6 | 461355.739825 | 431.742870 |

|       |      |               |            |
|-------|------|---------------|------------|
| cx-NA | 12-6 | 542581.039825 | 374.371428 |
| c-NA  | 12-6 | 542581.039825 | 374.371428 |
| o-NA  | 12-6 | 376752.770306 | 389.967870 |
| hc-NA | 12-6 | 56116.642717  | 78.698514  |
| h1-NA | 12-6 | 39029.528201  | 65.632257  |
| ho-NA | 12-6 | 0.000000      | 0.000000   |

### **Ceria-Mycolic Acid**

*Note: The Ce-oh, Ce-o and Ce-Oc potentials can be calculated using the Schroder methods as previously described (Freeman et al., 2007)*

|       |      |                 |              |
|-------|------|-----------------|--------------|
| Oc-c3 | 12-6 | 3836094.4214919 | 4552.1320343 |
| Oc-oh | 12-6 | 2725504.2942596 | 4518.5951133 |
| Oc-cx | 12-6 | 3401181.8507394 | 4036.0395651 |
| Oc-c  | 12-6 | 3401181.8507394 | 4036.0395651 |
| Oc-o  | 12-6 | 2180853.1017482 | 4040.0571577 |
| Oc-hc | 12-6 | 304800.0532923  | 789.7775657  |
| Oc-h1 | 12-6 | 203720.6706754  | 645.6789602  |
| Oc-ho | 12-6 | 0.0000000       | 0.0000000    |